Design and Development of Low Cost Cement Reinforced Polymeric Composite Material for Fabrication of Automotive Parts

A Thesis

Submitted in Partial Fulfillment of the Requirements for the Award of the Degree of

DOCTOR OF PHILOSOPHY

By

JAGANNATH SARDAR

(Roll No. 09610309)

Department of Mechanical Engineering

Indian Institute of Technology Guwahati

Guwahati-781039, India

November 2015

Dedicated to my parents and my sisters

who dedicated themselves for me

Department of Mechanical Engineering
Indian Institute of Technology Guwahati
Guwahati-781039, India

It is certified that the work contained in the thesis entitled "**Design and Development of Low Cost Cement Reinforced Polymeric Composite Material for Fabrication of Automotive Parts**" submitted by **Mr. Jagannath Sardar** to the Indian Institute of Technology Guwahati for the award of the degree of **Doctor of Philosophy** has been carried out under my supervision in the Department of Mechanical Engineering, Indian Institute of Technology Guwahati. This work has not been submitted elsewhere for the award of any other degree or diploma.

The thesis, in my opinion, has reached the standard fulfilling the requirements for the award of degree of Doctor of Philosophy in accordance with the regulations of the Institute.

12-11-2015

Dr. Dibakar Bandopadhya
Associate Professor
Department of Mechanical Engineering
Indian Institute of Technology Guwahati
Guwahati-781039, Assam, India

Acknowledgements

PhD, an abbreviation of only three words, teaches us how to live life with harmony of delight and the identity. It gives, in the same way, a magnificent and a phenomenal training ability of a person. Not only acquiring knowledge and ability to handle some meticulous work of a scientific platform, PhD also teaches how to converse, to deal with and also to make one comprehensible to others. In this context, I have interacted with a number of personalities, without their support, I may not reach this zenith of triumph.

At the very first, I take this opportunity to express my sincere gratitude to my respected supervisor, Dr. Dibakar Bandopadhya, Department of Mechanical Engineering, Indian Institute of Technology Guwahati, India, for accepting me as his PhD student along with his valuable guidance and steady encouragement throughout my PhD program. He provided me the complete freedom in my research and allowed me to work in my own way. He always has listened my ideas with endurance and constantly motivated to accomplish my goal. I have learnt from him, how to work with enthusiasm, energy, and full of life, yet remain unruffled and grounded. It is hard to express my gratitude with only a few words to his greatness and utmost personality. The best way to articulate my sincere gratefulness to him will probably be to comply the lessons I have learnt from him throughout my life.

My sincere acknowledgement, thenceforth, goes to Prof. D. Chakraborty and Prof. P. Mahanta, former Heads and Prof. A.K. Dass, present Head of the Mechanical Engineering Department. I express my gratitude to them for their encouragement, guidance, and support from the very beginning to the final stages of my research work. I am also indebted to the members of Doctoral Committee Prof. S.K. Dwivedy, Prof. D. Chakraborty and Dr. A. Perumal for their precious suggestions about critical issues related to my work. I am very much thankful to Dr. S. Senthilvelan because I have used his mold to fabricate the composite gear in our Advanced Manufacturing Laboratory. I will also drive to thank Dr. Ganesh R. Narayanan, Prof. Rajiv Tiwari and Dr. S. Kanagaraj, Dr. P. Biswas and other faculties of our department for their immense support, suggestions and encouragements directly or indirectly throughout my research work.

I would like to thank Technical staffs and Scientific Officers, Mr. S. Sarma Mr. J. Basumatary, Mr. M. Dowarah, Mr. R. Saikia, Mr. N. Borah and others of Department of Mechanical Engineering, and Mr. Chandan Borgohain, Mr. Madhurjya Borah of Central Instruments Facility for their enthusiastic technical support for various apparatus operation.

Sincere thanks to Mr. D. K. Saikia and Mr. N. Das for looking into my official deeds during the course of my stay.

Further, I owe to my seniors cum friends Dr. D. Biswal, Dr. C. Subramanian, Dr. S.K. Singh, Dr. R. Das, Mr. S. Kirtania for their support and help in the various ways. I am fortunate enough to get ample support from the technicians, Mr. D. Chetri, Mr. C. Banikya Mr. M. Sarma, Mr. D. Khaklary, Mr. N.K. Das Mr. M.K. Baishya and others directly or indirectly, to do jobs and experiments in the central workshop.

I am deeply indebted to dearest friend Dr. KV Kadambari for her immense help and support. In addition, I am also thankful to my friends Dr. B.K. Debnath, Dr. S. Basak, Mr. S.K Panda, Mr. S. Naskar, Mr. Krishnamohan, Mr. A. Ghatak, Mrs. M.D. Ghatak, Mr. C. Shravankumar, Mr. S. Anbarasu, Mr. R. Ghosh, Dr. A. Paul, Mr. B. Karmakar and many other individuals with whom I have come into contact during my stay in IIT Guwahati. Their friendships and hearty attachments have made my life colorful and precious.

It would not be completed if I do not admit some of my near and dear persons; they are my parents and my two sisters (Smt. Bithika Sardar and Smt. Sumati Sheuli). I am deeply grateful to them who always encouraged me for my research without knowing what PhD is. They were immersed into deep agony for long epochs by staying detach from any amusement, only to see me successful.

Last but not the least; I am especially indebted to my father who forced me to do PhD, instead of doing job.

Jagannath Sardar

November 2015 ***Jagannath Sardar***

Guwahati, India

Abstract

In the last few decades composite materials and the design and development technology have received great attention due to their numerous advantages over metallic materials. With the advancement of material processing technology, various micro and nanoparticles are now incorporated as filler materials into various matrix materials to improve the properties of composite materials results in excellent material performance. A variety of modern composite materials are existing nowadays in both structural and nonstructural elements for day-to-day life application in industrial as well as household appliances. The major advantages of polymeric composite materials such as low cost, ease of fabrication, high strength and modulus, reasonable fatigue and fracture resistance properties with respect to their density and excellent formability make them suitable for structural application substituting the need of metallic materials. Past researches indicate that spectacular enhancement and improvement in mechanical properties are achievable by varying small amount of filler particles concentration. The resulting mechanical properties of the composites are closely related to the microstructure achieved in processing of these materials. Failure of the polymeric composite depends on the percentage of filler materials incorporated into the matrix material although most of the cases it is observed that the high percentage of filler materials decreases the ductility of the composite materials. The mechanical properties of polymer composite depend on the filler-matrix material properties, matrix-to-filler interface and orientation of the filler materials and hence the properties of the end product made govern by the composite used.

Over the past decade, several composite materials have been developed and commercialized with specific application. However, there is serious limitation of finding a low cost composite material that can substitute the need of metallic materials for fabrication of automotive and other mechanical parts. Further, past researches indicate that no works, infact, carried out using Portland pozzolana cement (PPC) as filler materials and polypropylene as matrix material to fabricate the thermoplastic composite materials. In this work, thus attempts have been made to fabricate a low cost composite material using cement as reinforcing material into the polypropylene matrix that substitute the need of metallic material for industrial applications. Thus, in the present context it is relevant to try an inexpensive materials cement and polypropylene to design and develop a low cost thermoplastic composite material. In addition, few factors that govern the fabrication of this material are effectiveness, durability,

chemical reactivity, ease of processing, power consumption and excellent corrosion and fatigue resistant properties.

In this work, a low cost, non-hazardous and recyclable thermoplastic composite material is designed and developed for industrial applications. Detail fabrication procedures of the composite materials are outlined using cement particles as filler materials into the polypropylene matrix followed by Injection molding process. Several experiments are conducted to study the topographical features, dispersion of fillers into the matrix and thermal characteristics of the composite. Microstructural morphology of fabricated composite is studied using scanning electron microscope (SEM) and field-emission-SEM (FE-SEM). The morphological analysis shows that, the cement particles are adequately dispersed throughout the PP matrix. Crystallographic analysis of the composite is conducted by X-ray diffraction (XRD) analyzer. Thermogravimetric analysis (TGA), thermomechanical analysis (TMA) and differential scanning calorimetry (DSC) tests are conducted and thermal stability and degradation of the composite with temperature are studied.

Mechanical properties of the composite materials are evaluated in Instron universal testing machine, where, the experiments are conducted followed by ASTM D638 standard. Halpin-Tsai principle and rule-of-mixing series model are modified and applied to develop a mathematical model that describes the elastic modulus depending on the filler loading percentage and as well as the aspect ratio. Experimentally both the model is validated and it is found that theoretical results of the composite materials are closely agreed with the assumptions made to derive this model within the aspect ratio of 7 and 20. Dynamic mechanical analysis (DMA) of the materials has been carried out to investigate the change in storage modulus and the loss modulus with respect to temperature and subsequently the variation of loss factor of the material is ascertained.

A new type of polymeric composite material spur gear is designed and fabricated using the proposed composite material followed by injection molding technique. Several experiments are conducted with different percentages of cement materials with the polypropylene to optimize the composite material for gear fabrication. Tensile tests are conducted and the morphological studies of the fractured surface of the gear materials are investigated using scanning electron microscopy (SEM) and field-emission SEM (FE-SEM). Further, extensive experimental studies are carried out to evaluate the performance of the gear tooth under loading conditions. The experimental results validate the suitability of the proposed non-metallic spur gear for low cost industrial applications. Further, experiments are conducted to study the composite gear failure mechanism and resulting stress distribution along the contact

surface. A theoretical model is thus developed applying the Hertz's contact theorem that describes the stress profile along the contact surface.

The dynamic performance of the spur gear is evaluated under variable loads and speeds. For this, a gear-testing rig setup with accessories is modified and developed. The subsequent studies correlate the effect of temperature on the gear materials and its performance. Evaluation of heat loss measuring the heat emission in terms of surface temperature in dynamic condition is accomplished by an Infra-Red assisted camera, IR-TCM 384. In dynamic condition, the gear pair runs at a number of speeds with different loading conditions and subsequently results have been extensively studied to understand its feasibility. In addition, the composite spur gear material is subjected to friction and wear test both in adhesive and abrasive wear modes and the wear characteristics of the materials have been studied. Further, weight loss of the spur gear tooth owing to wear is quantified through direct measurement under a specific load and running condition.

An in-depth analysis and understanding of vibration characteristics of the proposed material is essential before designing any product using this class of material for structural and automotive applications. For this, composite material is subjected to free and forced vibration tests using the laser assisted vibrometer (LAV) to evaluate and characterize the damping at low frequency. The time response and Fast Fourier transformation (FFT) analysis of the materials have been carried out and subsequently the damping and loss factor of the materials are obtained. The effects of crack with respect to its position and depth on the composite beam samples have also been studied experimentally.

In addition, metal skinned sandwich panel with cement filled composite as core material was fabricated and underwent experimentation to estimate its performance for structural applications. An in-depth forced vibration characteristic and mechanical properties such as bending and tensile properties of the sandwich panel with both galvanized iron (GI) and aluminum (Al) skins have been assessed.

The thesis work results in design and development of a very low cost cement reinforced polymeric composite material. The proposed material is recyclable, durable and possesses excellent fatigue and corrosion resistant properties. A complex shaped, damage tolerant composite material spur gear has been designed and fabricated using the material for automotive industrial application. The primary benefit of using this low cost cement reinforced polymeric composite material gear is that a large weight saving can be obtained compared to metals. Further, on selecting large series of production of these gears, large cost

saving seem also feasible. In addition, the work boasts the idea to use cement particles as a cheaper, very effective strengthening filler materials with polypropylene as matrix material to fabricate composites without significant chemical and physical modifications for specific application.

Contents

List of Figures

List of Tables

Abbreviations

AC	:	*Alternating current*
AMP	:	*Ampere*
APDL	:	*Ansys parametric design language*
AFM	:	*Atomic force microscope*
$CaCO_3$	:	*Calcium carbonate*
Ca_3SiO_5	:	*Tricalcium silicate*
Ca_2SiO_4	:	*Dicalcium silicate*
$Ca_3Al_2O_5$	:	*Tricalcium aluminate*
$Ca_4Al_nFe_{2n}O_7$	:	*Calcium aluminoferrite*
CNTs	:	*Carbon nanotubes*
CSM	:	*Continuous stiffness measurement*
DGEBA	:	*Diglycidylether bisphenol a*
DMA	:	*Dynamic mechanical analysis*
DMF	:	*Dimethyl formaldehyde*
DSC	:	*Differential scanning calorimetry*
DTG	:	*Differential thermo-gravimetric*
EDX	:	*Energy dispersive x-ray*
FE-SEM	:	*Field-emission Scanning Electron Microscopy*
FFT	:	*Fast fourier transformation*
FRP	:	*Fibre reinforced plastic*
FSC	:	*Fatigue strength coefficient*
FTIR	:	*Fourier transformed infrared spectrophotometry*
GFRP	:	*Glass fibre reinforced plastic*
GI	:	*Galvanized iron*
GPa	:	*Giga pascal*
HCl	:	*Hydrochloric acid*
HDPE	:	*High Density polyethylene*
IR	:	*Infra-red*
HNO_3	:	*Nitric acid*
HP	:	*Horsepower*
H_2SO_4	:	*Sulfuric acid*
LAV	:	*Laser assisted Vibrometer*
LDPE	:	*Low Density polyethylene*
MFI	:	*Melt flow index*

MPa	:	*Mega pascal*
MWNTs	:	*Multi-walled Carbon nanotubes*
PA	:	*Polyamide*
PE	:	*Polyethylene*
PEEK	:	*Polyether ether ketone*
PEG	:	*Polyethylene glycol*
PET	:	*Polyethylene terephthalate*
PMMA	:	*Polymethyl methacrylate*
PNCs	:	*Polymer nanocomposites*
PP	:	*Polypropylene*
PPC	:	*Portland pozzolana cement*
g-MA	:	*Grafted malic anhydrite*
PSD	:	*Particle size distribution*
RMS	:	*Root means square*
RTM	:	*Resin transfer molding*
SEM	:	*Scanning electron microscopy*
SiO_2	:	*Silicon dioxide*
SRIM	:	*Structural reaction injection molding*
SWNTs	:	*Single-walled carbon nanotubes*
TEM	:	*Transmission electron microscopy*
TGA	:	*Thermo gravimetric analysis*
TMA	:	*Thermomechanical analysis*
UTM	:	*Universal testing machine*
UTS	:	*Ultimate tensile strength*
UV	:	*Ultra violet*
VGCF	:	*Vapor grown carbon fiber*
WAXRD	:	*Wide-angle X-ray diffraction*

Notations

A	:	*Projected contact area*
a/H	:	*Relative depth*
e	:	*Engineering strain*
E	:	*Elastic modulus*
E_a	:	*Activation energy*
E_i	:	*Modulus of the indenter*
E_r	:	*Reduced modulus*
$E(t)$	:	*Time dependent elastic modulus*
$E_U(t)$	:	*Modulus in unloading cycle*
$E_L(t)$	:	*Modulus in loading cycle*

F_n	:	*Applied normal load*
f	:	*Forced frequency*
f_n	:	*Natural frequency*
H	:	*Hardness of nanoindentation*
H_c	:	*Energy dissipation ratio*
Hz	:	*Unit of frequency in Hertz*
ΔH_c	:	*Normalized enthalpy of fusion*
ΔH_m	:	*Enthalpy of fusion*
J	:	*Joule*
K_w	:	*Specific wear rate*
kJ	:	*Kilo Joule*
kN	:	*Kilo Newton*
l/d	:	*Aspect ratio*
ℓ_c/ℓ	:	*Relative position*
Δm	:	*Mass loss*
N	:	*Newton*
n	:	*Order of reaction*
P_{max}	:	*Load measured at a maximum depth of penetration*
Q	:	*Amplification factor*
R	:	*Universal gas constant*
rpm	:	*Revolution per minute*
T	:	*Time period*
S	:	*Engineering stress*
S_c	:	*Contact stiffness*
S_d	:	*Sliding distance*
T_B	:	*Evaporation temperature*
T_c	:	*Crystallization temperature*
T_{dmx}	:	*Maximum degradation temperature*
T_{ds}	:	*Degradation starting temperature*
T_{dtg}	:	*Peak temperature at DTG*
T_g	:	*Glass transition temperature*
T_m	:	*Melting Temperature*
T_{wl}	:	*Temperature corresponding to weight loss*
V_{cem}	:	*Volume fraction of cement*
V_{filler}	:	*Volume fraction of filler*
W_{cem}	:	*Weight fraction of cement*
w_{cem}	:	*Weight of the cement*
W_f	:	*Weight percentage of filler material*
W_{fin}	:	*Final weight of the sample*

W_i	:	*Initial weight of the sample*
W_s	:	*Weight of the sample*
W_t	:	*Weight at a given temperature*
X_c	:	*Crystallinity%*
Y_{cem}	:	*Elastic modulus of cement*
Y_{comp}	:	*Elastic modulus of composite*
Y_{mat}	:	*Elastic modulus of matrix*
Y_{pp}	:	*Elastic modulus of polypropylene*
^oC	:	*Temperature in Celsius*

Greek symbols

α	:	*Fractional weight loss*
α_{max}	:	*Degredation quantity at maximum degradation rate*
β	:	*Geometrical constant*
γ_{se}	:	*Specific elastic strain energy*
δ_n	:	*Logarithmic decrement*
ε	:	*True strain*
ν	:	*Poisson's ratio*
η	:	*Damping loss factor (tan δ)*
η_0	:	*Orientation efficiency factor*
η_l	:	*Length efficiency factor*
2θ	:	*Regular spacing*
ξ	:	*Damping Ratio*
ρ_{comp}	:	*Density of composite (g/cm^3)*
σ	:	*Elastic Strength or Tensile Stress*
σ_{uts}	:	*Ultimate tensile strength of composite*
$\sigma_{0.2\%ys}$	:	*Yield strength at 0.2% offset*
ρ_c	:	*Density/ specific gravity of composite*
Φ	:	*Exponential factor*
φ	:	*Phase difference*
ψ	:	*Pre-exponential factor*
χ	:	*Stiffness ratio*
τ	:	*Shear stress*

Chapter 1

Introduction and Literature Review

1.1 Introduction

1.1.1 Definition, History and Background

Composite material is defined as a material made of at least two constituent phases, one is matrix and another is reinforcing which combined together with significant different physical and chemical properties (*Jose et al., 2012*). In polymer composite system, matrix can be classified into two broad categories, one is thermoplastic and another is thermoset. For reinforcing constituent mostly fibrous (e.g. continuous/short fibres and fabrics) and particles (micro/nanoparticles such as: calcium carbonate, saponite, ceramics/metal powder, wallostonite, flakes, talc, silica, montmorillonite and Indian bentonite nanoclay, carbon nanofubes/nanofibres etc.) are used to incorporate into matrix for fabrication of polymeric composite materials. Composites are a vast and important category of engineering materials, which have an ability to tailor deserved properties, combined with the intrinsic low density, and effectually low cost, makes these materials exceptionally attractive alternatives for a numerous applications.

Example of natural composite materials such as wood, bone and teeth are also made up of two or more constituents. For example, wood is made up of cellulose fibres as reinforcement in lignin matrix, where as bone and teeth are made up of toughened collagen matrix. Even whole human body is an example of natural biological composite with the combination of flesh and bones.

The first uses of manmade composites materials are found in the 1500 BC, when Egyptians and Mesopotamian citizens used a mixture of mud as matrix and straw as reinforcement to build strong and durable housings. Not only for housing, straw was used to provide reinforcement for composite commodities including pottery and naval application such as in boats. The Mongol citizens, in 1200 AD, invented the first composite for weapon as bows, using a combination of wood, bone, and animal glue. To enhance the strength of bows, they were pressed and wrapped up with bark of birch tree. This composite bow was the most powerful arm on earth until the invention of automatic weapons (*Ashby, 1987; Johnson, 2013*).

Norman de Bruyne extensively studied to develop fibre-reinforced composite material for commercial use in aviation industry during 1930s in the UK [202]. In 1932, a researcher at Owens-Illinois invented the process for mass production of glass fibre strands. Owens collaborated with the Corning company in 1935 and the production process was accepted by Owens Corning to produce its patented glass fibre. A suitable resin for combining the glass fibre with a polymer matrix was developed in 1936 by Du-Pont (*Johnson, 2013;* Marsh, 2006).

1.1.2 Importance and Usage of Composite Materials

Composite materials are reasonably cheaper than the metallic materials, however, sometimes incorporation of filler material into the matrix make them expensive. In this consideration, cheaper composite materials and manufacturing techniques get high interests. In spite of costliest nanomaterials, sometimes cheaper and easily available fillers are acceptable which provides desired properties of composites. Over the past two decades, the consumption of polymeric composite is radically increased in India as well as in other countries. Market research reveals that, consumption of composite materials, in India, has great potentials in various sectors such as chemical industries, wind power industries, aircraft, rail, marine application, automotive, textiles and many others. In this route, due to mass production capability and potential applications with good endurance properties, low cost, recyclability, ease of fabrication, the present research is being attempted to manipulate the injection molded composite material for various applications.

Varieties of modern composite materials are existing nowadays in both structural and nonstructural elements for day-to-day application in industrial as well as household appliances. The major advantages of polymer composite materials are as low cost, ease of fabrication, high strength and modulus, acceptable fatigue and fracture resistance values compared to their density and excellent formability make them suitable for structural application substituting the need of metallic materials (*Oprişan et al., 2010*). The major applications of the composite materials are found in aerospace, structures for military aircraft, commercial airlines, space shuttle and satellite systems similar to such structural parts. Similarly, in marine and automotive, as sports goods, in textile and chemical industries, electrical and biomedical applications, in civil constructions polymeric composite materials are getting wide recognition due to their specific advantages (*Jose et al., 2012*).

Apart from the direct application of polymer composite materials, the metallic sandwich panels are also used for structural applications. Some of the researchers investigated on the automobile leaf spring using glass fibre reinforced polymer composites as an alternative to metallic leaf spring. Over the few years, polymer is used as gear material; an alternative to metallic material. Mostly, nylon polymer is used for gear application due to its high abrasive resistant property (*Düzcükoglu, 2009; Mendi et al., 2006; Hoskins et al., 2011; Hakimian and Sulong, 2012; Kirupasankar et al., 2012; Senthilvelan and Gnanamoorthy, 2004*).

Over the decades, polypropylene (PP) is used as a matrix material for design and development of composite and its applications. However, very few works have been carried out where Portland pozzolana cement (PPC) is used as a filler material into the polymer matrix. Two patents are identified where cement material is used as filler to fabricate the composite material; Patents on: 'Oriented composite thermoplastic material with reactive filler' (*Maine and Newson, 2006*) and 'Toughened Polyethylene Terepthalate' (*Simmons and Simmons, 2008*). Further, research has been conducted on waste cement dusts as fillers incorporated with rubber compounds and it is observed that tensile strengths and modulus of the material enhanced satisfactorily (*Andrzej and Marek, 1984*). Thus, a thorough and scientific investigation is in demand on fabrication and characterizations of the composite materials in order to evaluate the properties for optimizing the materials to achieve optimal performance. However, till date, very limited works have been carried out that address the design and development of low cost polymeric composite materials suitable for industrial needs incorporating PPC as a filler material. In addition, few factors, which effectively get high interest of PPC filled thermoplastic composite materials are such as effectiveness, durability, chemical reactivity, processing difficulties and power consumption etc. Thus, in this work polypropylene as matrix material and cement as filler material is justified over other polymers and filler materials such as Nylon, Acetal, PMME, etc. and carbon nanotube/nanofibre, silicate pallets, montmorillonite nanoclay as filler respectively. Thus, it is relevant to try inexpensive materials polypropylene and cements for design and development of composite materials and finding suitable applications.

1.2 Polypropylene as a Matrix

Polypropylene is a semicrystalline polymer in nature of the combination of propylene monomer. Using the Ziegler catalyst, Giulio Natta invented polypropylene in the early 1950s (*Harper,* 1999) and it was characterized and obtained as isotactic polypropylene by

fractionation. In 1957, polypropylene was taken into account for commercial production by Italian firm Montecatini (*Pater, 2001; Morris, 2005*). Usually, the term polypropylene offers isotactic polypropylene obtained from Ziegler-Natta catalysis (*Burgt, 2002*).

The polymer structure of the isotactic polypropylene is shown below (Figure 1.1):

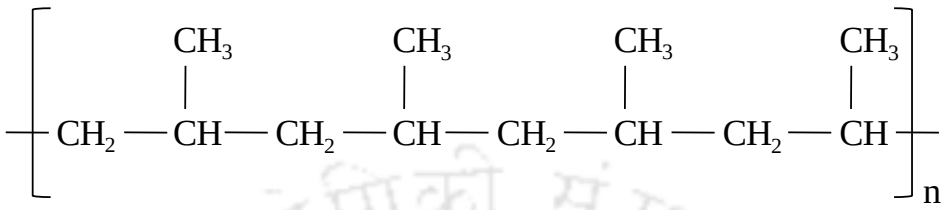

Figure 1.1 Chemical chain structure of isotactic polypropylene polymer

Polypropylene, is eventually, considered as a commodity polymer with enormous industrial as well as household applications potentials.. Major advantage of polypropylene is the recyclability of the polymer, which becomes an enormous interest for industrializations. Generally, recycled polypropylene is blended with virgin polypropylene for next stage end uses (*Harper, 1999*).

Polypropylene have found widespread applications in miscellaneous areas such as civil constructions, automotive, sports goods, household, textile and chemical industries, electrical and biomedical applications and marine constructions.

1.3 Inorganic Filler Particles

Usually, incorporation of inorganic fillers into organic polymers can result brittle nature of composite material. Addition of inorganic fillers at higher loading percentage, however, does not improve the mechanical and other properties of the material in every aspect because of inadequate dispersion of fillers throughout the matrix system. This limits the amount of fillers that can be incorporated into polymers to enhance the characteristics of the composite materials.

There are numerous inorganic particles are useful to incorporate into polymer/metal/ceramics matrices to fabricate composite materials for specific applications. For metal matrix, fillers improve high temperature creep characteristics and hardness as compared to pure metal. For ceramic matrix, fillers are incorporated to enhance its toughness and fracture properties. Similarly, for polymer matrix, inorganic fillers improve stiffness, strength, electrical and thermal properties (*García et al., 2004*).

To fabricate composite materials, there are several inorganic filler materials are available such as kaolin clay, talc, mica, phosphate Glass, Aluminum oxide (Al_2O_3), synthetic Na+ saponite clay, single-walled/multi-walled carbon nanotubes, carbon black, montmorillonite nanoclay (*Watari, et al., 1997; Cheng, et al., 2000; Gupta et al., 2010; Groner et al., 2006; Tetsuka et al., 2007; Martin et al., 2004; Kashiwagi et al., 2004; Golebiewski and Galeski, 2007; Sinha and Biswas, 1999*), wollastonite clay (*Zhuang et al., 1997; Tong, et al., 2003; Wang, et al. 2001*) and layered silicate, (*Pavlidou and Papaspyrides, 2008).*

1.4 Portland Pozzolana Cement as a Filler Material

Essentially cement material is used for construction of concrete for architectural buildings, roads, bridges, and other structures. The material has the tendency to mix up and aggregate (agglomerates) with water owing to its affinity to absorb water and become solid concrete material. It is also aggressive to acid like HCl, HNO_3, H_2SO_4 etc. Due to its small size in micron level and thus, can be used in polymers for manufacturing of the composites (*Maine and Newson, 2006; Simmons and Simmons, 2008*).

The main constituents of Portland pozzolana cement material are tricalcium silicate (Ca_3SiO_5), dicalcium silicate (Ca_2SiO_4), tricalcium aluminate ($Ca_3Al_2O_5$) and calcium aluminoferrite ($Ca_4Al_nFe_{2-n}O_7$). The formula of each of these minerals can be broken down into the basic calcium, silicon, aluminum and iron oxides (*Medvešček et al., 2006; Barron 2010*). In addition, fly ash also presents in the main ingredients of Portland cement. The density of the PPC is varied from 2.94 to 3.13 g/cc (F*elekoglu and Dulluc, 2007*).

Haecker et al., (*2003*) has shown that particle size distribution of cement observed by laser diffraction techniques are in the range of diameters between 1μm to 87.5 μm. Earlier, Bentz and Haecker, (*1999*) showed that particle size of Portland cement varies between 1 μm to 100 μm. In the present work, the particle size of PPC was measured using Inverted Metallurgical Microscope in our laboratory and it is found to be in the range of 14 μm to 118 μm. Thus, owing to the size limitation of the cement fillers, the cement particles and polypropylene matrix create the mechanical bonding due to absence of non reactive group on the surface of the cement particles.

1.4.1 Hydration of Portland cement

It is difficult to dope cement particles directly into the polymer because it could easily agglomerate rather than attaining homogeneous dispersion. It occurs due to high viscosity of

the melted polymer. In order to overcome this problem we need to process semi dispersion of the particles by hydration process. The hydration is done by adding water into the cement particles where, the process depends on the exposed time of cement particles in water. In hydration process, however, the exposed time generally kept very less such that the cement particles would make supernatant suspension with water rather than full hydration.

In the anhydrous state, four major minerals are usually present in Portland cement i.e., alite, belite, aluminate and a ferrite phase. The exothermic reaction (heat generation) occurs when water is added into Portland cement. The presence of limestone in Portland cement influences the rate and degree of cement hydration as well as the phase composition of hydrated cement paste (*Medvešček et al., 2006*). Medvešček et al., (*2006*) demonstrated that the hydration of Portland cement clinker minerals is essentially their reaction with water yielding a variable-composition complex microstructure. However, hydration of the cement for 24 h does not show any significant difference from nonhydrated sample (*Bishop et al., 2003*). This comprises amorphous or near-amorphous calcium silicate hydrated gel of nonstoichiometric composition with variable CaO/SiO_2 and H_2O/SiO_2 ratios of 1.5-2.0 and 3.0-4.0, respectively (CSH). The variables of the composition are: calcium aluminate hydrate ($3CaO \cdot Al_2O_3 \cdot 6H_2O$); ettringite, $3CaO \cdot Al_2O_3 \cdot 3CaSO_4 \cdot 32H_2O$; calcium monosulfoaluminate, $3CaO \cdot Al_2O3 \cdot CaSO_4 \cdot 12H_2O$ (monosulfate, MS), calcium hydroxide ($Ca(OH)_2$), carbonated silicate($6CaO \cdot 6SiO_2 \cdot CaCO_3 \cdot 2H_2O$), and/or aluminate hydrated phases ($3CaO \cdot Al_2O_3 \cdot CaCO_3 \cdot 11H_2O$) and calcium carbonate ($CaCO_3$) (*Makar and Chan, 2009*). It is also found that the weight loss of tricalcium silicate (Ca_3SiO_5) or alite is observed when hydration process takes place because of its decomposition through the exothermic process (*Lothenbach et al. 2008*).

1.5 Dispersion of Filler Materials into Matrix

Several researchers worked on the dispersion procedures of various nano-materials and prove to be indispensable as quality dispersion of nanomaterials into the matrix material, highly influence the properties of the composite material and hence the end product developed. Sandler et al., (*1999*) demonstrated the dispersion of CNTs into epoxy resin. The procedure they have followed which revealed that untreated catalytically-grown CNTs are first dispersed in ethanol in an ultrasonic bath at room temperature for 1 h. After mixing, the ethanol-based solution is added into the resin and the suspension is stirred for 1 h at 2000

rpm. During stirring, the temperature of the resin is kept at 80ºC using a silicone oil bath in order to maintain a low viscosity of the resin. In this case, they used thermoset matrix which remains in liquid phase at room temperature and the viscosity of epoxy is less compared to any thermoplastic polymer. A complete dispersion of the nanotubes into the polymer matrix yet to be studied in vast because nanotubes easily agglomerate due to its Intrinsic van der Waals attraction among each other.

Park et al., (*2002*) reported that CNTs can be fairly dispersed into continuous polymer system by the help of in-situ polymerization. They have used aromatic polyimides as a continuous polymer matrix and SWNTs as a dispersing material for reinforced thermoplastic nanocomposites. The procedure what they described is as a solution of dimethylformamide and 0.05 wt% SWNTs was prepared by homogenizing stirred for 10 min by a 6 mm diameter rotor at 750 rpm and sonicated for one and a half hours in an ultrasonic bath at 40 kHz. The sonicated Dimethyl Formaldehyde (DMF) and SWNTs solution was transferred into a three neck round bottom flask which is equipped with a mechanical stirrer, nitrogen gas inlet, and drying tube outlet filled with calcium sulfate. After stirring for 10 min, the diamine was added into the SWNTs solution. The SWNTs and diamine mixture continued to be stirred for 30 min before adding the dianhydride of polyamide. The entire reaction was carried out in the flask immersed in an ultrasonic bath at 40 kHz until the solution viscosity increased and stabilized.

Sennett et al., (*2003*) have reported dispersions of MWNTs in polycarbonate matrix by mixing in a conical twin-screw extruder followed by fiber-spinning apparatus.

Prashantha et al., (*2008*), reported the dispersion mechanism of MWNTs in polypropylene matrix. They demonstrated that, polypropylene/MWNTs nanocomposites produced by mixing homo polypropylene granules and 2 wt% polypropylene-g-MA with the commercial masterbatch containing 20 wt% of MWNTs in a co-rotating twin screw extruder at barrel temperature of 195–210°C, and a screw speed of 50 rpm. Similarly, Bikiaris et al., (*2008*) also demonstrated the dispersion technique of MWNTs in polypropylene matrix by melt mixing in a HaakeeBuchler Reomixer (model 600).

1.6 Compounding and Fabrication of Composites

The superiority of the composite product is heavily reliant upon the efficiency of the compounding technique for the overall properties especially, mechanical properties point of view. The melt mechanical mixing is commonly used technique for incorporation of micro as

well as nanoparticles into polymer. Employing this technique, the dispersion of the filler occurs in the molten state of the polymer. In addition, the purpose of compounding is to generate a homogeneous blend that certainly helps understanding the factors that govern and control the mixing.

Mixing: Currently, three methods are commonly used to incorporate CNTs into polymers which are called compounding techniques i.e., solution mixing, in-situ polymerization and melt compounding or melt mechanical mixing (*Zou et al., 2004*).

The term mixing refers to the operations that would have a propensity to reduce inhomogeneities or gradients in concentration, temperature, size of a dispersed phase, or other properties of materials. The objective of the mixing process is usually to achieve a standardized dispersion of the minor constituent into the major phase.

Fabrication: One of the leading techniques to fabricate the polymer composite is injection molding technique. Apart from this technique, there are numerous ways to fabricate the same composites for example, compression molding, resin transfer molding (RTM), autoclave molding, structural reaction injection molding (SRIM) etc. In injection molding process, nanomaterials doped polymer chips are fed into the machine and accordingly the melted polymers with nanomaterials are filled into the mold. For making samples, processing parameters like temperature, time, injection pressure, screw speed etc. are required to be prefixed.

1.7 Brief Overview on Polymeric Composite Materials

Eventually, mechanical properties of thermoplastic composites such as tensile and compression strength, impact strength, bending and shear strength have been enhanced using a wide range of filler materials such as nanoclay, carbon nanotubes/nanofibres (*Seung et al., 2008*), silicate pallets, ceramic powder, short fibres (*Pavlidou and Papaspyrides, 2008*) etc. Various continuous high performance unremitting fibres like carbon/graphite fibre, glass fibre, aramid and boron/ceramic fibres (*Dickson et al., 1989*) are being used to fabricate composites for high demanding industrial applications. Gas barrier, thermal and electrical properties are also being modified using special filler materials such as phosphate Glass, Aluminum oxide (Al_2O_3), synthetic Na+ saponite clay, single-walled/multi-walled carbon nanotubes, carbon black and montmorillonite nanoclay etc. (*Gupta et al., 2010; Groner et al., 2006; Tetsuka et al., 2007; Martin et al., 2004; Kashiwagi et al., 2004; Golebiewski and Galeski, 2007*).

Alongside, modified layered silicates (organoclay) are increasingly used for reinforcement of polymeric materials (*Lertwimolnun and Vergnes, 2005*). The dispersion of such minerals at the level of a few nanometers induces a significant improvement in mechanical properties, flame resistance and barrier properties, compared with the pure polymer (*Ray and Okamoto, 2003*). In addition, in the recent past, it is observed that the Portland cement can also be doped into the polymers to manufacture the composites. Maine and Newson (*2006*) took patent where they used Portland cement as a filler into the polypropylene matrix. Simmons and Simmons (*2008*) also took patent; where, they used thermoplastic PET (Polyethylene Terephthalate) as a matrix and cement particles as filler.

Thermoplastic polymers which can be reshaped by applying heat having good extensibility but the mechanical point of view, such as, tensile strength and modulus, stiffness, fracture strength, shear strength and modulus, are inferior compared to non polymeric materials. Thus, these properties can be improved using different fillers into the polymer as said earlier. Polypropylene is extensively used in many fields such as housing industries, automobiles, electricity and electronics industries and many more fields because of its low density, less toxicity, excellent electrical resistance, and ease of processing and molding. However, pure polypropylene is highly inflammable at room temperature and leaves almost no carbon residue, the presence of which enhances fire protection. Flame retardants are sometimes required to be added during compounding to improve the antiflame properties of polypropylene.

It is also observed that mechanical, electrical, thermal and magnetic properties of the composite mostly depend on the filler materials and the way of dispersion throughout the polymer. Therefore, dispersion of the filler materials and its subsequent effect on the composite materials serves the purpose to characterize the polymer composites. Nowadays researchers are using maleic anhydride-grafted polypropylene to obtain proper bonding between matrix and filler materials and homogeneous dispersion of fillers into the polymer matrix, because of the non-polar nature of polypropylene (*Raka et al., 2009; Gutiérrez et al., 2010; Fung et al., 2003*).

1.8 Characterizations and Structural Analysis of Composites

Evaluations of various characteristics of the polymeric composite materials are indispensible before application. The common characterization techniques such as thermogravimetric analysis (TGA), differential scanning calorimetry (DSC), X-ray diffraction analysis,

morphological analysis (SEM, FE-SEM, AFM) and many more tools are employed for polymer composite materials. However, the presence of filler materials into polymer give improved thermal, mechanical and other properties in accordance with the optimum percentage of filler materials.

For the structural applications, researchers give importance in mechanical properties, structural investigation of sandwich panels with bending deformation analysis as well as vibration analysis. In recent advancement of technology on structural analysis, researchers get more interest in investigation of effects of crack vibration for structural applications. This includes the crack identification and assessing the effect of crack on the mechanical parts.

The nanoparticles and nanocomposites can be characterized using various emerging technologies. Generally, characterizations of the materials are required to predict or to observe the intrinsic properties of the materials. Various techniques have been employed widely to characterize the nanocomposites materials. The commonly used powerful characterization tools are Scanning Electron Microscopy (SEM), Transmission Electron Microscopy (TEM), wide-angle X-ray diffraction (WAXRD), Differential Scanning Calorimetry (DSC), Fourier Transformed Infrared Spectrophotometry (FTIR), Thermo Gravimetric Analysis (TGA) etc.

The SEM provides images by which huge information of surface features associated with the sample can be obtained. TEM allows a qualitative understanding of the internal structure, spatial distribution of the various phases, and views of the defective structure through direct visualization (*Hussain and Hojjati, 2006*).

WAXRD technique gives the information about the nanocomposite structures with the help of kinetics of polymer melt intercalation. Based on this, one can conclude the percentage aggregation of the nanoparticles into the polymer (*Manchado et al., 2005; Raka et al., 2009*).

Generally, a DSC technique is used widely to characterize the polymers for checking their composition, glass transition temperatures (T_g), melting temperatures (T_m) and crystallization percentage as well as crystallization temperature (T_c) and time (*Zeng et al.,2006; Garcia et al., 2004; Jose et al.,2008*). Zeng et al., (*2006*) has shown that double melting peaks can be observed in the curves of pure lab-synthesized polyamide (PA1010) and MWNTs/PA1010 composites with MWNTs contents < 5.0 wt%.

TGA is performed on samples to determine changes in weight in relation to the change in temperature (*Zeng et al., 2006; Jose et al., 2008*). Such analysis relies on a high degree of precision in three measurements i.e., weight, temperature, and temperature change. It is commonly employed in research and testing to determine characteristics of polymeric

materials such as degradation temperatures, absorbed moisture content of materials, the level of inorganic and organic components in materials, decomposition points of explosives, and solvent residues etc.

FTIR is used to record the infrared spectrum of a chemical substance or mixture of nanocomposite materials. This spectrometer gives data for all wavelengths simultaneously.

Choi et al., (*2006*) reported the observation on Multi-walled carbon nanotubes (MWNTs)/polysulfone (PSf) blend membranes. They concluded based on FTIR spectrum, the modified MWNTs show –COOH and –OH functional groups. The peak at 1715 and 3435 cm^{-1} are in correspondence to CO and –OH stretching, respectively, indicating the existence of carboxyl groups in the modified CNTs.

Chen et al., (2006) have obtained similar observations on Nylon 6 nanocomposites after extensive characterization. They discussed about the formation of MWNTs–NH_2 and was confirmed through the FT-IR analysis. A fine dispersion of MWNTs throughout nylon 6 matrix was observed by SEM and TEM.

Valentini et al., (*2003*) reported on the characterization of SWNTs/polypropylene nanocomposites. They observed that the polymer is intercalated between nanotubes into bundles at the low frequency Raman bands when the concentration of nanotubes is low. However, when the nanotube concentration is high, nanotubes do not allow for intercalation of a high quantity of polymer in between the nanotubes bundles.

Marosfoi et al., (*2006*) carried out thermogravimetric analysis (TGA) and varied temperature Raman spectroscopic measurements on the polypropylene/carbon nanotube composites. They reported that the incorporation of carbon nanotubes into polymer matrix increased the thermal stability compared to the virgin polypropylene. In addition, the TGA and Raman Spectroscopy also provide further information about the thermal decomposition of the composites.

Dong et al., (*2008*) also reported on polypropylene/organoclay nanocomposites after conducting experiments such as, the X-ray diffraction (XRD), SEM, TEM and dynamic mechanical analysis (DMA). The prevalence of intercalation with a certain level of localized exfoliation is observed by XRD, homogeneous dispersion is observed in the morphologies by SEM, TEM analysis. While quantitative verification by XRD and SEM analyses demonstrate the prevalent intercalated nanocomposites structure and higher clay content could deteriorate the uniform clay dispersion as a result of large tactoids. DMA analysis shows that the dynamic elastic modulus drastically decreases with the increase of temperature.

Similar characterization techniques have been employed for characterizing the different nanocomposites by several researchers. Where, different characterization techniques such as, the UV/visible spectroscopy, Contact Angle Goniometer, XRD, Rheometer, DSC, Fourier Transform Infrared (FTIR) spectroscopy, SEM, Atomic Force Microscope (AFM), TGA, TEM, DMA etc. techniques revealed the intrinsic properties of the nanocomposites.

1.9 Mechanical Properties of Composites

An extensive research works have been done to evaluate the mechanical properties of the composite materials as it is essential for engineering materials. In this context, fabricated composite materials underwent various mechanical testing to evaluate its approximate behavior during its application. In this context, 3-point bending, short term fatigue of loading-unloading, effect of circular notches over mechanical properties of the composites and dynamic mechanical analysis (DMA) are performed (*Daniels et al., 1971; Christiansen et. al., 1972; Sugimoto*[I-II] *et. al., 2007; Clorius et. al., 2000; Prabhakaran, 1979*). The structural behaviors, analysis and various properties of the composite materials are discussed in the following sections. To verify influence of MWCNTs in polypropylene matrix as a reinforcement factor and are investigated using Halpin-tsai, and modified rule-of-mixing theory. Several researchers have shown that the reinforcement factor depends on the physical and mechanical properties of the filler materials (*Li and Cho, 2003; Landro and Lorenzi, 2009*).

Luo and Daniel (*2003*) have shown higher composite modulus is achievable for randomly oriented filler composite by controlling and maintaining the dispersion rate. Maleic anhydride-grafted polypropylene (non-polar nature) is mostly used for attaining homogeneous dispersion of filler into the polypropylene matrix and to ensure proper bonding between polypropylene matrix and filler materials (*Raka et. al., 2009; Gutiérrez et. al., 2010; Fung et. al., 2003*). Mechanical characteristics and performance mostly depend on the microstructure and the strength of the bond between the filler to filler directly or filler to filler via matrix (*Chabert et. al., 2003*). Dynamic mechanical analysis (DMA) becomes essential to determine the viscoelastic as well as thermal characteristics of polymeric materials. In general, DMA test performed over a wide range of temperature helps to understand the viscoelastic behavior of composite materials. Significant works on dynamic mechanical analysis (DMA) have been carried out on particulate polymer composites to explore the effect of addition of filler percentages and for measuring heat deflection (*Bao and Tjon, 2008,*

Chabert et al., 2003) and glass transition temperature to figure out the behavior of filler-matrix interface etc. (*Jin et al., 2001; Sohn et al., 2003; Kanny et al., 2008*). Kanny et al., (*2008*) studied the dynamic mechanical properties of clay–polypropylene nanocomposites. They have observed that, at 20ºC the storage modulus of polypropylene increases when percentage incorporation of nanoclay shoots up to 3%. Sohn et al., (*2003*) have also shown the dynamic elastic modulus increases with the loading percentage of filler materials.

Jin et al., (*2001*) have extensively studied on the dynamic mechanical behavior of MWNTs/PMMA (Polymethyl Methacrylate) composites at different temperatures. They observed that the increment of loading percentage of MWNTs in PMMA composites, the storage modulus is increased particularly at higher temperatures and loss factor of the composite shows some broadening. Similarly, Allaoui et al., (*2002*) have demonstrated on the MWNT/epoxy composite that the Young's modulus and the yield strength have been doubled and quadrupled (4^{th} time) for composites with respectively 1 and 4 wt% nanotubes, compared to the pure resin matrix samples. Goh et al., (*2003*) have extensively studied on the dynamic mechanical properties of multi-walled carbon nanotube/phenoxy resin composite. They found that if dispersion of MWNTs are maintained upto 14% in phenoxy resin, the storage modulus can be reached more than 600 MPa. Tang et al., (*2003*) have examined the mechanical properties of MWNT/HDPE nanocomposites thin plate. They employed small punch test technique. In this technique a small disk of the material is prepared and is clamped over a circular guide hole between two rigid dies. The specimen is then subjected to a lateral indenter driven at a constant displacement rate through the guide hole as the indenter force and displacement are recorded. They concluded that the loading configuration involves lateral bending and large, biaxial deformation, although the experimental results do not directly yield the usual mechanical properties such as yield stress, elastic modulus, etc. Furthermore, the small punch test results show that the stiffness, the yield strength, and the fracture toughness of MWNT/HDPE composite films all increase with the increasing percentage of MWNTs. Zou et al., (*2004*) have reported examining the mechanical properties on the MWNT/HDPE composites with MWNT content of 1.0%, the elongation–content curve shows a transition, the tensile strength and modulus of the composites versus MWNTs content shows a similar tendency to that of the impact strength. They also claimed that the flexural properties of HPSM (HDPE/PEG/SiO2/MWNTs), unlikely the tension and impact results, the flexural strength and the corresponding modulus increased with the MWNTs content.

Manchado et al., (*2005*) reported that the percentage SWNTs and Carbon Black (CB) increases in the polypropylene polymer, the Young's modulus and max. strength gradually increases upto a certain limit. The tensile modulus goes from 0.85 GPa for pure polypropylene to 1.19 GPa at the loading of 0.75 wt% SWNTs in nanocomposites. However, further increase in the loading percentage of SWNTs allowing the tensile modulus as well as ultimate strength remarkably decreased. They also observed that the storage modulus of the composite gradually increases with increase of the loading percentages of SWNTs.

Similar observations have been made by Zeng et al., (*2006*) that increasing the MWNTs content from 1.0–30.0 wt% into $Nylon_{1010}$ increases the corresponding Young's modulus from 27.4% (1301 MPa) to 87.3% (1912 MPa), respectively but the elongation at break drastically changes with increasing the % of MWNTs. And for DMA test they reported that the storage modulus of the materials increases significantly upon addition of MWNTs. The composite with 1.0 wt% MWNTs displays 105% increment of storage modulus over pristine $Nylon_{1010}$ polymer. Zhang et al., (*2006*) investigated the mechanical and dynamic mechanical analysis on the SWNTs/HDPE nanocomposites. They observed that the addition of 0.5 wt% SWNTs leads to the increase of tensile strength and initial modulus by approx. 30% and 20%, respectively. And the loading level of 2.6 wt% causes the increment of 65% and 50%, respectively. Hence, they concluded that the high increases of the mechanical properties in the said composites are attributed to the homogeneous dispersion of SWNTs in HDPE. To the mechanical properties point of view, it is shown that the enhancement of tensile properties of different polymer composites can be done by the incorporation of MWNTs as well as SWNTs. Xiao et al., (*2007*) reported that CNT based low density polyethylene (LDPE) composite yields higher stress with higher % of CNT, at the same time they reported that 1-5% of CNT gives the fair strain % and at the same time, modulus is improved with higher % of CNTs.

Bao and Tjong (*2008*) prepared the polypropylene nanocomposites which filled with 0.1, 0.3, 0.5 and 1.0 wt% MWNTs. They tested the nanocomposite samples at various strain rates up to post-yielding using strain gage extensometer to measure the axial strain of the specimens in low strain region (≤0.02). The cross-head speeds were kept in the range of 0.05–500mm/min. They observed that the additions of very small amounts of MWNTs to polypropylene improve its yield strength, Young's modulus and stiffness significantly. The stiffness of polypropylene increases dramatically by 31% by adding 0.3–0.5 wt% MWNTs. In dynamic mechanical analysis, the effect of MWNTs of only 0.3–0.5 wt% is observed that the storage modulus shoots up from 1.88 to 2.5 GPa i.e. 33% more over pure polypropylene.

Along with, at different temperature and different strain rate, tensile behaviors of nanocomposites were discussed in this work. Prashantha et al., (*2008*) also have shown similar results on MWNTs/polypropylene composites. Similar explanations have been given by many researchers that CNTs can directly influence the reinforcement of any kind of polymer composites. Thus, past literatures established the fact that the mechanical properties and dynamical properties of polymer composites can be enhanced by incorporation of CNTs for any certain of percentage.

1.10 Fatigue Behavior of Polymeric Composite Materials

Zhou et al., (*2005*) investigated the thermal, mechanical and fatigue behavior of talc/polypropylene and polypropylene/clay nanocomposites. They explained that the nanophased polypropylene exhibited the highest fatigue performance, and fatigue strength coefficient, σ_f, of nanophased polypropylene is 13.3% higher than the neat polypropylene and 50% higher than that of talc-filled polypropylene. Along with, they revealed that the 40 wt% talc particles increase the modulus, but decrease the yield strength. However, 5 wt% nanoclay can improve both the modulus and yield strength by 90% and 5%, respectively.

Kultural and Eryurek (*2007*) reported that all the polypropylene composites samples (40, 20 and 0% $CaCO_3$) show an infinite life (>10^7 log cycles) below a certain stress ratio such that the curve becomes parallel to x-axis and conforms to an endurance limit.

According to the experimental results, it has been concluded that fatigue strength of pure polypropylene is better than the filled ones, and increasing $CaCO_3$ content causes a reduction in fatigue strength. With these results, they observed that during cyclic loading of composites the temperatures increases, while polypropylene with 40% filler is more susceptible to hysteretic heating than polypropylene with 20% filler and pure polypropylene.

Ramkumar and Gnanamoorthy, (*2008*) analyzed the axial fatigue behavior of $Nylon_6$ and hectorite clay/ $Nylon_6$ composites at room temperature. It is observed that less modulus drop and temperature rise are associated with the polyamide-6 nanocomposites although both the pristine and nanocomposite samples survived for 10^5 cycles at low applied stress levels. At high stress levels, polyamide-6 samples exhibited a rapid drop in modulus, unstable rise in temperature, localized neck formation, and thermal softening which were not observed in nanocomposite samples.

Charles et al., (*2010*) explained after extensive experimentation on Nylon/ silicate hectorite clay reinforced nanocomposite for fatigue analysis. The nanocomposite samples which are

tested at low stress levels (40 and 43 MPa, corresponding to loads 150 and 175N, respectively) and at low rolling speed of 1000 rpm, have sustained 2 million working cycles. The nanocomposites exhibited a less contact fatigue life at high rolling speeds even at low stress level. At high contact stress, corresponding to the load of 225N at 2000 rpm, the sample sustained for only about 0.17 million cycles which is low compared with the life of samples tested at low stress and rolling speed. The polymer nanocomposites (PNCs) samples exhibited a large fatigue life reduction with increasing contact stresses at various rolling speeds.

Manjunatha et al., (*2010*) reported on tensile fatigue behavior of silica nanoparticle-modified glass fibre reinforced epoxy composite. They observed that the addition of silica nanoparticles enhances the fatigue life of the composite by about three to four times over the entire range of stress levels. Further, in bulk epoxy to a lesser extent, the fatigue strength coefficient (FSC) of glass fibre reinforced plastic (GFRP) composite increased, by 13% due to nanoparticle-modified epoxy matrix.

1.11 Manufacturing of Non-metallic Composite Gear

Several researchers have proposed and developed polymeric composite gears as alternatives to metallic gears (*Düzcükoglu, 2009; Mendi et al., 2006; Hoskins et al., 2011 ; Hakimian and Sulong, 2012 ; Kirupasankar et al., 2012*). Mendi et al., (*2006*) demonstrated that due to reinforcement, and residual compression stress in the tooth profile is more effectual in increase fatigue strength. Endo et al., (*2006*) developed micro-gears of carbon nanotube as a filler into Nylon polymer and investigated its workability based on its applications. Kirupasankar et al., (*2012*) shown that the enhancement in mechanical properties of Nylon 6-nanoclay composite gears results in higher torque transmission efficiency and fatigue failure compared to pristine polyamide gear. Senthilvelan and Gnanamoorthy, (*2004-2007*) and Mao, (*2007*) have also discussed the detailed fabrication of polymeric composite gears using various materials such as glass and carbon fiber reinforced Nylon 66. They studied the effect of various parameters on the performance of the composite gear such as fiber length, gear tooth fillet radius, topography, fatigue and failure, tooth deflection, friction and wear etc.

Wright and Kukureka (*2001*) fabricated composite gears of fibre-reinforced polyamide-66 thermoplastic polymer followed by Injection-molding process. They worked mostly on the performance of the composite gear and detailing on the wear performance. However, they did not address influence of filler percentages as well as filler aspect ratio on the tensile

properties. These parameters significantly influence the mechanical properties of the composite materials for gear fabrication and its performance. Alongside, there are numerous models have been developed on various gear systems to correlate the dynamic behavior of gears with different aspect such as quasi-static surface wear, wear depth, stress analysis and nonlinear contact deformation analysis using, Hertz's cylinder contact theorem (*Ivana et al., 2009 ; Sunil et al., 2010 ; Savage et al., 1986 ; Abbes et al., 2011; Ding, 2007 ; Draˇca, 2006*). Generally, maximum wear occurs at the dedendum region for both the driver and driven gears due to sliding action in the contact area (*Draˇca, 2006*). In Hertz's contact theorem, the entire applied load is assumed compressive load. Teeth deformation depends upon this load and the modulus of the gear materials.

Research has been emphasized on the polymeric composite spur gear properties using Hertzian contact theorem.

1.12 Performance Analysis of Non-metallic Composite Gear

To investigate the performance of the gears, Gauvin et al., (*1984*) investigated on the surface temperature of the Nylon gear as driver and steel gear as a driven using infrared radiometer and reported that the surface temperature is found to be 110ºC. Heat loss during running of the Acetal polymeric composite gears was investigated under variable speeds and running condition. It is observed that sudden gear failures occur at 500 rpm and at 1000 rpm for an applied torque range of 5-35 Nm on the driver gear. The temperature rise is found to be proportional to the torque limits up to 8 Nm, though higher speed may lead to rise in surface temperature farther (Mao, *2007*). For gear running at 1000 rpm, the contact and non-contact flanks surface temperature rises up to 110ºC and 90ºC respectively when the applied torque is 9 Nm. Further, at 2500 rpm with 10 Nm applied torque, the surface temperature of the Acetal composite gear rises up to 140ºC (*Hooke et al., 1993*). Similarly, Polycarbonate/Acrylonitrile butadiene styrene (PC/ABS) composite spur gear failed at 75ºC with an applied load of 20.5 N/mm and with a speed of 1500 rpm (*Yakut et al., 2009*). Glass fibre reinforced PEEK and PA66 polymer composite spur gear also underwent experimentation where the temperature shoots up from 61ºC to 74ºC for an applied torque of 4.5 Nm with a speed of 257 and 494 rpm respectively (*Dighe et al., 2014*).

Similar experiment have also been done by Melick and Dijk, (*2010*); they observed that the glass fibre reinforced Nylon gear flank temperature to be very close to 140ºC at 3000 rpm with applied torque of 10Nm with oil spray is used. The glass fibre reinforced Nylon-6

polymeric composite gear show temperature rise up to 60-70ºC with a speed of 1200 rpm subjected to 8 MPa tooth bending stress (*Senthilvelan and Gnanamoorthy, 2007*). Similar to composite materials gear, steel spur gear was also subjected to APDL (ANSYS Parametric Design Language) test to investigate its performance. It is observed that for an applied torque of 150 Nm and with a speed of 2000 rpm, the temperature of the contact surface rises to 93ºC even with proper lubrication (*Jie et al., 2013*).

1.13 Damping Characteristics of Polymeric Composites

Damping in composites involves a variety of energy dissipation mechanisms that depend on vibrational parameters such as frequency and amplitude and environmental conditions such as temperature and moisture. In fiber-reinforced polymers, the most important damping mechanisms appear to be

1. Viscoelastic behavior of matrix and/or fiber materials
2. Thermoelastic damping due to cyclic heat flow from regions of compressive stress to regions of tensile stress
3. Coulomb friction owing to slip in unbonded regions of fiber/matrix interface
4. Sometimes, yet to be understood dissipation occurs at sites of cracks or delaminations in composite. Gibson, (*1992*) has shown that the loss factor of Boron fibre/Epoxy composites depend on the fibre aspect ratio. It seems loss factor decreases with increase in aspect (*l/d*) ratio.

Gassan and Bledzki (*2000*) investigated on specific damping capacity of jute fibre reinforced polypropylene composite material for its structural performance. Kultural and Eryurek (*2007*) investigated fatigue performance of polypropylene with different percentage of calcium carbonate and confirmed that the filler loading influence not only the fatigue performance but also the damping properties. Enhanced stiffness along with good damping characteristics of thermoplastic composite material suits many anti-vibration applications. A number of researches have been performed to understand the influence of reinforcement on damping characteristics of polymeric composite materials (*Gibson, 1992, Chandra et al., 1999; Finegan et al., 2003; Adams and Maheri, 2003; Zhou et al., 2004; Auad et al., 2009; Kordani et al., 2010*).

Finegan et al., (*2003*) also reported that composites having very low fiber aspect ratios should have higher damping loss factor than those having high fiber aspect ratios. They examined the vapor grown carbon fiber-polypropylene (VGCF/polypropylene) nanocomposites and

concluded that the carbon nanofiber aspect ratios of approximately *l/d=19* yields the highest predicted damping. It is observed inversely, that storage and loss modulus increases with increase of aspect ratio. Zhou et al., (*2004*) extensively investigated and modeled on SWNT/epoxy composites for damping characteristics. They found that the damping characteristics of SWNT-based composites depend on the critical bonding stress, material deformation, and SWNT weight ratio. At the same time the choice of fillers significantly affects the maximum loss factor one can achieve where, the size and surface area that fillers possess is one of the dominant factors. Rajoria and jalili (*2005*) experimented on the damping behavior of carbon nanotube-epoxy composites. They discussed that enhancement in damping ratio is more dominant than enhancement in stiffness by incorporating carbon nanotube. Multi-walled nanotubes are observed to be a better reinforcement than single-walled nanotubes. Up to 700% increase in damping ratio is observed for multi-walled nanotube (5% by weight)-epoxy beam as compared to the plain epoxy beam.

In addition, Auad et al., (*2009*) revealed that nanocomposites containing SWNTs or MWNTs where, high damping can be achieved by taking advantage of the weak bonding and interfacial friction between individual nanotubes and the matrix. They explained that variable amounts (0.5–3 wt%) of oxidized SWNTs were dispersed by ultrasonication in precursors of an epoxy elastomer based on the reaction of diglycidylether of bisphenol A (DGEBA) and a polyoxypropylene with average molar mass of 2000, end-capped with primary amine groups. Cured elastomers exhibited a large increase of the loss modulus with increasing amounts of SWNTs. For 3 wt% SWNTs, an increase in loss modulus was about 1400% at room temperature. When temperature was increased up to 140ºC the loss modulus of the nanocomposite stayed practically constant while one of the matrix dropped to a negligible value. Further, Kordani et al., (*2010*) showed that the damping characteristics of the CNTs/Epoxy composite beam vary significantly between the specimens with and without nanotubes. The maximum damping ratio of the 0.5 wt% SWNTs -specimen is much higher than those of the 0.5 wt% MWCNT-specimens and the neat specimen.

1.14 Effects of Crack on Performance of Composite Materials

Cracks formation in structural elements have various reasons. Reasons for the formation of crack can be involved due to restricted fatigue strength, mechanical defects, or localized cracks which takes place inside the material during manufacturing processes (*Ostachowicz and* Krawczuk, *1991*).

Haisty and Springer (*1991*) developed a general finite beam element having symmetric discontinuity in the form of a double sided open crack for use in damage assessment. Ostachowicz and Krawczuk (*1991*) modeled the effect of cracks on the natural frequencies of a cantilever beam. They configured on two types of cracks; single sided and double sided. Krawczuk and Ostachowicz (*1992*) investigated on the parametric vibrations of the beam with crack configuration. The opening of crack essentially assumed to be changed with respect to time by the periodic manner. In half of the cycle was assumed open and the other half it was assumed that the crack closing sinusoidally from entirely open to the completely closed and vice versa. Sinha et al., (*2002*) investigated and proposed a simplified model for the identification and prediction of location of cracks in structural beams. Krawczuk et al., (*2000*) studied on the elastic beam by finite element method with a transverse elastic-plastic crack phenomena. Friswell and Penny (*2002*) investigated on the crack identification for structural health monitoring and its remedy. They investigated the effect of open cracks and breathing cracks on system response and natural frequencies during structural vibration.

1.15 Application of Composite Materials

Over the past three decades polymer composites are getting wide recognition in applications with a great percentage compared to other materials in military, civil, naval, aviations, aeronautical, automobile, orthopedic medical, electrical and electronic applications. In military and civil applications, mostly the fibre reinforced polymer (FRP) composites are used. Few examples of the fibre reinforced plastic (FRP) applications are such as wind turbine blades, skylight, dome, industrial roof, boats, automobile body parts and so on. Some of the researchers investigated on the automobile leaf spring using glass fibre reinforced polymer composites.

The major applications of the composite materials are in aerospace, structures for military aircraft, commercial airlines, in space shuttle and satellite systems similar to such structural parts. Similarly, in marine, automotive, as sports goods, in textile and chemical industries, electrical and biomedical applications, civil constructions made of polymeric composite materials are getting wide recognition due to their specific advantages (*Jose, 2012*). There are various other industrial applications of polymer composites are also observed today. Apart from the direct application of polymer composite materials, the metallic sandwich panels are also used for structural applications.

Today the modern world is moving fast with the sensible advancement in the field of technology, economics and life styles. Now-a-days, design, development and performance of composite material, which is one of the most important sectors in industrial and household applications, have driven the world enormously for accomplishment since its inception.

1.16 Motivation and Scope

Past literatures indicate that, a variety of modern composite materials are available nowadays both in structural and nonstructural elements for day-to-day life application in industrial as well as household appliances. The major advantages of polymer composite materials such as: low cost, ease of fabrication, high strength and modulus, acceptable fatigue and fracture resistance values compared to their density and excellent formability make them suitable for structural application substituting the need of metallic materials (*Oprişan, 2010*).

Over the past decades, polypropylene is used as a matrix material for design and development of composite and its applications. However, very few works have been carried out where Portland pozzolana cement (PPC) is used as a filler material into the polymer matrix. A Patent on: 'Oriented composite thermoplastic material with reactive filler' (*Maine and Newson, 2006*) is identified where cement material is used as fillers to fabricate the composite material; Another patent on, 'Toughened Polyethylene Terepthalate (PET)' where Portland cement is used into recyclable PET polymer and it is observed that 5-15wt% Portland cement particles greatly enhance the toughness, elastic modulus and improved resilience properties of the composite (*Simmons and Simmons, 2008*). For light to medium duty industrial applications, the proposed cement reinforced PP composite material is used to fabricate the spur gear due to its specific advantages over other composites and metals. For this, the research has been accentuated to fabricate the composite spur gear and its performance analysis. As the trends, i.e., metallic gears are mostly used in automobiles and other industrial applications for their advantages such as durability, availability, smooth workability and reliability on performance. Although, disadvantages such as high cost, higher wear, more weight to power consumption limits usages of metallic gears applications. To remediating these problems, metallic gears can be replaced by proposed composite gears as the latter have certain advantages such as cheaper than metals and other polymers. The cost of polypropylene is Rs. 80-100/kg and density is 0.9 g/cc which is quite lesser than other polymers such as Nylon, PEEK, PET, Acetal etc. as well as any metals which leads to less weight to power consumption for gear application. It is also inactive to chemicals such as

concentrated acids, proves durable and ease of processing and fabrication, since the melting temperature is 190ºC. Further, waste cement dusts as filler materials was incorporated into the rubber compounds results in improved tensile strength and modulus (*Andrzej and Marek, 1984*). Thus, a detailed scientific investigation is in demand on fabrication and characterizations of the composite materials in order to optimize the material properties to achieve optimal performance.

However, till date, very limited works have been carried out that address the design and development of low cost polymeric composite materials suitable for industrial needs incorporating cements as a filler material. In addition, few factors such as effectiveness, durability, chemical reactivity, processing difficulties and power consumption etc. get high interest for PPC filled thermoplastic composite materials. This motivates to explore the grey areas exist on design and development of low cost composite materials for fabrication of non-metallic parts substituting the need of metallic parts. Hence, it is relevant and justifiable to try very low cost polypropylene as matrix material and cement as filler material over other polymers such as Nylon, Acetal, PMME, etc. and carbon nanotube/nanofibre, silicate pallets, montmorillonite nanoclay as filler materials respectively.

This work primarily focuses on to fabricate a low cost, recyclable and durable cement based composite material proves to be an advanced, alternative and unique material for next generation that substitute the need of metallic materials in industrial applications. The improved mechanical and thermal properties of the composite material validate its suitability for fabrication of non-metallic spur gear for small-to-large duty device applications.

The motivations along with scope of the present work are briefly outlined as follows:

- Fabrication of a low cost, non-hazardous and recyclable thermoplastic composite for industrial applications such as polymeric composite gears, rotor and propeller blades, automotive body parts and other structural applications etc. In addition, fabricated composite materials are subjected to thermo-mechanical analysis (TMA), thermo-gravimetric analysis (TGA) and differential scanning calorimetry (DSC) test to understand the thermal stability and fire retardant properties of the fabricated thermoplastic composite materials. Further, rheological properties of the material have been evaluated to find out the correlation between viscosities of the materials with respect to temperature.

- It is essential to investigate the resulting mechanical properties of the composite material as the small amount of filler particles concentration significantly affects the properties of the composite material and its performance. Mechanical characterizations such as tensile behavior, correlation of reinforcement factor with mechanical properties, effect of circular notch size in mechanical properties, bending deformation and short-term fatigue analysis are carried out. In addition, dynamic mechanical analysis (DMA) of the composites is also carried through.

- An inexpensive, lightweight, recyclable thermoplastic composite spur gear was manufactured using proposed composite materials for light to medium duty device applications.

- Geometrical structure of the developed product depends on the parameter like loading-unloading condition and temperature fluctuation that severely influence the material performance and shorten the product life. Direct performance analysis of the fabricated composite spur gear has been carried out to evaluate its load bearing capacity. A theoretical stress model is developed that correlate experimental results and describe stress distribution along the tooth contact surface using the modified Hertz's contact theorem.

- Modification of a dynamic test-rig setup is carried out to study the dynamic performance of the gear subjected to variable loads and speeds and equipped with an online Infra-Red assisted camera to monitor the temperature emission during running condition.

- Investigation and assessment of friction and wear behavior of composite materials are necessary before finding suitable application of the product. Thus, wear characteristics of the composite material under adhesive and abrasive modes are evaluated using standard pin-on disc arrangement. These include evaluations of weight loss and wear volume after a certain period of running of gear pair and quantifying optimum wear characteristics.

- Experimentation and investigation of damping and vibration characteristics on the effect of cracks of the fabricated composite cantilever beam for vibration prone structural applications. In addition, metal skinned sandwich panel with cement filled composite as core material was fabricated and underwent experimentation to estimate

its performance for structural applications; an extended application of fabricated composite material.

1.17 Objectives and Methodology

The specific objectives of this research work are outlined below along with the specific contributions to the field of design and development of low cost composite materials suitable for industrial application. The main objectives are:

- Fabrication of Portland pozzolana cement reinforced polypropylene thermoplastic composite.
- Characterizations of the fabricated composite followed by morphological and microstructural analysis of the fabricated composite material using scanning electron microscope (SEM), field-emission SEM (FE-SEM), atomic force microscope (AFM), X-ray diffraction (XRD), Raman spectroscopy and Fourier transform infra-red (FT-IR) analysis to understand the crystallization, dispersion of PPC and possible exfoliation of the filler particles into the polymer matrix. Further, employing nanoindentation technique to investigate the localized mechanical properties of the composite.
- Thermal characterizations followed by thermo-mechanical analysis (TMA), thermo-gravimetric analysis (TGA) and differential scanning calorimetry (DSC) test to study the thermal stability and fire retardant properties. In addition, investigation on rheological properties of the fabricated composite.
- Mechanical characterizations such as tensile behavior, correlation of reinforcement factor with mechanical properties, effect of circular notch in mechanical properties, bending deformation and short-term fatigue analysis. In addition, studies on effect of filler materials into polymer matrix using Halpin-Tsai and rule-of mixing series model.
- Fabrication of spur gear alternative to metallic gear using Injection molding technique. Experimental evaluation and optimization of compositions for gear material and tooth performance analysis subjected to load and other parameters. In addition, modification of Hertz's contact theorem to correlate the experimental results

and evaluation of stress distribution along the tooth contact surface using the modified dynamic mechanical analysis (DMA) of the composite materials.

- Modification of a dynamic test rig setup to study the dynamic performance of the gear equipped with an online Infra-Red assisted camera to monitor the surface temperature during running condition.
- Investigation and assessment of friction and wear behavior of composite materials under adhesive and abrasive modes using standard pin-on disc arrangement. Further, evaluations of weight loss and wear volume after a certain period of running of gear pair and quantifying optimum wear characteristics.
- Experimentation and investigation of vibration characteristics on the effect of cracks of the fabricated composite cantilever beam. Fabrication of metal-skinned sandwich panel with cement filled composite as core material and underwent experimentation to estimate its performance for structural applications.

1.18 Organization of the Thesis

The thesis of this research work has been organized attentively in the direction of PPC reinforced polypropylene composite material, its characterizations, performance analysis and its applications. Chapter 1 furnishes a brief introduction about composite materials, their usefulness and applications in industries followed by literature review. Motivation of the present work, objectives and thesis organization are discussed.

Chapter 2 deals with the fabrication of a low cost, non-hazardous and recyclable cement reinforced polypropylene thermoplastic composite material for industrial applications and evaluation of its thermal characteristics. Fabrication of composite using cement particles as filler material of varying quantities into the polypropylene matrix using Injection molding process is discussed in this chapter. Several experiments are conducted to study the topographical features, dispersion of fillers into the matrix and thermal characteristics of the composite. Micro-structural morphology of fabricated composite is studied using Scanning Electron Microscope (SEM) and Field-emission (FE-SEM). Crystallographic analysis of the composite is conducted by X-ray diffraction (XRD) analyzer. Thermo-gravimetric analysis (TGA), thermo-mechanical analysis (TMA) and differential scanning calorimetry (DSC) tests are conducted and thermal stability and degradation of the composite with temperature are

studied. The experimental investigations, characterizations and performance of the composite material demonstrate its effectiveness for industrial applications.

In Chapter 3, the characterizations and evaluation of mechanical properties of the composite materials are presented. Mechanical properties of polypropylene and its cement filled composite materials are evaluated using Instron universal testing machine. The experiments are conducted following ASTM D638 standard. Failure of the polymeric composite materials depend on the percentage of filler materials incorporated into the matrix although most of the cases it is observed that the high percentage of filler materials decreases the ductility of the composite materials. The morphological studies of the fractured surface of the gear materials are carried out using scanning electron microscopy (SEM) and field emission SEM (FE-SEM). Halpin-Tsai principle and rule-of-mixing series model are modified and applied to develop a mathematical model that describes the elastic modulus depending on the filler loading as well as the aspect ratio. Experimentally both the models are validated and it is found that the theoretical results are in close agreement with the assumptions made to derive this model.

In Chapter 4, development and fabrication of a new type of polymeric composite material spur gear using low cost cement particles as filler into the polypropylene matrix are presented. Polypropylene granules are mixed with cement particles and an injection-molding process is used to manufacture the thermoplastic composite gear. Several experiments are conducted with different percentages of cement particles into polypropylene matrix to optimize the gear material for fabrication. In addition, dynamic mechanical analysis (DMA) of the material has been carried out to find out the change in storage modulus and loss modulus of the material and to assess the variation of damping properties with respect to temperature. Further, extensive experimental studies are carried out to evaluate the performance of the gear tooth under loading conditions. The experimental results validate the suitability of the proposed non-metallic spur gear for low cost industrial applications. Several experiments are conducted to study the composite gear failure mechanism and resulting stress distribution along the contact surface. For this, experimental data are used and Hertz's contact theorem is applied to develop a theoretical model that describes the stress distribution along the contact surface.

Chapter 5 deals with the modification and development of a gear-testing rig setup with its accessories. The fabricated composite spur gear is subjected to variable loads and speeds to evaluate its dynamic performance and heat emission due to friction. The subsequent studies

further correlate the effect of heat on the gear material and its performance. Evaluation of heat emission in dynamic condition is aided by an Infra-Red assisted camera, IR-TCM 384. In dynamic condition, the gear pair runs at a number of speeds with different loading conditions and subsequently results have been extensively studied to understand its feasibility. In this work, the composite spur gear material is tested to evaluate its friction and wear characteristics in both adhesive and abrasive wear modes. Weight loss due to wear of the gear is evaluated through direct measurement under a specific load and running condition.

Chapter 6 describes the free vibration characteristics of the fabricated composite materials. It is essential to study the damping characteristics of the composite materials suitable for structural and automotive applications. Damping characteristic of the material is evaluated using three types of cantilever beam viz. an intact, a single sided open crack and a double-sided open crack. Laser assisted vibrometer (LAV) is used and a low magnitude force is applied on the tip of the beam. Further, specimens of variable notch sizes are prepared and experiments are conducted to study and investigate the material performance. In addition, metal faced-composite core sandwich beams are fabricated and subjected to vibration and mechanical properties analyses to understand its feasibility for structural applications. Results of these experiments are prescribed and discussed in details in the chapter 6.

Finally, Chapter 7 provides a summary of the contributions of the thesis and highlights the few prospects on the future works.

Chapter 2

Fabrication and Characterizations of Composite Materials

2.1 Introduction

Fabrication and the characterizations of polymeric composite materials are essential before designing any product and finding its application. Incorporation of filler materials into polymer matrix not only gives desired reinforcement but also improves the properties like rheological, thermal, thermo-mechanical and microstructural morphology which directly influence the materials performance. The common characterization techniques such as thermo-gravimetric analysis (TGA), differential scanning calorimetry (DSC), X-ray diffraction analysis (XRD), morphological analysis (SEM, FE-SEM, AFM) and many more techniques are employed to polymer composite materials. However, the presence of filler materials into the polymer impart improved thermal, mechanical and other properties in relation with the optimal percentage of filler materials.

In this chapter, Portland pozzolana cement based polypropylene composite fabrication and characterizations using various techniques are discussed. Initially, polypropylene granules (H110MA) are processed by adding 3% grafted polypropylene (OPTIM-P-425) with 5%, 10% and 15% (wt) cement solutions separately at 120^0C and dried at room temperature for 72 hours. In this study three varying quantities of cement materials are taken to better understand the effect of filler materials on mechanical and thermal characteristics of the composite. The composite is then fabricated by injection molding technique using the modified polypropylene pallets. Several experiments are conducted to evaluate the morphological features, microstructure and thermal stability of the composites. Microscopic and morphological analysis of the composite is carried out by the scanning electron microscope (SEM) and the results are showing the adequate dispersion of the cement particles. Investigation of possible exfoliation and crystallographic analysis of cement particles into the polypropylene matrix are carried out by X-ray diffraction (XRD) test. The thermal degradation and stability of the composites due to temperature fluctuation are studied by thermo-gravimetric analysis (TGA), differential scanning calorimetry (DSC) and thermomechanical analysis (TMA) tests. Nanoindentation technique is used to investigate the localized mechanical properties of the composites. Along with this, Raman spectroscopy and

FI-IR analysis are also conducted to characterize the fabricated composite materials. The Rheological properties of the composite materials are also investigated to find out the rate of change of viscosity of the composite materials with respect to temperature.

2.2 Materials and Methods

Cement reinforced polypropylene composites have been prepared using graded polypropylene homopolymer i.e. H110MA purchased from the Reliance Industries Limited having the characteristics of melt flow index (MFI) (at 230°C / 2.16kg) is 11/10 (g/min) and heat deflection temperature (at 455 kPa) is 104ºC. Better and improved of bonding between polypropylene matrix and filler material is achieved by using grafted polypropylene (*Cai et al., 2007*). For this purpose, grafted polypropylene (OPTIM-P-425) is used. The fabrication of the polypropylene composite consists of two phases and are discussed subsequently.

2.2.1 Cement Coating on the Surface of Polypropylene Pallets

The cement solution is prepared using distilled water with water to cement proportion of 3:1. The solution is then stirred up for 45 minutes in an ultrasonic chamber and then piled up with the polypropylene granules in a steel bowl for 30 minutes. Cement-water supernatant suspension and the polypropylene granules are then stirred mechanically at 100ºC until the cement particles are fully coated on the surface of the granules. The processed materials are then dried at room temperature for 72 hours in order to remove the entrapped moisture from the materials. The topography of the Portland pozzolana cement is studied using LEO 1430 VP scanning electron microscope (SEM) supplied by LEO Electron Microscopy Inc. The topography of the cement, the corresponding energy dispersive X-Ray (EDX) graph of the topography and cement coated polypropylene granules are illustrated in the Figure 2.1(a)-(c) respectively. As shown in the Figure 2.1(b), the EDX graph of the cement topography, it is observed that the main constituents of the cement are Calcium (Ca), Iron (Fe), Silicon (Si), Aluminum (Al) and Oxygen (O).

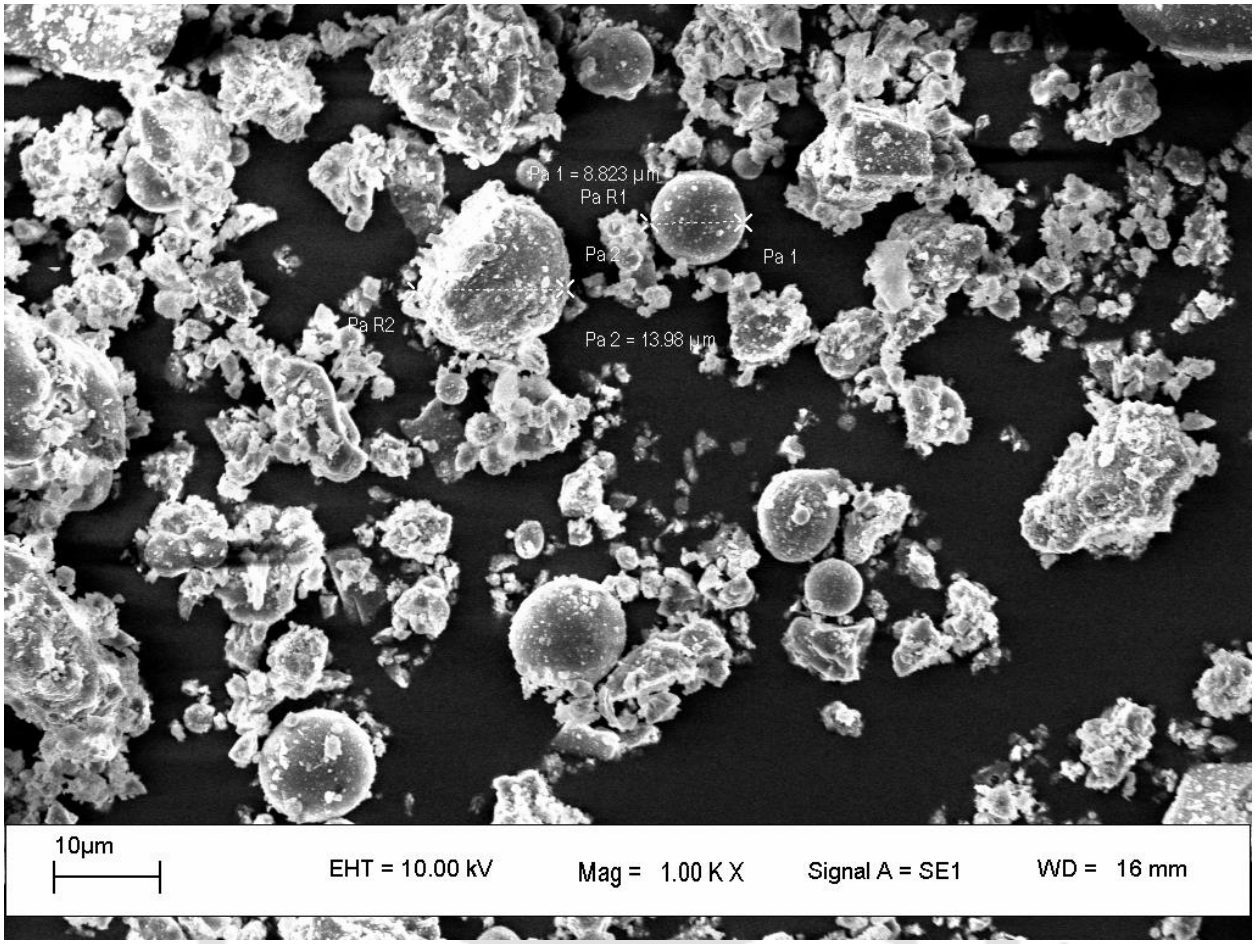
Pa 1 = 8.823 µm
Pa R1
Pa 2
Pa 1
Pa R2
Pa 2 = 13.98 µm
10µm
EHT = 10.00 kV
Mag = 1.00 K X
Signal A = SE1
WD = 16 mm

(a)

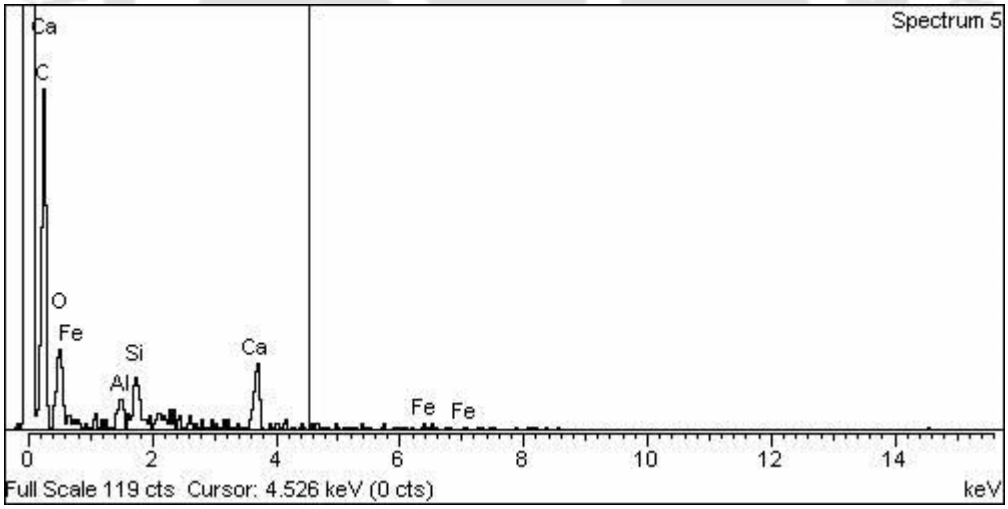
Spectrum 5
Ca
C
O
Fe
Si
Al
Ca
Fe
Fe
0
2
4
6
8
10
12
14
Full Scale 119 cts Cursor: 4.526 keV (0 cts)
keV

(b)

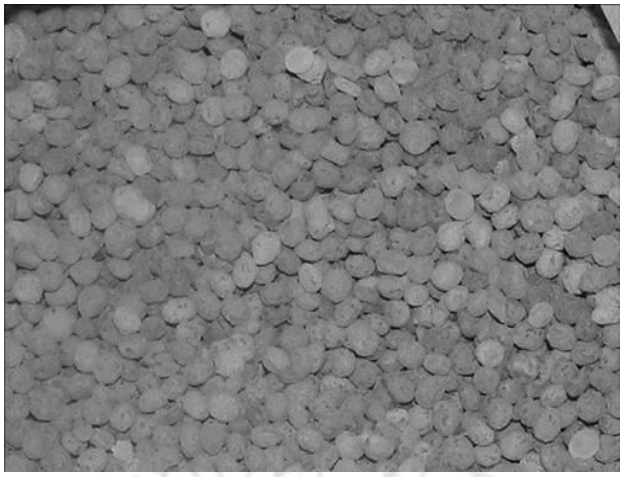

(c)

Figure 2.1 (a) SEM topography of Portland pozzolana cement, (b) corresponding EDX graph of the Portland pozzolana cement and (c) cement coated polypropylene pallets

2.2.2 Injection Molding

The dry up cement coated polypropylene granules are then used for injection molding process. The schematic configuration of the molding setup is shown in the Figure 2.2, while Figure 2.3 shows the original setup of injection molding machine (JTS 40, TEXAIR- Plastics & Hydraulics, Coimbatore, India). The processing parameter i.e. temperatures are kept constant for the three consecutive heaters i.e. at 220ºC, 225ºC and 230ºC from entrance to the sprue accordingly, while the sprue (nozzle) temperature is maintained at 50ºC. Injection shot capacity of the machine is 100 g/s. Other injection parameters are adjusted as: Injection pressure: 6 MPa, injection time: 8s, cooling time: 12s and mold temperature: 28ºC. The step-by-step flow chart for fabrication of the cement reinforced composite gear is shown in the Figure 2.4.

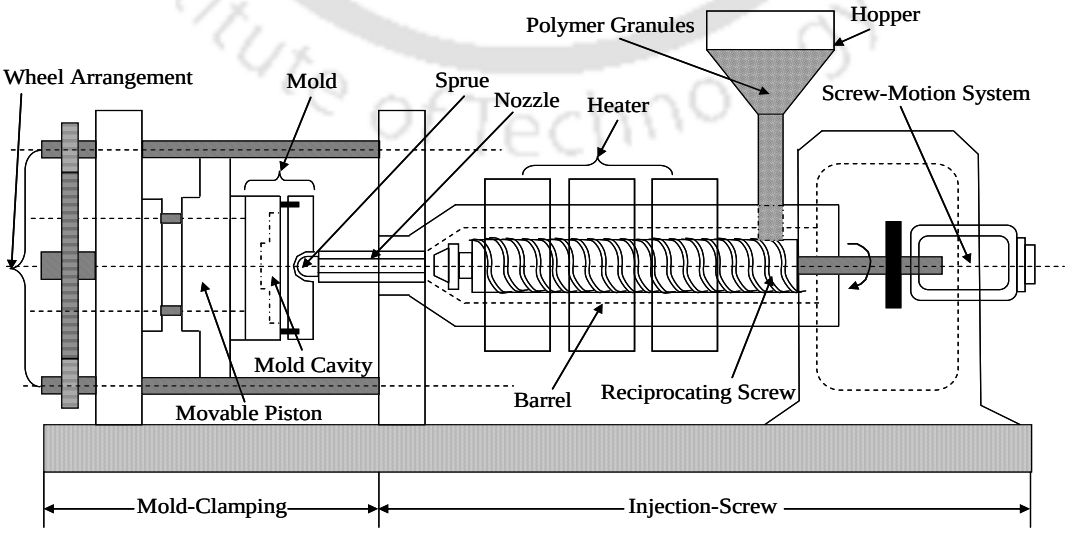

Figure 2.2 Schematic diagram of Injection molding setup

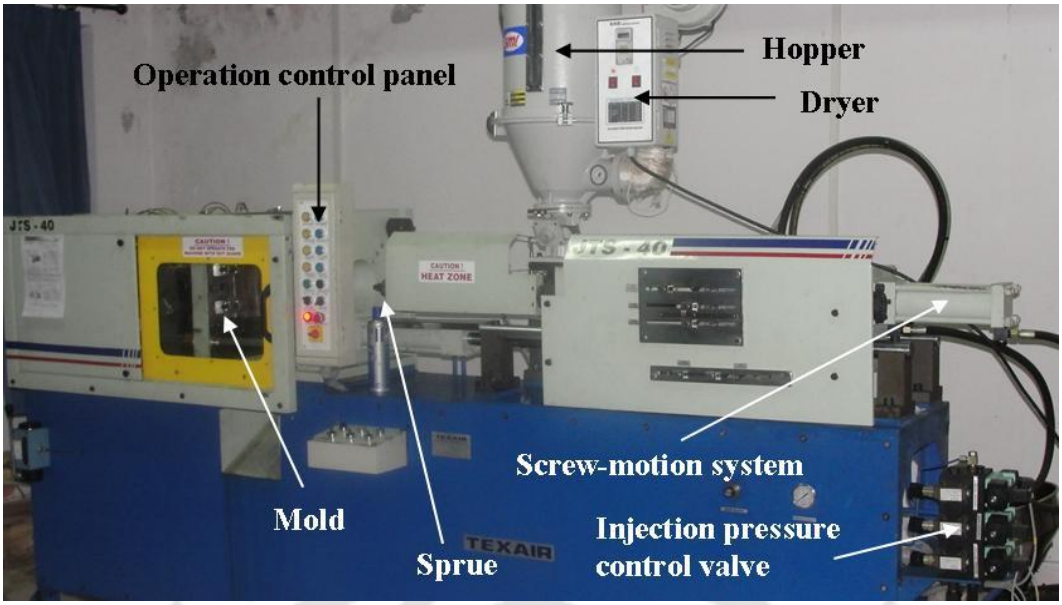

Figure 2.3 Injection molding setup

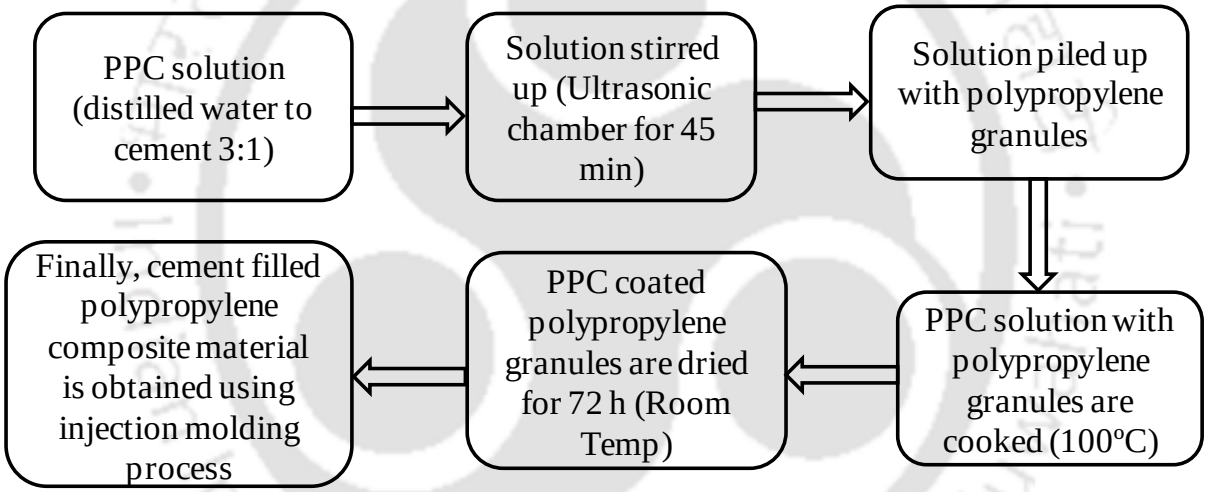

Figure 2.4 Flow chart for cement filled polypropylene composite gear fabrication

Figure 2.5 shows two samples of the fabricated composite. Table 2.1 enlists all the parameters and physical properties of the dog bone shaped composite samples with varying percentage of cement materials.

Figure 2.5 Cement filled polypropylene composite sample

Table 2.1 Physical property of the composite samples (tensile sample)

Filler content	Sample weight (g)	Filler weight (g)	Density (g/cc)
0%	7.21	0	0.91
5%	7.42	0.371	0.94
10%	8.33	0.833	0.98
15%	9.14	1.371	1.01

2.3 X-ray Diffraction Analysis of the Composite Materials

X-ray diffraction (XRD) analysis is carried out using Bruker D8 Advanced X-ray diffraction measurement system (Bruker corporation-Germany), equipped with Beryllium Detector. The setup employs X-ray of wavelength 1.54 Å, supplied at 40kV and 40mA. The data are stored at a scan rate of 0.3º/min while the range of cycles are kept at 2θ = 5º-60º for all the samples. Figure 2.6 shows the XRD pattern of the Portland pozzolana cement-fly ash based material. It is observed that the major peaks are appeared to be in the range of 2θ = 26º-42º. The first major peak at 2θ = 26.55º confirms the presence of C_3S (Tricalcium silicate) - Alite or other silicate compound and the corresponding regular spacing of the crystal plane is 0.34 nm; calculated using the Bragg's Law of diffraction principle as given below eqn. (2.1):

$$n\lambda = 2d\sin\theta \tag{2.1}$$

where, n is an integer number, λ is the wavelength of incident X-ray wave, d is the spacing between the planes in the atomic lattice, and θ is the angle between the incident X-ray and the scattering planes. Further, the major peaks at 2θ = 29.4º, 32.1º, 32.55º, 38.85º, 34.3º, 39.25º, 41.2º are associated with the crystal planes of regular spacing as 0.30, 0.28, 0.27, 0.23, 0.26, 0.23, 0.22 nm respectively are observed. All the major peaks confirm the presence of C_3S (Tricalcium silicate) – Alite and C_2S (Dicalcium silicate) – Belite. Additional small peaks validate the presence of C_4AF (Tetracalcium aluminoferrite)-Ferrite, C_3A - Tricalcium Aluminate, CaO - free Lime, MgO – Periclase along with the other major compounds such as Alite and Belite (*Katsioti et al., 2009*).

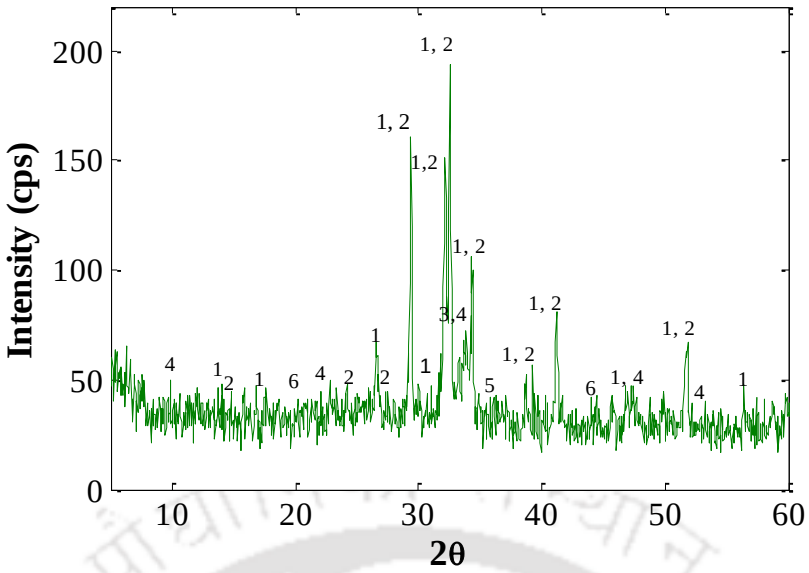

Figure 2.6 XRD patterns of Portland cement (1-C_3S, 2-C_2S, 3-C_3A, 4-C_4AF, 5-CaO_f-Free lime, 6-MgO)

In general, absence of major peaks of the filler material indicates the possible exfoliation of the filler into the polymer matrix system (*Raka et al., 2009*). Figure 2.7(a) shows the X-ray diffraction patterns of the composites of varying percentage (5%, 10% and 15%) of cement. Since, major peaks of cement particles are absent in the diffraction patterns of composite materials which reveal the possible exfoliation of cement particles in the polypropylene matrix takes place. This observation is justified due to the effect of strong interface between polar groups of polypropylene-g-MAH molecule and the cement particles. It is anticipated that the typical α-form (monoclinic) polypropylene crystal exists during the formation of composite. The major peaks at 2θ = 16.9º and 2θ = 21.15º with corresponding spacings of the crystal planes (040) and (111) are 0.524 nm and 0.42 nm respectively, confirms the complete absence of the β-crystal (hexagonal) form of polypropylene into the composite (*Zhang et al., 2007*). Thus, the X-ray diffraction patterns are highlighting the fact that the addition of cement particles of varying quantities does not affect the crystallographic nature of polypropylene. In addition, pure polypropylene and the composites show the monoclinic crystalline (α) structure with planes of reflections at (110), (040), (130), (111) and (041) (*Bhattacharyya et al., 2003*) while the corresponding crystal spacings are of 0.63, 0.52, 0.48, 0.42, 0.41 nm as indicated in the Figure 2.7(a) and (b) respectively.

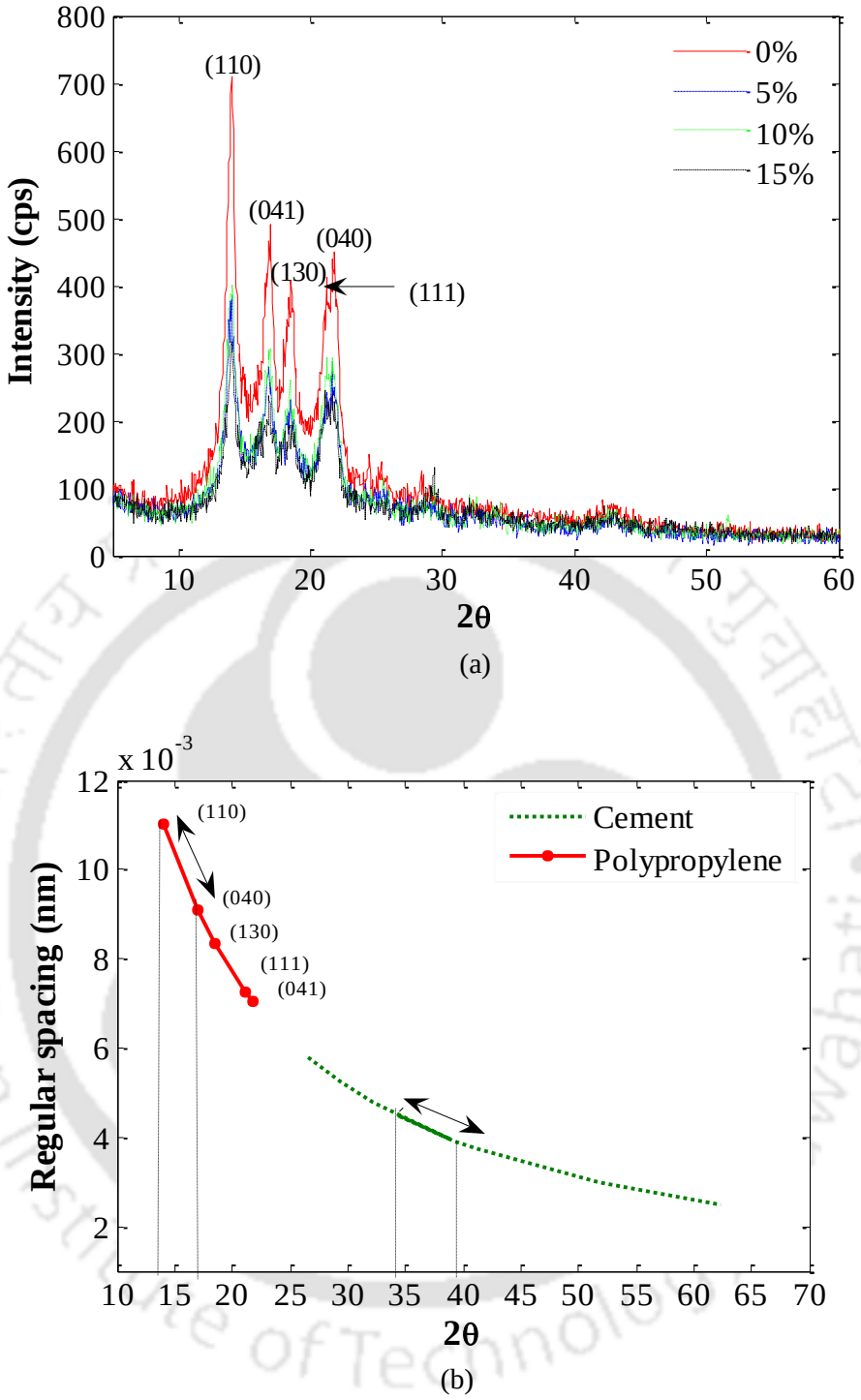

Figure 2.7 (a) XRD patterns of polypropylene and Portland cement filled composites and (b) regular spacing of crystallographic planes

2.4 Investigation on Effect of Temperature on Composite Materials

2.4.1 Thermogravimetric Analysis (TGA)

Thermal stability is also an important property of thermoplastic polymer composite requires to be investigated before various applications in an environment prone to temperature

fluctuation. thermo-gravimetric analysis (TGA) and differential scanning calorimetry (DSC) analysis, thus, carried out to investigate the thermal behaviors of polypropylene and its cement filled composite. TGA is carried out on a Mettler Toledo TGA/SDTA 851e/LF/1100, Switzerland, instrument in Nitrogen gaseous environment. The composite samples are converted into powder form of an amount of 12-35 mg to provide a suitable sample for the test. While DSC analysis is carried out on NETZSCH instrument, model no. STA 449 F3, Jupiter®, (Germany), instrument in Argon gaseous environment. Both the cases, the heating rate is kept at 10ºC/min. and temperature is maintained at 25ºC to 600ºC. Figure 2.8(a) and 2.8(b) show the TGA and differential thermo-gravimetric (DTG) patterns of polypropylene and the composite respectively. Figure 2.8(a) shows the weight loss of pure polypropylene starts at a temperature of 271ºC and continue till to full degradation is completed. For 5%, 10% and 15% cement reinforced composites, it is observed that the starting and peak point of thermal degradation is observed to be around 312-490ºC, 360-492ºC, and 376-488ºC respectively. The initial shift of decomposition temperature is observed to be 41ºC, 89ºC and 105ºC for 5%, 10% and 15% cement reinforced composites respectively with respect to pure polypropylene, indicate better thermal stability of the composite due to the presence of cement particles.

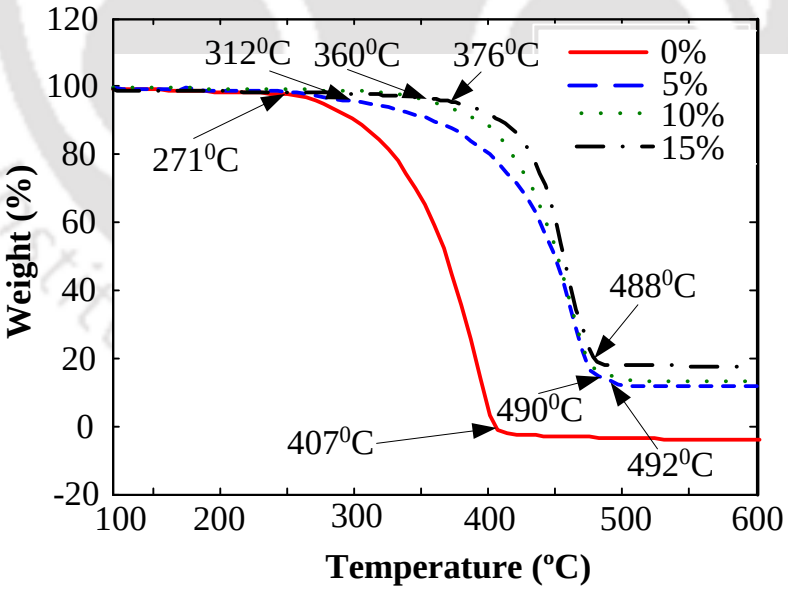

(a)

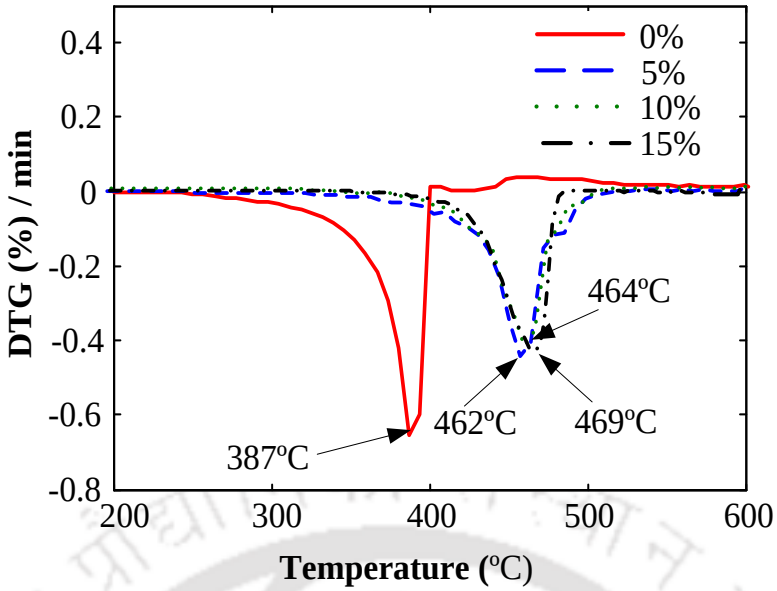

(b)

Figure 2.8 (a) TGA patterns of polypropylene and composites and (b) DTG patterns of polypropylene and composites

It is further observed that the thermal degradation of 5% cement reinforced composite starts much earlier although the stability and sustainability of the composite much longer as compared to other cement reinforced composites and pure polypropylene. For 15% cement reinforced composite, it is observed that thermal degradation starts lately at 376ºC indicates better sustainability at high temperature. Thus, with the percentage increase of cement materials to the composite, dramatic shift of thermal degradation is observed. Figure 2.8(b) shows the degradation rate of all composite samples. The maximum degradation rate of pure polypropylene is observed to be at 387ºC, while 462ºC, 464ºC and 469ºC for 5%, 10% and 15% cement reinforced composites respectively.

The degradation starting temperature (T_{ds}), maximum degradation temperature (T_{dmx}), temperature corresponding to weight loss (T_{wl}) and the differential thermo-gravimetric peak temperature (dW/dT) (T_{dtg}) are obtained from the DTG curve (Figure 2.8(b)) and summarized in the Table 2.2. As given in the Table 2.2, for example, 6% weight loss of 10% cement filled polypropylene composite material takes place when the temperature is 372ºC. Similarly, the weight loss (%) of the material can be calculated at a particular temperature.

Table 2.2 Characteristic thermal decomposition temperatures of polypropylene and cement reinforced composites

Filler content	T_{ds} (°C)	T_{dmx} (°C)	T_{dtg} (°C)	T_{wl} (°C) at weight loss (%)				
				2%	4%	6%	8%	10%
0%	271	407	387	231	268	282	295	302
5%	312	490	462	262	292	321	343	364
10%	360	492	464	287	359	372	391	403
15%	376	488	469	290	365	387	401	410

2.4.2 Differential Scanning Calorimetry (DSC)

The DSC patterns of polypropylene and the composite are shown in Figure 2.9. It is anticipated that addition of cement particles in polypropylene decreases the enthalpy of fusion, which attribute to the non-ignition property of the composite.

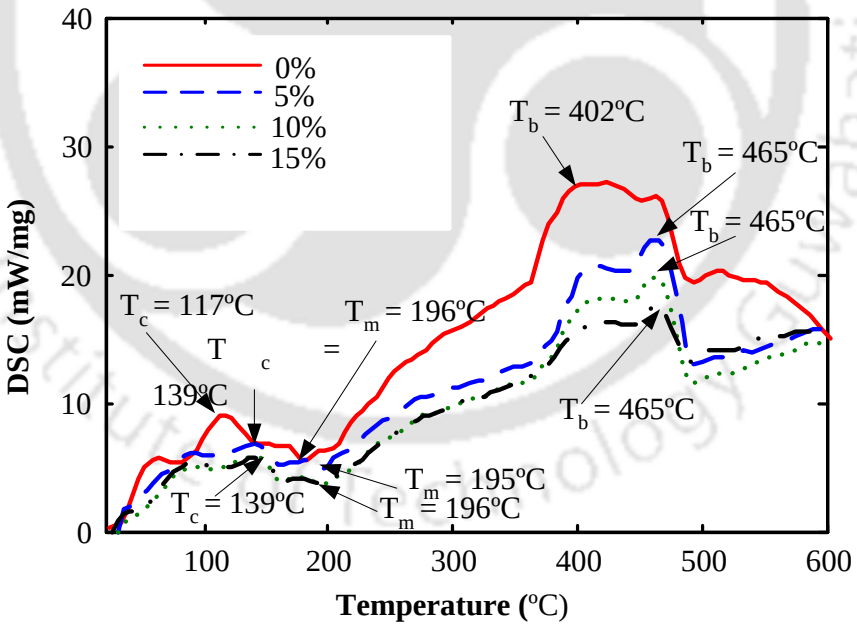

Figure 2.9 DSC patterns of polypropylene and cement reinforced polypropylene composites

The melting points of composites demonstrate the possible degree of crystallization of the composites (*Kanagaraj et al., 2007*). The crystallization onset temperature (T_c) rises about 22°C (from 117°C for the pure polypropylene to 139°C for composite). The evaporation temperature (T_b) of the samples are 402°C, 465°C, 465°C and 465°C for pure polypropylene,

5%, 10% and 15% cement reinforced composites respectively. It is also observed that the melting points of the composite samples are significantly affected by the presence of cement particles. Even though, the melting points of the composites are higher compared to pure polypropylene, although the normalized enthalpy of fusion decreases for each composite. The degree of crystallinity of the composites are calculated from the DSC analysis taking into account the heat of fusion 209 J/g for 100% crystalline polypropylene (*Garcia et al., 2004; Jose et al., 2008*) and the results are summarized in the Table 2.3.

Table 2.3 Results obtained from continuous DSC analysis for fabricated composite materials

Filler content	**Melting temperature (T_m) [ºC]**	**Crystallinity temperature(T_c) [ºC]**	**Evaporation temperature(T_b) [º C]**	**Enthalpy of fusion (ΔH_m) [J/g]**	**Crystallinity (X_c) [%]**
0%	178	117	402	96.92	46
5%	195	139	465	71.28	36
10%	196	141	465	78.60	42
15%	196	141	465	78.56	44

The degree of crystallinity can be expressed as eqn. (2.1) (*Jose et al., 2008*):

$$X_c = \frac{\Delta H_m}{\Delta H_c} \times 100\% \qquad (2.1)$$

Where, X_c is the degree of crystallinity, ΔH_m is the enthalpy of fusion of the sample and ΔH_c is the normalized enthalpy of fusion of 100% crystalline polymer (*Jose et al., 2008*). For composite samples, the degree of crystallinity is given as (*Fortunati et al., 2010*):

$$X_c = \frac{\Delta H_m}{\frac{\left(100 - W_f\right) \times \Delta H_c}{100}} \times 100\% \qquad (2.2)$$

where, W_f is the weight percentage of filler material. It is observed that the enthalpy of fusion decreases as percentage of cement increases and the degree of crystallinity changes significantly.

2.4.3 Evaluation of Activation Energy (E_a) of Composites

The activation energy of thermal decomposition of the composites is obtained from the TGA analysis using Horowitz–Metzger eqn. (*Jose et al., 2008; Sridhar et al., 2009*).

$$ln\left[\frac{1-(1-\alpha)^{n-1}}{T^2}\right]=ln\frac{R}{\Delta E_a}\left[1-\frac{2RT}{E_a}\right]-0.434\frac{E}{RT} \quad (2.3)$$

where, T is temperature (K), E_α is activation energy in J/mol, R is universal gas constant 8.3136 J /mol-K, n is the order of reaction and α is the fractional weight loss at a particular temperature. The fractional weight loss (α) can be expressed in eqn. (2.4):

$$\alpha=\frac{W_i-W_t}{W_i-W_f} \quad (2.4)$$

where, W_i and W_f are the initial and final weight of the sample respectively. While W_t is the weight at a given temperature. For n = 0, eqn. (2.3) is reduced to:

$$ln\left[\frac{-ln(1-\alpha)}{T^2}\right]=ln\frac{R}{\Delta E_a}\left[1-\frac{2RT}{E_a}\right]-0.434\frac{E_a}{RT} \quad (2.5)$$

The n-value can be estimated using the following Expression (*Saikrasuna and Saengsuwan, 2009*):

$$n=\left[(1-\alpha_{max})E_a e^{\Phi}\right]\times\frac{e^{-\frac{E_a}{RT_{max}}}}{R\left(\frac{d\alpha}{dt}\right)_{max}} \quad (2.6)$$

where, α_{max} is the degradation quantity at maximum degradation rate. The exponential factor Φ can be calculated using the following expression (*Saikrasuna and Saengsuwan, 2009*):

$$\Phi=ln\left[n(1-\alpha_{max})^{n-1}\left(\frac{\psi R}{E_a}\right)\right] \quad (2.7)$$

where, ψ is the pre-exponential factor. Therefore, a plot of $-ln\left[\frac{-ln(1-\alpha)}{T^2}\right]$ against $\frac{1000}{T}$ is constructed, as shown in Figure 2.10. Activation energy E_a is calculated from the slope using the expression as eqn. (2.8):

$$E_a=2.303\times R\times m \quad (2.8)$$

where, m is the slope, obtained from the approximated straight line as shown in the Figure 2.10.

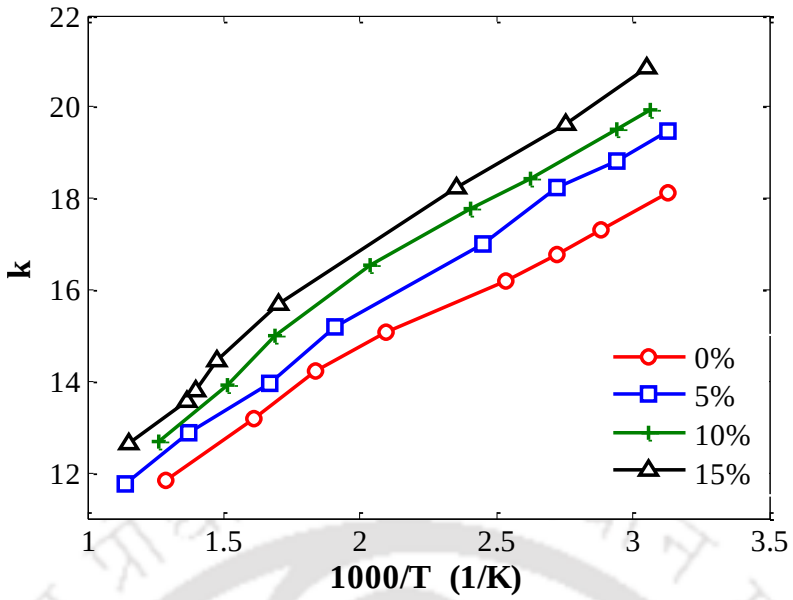

Figure 2.10 k [where k = $-\ln\left[\frac{-\ln(1-\alpha)}{T^2}\right]$] against $\frac{1000}{T}$ (1/K) curve

Activation energy is the least amount of energy required to initiate a chemical reaction for a material. Figure 2.11 demonstrates the gradual increment of activation energy of the composite due to percentage increase of filler material which attributes the uniform dispersion of the filler material throughout the polypropylene matrix. The activation energy (E_a) of polypropylene is calculated and it is found to be approximately 63 kJ/mol. The activation energy of 5% cement reinforced composite is considerably high as 72.5 kJ/mol.

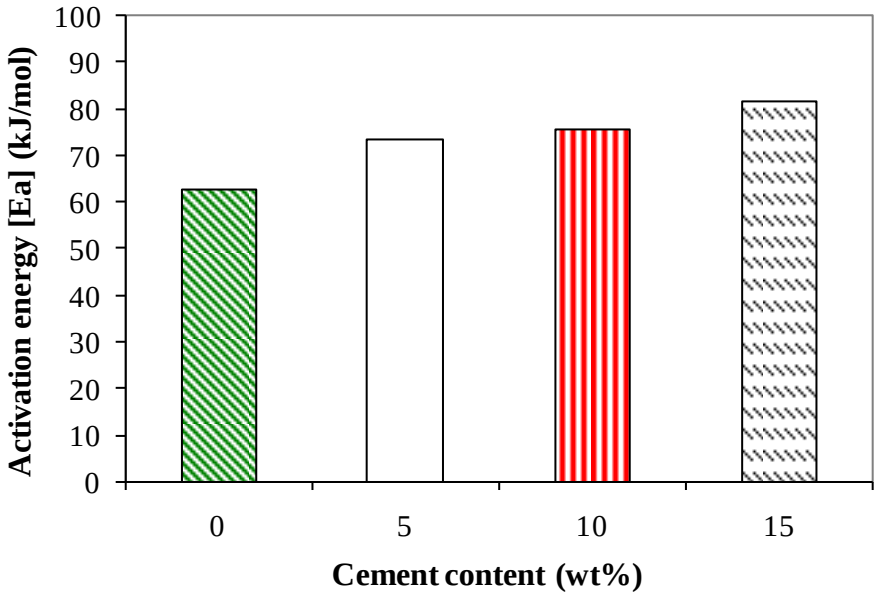

Figure 2.11 Variation of activation energy with respect to filler loading weight fraction

While, for 10% and 15% cement reinforced composites, the activation energy is obtained as 76 kJ/mol and 82 kJ/mol respectively. The fact is attributed that the addition of cement particles significantly enhanced the thermal stability of the composite.

2.5 Thermomechanical Analysis (TMA)

Thermomechanical analysis (TMA) is one of the important techniques for characterization of thermal properties polymeric composite materials. In the TMA, the thermomechanical properties of such as Glass transition temperature (T_g), coefficient of thermal expansion, thermal conductivity, heat deflection temperature, creep modulus, creep relaxation, viscoelasticity etc (*Price, 2002*), can be estimated. During testing, the loading or force applied to the sample can be varied with TMA probe. In the TMA analysis, the thermal expansion of the composites is found to be decreasing with the increase of fillers loading. Portland pozzolana cement which acts as filler is a suitable material for preventing the thermal expansion of the composite materials initiates by temperature fluctuation as well as atmospheric changes. The TMA instrument setup and samples are shown in the Figure 2.12 and 2.13 respectively.

Figure 2.12 TMA analyzer (TMA/SS6000)

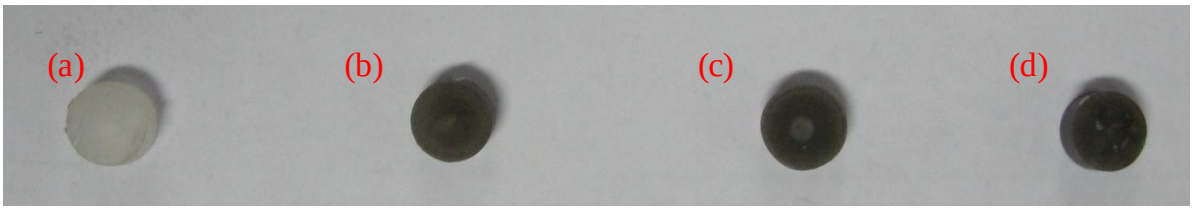

Figure 2.13 (a) Polypropylene, (b) 5%, (c) 10% and (d) 15% cement filled composite samples

Figure 2.14 reveals that the linear thermal expansion depends not only on the rehological properties of the polymer but also on the filler properties and the filler loading percentages. Test results indicate that the cement filled polypropylene composites have less linear expansion rate compared to pure polypropylene. The linear expansion decreases with percentage increase of cement particles loading. 15% cement reinforced composite shows

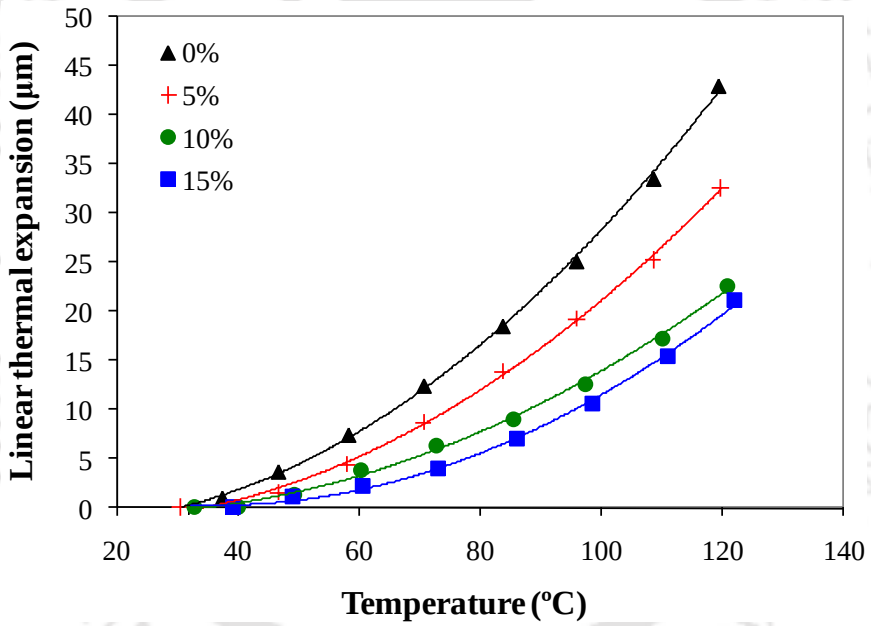

Figure 2.14 TMA plots of polypropylene and its composite samples

minimum expansion compared to the other composites as well as pure polypropylene. This happens due to decrease of viscosity of the composite materials with the percentage increase of filler materials. 5% cement reinforced composite shows around 30% decrease of linear

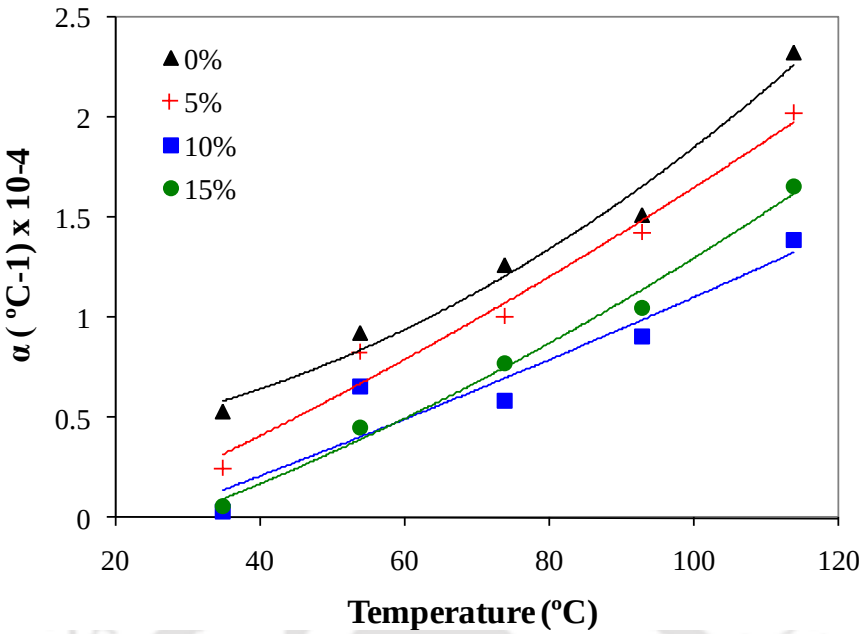

Figure 2.15 Coefficient of thermal expansion plot of polypropylene and its composite samples

expansion than pure polypropylene, while 10% and 15% cement reinforced composites show 48% and 52% decrease of the same properties respectively. Similarly, Figure 2.15 demonstrates the coefficient of thermal expansion and observed to be decreasing when the cement loading percentage decreases.

2.6 Nanoindentation Test

2.6.1 Principle and Procedure

Nanoindentation tests are conducted on CETR Nanoindenter (UMT-2, Figure 2.16) using a Berkovich indenter tip (tip radius 50 nm) on a polished composite samples. A total of two indentations are performed on each specimen using the continuous stiffness measurement (CSM) technique and the average values of indentations are presented in this work.

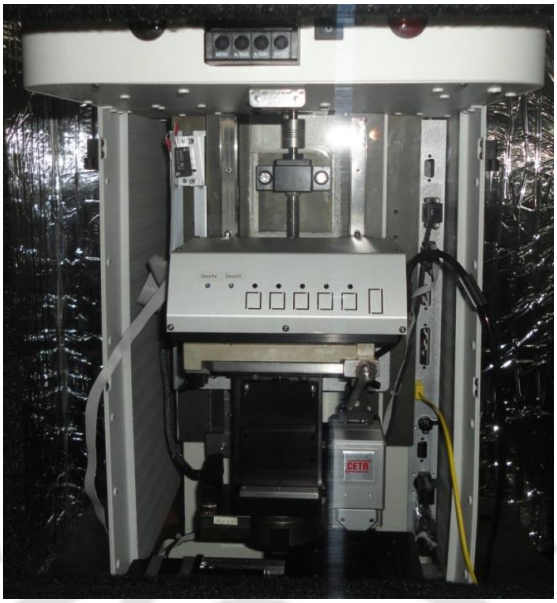

Figure 2.16 CETR Nanoindenter (UMT-2)

Figure 2.17 shows the representative load vs. displacement curves for pure polypropylene matrix and for the 5, 10 and 15% cement filled composites. Continuous nanoindentation is performed following six steps: indenter approach to the surface, loading to peak load for 24 s, holding the indenter at peak load i.e. creep for 10 s and allowing thermal drift for 5 s, unloading 90% of peak load for 20 s, holding the indenter after approximate 90% unloading for 15 s, and finally, unloading completely. This curve of quasi-static loading vs. indentation depth comprises of both elastic and plastic deformations. This is, from the starting of the unloading slope, the conventional elastic indentation stiffness is calculated (*Wong et al., 2006*). The indentation is monitored and applied on the polished surface of the composites and as well as pure polypropylene samples also. The instrumented indenter operating under continuous stiffness measurement (CSM) technique can sensitively assess local stiffness as the indenter tip traverses the polished surface of the composite medium (*Wong et al., 2006; Thome´ et al., 2009*).

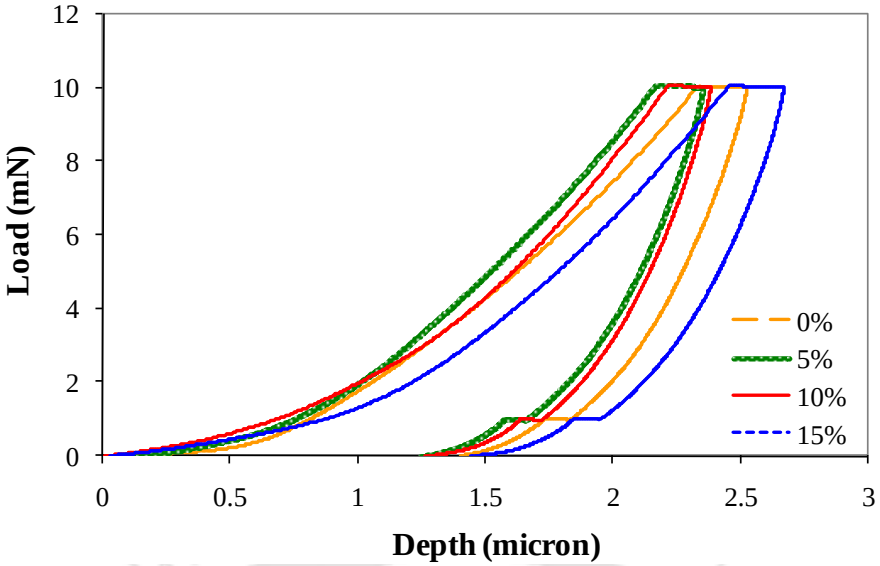

Figure 2.17 Load vs. depth of the composite materials for nanoindentation

An unremitting stiffness measurement that implicated a progressive series of loading and unloading cycle is conducted until the final indentation depth is achieved, generating a series of hardness and modulus values as a function of indentation depth (*Fang and Chang, 2004; Fang et al., 2005*).

Hardness (*H*) and elastic modulus (*E*) are calculated from the load–displacement results. When, the indenter penetrates into the specimen, both elastic and plastic deformation takes place out of which only the elastic segment of the displacement is retrieved during unloading condition. According to Oliver and Pharr (*1992*), hardness of nanoindentation can be defined as:

$$H = \frac{P_{max}}{A} \tag{2.10}$$

where P_{max} is the load measured at a maximum depth of penetration in an indentation cycle; A is the projected contact area of the hardness impression. The elastic modulus of the sample can be derived from the initial unloading contact stiffness (S). This contact stiffness, expressed as $\frac{dP}{dh}$, is the slope of the initial part of the unlading curve (*Oliver and Pharr 1992; Lee et al., 2007*). A relation among contact stiffness, contact area, and elastic modulus can be expressed as:

$$S_c = \frac{dP}{dh} = 2\beta E_r \sqrt{\frac{A}{\pi}} \tag{2.11}$$

Where, β is a constant which depends on the geometry of the indenter (β = 1.034 for Berkovich tip) and E_r is reduced elastic modulus, which attributes that elastic deformation occurs in both the sample and the indenter.

The sample elastic modulus (E) can then be calculated as (*Oliver and Pharr 1992; Lee et al., 2007*):

$$E = \left(1 - \nu^2\right)\left(\frac{1}{E_r} - \frac{1 - \nu_i^2}{E_i}\right)^{-1} \tag{2.12}$$

where ν and ν_i are the Poisson's ratios of the specimen and indenter, respectively, while E_i is the modulus of the indenter E_r is the reduced modulus. Table 2.4 shows a series of hardness, indentation Young's modulus and reduced modulus values of polypropylene matrix and its composites obtained by continuous nanoindentation with 1 mN/s indentation rate. The variation of the values may be due to the roughness of the samples and its different compositions (*Odegard et al., 2005*).

Table 2.4 Nanoindentation properties of the composite materials

Filler content	Indentation Young's modulus (GPa)	Reduced modulus (GPa)	Hardness (GPa)
0%	3.36	3.45	0.048
5%	3.97	3.05	0.062
10%	3.03	3.10	0.061
15%	3.75	3.83	0.046

Figure 2.18(a)-(c) illustrate the indentation stiffness, tensile stiffness and bending stiffness as a function of filler percentages are calculated through indentation, tensile and bending tests. The indentation stiffness is compared to the stiffnesses obtained from (i) standard tensile and (ii) 3-point bending tests using the specimens discussed in the chapter 3. Figure 2.18 shows the stiffnesses of unreinforced polypropylene and 5, 10, 15% cement filled polypropylene composites obtained from the nanoindenter and from the uniaxial tensile and 3-point bending tests. As shown in Figure 2.18 (a), it is observed that indentation stiffness increases when cement content increases except pure polypropylene; the probable reason could be the high variation of surface roughness of polypropylene sample. It can be attributed from the results that higher cement contents provide significantly higher resistance against materials

deformation under both tensile and bending. Similarly, indentation stiffness of the material indicates that higher percentage of cement fillers provide considerably greater resistance along with the puncture deformation of the materials. This finding can be streamlined by the fact that the cement possesses inherent stiffness higher than the matrix material.

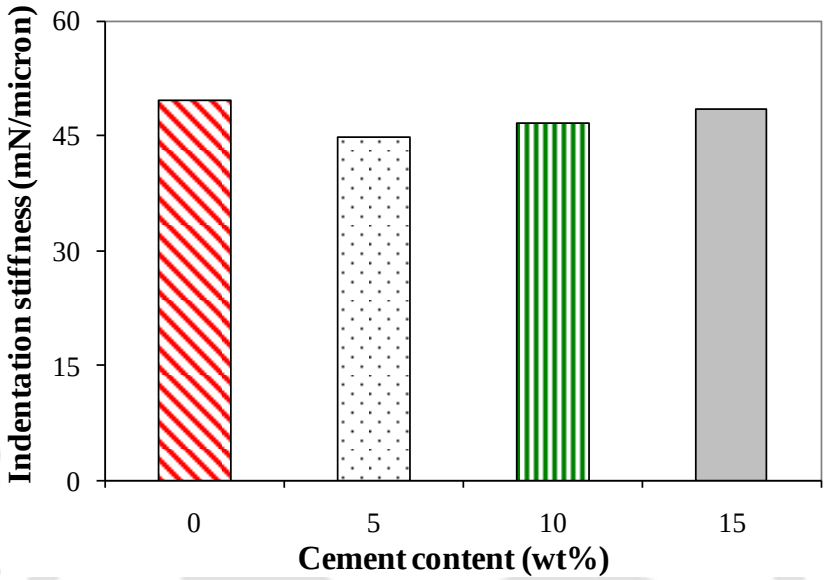

(a)

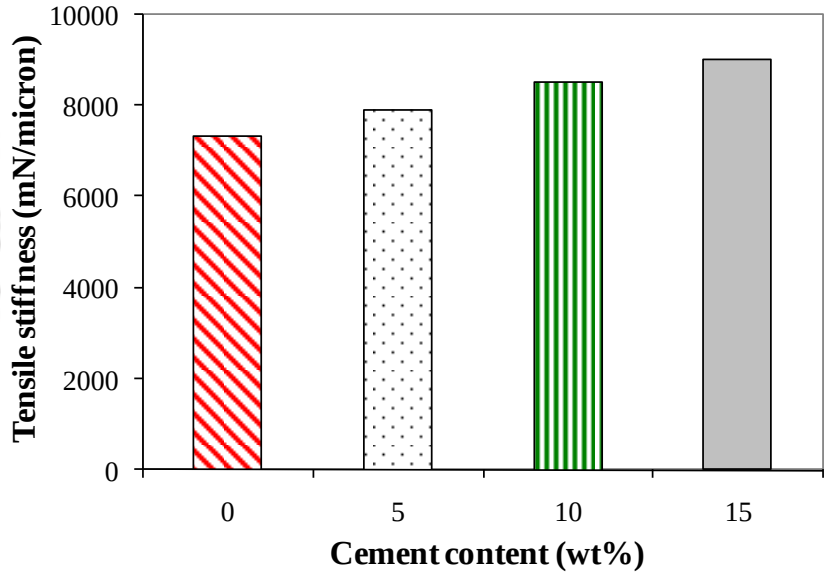

(b)

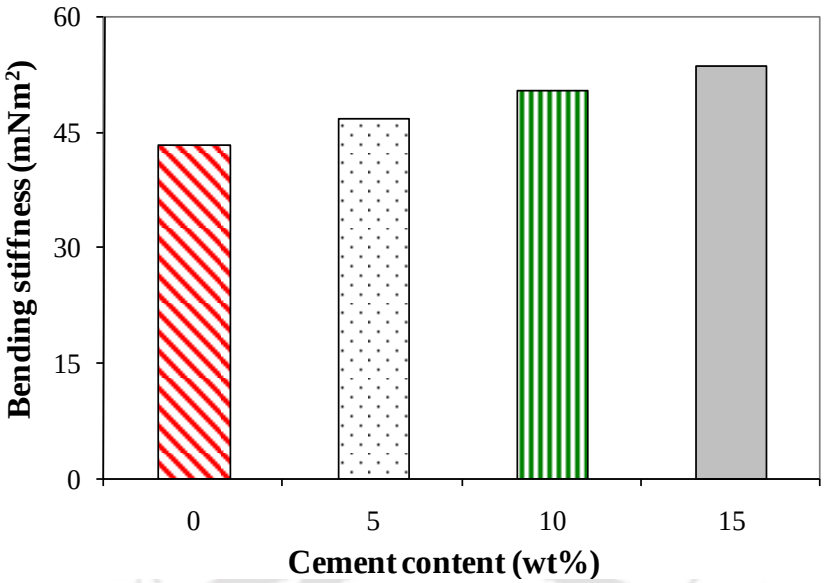

(c)

Figure 2.18 Variation of different stiffness (a) continuous indentation stiffness, (b) tensile stiffness and (c) bending stiffness with respect to filler content

Further, nanoindentation gives measure of the work done by loading and unloading cycle and are evaluated. Figure 2.19 shows the work done for the elastic and plastic deformation of the materials. It is observed that both the cases work done for elastic and plastic deformation decreases as cement contents increases. This finding can be rationalized by the fact that the cement particles enhanced inherent energy absorption during plastic deformation higher than the elastic deformation for pure polypropylene as well as its composites. At the same time, it is observed that work done decreases owing to the increase of cement contents, results in increase of brittleness as well as stiffness of the composites.

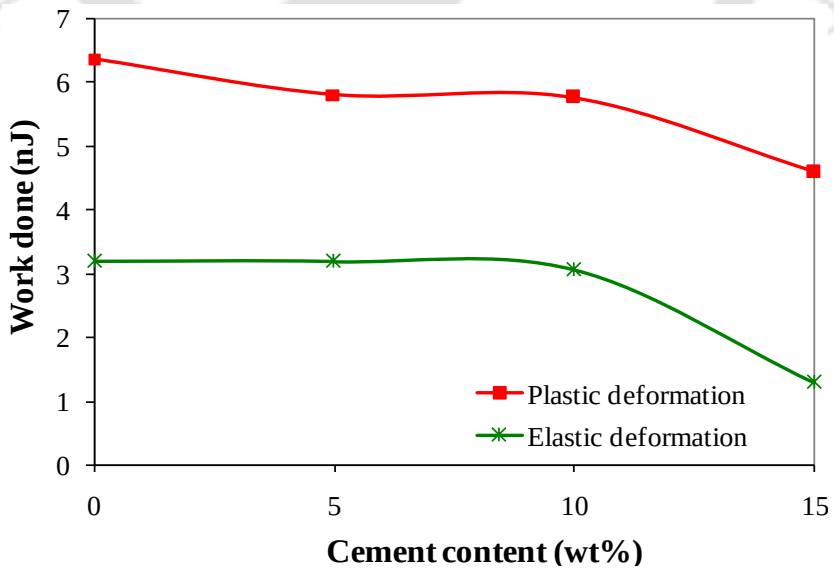

Figure 2.19 Work done due to plastic and elastic deformation subjected to nanoindentation test

2.7 Raman Spectroscopy

Raman spectroscopy is a powerful technique, useful to characterize various composite materials. In order to understand the degree of crystallinity and vibrational characteristics of chemical bonds of the composite materials, Raman spectroscopy technique is employed at an excitation wavelength of 633 nm of HeNe Laser, in LabRam HR800 Raman spectroscope (Huriba Jobin) as shown in the Figure 2.20.

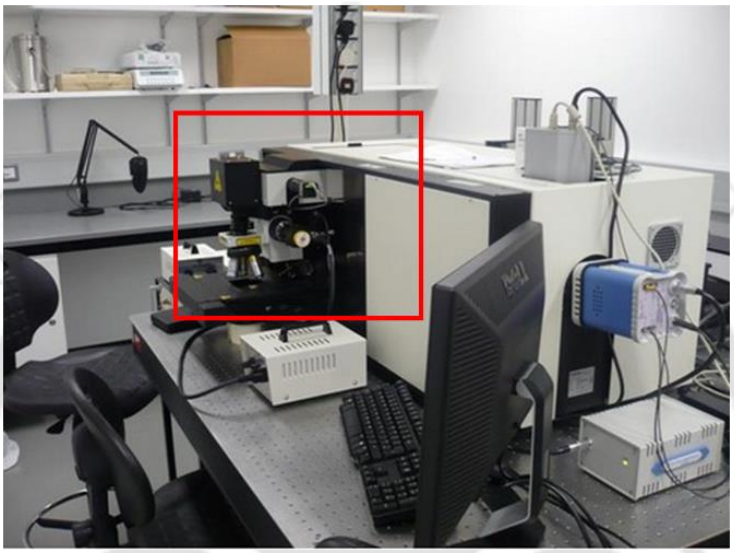

Figure 2.20 Raman spectroscopy

The Raman spectra of pure polypropylene and cement reinforced polypropylene composites samples are measured and is shown in Figure 2.21(a) and 2.21(b) respectively. The Raman peaks at 810, 844 and 1335 cm^{-1}, are assigned to the CH_2 rocking, C–C stretching and CH_2 twisting modes. Several medium peaks decreased with treatment time such as the peak at 975 cm^{-1} for the asymmetric rocking CH_3, mixed with the CH_2 rocking and C–C stretching modes, 1156 cm^{-1} for the CH bending, and 1170 cm^{-1} for the CH_3 rocking and C–C wagging modes (*Ahmed et al., 2010*). The bands at 840 and 890 cm^{-1} can be found in both visible

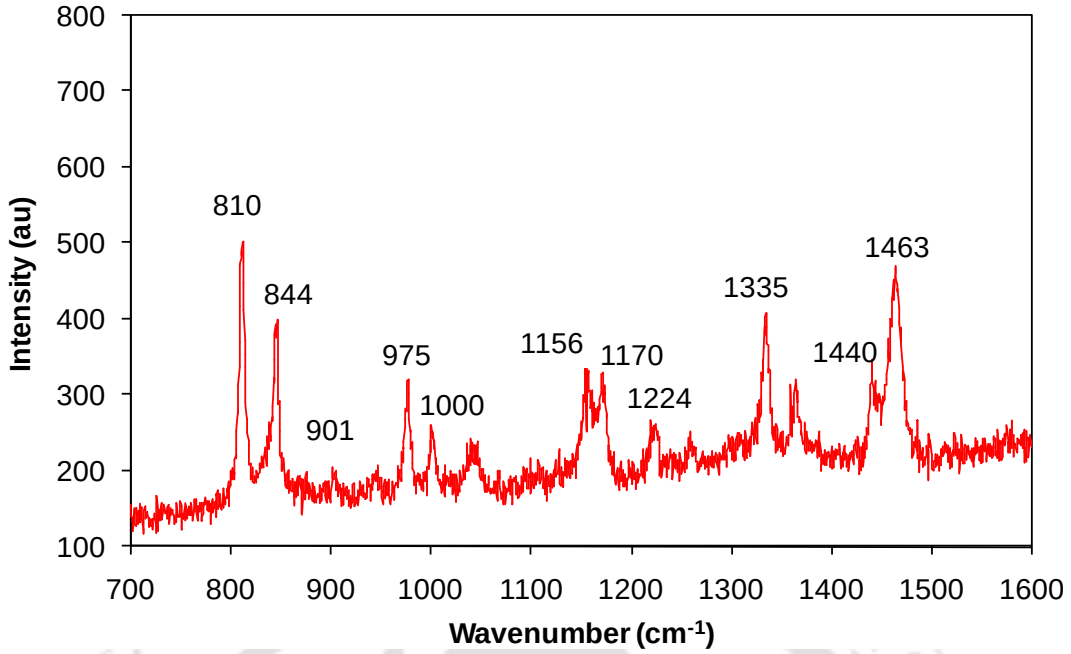

(a)

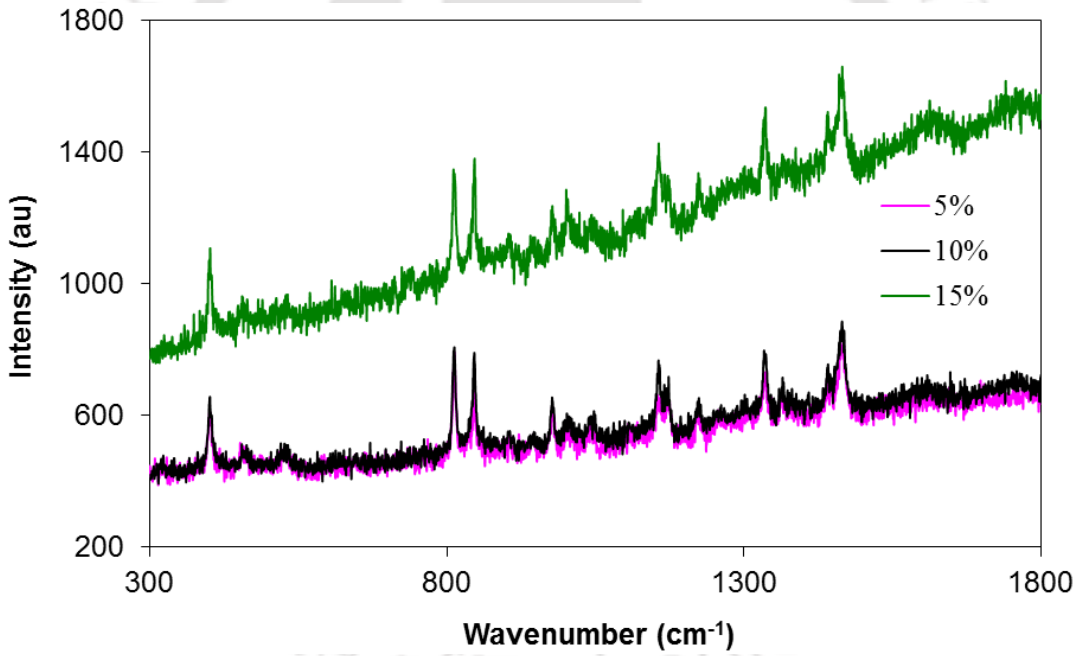

(b)

Figure 2.21(a) Raman spectroscopy of polypropylene matrix and (b) Raman spectroscopy of cement filled polypropylene composites

light spectra of C_3S, which can be assigned unambiguously to silicate stretching vibrations (*Newman et al., 2005*). Portland pozzolana cement shows the Raman shift at 1070 cm^{-1} for $CaCO_3$ **(***Lackhoff et al., 2003*). As illustrated in Figure 2.21(b), the cement filled composites spectrum exhibits a distinct peaks at different wavenumber, which does not conflict with peaks from cement as seen in the reference (*Lackhoff et al., 2003*). These peaks are perfectly

matches with the pure polypropylene. Since the intensity of the band at 810 cm^{-1} and 844 cm^{-1} rises, it is the evidence of degree of crystallinity that rises in both the pure polypropylene and its composites (*Arruebarrena et al., 1995*).

2.8 FT-IR Analysis

Fourier transform infrared spectroscopy (FT-IR) is a characterization technique that provides the information of the orientation of the polymer chain and proves the evidence of the presence of the functional group of the material and its chemical reaction. FT-IR analysis has been carried out to study the chemical interaction of the cement particles with the polypropylene matrix compound and its bonding. Characterization of compounds via infrared spectroscopy is not limited to organic compounds only but also to Inorganic compounds of the materials as well. The inorganic compound that generally forms covalent bonds with a molecular ion fragment, cation or anion produces a characteristic absorption spectrum with associated group frequencies. All complex ionic compounds containing more than one atom and coordination, exhibit compounds characteristic spectra. FT-IR spectroscope setup (NICOLET iS10, Thermo Scientific and OMNIC-software) is shown in the Figure 2.22.

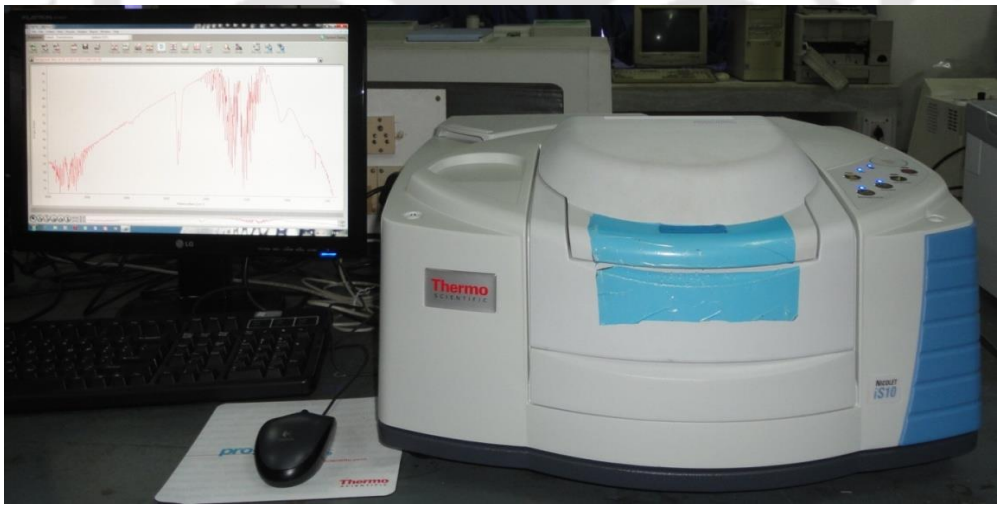

Figure 2.22 FT-IR Spectroscope (NICOLET-iS10)

Simultaneously, the FT-IR spectroscopy patterns are shown in Figure 2.23 and 2.24 of cement particles, and polypropylene and its cement reinforced composites. Absorption bands at 1459 cm^{-1} broadband and 928–659 cm^{-1} attribute to a strong peak arises from CO_2 vibration from $CaCO_3$ as calcite. These bands are present in sample, indicating the reaction between $Ca(OH)_2$ and CO_2 occurred. In Portland cements, a broadband of 928–815 cm^{-1}

arises from C–S–H vibration (*Parande et al., 2011*). The sharp vibration band at 3500 cm^{-1} corresponds to OH stretching and it is designed to be the calcium hydroxide. Other bands at 2923, 1646, 1123, 659 cm^{-1} indicate the presences of gypsum. A sharp shoulder peak at 815 cm^{-1} gives evidence of sulfite.

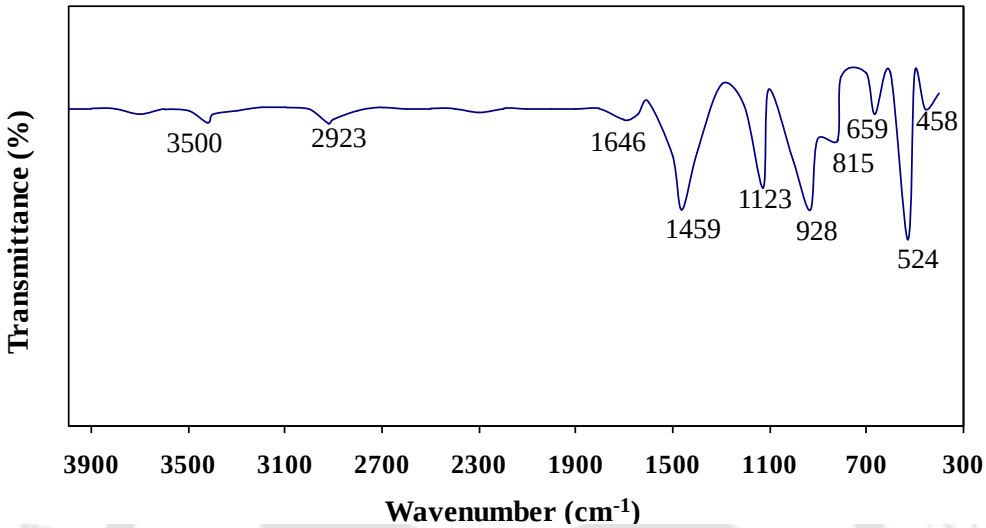

Figure 2.23 FT-IR for Portland pozzolana cement

The FT-IR spectra of the polypropylene sample and its cement based composites are analyzed and shown in Figure 2.24. The broad peaks at approximately 2946 cm^{-1} and 2914 cm^{-1} are assigned to the CH_3 and CH_2 asymmetric stretching modes, respectively. The prominent band is observed because of the symmetric and asymmetric vibrations of the methyl group near 1381 cm^{-1} and 1460 cm^{-1}, respectively, which are characteristics of polypropylene (*Dikobe and Luyt, 2009; Idrus et al., 2011; Zhou et al., 2013*). A broad absorption band between 1640 and 1800 cm^{-1}, assigned to the C-O and C-C stretching vibrations and is observed in the composites samples. However, the most significant difference between the FT-IR spectra of pristine polypropylene and its cement based composites as is seen in the region of 2840–2965 cm^{-1} where the different CH_2 peaks increased as cement content increases. In general, cross-linking between polypropylene and cement particles are occurred in the composites. In this case, the FTIR analysis also indicates that the amount of CH_3 groups decreased with increasing cement loading percentage and transformed into CH_2 groups inducing cross-linking **into** polypropylene, which may be associated with the dominating nature of cross-linking rather than stretching of polymer chain (*Ahmed et al., 2010*).

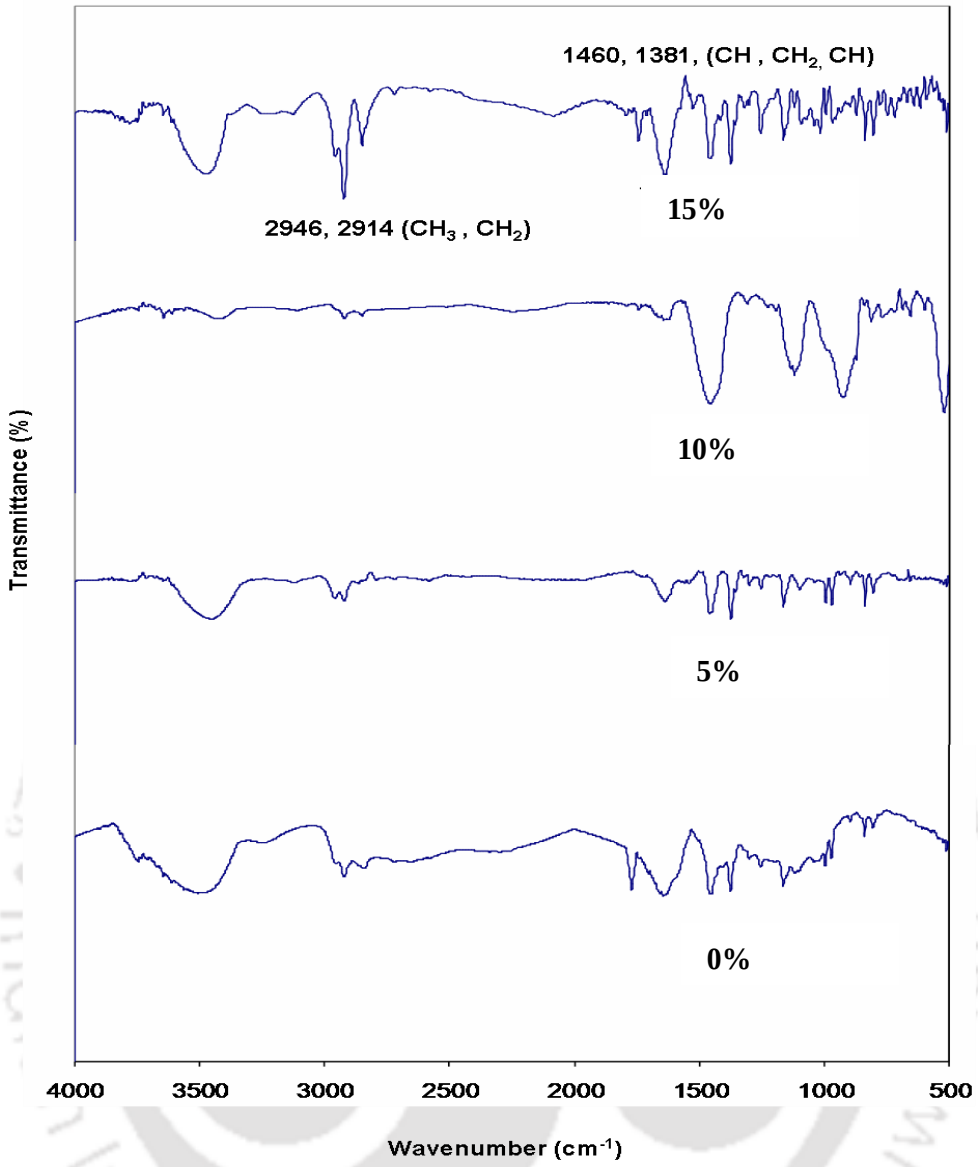

Figure 2.24 FT-IR spectra for pristine polypropylene and cement reinforced composites

These observations from the analysis suggest that cement particles has a strong influence on the structural and physical properties of polypropylene. Besides this, a broad absorption band at 3610 cm^{-1} is observed to be the characteristics of hydroxyl absorbed onto the cement particles. Hence, the results indicated strong interaction between polypropylene and cement particles. This interaction explains the enhancement of interfacial bond between hydroxyl group of cement particles generated from the $Ca(OH)_2$ and carboxyl group of polypropylene.

2.9 AFM- Analysis and Surface Roughness

Atomic force microscopy (AFM) is used to determine surface topography and roughness of cement reinforced polypropylene composites. AFM analysis is performed on a non-contact

mode AFM microscope (Agilent 5500, scanning probe microscope, USA). Figure 2.25(a-c) illustrates the surface properties of pure polypropylene and its cement reinforced composites in 2D phase images and topographies. In comparison to the pure polypropylene with a relatively smooth surface (Figure 2.25(a)); the surface of the composite materials exhibit increased roughness (Figure 2.25(b–d)). This is more evident from R_a (average surface roughness), the ten point height and R_z i.e., root means square (RMS) of surface roughness values summarized in Table 2.5. Results show that the surface roughness increases with the percentage increase of cement fillers. AFM image of 5% cement reinforced composite shows well structured morphology that also verify the cement surfaces are oriented parallel to the outer surface. Generally, The obtained AFM results indicate that increase of filler amount gives less exfoliation and increase structural randomness, results in higher roughness (*Ataeefard and Moradian, 2011*). Thus, it is concluded that, higher the cement content gives less ordered structures anticipating the less exfoliation of cement particles in the polypropylene matrix, say for 10% and 15% cement reinforced composite materials. It is further observed that well interacted or exfoliated cement filler into polypropylene composites give better-structured and oriented morphology. Further, the 10% and 15% cement reinforced composites show micro crack formation on the surface of the sample owing to the brittleness of the structure.

Table 2.5 Surface roughness of the polished specimens

Filler content	**10 point height (µm)**	**R_a(µm)**	**R_z(µm)**
0%	15.00	2.36	2.45
5%	18.60	2.97	3.05
10%	19.32	3.03	3.10
15%	26.46	3.25	3.33

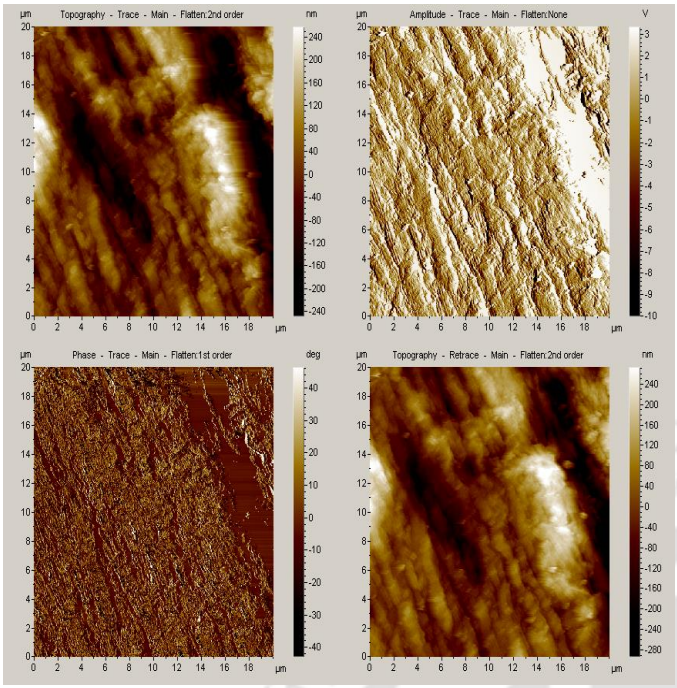

(a)

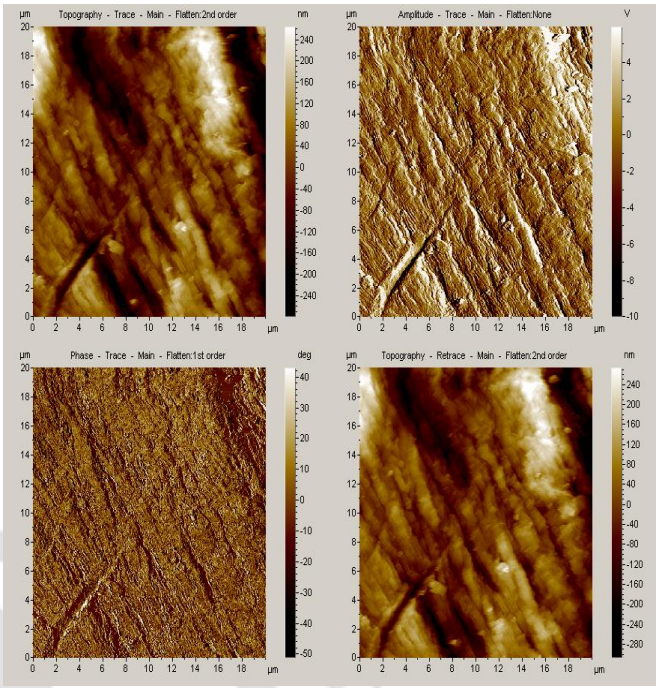

(b)

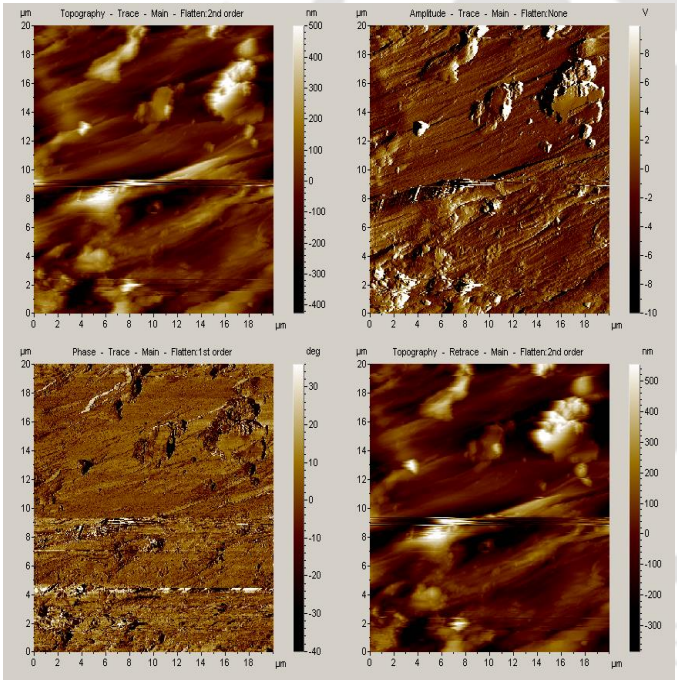

(c)

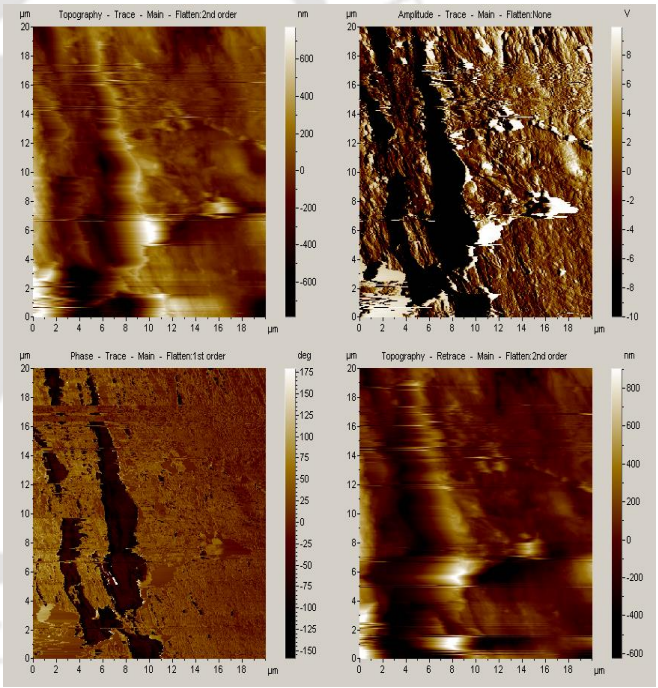

(d)

Figure 2.25 2D phase images with topographic images of atomic force microscopy of (a) polypropylene, (b) 5%, (c) 10% and (d) 15% cement reinforced composites

2.10 Rheological Behavior of Composite Materials

The rheological behavior of the pure polypropylene and its composites are investigated by using a torque sensitive capillary rheometer to study the viscoelastic properties of the composite materials. Ristolainen et al., (*2005*) investigated rheological behavior of

polypropylene/Organoclay composites and its relationship with degree of exfoliation of organoclay at 210°C. A similar study led by Solomon et al., (*2001*) focus on the rheological behavior of polypropylene and amine-exchanged montmorillonite hybrid composite under low amplitude oscillatory shear for a temperature range of 165-210°C. These investigations clearly show a dependence of the shear viscosity versus the shear rate at fixed temperature (200°C).

Rajesh et al., (*2012*) have reported that the magnitude of complex viscosity of polypropylene-clay composite is higher when the clay concentration increases. Similar study has also been undertaken by Muksing et al., (*2008*). They studied the flow properties of polypropylene and its clay composites at three test temperatures of 190ºC, 200ºC, and 210°C when the range of apparent shear rates varied from 50 to 8000 s^{-1}. These results revealed that the apparent shear stress of both unfilled and organobentonite-filled polypropylene nanocomposites increases approximately and linearly with the increasing apparent shear rate.

In order to build a consistent law for the rheological behavior of cement reinforced polypropylene composite materials versus shear rate and frequency, the shear viscosity is measured for a very large shear rate range: (10^{-1}–10^{4} s^{-1}) at 200°C. A PHYSICA MCR101 rheometer test setup is used for these measurements (Figure 2.26). The logarithmic plot of shear viscosity versus shear rate for polypropylene and other cement reinforced composites are obtained at 200°C and is shown in the Figure 2.27.

Figure 2.26 PHYSICA MCR101 Rheometer

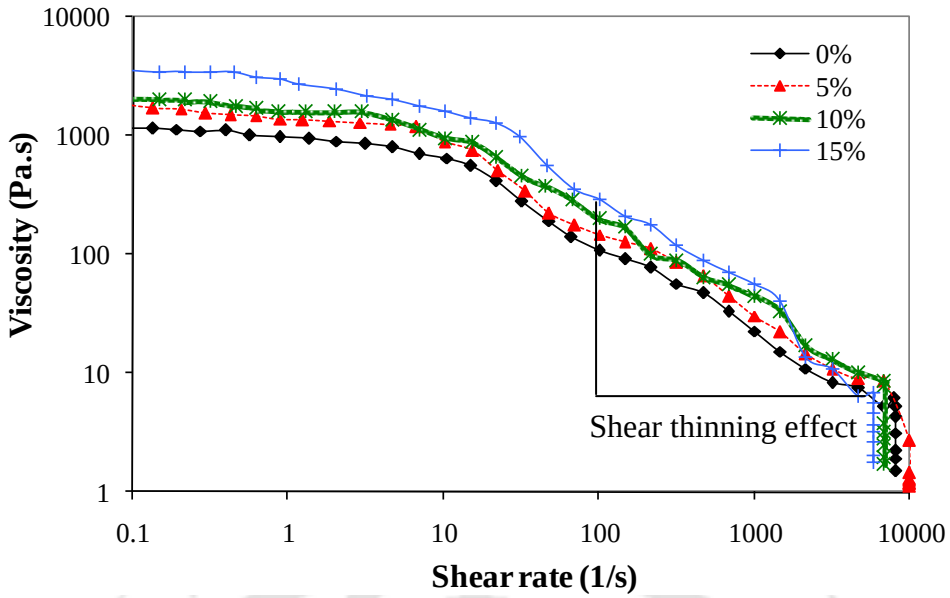

Figure 2.27 Shear viscosity vs. shear rate at 200°C for the polypropylene and the cement filled composite materials

At fixed temperature, the shear viscosity of the pure polypropylene and its composites decreases with the increase of the shear rate. These viscosity curves clearly indicate the significant effect of the cement content. When the shear rate is in the range 100-10000 s^{-1}, the cement reinforced composites exhibit a shear thinning effect i.e., pseudoplastic effect while the neat polypropylene exhibits only small shear rate dependence, revealing a Newtonian plateau (linear viscosity) (*Solomon et al., 2001; Muksing et al., 2008*). The logarithmic plot of shear stress versus the shear rate for pure polypropylene and the other composites at fixed temperature (200°C) are apparently shown in Figure 2.28. With an increase in cement loading, the shear stress increases, although the difference is small and tends to converge at high shear rate.

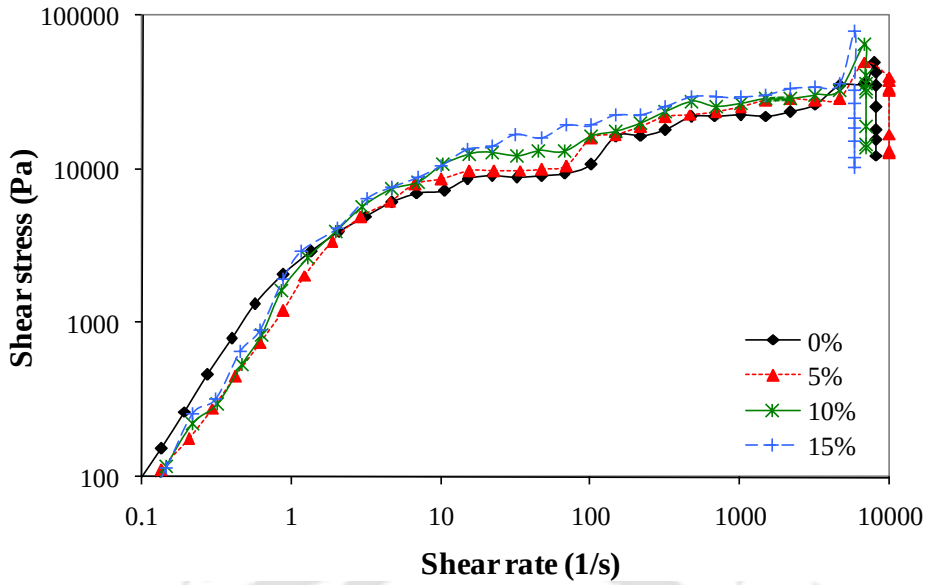

Figure 2.28 Shear stress vs. shear rate (1/s) at 200°C of polypropylene and other composites

The change in torque amplitude with respect to time is shown in Figure 2.29. It is observed that the torque increases with the cement loading and in general, the mixing torque decreases with time to a limit torque. This further can be correlated with the temperature of the composites results in decrease of the polypropylene shear viscosity. Further, due to the solid state of the cement reinforced composites when it is introduced into the mixer, very high values of the torque are measured up to 360s. As the polypropylene is softened with the heating, results in rapid decrease of the torque required. It takes around 200s to introduce cement reinforced composite to solid state. It explains the fact that the beginning of effective mixing phase starts after 275s. However, the shear viscosity of the cement reinforced composites, at the same order of shear rate, higher than the polypropylene; the effect of the cement content is observed to be less important than at low shear rates.

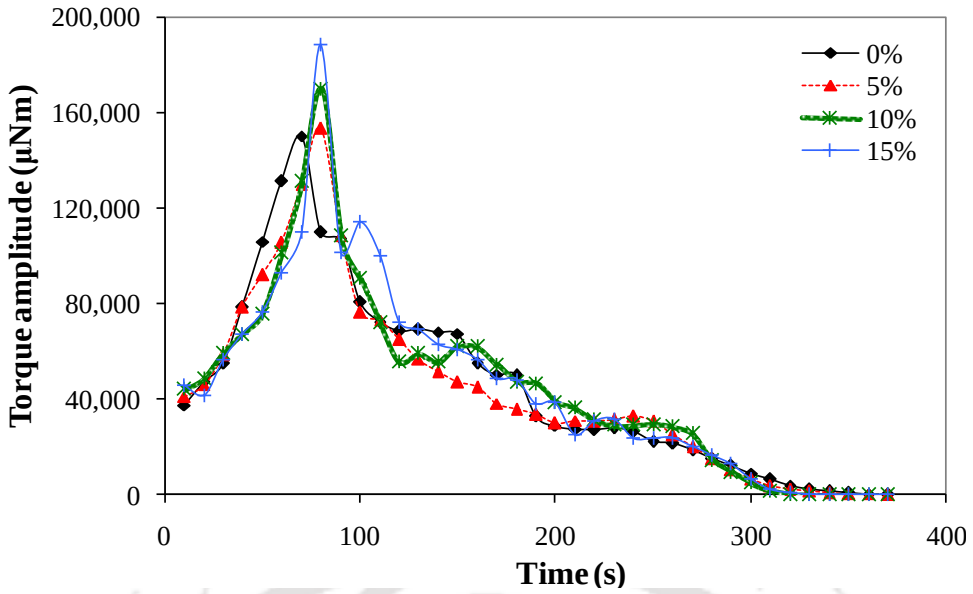

Figure 2.29 Variation of torque amplitude for pure polypropylene and the other composites

2.11 Summary

In summary, a new type of polypropylene based composite material has been developed using Portland pozzolanic cement particles as filler material for industrial applications. The work boasts the idea to use cement particle as a cheaper, though effective, strengthening polymer material without any significant chemical and physical modifications. The chapter emphasized on DSC, TGA, XRD, morphological analysis, TMA for vast investigation of the composite materials prepared by incorporating of cement particles with different loading percentage in polypropylene matrix. The morphological study of the fractured composite shows adequate bonding between the polypropylene matrix and the cement particles. It is observed that no crystallographic changes occur in the matrix with the incorporation of cement particles at high loading rate. Further, the absence of major peaks is understood to have the possible exfoliation of the cement particles into the polymer matrix. Thermal properties analysis reveals that the thermal stability and fire retardant property of the composite are improved with the percentage increase of cement particles.

Along with this, various characterization techniques are also employed such as, nanoindentation, Raman spectroscopy, FT-IR and AFM. Rheological behaviors of the fabricated composite materials have also been studied to evaluate the viscoelastic properties. Nanoindentation test is conducted to study the localized mechanical behaviors of the composite materials which correlate the global properties of the proposed materials. Raman spectroscopy and FT-IR analysis reveals that the band peaks of the filler materials do not

mingle with the composite materials indicating adequate bonding between fillers with the matrix. AFM results show that, increase of filler amount gives less exfoliation and less order of structure; hence, results in higher surface roughness of the composite materials. It is observed that 10% and 15% cement reinforced composite structures show less ordered due to less exfoliation of cement particles into the polypropylene matrix. Well interacted/exfoliated cement reinforced polypropylene composite materials show well structured and oriented morphology of composite. Apart from this, the 10% and 15% cement reinforced composites show micro-crack formation on the surface of the sample due to the brittleness. Further, the rheological analysis shows, viscosity and shear stress depend upon the filler loading % as well as the temperature. The high dispersion of filler materials into the polymer, demands that the initial shear stress as well as the applied torque is required to be at higher rate.

Chapter 3

Investigation and Evaluation of Mechanical Properties of Fabricated Composite Materials

3.1 Introduction

Geometrical structure of the product developed, material deformities, presence of cracks, cavities severely affects the material performance and ultimately leads to material failure. Thus, investigation on mechanical properties of the polymeric composite material is indispensible before its applications. Several experiments are conducted to study and investigate the material performance with notches. Samples of various notch sizes are prepared and tensile properties of the composite material are studied by conducting experiment using Instron Universal testing machine. It is observed that tensile properties of the composite material significantly changes owing to the presence of notches and percentage variation of the cement fillers. In addition, the performance and service life mostly depends on the fatigue characteristics of the composite materials. The strain energy during fatigue analysis depicts the material durability and performance. It is, eventually, thus depends on the stiffness as well as hysteretic characteristics of the materials which led to material failure. Thus, the fabricated cement reinforced composite materials underwent to short-term fatigue analysis to evaluate its performance prior to putting into service and in real time applications. Further, it is essential to know the effect of reinforcement on mechanical properties of the material. Hence, a theoretical investigation have been, subsequently, carried out using the Halpin-Tsai and modified rule-of-mixing model to understand the effect of reinforcement factors viz. filler concentration, aspect ratio and elasticity to figure out the optimal mechanical properties of the material. In the rule-of-mixing series model, it is observed that length efficiency factor (η_l) is a function of the volume fraction of the filler materials. Thus, it is necessary to modify the rule-of-mixing series model incorporating the length efficiency factor as a function of the volume fraction of the filler materials.

3.2 Tensile Mechanical Behavior of the Composites with Circular Notches

The tensile mechanical properties of cement filled composite materials with varying circular notch size are obtained followed by the ASTM standard D638 using Universal Testing

Machine (UTM), Instron Tensile Tester. The tests are carried out at a crosshead speed of 2 mm/min at room temperature. The mechanical properties i.e. tensile true stress-strain of pure polypropylene, 5% , 10% and 15% (weight) cement filled composites are obtained experimentally and are illustrated in the Figure 3.1(a) to Figure 3.1(d) respectively.

Samples are prepared keeping the width constant while the circular notch diameter is selected as 2.5, 4.5 and 5.5 mm where diameter to width ratio varies as 0.192, 0.346 and 0.424. The position of the circular notch is kept at the middle of the tensile sample anticipating the fracture of the sample is to be found at the middle with uniform stress distribution. The tensile strength of the composites of the unnotched and notched conditions is shown in Table 3.1 as a function of specimen filler contents and circular notch diameter along with the standard deviation (SD). Where, true stress is defined as the applied load acting on the instantaneous cross-sectional area and true strain is defined as the rate of instantaneous change in gauge length of the tensile sample (*Dieter, 1961*).

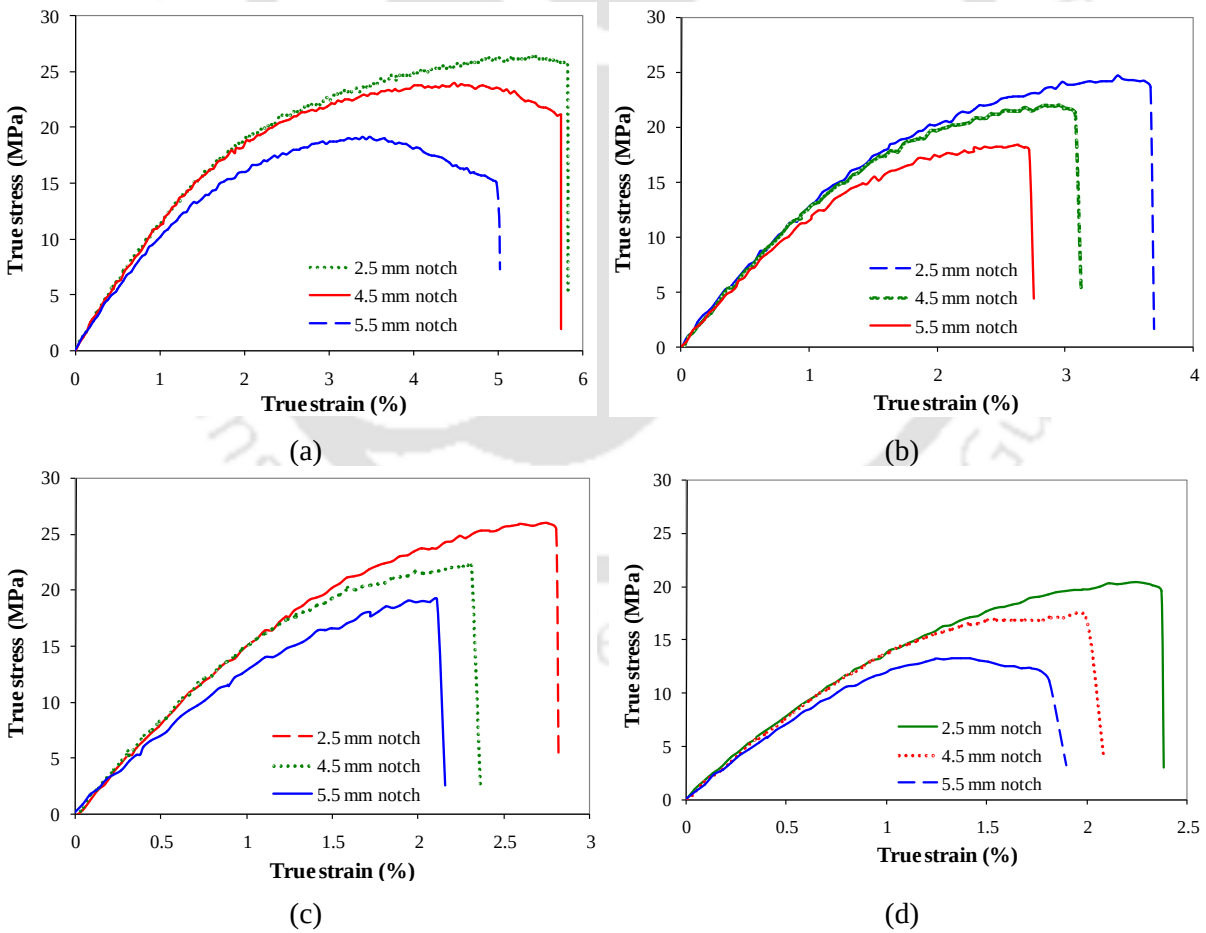

Figure 3.1 True stress-true strain behavior of (a) 0%, (b) 5%, (c) 10% and (d) 15% cement reinforced polypropylene composite with varying circular notch size

The tensile strength of the composites with respect to circular notch-to-width ratio for notched and un-notched conditions is shown in Figure 3.2. Figure 3.3 shows the variation of work-of-rupture strength for both notched and un-notched condition as the filler loading percentages varies from 0 to 15 %. It is clearly observed that with notches, the tensile strength of the composite significantly decreases in addition to the percentage increase of cement materials. Further, decrease in notched strength with increase in notch size corresponds to the stress concentration factor around the vicinity of the circular notch may lead to failure of the composite as a whole.

Table 3.1 The tensile strength of notched and unnotched specimens of composite materials

	Tensile strength (MPa)							
		SD		**SD**		**SD**		**SD**
Notch (mm)	**0%**		**5%**		**10%**		**15%**	
0	29.44	1.40	30.65	2.02	31.52	1.58	24.07	2.11
2.5	25.05	1.80	25.81	1.64	26.19	1.56	19.94	1.75
4.5	22.97	1.32	23.4	1.54	24.23	2.02	16.63	1.70
5.5	18.48	2.05	18.89	1.43	19.58	1.82	13.06	2.24

In addition, the detailed mechanical properties of pure polypropylene and cement reinforced composite materials are vastly discussed in the chapter 4. Further, another important observation is made, while the gross stress is used in the fracture analysis and the two-parameter analysis, the net stress for the specimens with circular notches tends to level off (Figure 3.2). The isotropic composite materials under the investigation show a similar trend of the notched strength reaching a limiting value (*Prabhakaran, 1979*).

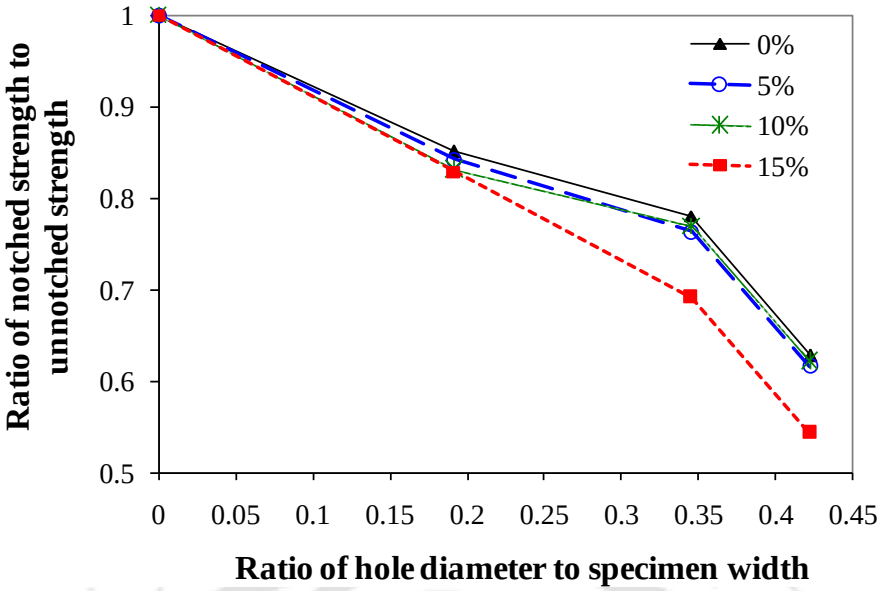

Figure 3.2 Variation of net notched strength with circular notch size

The experimental work of rupture of the fabricated composite samples and pure polypropylene are evaluated by calculating the area under the curve starting from up to the fracture point of the specimens. It is observed from the analysis that, the work-of-rupture is a function of the ratio of circular notch diameter to the specimen width as shown in the Figure 3.3. In the course of this investigation, an important aspect is taken into account that net work of rupture of the specimen with varying circular notch diameter tends to level off and reaches a limiting value even though maintaining the same width of the specimen (*Prabhakaran, 1979*).

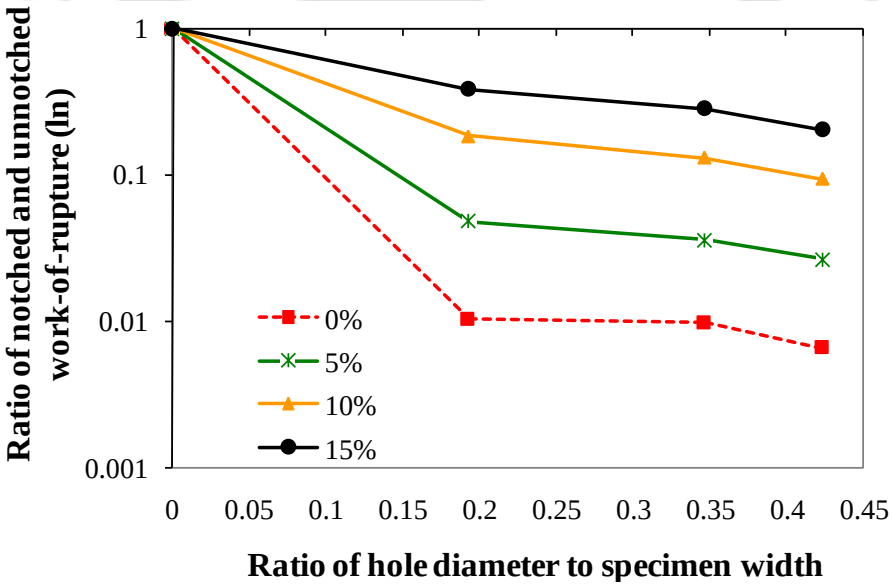

Figure 3.3 Variation of work-of-rupture with circular notch size

The morphology of the fractured surface of composite is studied under LEO 1430 VP Scanning Electron Microscope supplied by LEO Electron Microscopy Inc. The fractured surface of the specimen is prepared by gold coating (as the composite is non-conductive) and examined under high voltage (10kV) with 500 times magnification. Figure 3.4 illustrates the micrograph of the fractured surface of 15% cement filled polypropylene composite. The result shows adequate dispersion of cement particles in the polypropylene matrix. The results thus validate the certain bonding between the matrix and filler material. Further, it is anticipated that the bonding is improved and enhanced due to the presence of grafted polypropylene.

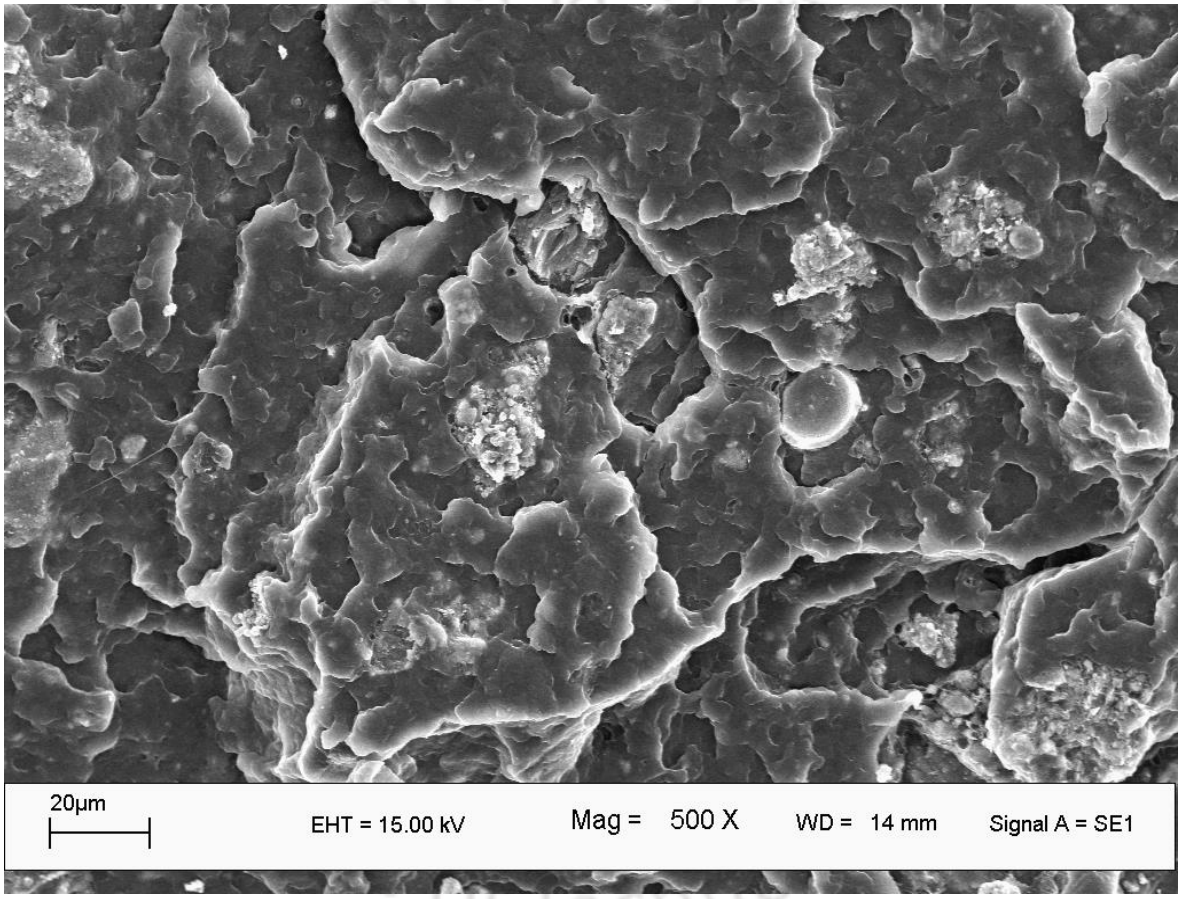

Figure 3.4 SEM image of the fractured surface of 15% cement filled composite with 500 × magnification

3.3 Short-term Fatigue and Bending Analysis

3.3.1 Fatigue Behavior on Short-term Loading-Unloading

The hysteresis loop of the stress–strain relationship is obtained during each loading cycle in the fatigue test at a frequency of 1 Hz, where, each hysteresis loop consists of loading and unloading curves. Figures 3.5 and 3.6 show the loading-unloading curves of the hysteresis

loops evaluated during the experiments. A typical example is shown at each stress level under respective loading conditions. The results indicate that the deformation behavior of the composite specimen depends on the loading conditions and the cycle selected.

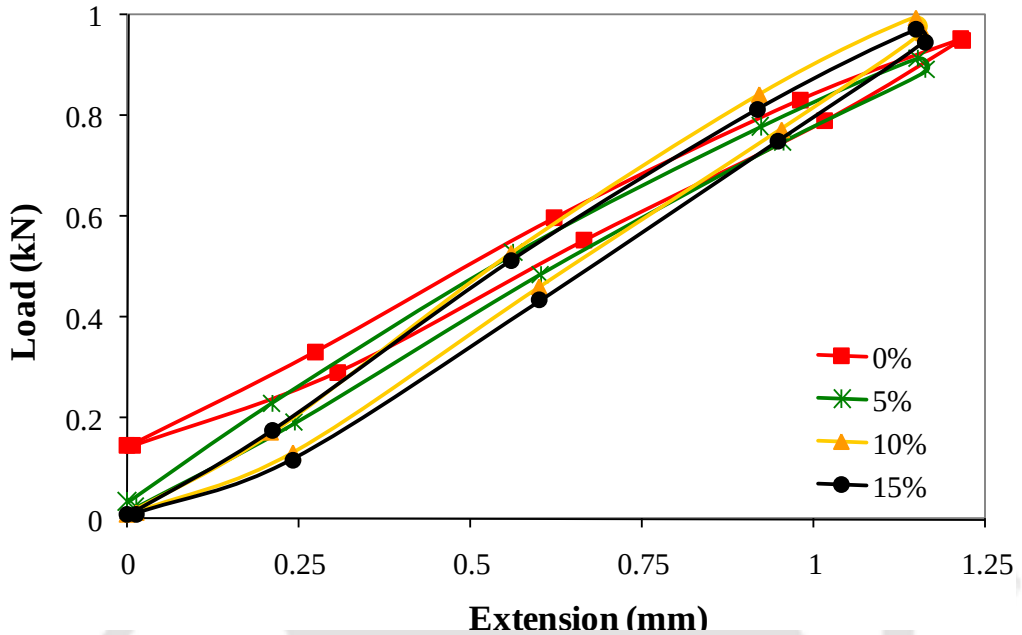

Figure 3.5 Load vs. extension of the composite materials

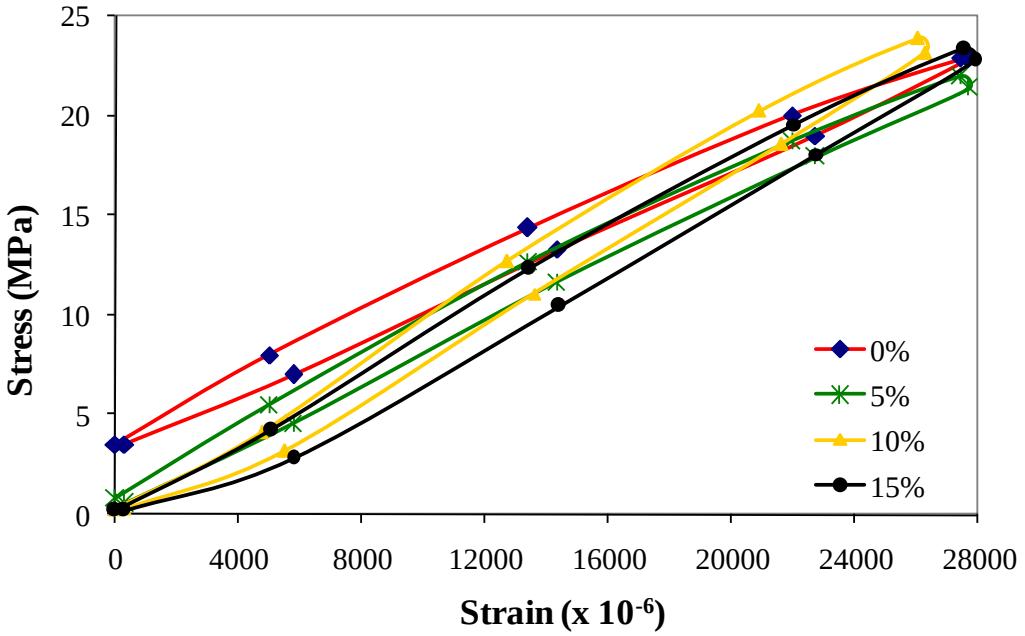

Figure 3.6 Stress–strain curve indicates hysteresis of the composite materials

The tension-compression effect of the specimen is observed across the thickness while maintaining the same frequency of the cyclic load is applied. This is considered to be the reason that the fatigue life of the composite specimen is highly dependent on the loading

conditions. Therefore, not only the stress level but also the strain should be taken into consideration to explicate the fatigue behavior of specimens under various loading conditions (*Sugimoto and Sasaki*[I-II], *2007*).

Further, strain energy i.e. mechanical work done per unit volume of the composite specimen is calculated and illustrated in the Figure 3.7(a). The strain energy reflects the deformation behavior of a specimen during loading from zero to the peak value. The fatigue behavior of polymeric composite material causes significant dissipation of energy under loading-unloading condition. Energy dissipation ratio, denoted by H_c, can be defined as the ratio of energy loss per cycle, i.e. measured from the area enclosed by the loading-unloading curve to the strain energy per cycle, i.e. area enclosed by the loading curve as shown in the Figure 3.7(b). The energy dissipation ratio is used as an index of fatigue performance of the composite material (*Sugimoto and sasaki, 2008*).

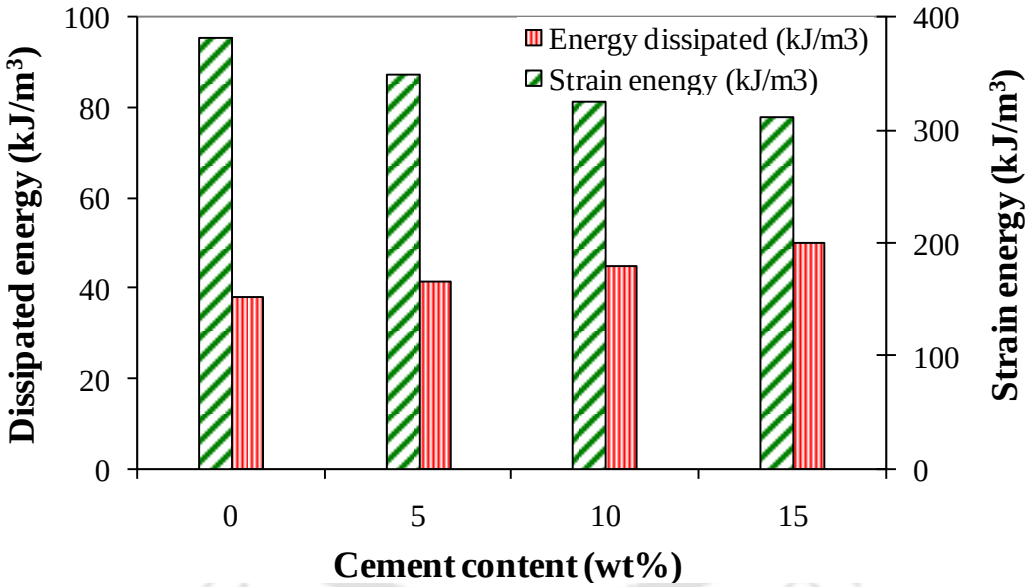

(a)

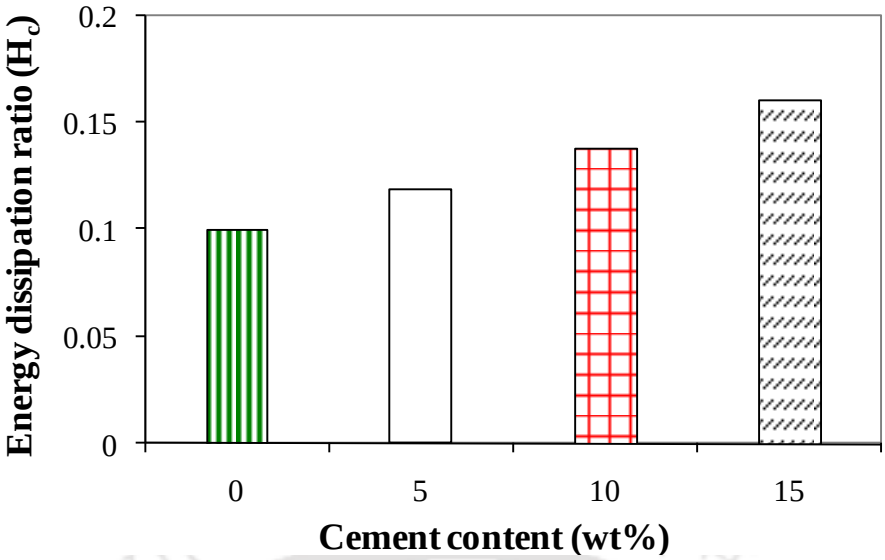

(b)

Figure 3.7 Variation of (a) dissipated strain energy and (b) energy dissipation ratio with the filler loading (wt%)

Clorius et al., (*2000*) demonstrated that, the stiffness decreases during the fatigue life of the materials and gives a fatigue life dependent elastic modulus, *E(t)*. The time dependant elastic modulus in unloading cycle, denoted by $E_U(t)$, is not same as the time dependent elastic modulus, $E_L(t)$, in loading condition. The ratio of $E_U(t)$ *to* $E_L(t)$ is denoted as the stiffness ratio. The stiffness of the material is observed to be fatigue life dependant and is governed by the time dependant elastic modulus. This stiffness ratio is obtained in loading-unloading sequences is determined at any given time of the fatigue life of the materials and can be expressed as:

$$\textit{Stiffness ratio } (\chi) = \frac{E_U(t)}{E_L(t)} \tag{3.1}$$

The stiffness ratio (χ) depends on the filler loading %, as such the stiffness ratio increases with increase of filler materials. The total loading-unloading cycle time has been assumed as a total fatigue life of a sample because the experiment has been done in order to evaluate short term fatigue performance of the composite materials. The total experimental time has segregated into four relative fatigue life of each sample and it is observed that fatigue life significantly varies with the stiffness ratio as shown in the Figure 3.8.

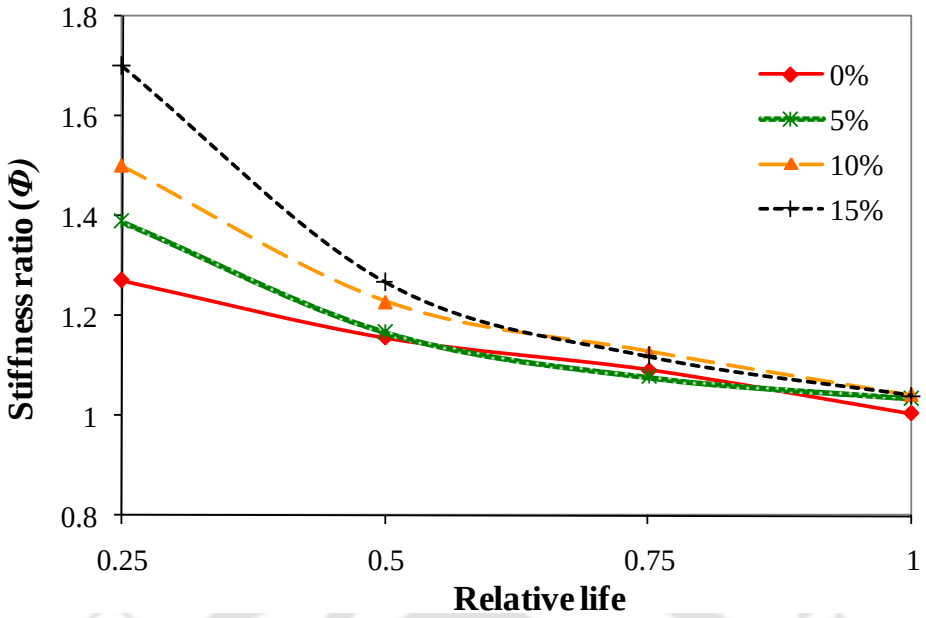

Figure 3.8 Variation of stiffness ratio with relative life

3.3.2 Bending Deformation Analysis

To understand the shear deformation under loading condition, the 3-point bending tests of composite materials are conducted in universal testing machine (INSTRON- 8801) followed by the ASTM standard D790. The load-deflection graph of the test results are represented in the Figure 3.9.

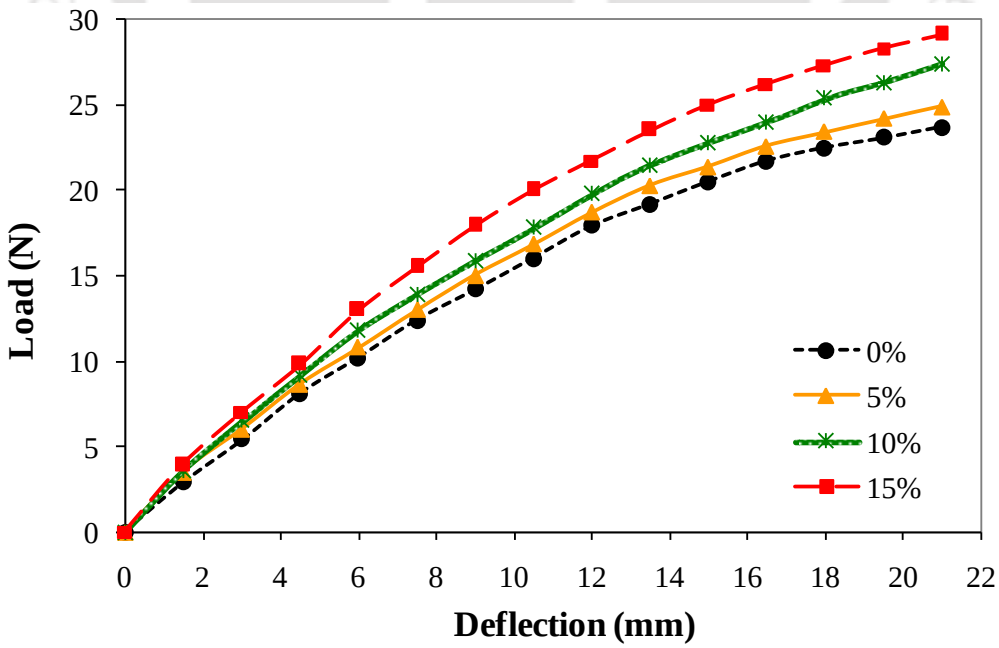

Figure 3.9 Load-deflection behavior of composite materials

From the test results, the interlaminar shear stress, which is at a maximum at the neutral axis, is calculated with the aid of the standard relationship (*Christiansen et. al., 1972*). The tensile and the shear stresses are calculated for the composite (where it is maximum) and is given by the expression:

$$\sigma = \frac{3P}{2BD}\left(\frac{L}{D}\right) \tag{3.2}$$

$$\tau = \frac{3P}{4BD} \tag{3.3}$$

where τ is the interlaminar shear stress at the neutral axis, P is the applied load, B the width and D the thickness of the specimen. The load is measured at the first major maximum in the load deflection curve as shown in Figure 3.9. The results obtained for the complete range of composite samples using the load deflection results are illustrated in the Figure 3.10.

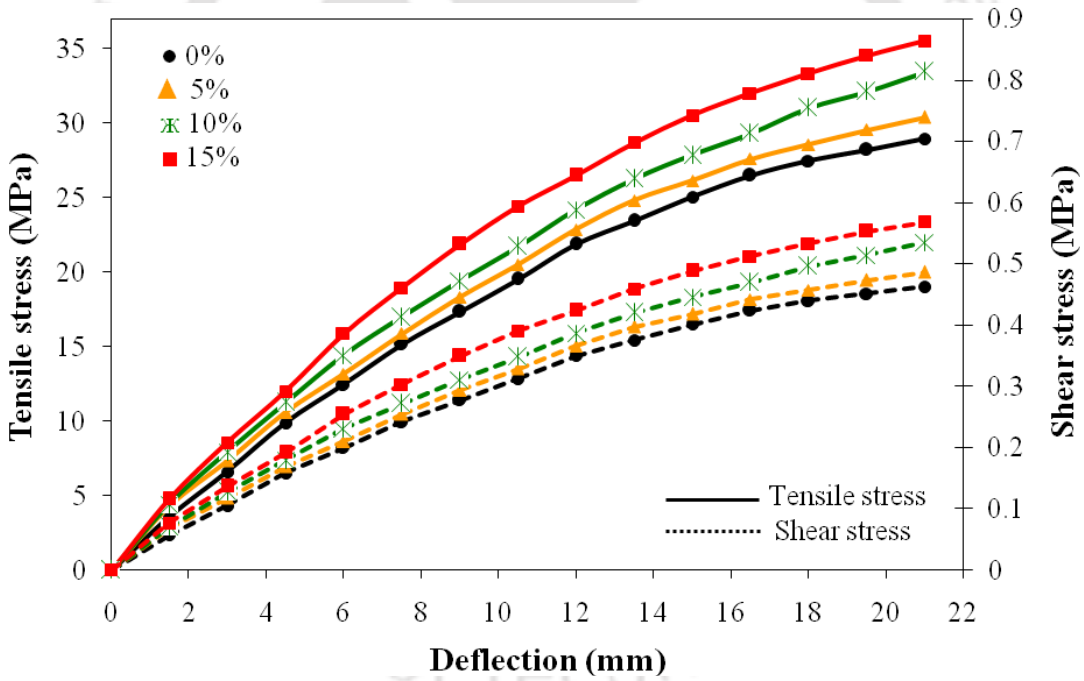

Figure 3.10 Variation of tensile stress and shear stress vs. deflection of the composite materials

In the Figure 3.11, the demarcation of failure region over tensile and shear has shown. The straight line represents the boundary between tensile and shear failures according to inequality which differentiates between shear and tensile failure of the composite materials (*Daniels et al., 1971*).

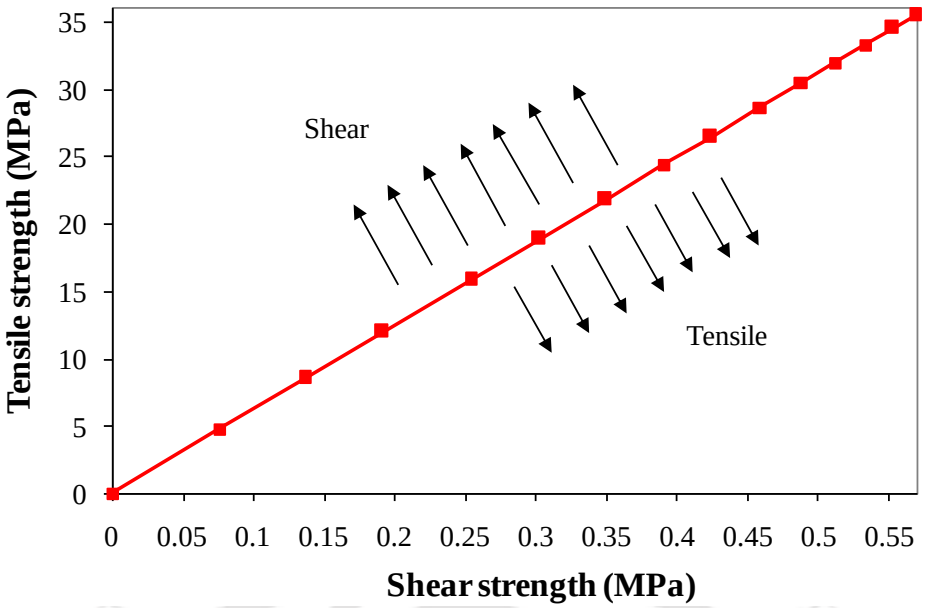

Figure 3.11 Tensile strength vs. shear strength at the failure region

3.4 Theoretical Modeling to Predict the Elastic Modulus of the Composites

According to the modified self-consistent micromechanics model of Halpin-Kardos (*Halpin and Kardos, 1976*), and modified series model of rule-of-mixing, Jonathan et al., (*2006*) and Kanagaraj et al., (*2007*) modified the model for high density polyethylene/carbon nanotubes (HDPE/CNT) nanocomposites where they have assumed that CNT's are randomly oriented into HDPE matrix as short fibre arrangement. The aspect ratio (l/d) of the CNT as short fibre was considered as 84.2.

In this study, it is essentially assumed that cement particles and polypropylene matrix are very well-bonded, equally expands during the tensile test, while cement particles are homogeneously dispersed throughout the polypropylene matrix system. In addition, the cement particles are considered to be mineral filler, where final shape can be assumed as a mixture of different shapes like sphere, cube, block, plate/flake, fibre etc. The aspect ratio (l/d) of those shapes can be varied as for 1 (sphere and cube), 2-4 (block), 20-200 (plate/flake), >200 (fibre) [186]. Further, assumption is made that there is no voids in the composite samples. The elastic modulus of cement is considered as 20×10^3 MPa where the fly ash content is 30% (*Siddique, 2003*). The elastic modulus of polypropylene is 1325.286 MPa (detailed about tensile properties of pure polypropylene and cement reinforced composite materials are discussed in the chapter 4) obtained experimentally for this study. The modified model is expressed in the eqn. (3.4) and eqn. (3.5).

$$\frac{Y_{comp}}{Y_{pp}} = \frac{3}{8}\left[\frac{1+2\left(\frac{l}{d}\right)\eta_l V_{cem}}{1-\eta_l V_{cem}}\right] + \frac{5}{8}\left[\frac{1+2\eta_t V_{cem}}{1-\eta_t V_{cem}}\right] \quad (3.4)$$

where, Y_{comp} and Y_{pp} are the elastic modulus of composite and polypropylene respectively,

$$\text{where } \eta_l = \left[\frac{\left(\frac{Y_{cem}}{Y_{pp}}\right)-1}{\left(\frac{Y_{cem}}{Y_{pp}}\right)+2(l/d)}\right] \text{ and } \eta_t = \left[\frac{\left(\frac{Y_{cem}}{Y_{pp}}\right)-1}{\left(\frac{Y_{cem}}{Y_{pp}}\right)+2}\right]$$

where, V_{cem} denotes volume fraction of cement into polypropylene and *l/d* is the average aspect ratio of cement particles. In this work the cement particles were taken as (wt/wt) % and the volume fraction was calculated. Weight fraction of cement is expressed as:

$$W_{cem} = \frac{w_{cem}}{100}$$

where w_{cem} is weight of the cement in polypropylene matrix. Similarly, the Volume fraction of cement is expressed as

$$V_{cem} = \frac{\rho_{comp} W_{cem}}{\rho_{cem}}$$

where ρ_{comp} and ρ_{cem} are the theoretical specific gravity of composites and Portland Pozzolana Cement respectively. Further, according to modified series model, the composite elastic modulus can be written as (*Cox, 1952; Jonathan et al., 2006*):

$$Y_{comp} = \left[\eta_l \eta_0 Y_{cem} - Y_{pp}\right] V_{cem} + Y_{pp} \quad (3.5)$$

where, η_l denotes the length efficiency factor which can be written as

$$\eta_l = 1 - \frac{Tanh\left\{a\left(\frac{l}{d}\right)\right\}}{a\left(\frac{l}{d}\right)} = \frac{e^{2p}(p-1)+(p+1)}{p(e^{2p}+1)}$$

where, $p = a\left(\frac{l}{d}\right)$; $a = \sqrt{\frac{-3Y_{pp}}{2Y_{cem}\, ln(V_{cem})}}$; where, η_0 = 1/5 (Orientation efficiency factor for random orientation) (*Jonathan et al., 2006*).

Theoretical results are obtained using eqn. (3.4) and (3.5) and experimental results have been shown in the Figure 3.12. The experimental results make close agreement to the theoretical results when the aspect ratio (*l/d*) is considered as 45.

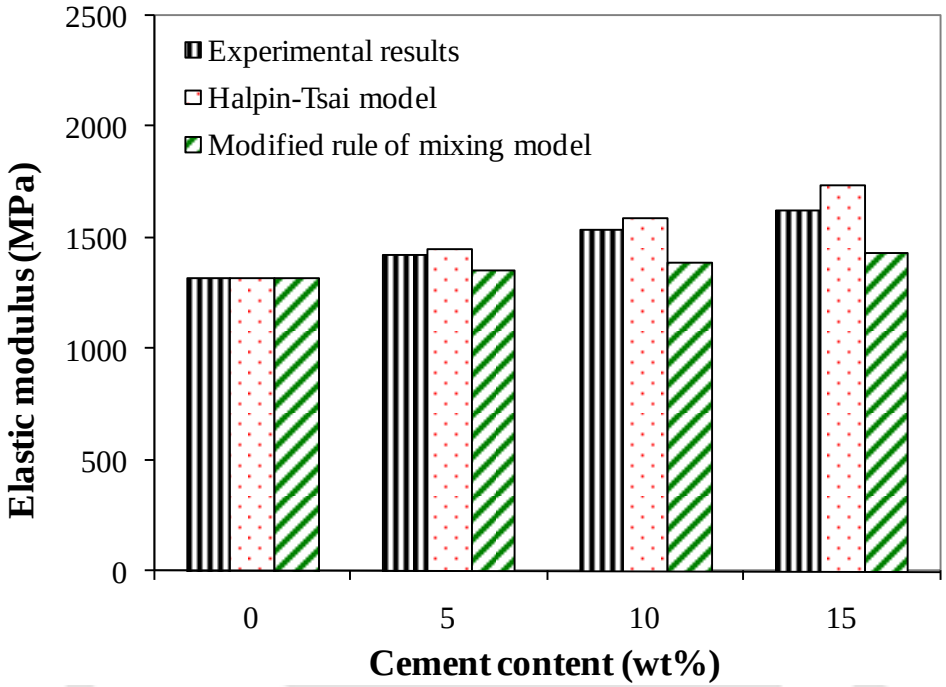

Figure 3.12 Comparison of experimental and theoretical values of Elastic modulus of cement-polypropylene composites

Both models have two factors in common, the stiffness is predicted in a scale taking into account both volume fraction and aspect ratio. In both the cases a more or less linear increase of modulus with volume fraction is predicted. This suggests that a good measure of the reinforcement is given by $\frac{dY_{comp}}{dV_{filler}}$ at low volume fraction of filler (V_{filler}). This takes into account for both the magnitude of the stiffness increase and the amount of fibre required to achieve it and has the advantage that it can easily be extracted from experimental data. The factor, $\frac{dY_{comp}}{dV_{filler}}$ will be used to represent the magnitude of the reinforcement effect. For simplification, this quantity is written as $\frac{dY_{comp}}{dV_{filler}}$ and refer to it as the reinforcement. This will be used to compare the results with the literature. Jonathan *et al.*, (2006) have given the expression of the magnitude of the reinforcement as eqn.(3.6).

$$\frac{dY_{comp}}{dV_{filler}} = \left(\eta_l \eta_0 Y_{filler} - Y_{mat}\right) \tag{3.6}$$

From the eqn. (3.5), it is observed that η_l is the function of V_{filler}, however past works, neglected the counter part of the derivatives of the main eqn. (3.5). Since η_l is the function of V_{filler} the approximate derivatives of the eqn. (3.6) can be expressed as,

$$\frac{dY_{comp}}{dV_{cem}} = \left[\eta_l \eta_0 Y_{cem} - Y_{pp}\right] + V_{cem}\left[\frac{\partial \eta_l}{\partial V_{cem}} \eta_0 Y_{cem}\right]$$

Thus, on substitution the final expression is obtained as, after substituting

$$\frac{dY_{comp}}{dV_{cem}} = \left[\eta_l \eta_0 Y_{cem} - Y_{pp}\right] + \frac{\left[a^2\left(\frac{l}{d}\right)\left(\frac{e^{2a\left(\frac{l}{d}\right)}-1}{e^{2a\left(\frac{l}{d}\right)}+1}\right)^2 + a\left(\frac{e^{2a\left(\frac{l}{d}\right)}-1}{e^{2a\left(\frac{l}{d}\right)}+1}\right) - a^2\left(\frac{l}{d}\right)\right]\eta_0 Y_{cem}^2}{3Y_{pp}\cdot\left(\frac{l}{d}\right)} \tag{3.7}$$

where, *l/d* is the average aspect ratio of the cement particles and $a = \sqrt{\frac{-3Y_{pp}}{2Y_{cem}\, ln(V_{cem})}}$.

Similarly, for the Halpin and Kardos (*Halpin and kardos, 1976*) model, the Halpin-Tsai model for random orientation and the magnitude of the reinforcement is approximated as given below eqn. (3.8):

$$\frac{dY_{comp}}{dV_{cem}} = \frac{3}{8} Y_{pp}\left[\frac{\left(1+2\left(\frac{l}{d}\right)\right)\eta_l}{\left(1-\eta_l V_{cem}\right)^2}\right] + \frac{15}{8} Y_{pp}\left[\frac{\eta_t}{\left(1-\eta_t V_{cem}\right)^2}\right] \tag{3.8}$$

Elastic modulus is calculated using the modified Halpin-Tsai model with varying aspect ratio and represented in the Figure 3.13(a). It is anticipated that the elastic modulus varies with the aspect ratio of the filler materials according to the relationship given in eqn. (3.7). As shown in the Figure 3.13(a), the optimum aspect ratio of the filler materials is calculated as 213 when the modulus is almost saturated. Further, it is also observed that the modulus of the composite depends on the percentage of the filler materials as well and the modulus reinforcement depends on the aspect ratio (Figure 3.13(b)) as well. Modulus reinforcement, $\frac{dY_{comp}}{dV_{cem}}$ is calculated using eqn. (3.7), with Y_{pp} = 1325.286 MPa, Y_{cem} = 20000 MPa for a volume fraction of 1.5667%, 3.2667% and 5.05% of cement. It is interesting to note that

since the modulus reinforcement is a rate of change of elastic modulus with respect to the aspect ratio and do not affect by the filler volume fraction and can be justified from the Figure 3.13(b).

3.4.1 Results and Discussions

As shown in the Figure 3.13(c), the modulus reinforcement versus elastic modulus of all the composite samples show the slope of the straight lines of 5%, 10% and 15% cement filled composite are approximately 89º, 88º and 87º respectively. This signifies that for each 5% cement loading enhancement, the slope decreases by 1º.

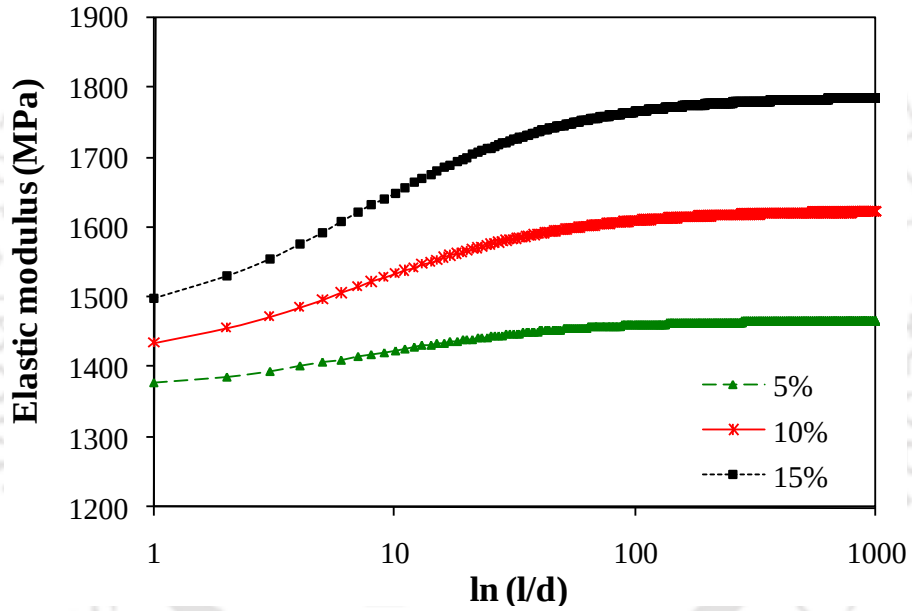

(a)

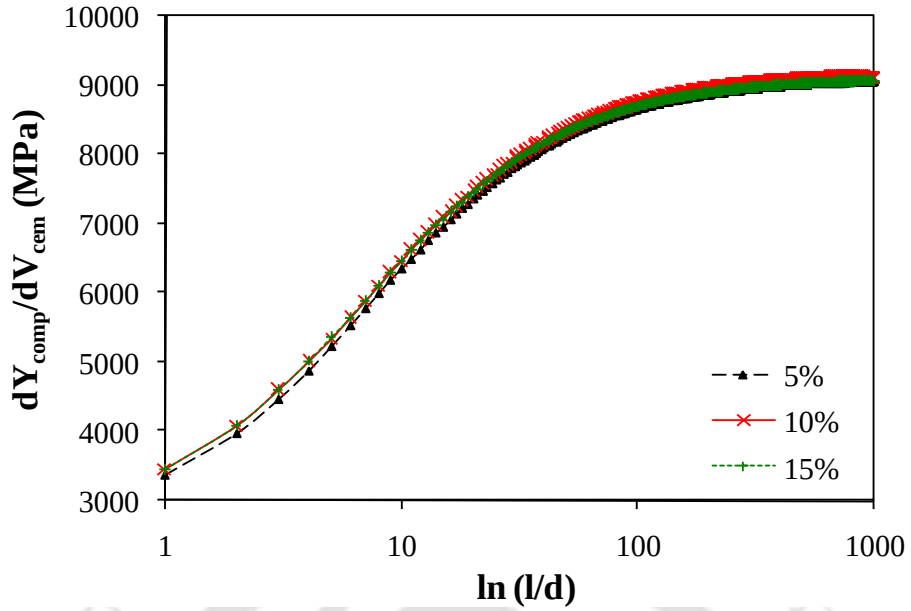

(b)

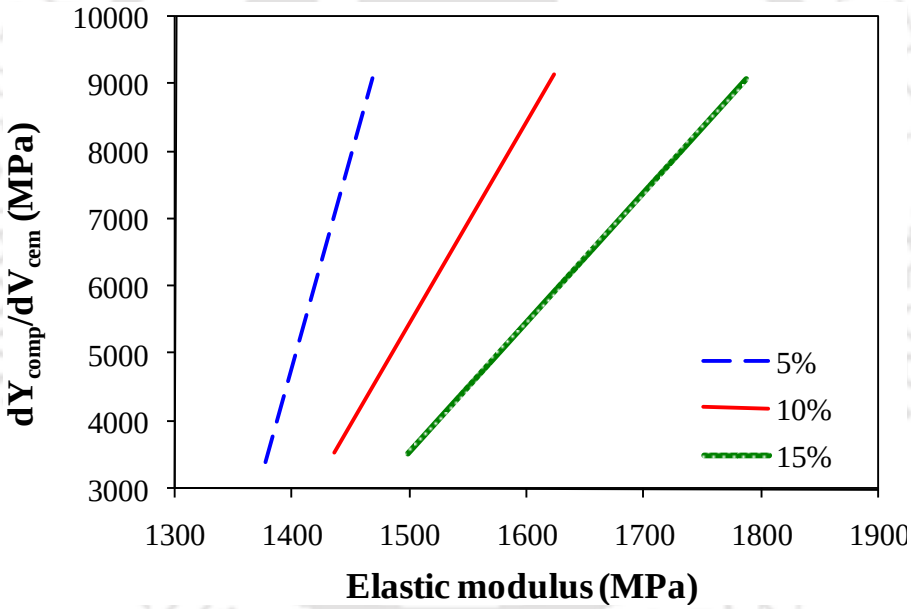

(c)

Figure 3.13 (a) Elastic modulus vs. aspect ratio of composite samples using modified Halpin-Tsai model, (b) Modulus reinforcement vs. aspect ratio plot and (c) Modulus reinforcement vs. elastic modulus

Similarly, the elastic modulus is also calculated using the rule-of-mixing model (*Jonathan et al., 2006*) with varying aspect ratio and presented in the Figure 3.14(a). It is observed that the elastic modulus dramatically varies with the aspect ratio and stabilized when the aspect ratio reaches about 220. Further, from the result, it is also observed that the elastic modulus increases when the filler concentration increases. From the Figure 3.13(a), the optimum aspect ratio of the filler materials is also calculated and approximately 213 when the modulus

is almost saturated. Here, an interesting point i.e, when the aspect ratio is less than 7 the elastic modulus of composite is less than the pure polymer which is insignificant for the composites. At the same time, when the aspect ratio is 7, all the composites (5%, 10% and 15% cement filled composite) are showing approximately the same elastic modulus and is equal to the elastic modulus of pure polypropylene. In addition, it is also observed that the modulus of the composite depends on the percentage of the filler materials as well. Similarly, the modulus-reinforcement is also depends on the aspect ratio (Figure 3.14(b)) where, modulus reinforcement is calculated using eqn. (3.7), on modification of the rule-of-mixing model.

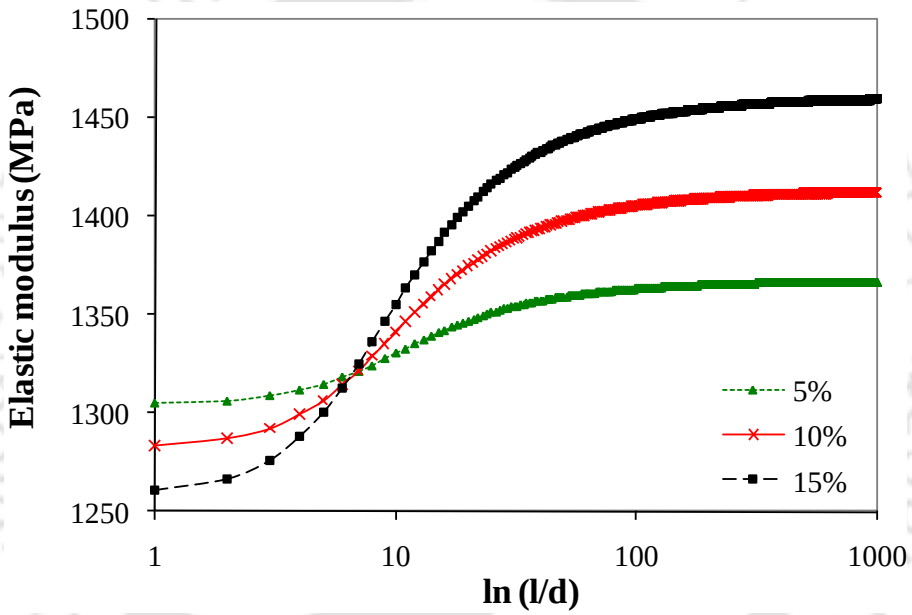

(a)

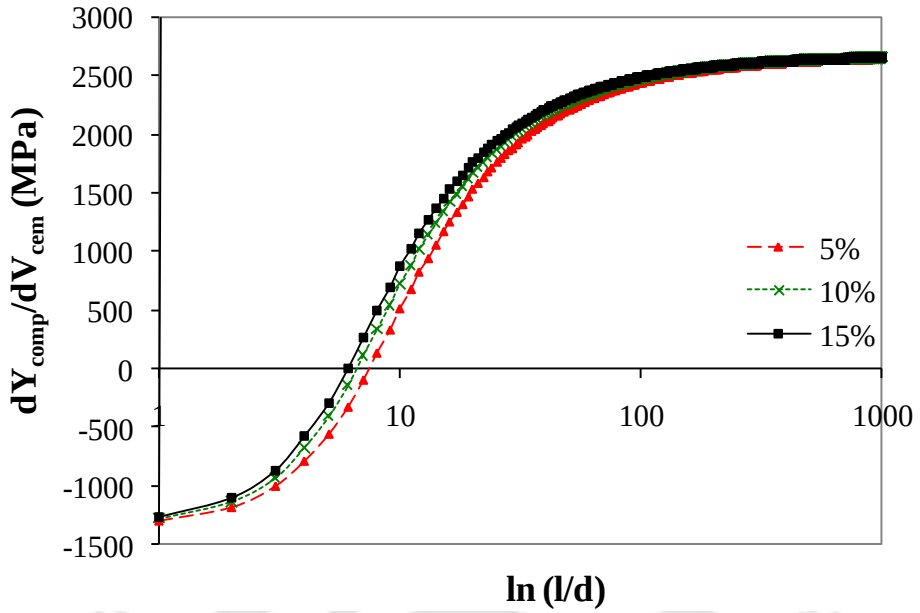

(b)

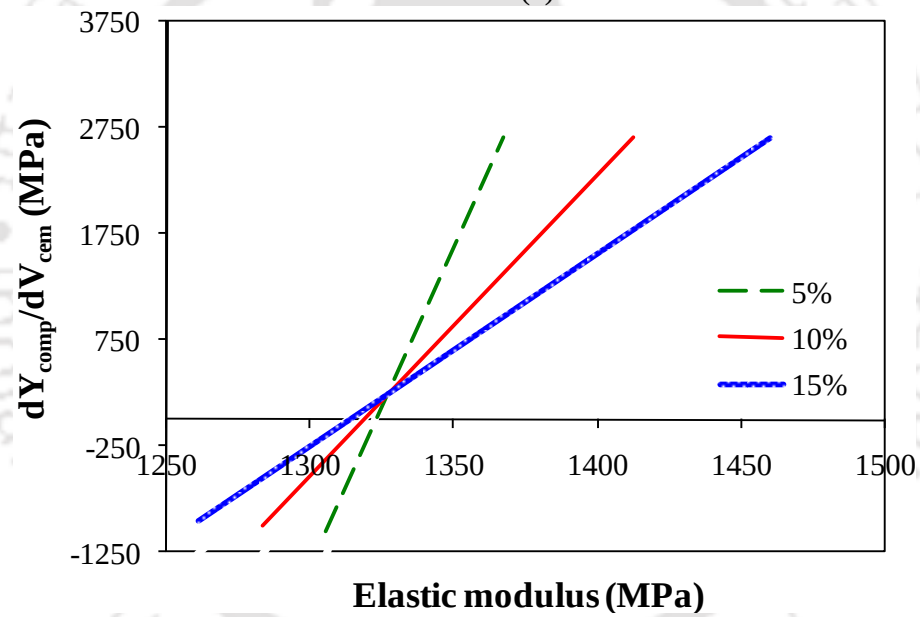

(c)

Figure 3.14 (a) Elastic modulus vs. aspect ratio of composite samples using rule of mixing, (b) Modulus reinforcement vs. aspect ratio and (c) Modulus reinforcement vs. elastic modulus

The approximate derivative of the eqn. (3.5) is expressed as in the eqn. (3.7). The calculation is being done with E_{pp} = 1325.286 MPa, E_{cem} = 20000 MPa for a volume fraction of 1.5667%, 3.2667% and 5.05% of cement materials. It is worth to be noted that the modulus reinforcement or the reinforcement effect is a rate of change of elastic modulus with respect to the aspect ratio and thus remain unaffected by the filler volume-fraction, which is demonstrated in the Figure 3.13(b). While in the case of rule-of-mixing model, with an aspect

ratio range 2-75, the reinforcement effect is observed to be affected by the volume fraction of the filler materials (Figure 3.14(b)).

Similar to the analysis carried out as shown in the Figure 3.13(c), the modulus reinforcement versus elastic modulus of all the composite samples show the linear relationship which is presented in the Figure 3.14(c). The slope of the straight lines of 5%, 10% and 15% cement filled composites are approximately 89º, 88º and 87º respectively. This signifies that for each 5% cement particles increment, the slope is decreased by 1º.

3.5 Summary

In summary, we have vastly investigated the composite materials prepared by incorporating PPC particles of different loading percentage in polypropylene thermoplastic matrix. The mechanical properties of pure polypropylene, 5%, 10% and 15% cement reinforced composites with various circular notch incorporated on the samples are studied, followed by ASTM D638 standard. Experimental results, tabulated in the Table 3.1, indicate that the ultimate tensile strength increased about 4% and 7% for 5% and 10% cement reinforced composite materials respectively as compared to pure polypropylene. However, 18% decreased for 15% cement filled composite is observed due to the brittleness of the material. For circular notch tensile, it is observed that the circular notch size presence onto samples significantly affects the mechanical performance of the materials. The microstructures of the fractured surface of the composite materials have been examined and it is observed that up to a certain percentage of filler, the composite exhibits ductility. Mechanical characterization and analysis of the composites have been carried out and it is observed that with the percentage increase of cement materials, the mechanical properties enhanced up to a certain percentage of filler material. Based on the modified Halpin-Tsai and modified rule-of-mixing series model, the results are further, analyzed. It is observed that the elastic modulus depends on the filler loading as well as the aspect ratio. The comparison between experimental and modified Halpin-Tsai model and modified rule of mixing series model give a close agreement with certain aspect ratio of the fillers. The results validate the assumptions made to derive the equations are closely agreeing with the experimental conditions.

Chapter 4

Design and Fabrication of Composite Material Spur Gear

4.1 Introduction

The demand for seeking alternatives to metallic gears in industry has led to the development of composite material gear. In this work, efforts have been given to develop low cost composite material spur gears using cheap materials i.e., polypropylene as matrix and cement as filler materials. Till date, metallic gears are mostly used in automobiles and industrial applications for their advantages such as durability, availability, smooth workability and reliability on performance. Although, disadvantages such as cost, high wear, more weight to power consumption limits usages of metallic gears in light scale (duty and weight) device applications. To amend these problems, metallic gears can be replaced by composite gears as the latter have certain advantages such as cheaper than metals, less weight to power consumption, durable, ease of processing and fabrication. Past researches show that dramatic enhancement and improvement in mechanical properties achievable by varying small amount of filler particles concentration. The resulting mechanical properties of the composites are closely related to the microstructure achieved in processing of these materials. The mechanical properties of polymer composite depend on the filler-matrix material properties, matrix-to-filler interface and orientation of the filler materials and hence the properties of the end product made govern by the composite used. Luo and Daniel, (*2003*) has shown, higher composite modulus can be achieved for randomly oriented filler composite by controlling and maintaining high dispersion rate. Mechanical characteristics of the material mostly depends on the microstructure and the strength of the bond between the filler- to-filler directly or filler to filler via matrix (*Chabert et al., 2003*). Maleic anhydride (grafted polypropylene; non-polar nature) is mostly used for attaining homogeneous dispersion of filler in the polypropylene matrix and to ensure proper bonding between the polypropylene matrix and filler materials (*Raka et al., 2009; Gutiérrez et al., 2010; Fung et al., 2003*).

The temperature dependent dynamic parameters like dynamic modulus, storage modulus, loss modulus and loss factor provides knowledge of relations between the polymer matrix and the filler. Even though, it is observed that failure of the composite depends on the percentage of filler materials incorporated into the matrix, however, most of the cases, the high percentage of filler materials decreases the ductility of the materials (*Sohn et al., 2003*).

Until now, huge progress has been made in forming micro/meso scale devices using the methodology and materials such as gears adopting molding, electroforming processes using electro-platable metals, alloys and poly-methylmethacrylate (PMMA) (*Sun et al., 2009*). The choice of composite materials applications in fighter aircraft was perceived by a need to reduce weight and to improve strength, reliability and maintainability suitable for aerospace applications. The F-22 fighter aircraft has demonstrated the feasibility and benefits of introducing processes such as resin transfer molding (RTM) to improve the affordability of composite materials in combat aircraft applications. Further, these composite materials not only reduce the weight but also possess excellent characteristics of corrosion and fatigue resistant. In addition, significant contribution can be achieved by designing composite materials which proves superior cost-effectiveness compared to conventional metals (*Deo et al., 2001; Anon, 1999*). A composite landing gear component for a fighter aircraft was developed as replacement of a steel component using resin transfer molding (RTM) technique for fabrication of structural components. The objective was to achieve a weight reduction of 20% and a cost reduction up to 15% (*Thuis, 2002*).

Further, past researches show that few works have been carried out to evaluate the dynamic mechanical properties of the composite materials used for fabrication of gears. In addition, few works deal with the failure analysis and the resulting topographical structures of the composite materials. This motivates to explore the grey areas exist on design and development of low-cost nonmetallic mechanical parts such as gear suitable for lightweight industrial application. Thus, it is relevant to try very inexpensive materials such as polypropylene and cements for design and development of composite materials and finding suitable applications of it. The particle size distribution of Portland cement particles is in the range of 0.1 to 100 μm and the aspect ratio (L/W) i.e. length/width ratio varies between 1.27 - 1.46. A literature has been added into the texts, where much more in-depth analysis has been made on particle size distribution (PSD) and particles shape (*Holzer et al., 2010*). In this work, a new type of polymeric composite gear is fabricated using fly ash based cement particles as a reinforced material into polypropylene matrix followed by injection molding process.

The main objectives of this work are:

(i) Fabrication of a low cost composite material spur gear alternative to metallic gear

(ii) Experimental evaluation and optimization of compositions for gear material and tooth performance analysis

Composite gear materials of three weight percentages of fillers are prepared and tested under dynamic load to evaluate the mechanical properties. Morphological analysis is carried out by scanning electron microscope (SEM) and field-emission SEM (FE-SEM) to investigate the topographical features of the fractured surface and deformed gear tooth, bonding between fillers and the matrix, dispersion and failure mechanism. Further, dynamic mechanical analysis (DMA) has been carried out to study the viscoelastic properties of the composite and the effect of temperature on it during loading. The experimental study and obtained results are instrumental to select the right combination of constituent materials for fabrication of the proposed gear. Gear tooth performance is evaluated by using Instron universal machine applying direct load on the tooth and also fatigue testing the gears tooth under dynamic load. The experimental study and the results indicate that the developed gear is suitable for academic and industrial application. In addition, a theoretical model has been developed following the Hertz contact theorem that describes the stress profile along the tooth contact region of two meshed gear.

4.2 Manufacturing of Composite Spur Gear

The materials required for fabrication of composite gears include, the graded homopolymer, H110MA, is (purchased from Reliance Industries Ltd.) having the characteristics like melt flow index (MFI) (at 230°C / 2.16kg) and heat deflection temperature (at 455 kPa) are 11/10 (g/min) and 104^0C respectively. The grafted polypropylene (OPTIM-P-425) is used as bond enhancer i.e. improves the quality of bonding (*Cai et al., 2007*) between the matrix and the fillers. The detail schematic representation of fabrication of composite material spur gear is shown in the Figure 4.1. Initially, cement solution is prepared using distilled water with water to cement particles is taken as 3:1 proportion. All the subsequent step-by-step procedures are followed up and schematically represented in the Figure 4.1.

The schematic layout of preprocessing of gear materials before starting of the injection molding and the injection molding setup has been discussed and has been shown in the chapter 2, Figure 2.1 and Figure 2.2. The details of the molding setup are maintained such as injection screw diameter: 32 mm; screw length to diameter (L/D) ratio is 16. Temperatures of the three consecutive heaters are maintained at 220ºC, 225ºC and 230ºC from entrance to the sprue accordingly, while, the sprue (nozzle) temperature is preset to 50ºC. Other injection parameters are adjusted to: injection shot capacity 100 g/s, injection pressure 6 MPa, injection time 8s, cooling time 12s and mold temperature 28ºC.

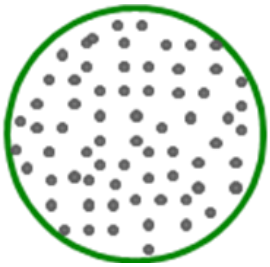 Step I	Portland pozzolana cement particles are used as filler materials with polypropylene matrix.
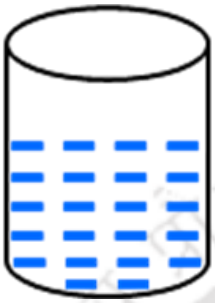 Step II	Distilled water is prepared in the laboratory, using a portable unit of distilled water plant. Distilled water is then used to prepare the cement solution in an ultrasonic chamber.
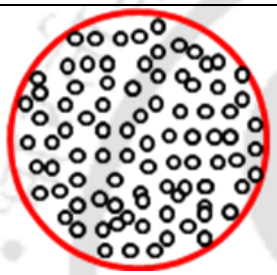 Step III	Polypropylene granules are mixed with the liquid cement solution and stirred subsequently for better adhesion.
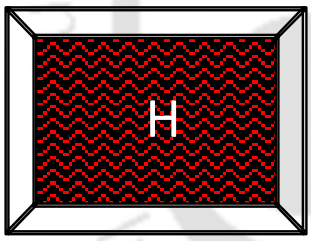 Step IV	Hot plate is used to evaporate the water, maintained at 100ºC. In a process cement particles are coated on the surface of the polypropylene granules.
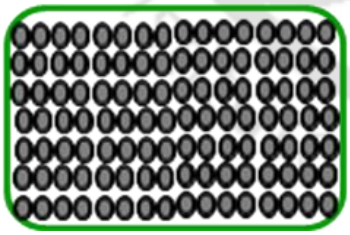 Step V	Cement coated polypropylene granules are then collected in a tray and prepared to be fed into injection molding machine.
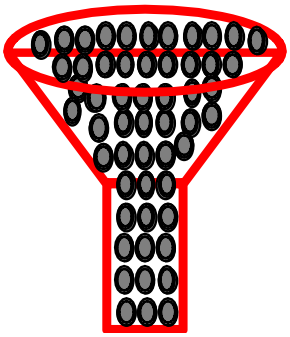 Step VI	Before feeding into the injection molding machine, the processed cement coated granules are dried in the injection molding hopper at 80ºC for 2 h. Subsequently, the materials are then fed into the machine.

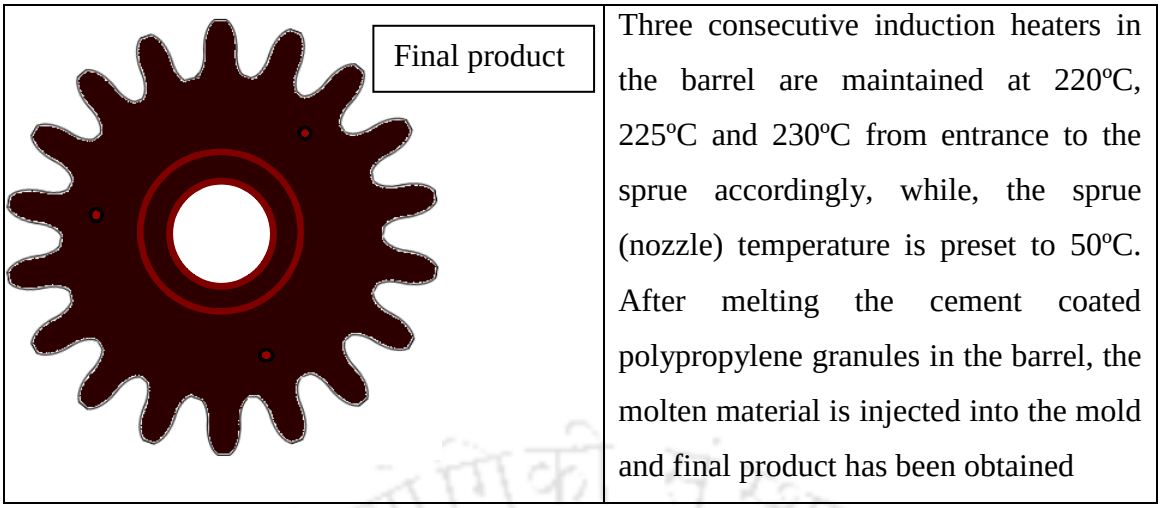

Figure 4.1 Flow chart for cement filled polypropylene composite gear fabrication

4.3 Experimental Study: Optimization of Gear Materials

4.3.1 Tensile Properties

The tensile mechanical properties of the gear materials are studied by using Instron universal testing machine (ASTM D638) digitally controlled by the closed loop servo hydraulic dynamic machine (100 kN, maker, Instron, model no. 8801) with a cross head speed of 1 mm/min at room temperature. Figure 4.2(a) shows the schematic diagram of the test specimen of gear material, Figure 4.2(b), (c) and (d) are showing the various stage results after the samples are deformed while Figure 4.2(e) shows the deformed specimen with setup under testing. It is observed that with 5 % and 10 % cement filled gear materials experienced ductile failure while 15 % cement filled gear material exhibits the brittle fracture. Thus, it is observed that as the percentage of the cement fillers increases, the ductility of the composite material decreases while brittleness improved and reaches an optimal value.

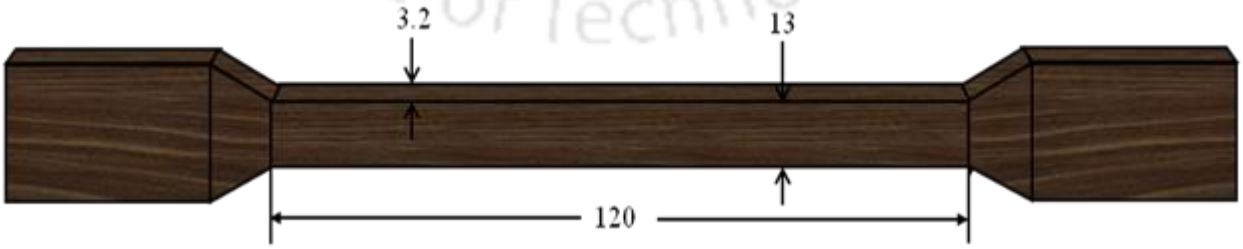

(a)

(b) (c) (d)

(e)

Figure 4.2 (a) Schematic of tensile test sample (all dimensions are in mm) and (b) 5%, (c) 10% with ductile failure, (d) 15% cement filled composite gear materials undergoes brittle failure under tensile load and (e) tensile failure of the 10% cement reinforced composite specimen on the experimental setup

After tensile failure, experimental data are collected at constant rate of elongation (CRE) of 1 mm/min and the true stress and true strain % are calculated using eqn. 4.1(a) and eqn. 4.1(b) as (*Ling, 1996*):

$$\sigma = S(1+e) \quad 4.1(a)$$

$$\varepsilon = ln(1+e) \quad 4.1(b)$$

Where, engineering stress and strain are denoted by 'S' and 'e' respectively. Figure 4.3 shows the true stress and strain behavior of the composite materials under uniaxial tensile

load. It is observed that modulus of elasticity increases with % increase of cement particles leads to % decrease of strain value. For pure polypropylene and 5%, 10%, 15% cement filled composite gear materials, modulus of elasticity are obtained as 1325.29, 1430.56, 1540.5, 1629.48 MPa respectively.

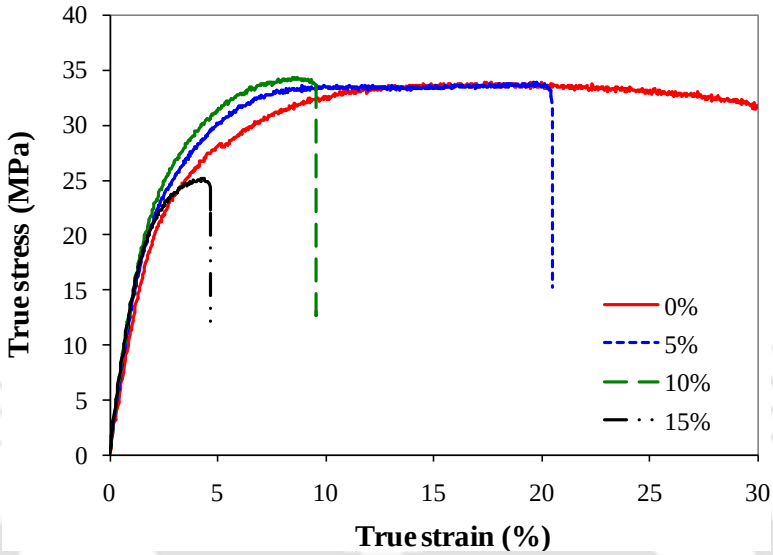

Figure 4.3 True stress-strain behavior of polypropylene and other composite gear materials

In the Figure 4.4(a), the variation of ultimate tensile strength and elastic modulus of composite gear materials of different compositions are shown. The tensile test results are given in the Table 4.1. Figure 4.4(b) shows the change in load bearing capacity as well as 0.2% yield strength of the material with respect to the percentage of cement fillers loading. It is observed that ultimate tensile strength increases by 4% and 7% as the filler percentages changes from 5% to 10% respectively. Further increase in fillers loading decreases the tensile strength by 18% for 15% composite material. Also, the modulus of elasticity of gear materials changes remarkably with higher loading of cement particles in the polypropylene matrix. With 5%, 10% and 15% of cement fillers loading, it is observed that the elastic modulus of the composite increases by 8%, 16.24% and 23% compared to 100% polypropylene.

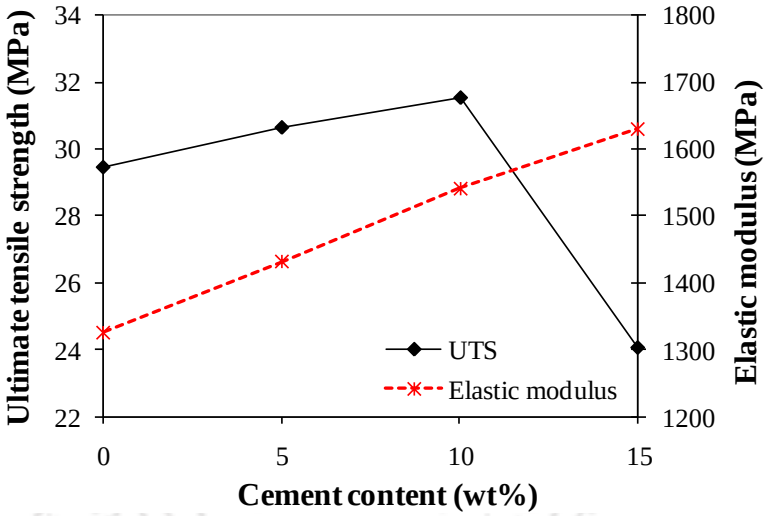

(a)

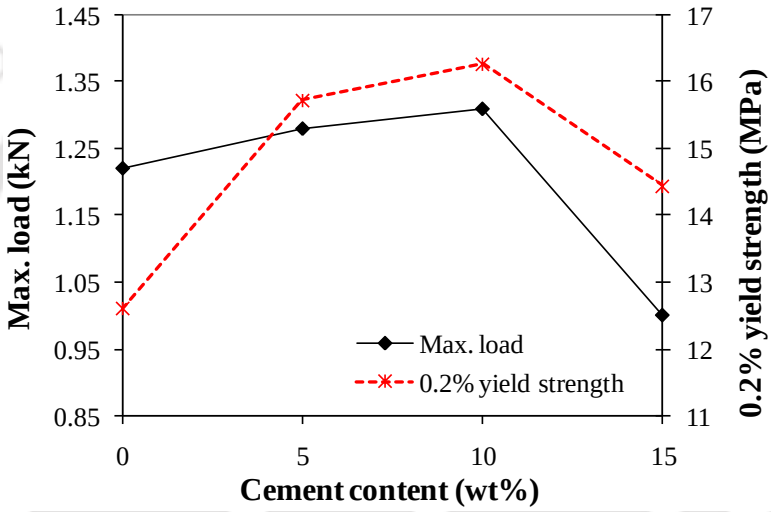

(b)

Figure 4.4 (a) Ultimate tensile strength and elastic modulus, (b) variation of maximum load and yield strength at 0.2% offset with the filler % of composite materials

Table 4.1 Tensile test results of cement reinforced composite materials

Filler	UTS (MPa)	SD	Modulus of elasticity (MPa)	SD	Max. Load (kN)	SD	0.2% Yield Strength (MPa)	SD
0%	29.44	1.40	1325.29	2.25	1.22	1.85	12.60	1.64
5%	30.65	2.02	1430.56	3.05	1.28	2.12	15.73	1.52
10%	33.52	1.58	1540.5	2.12	1.31	1.78	16.27	2.03
15%	24.07	2.11	1629.48	2.23	1.00	1.88	14.44	1.97

In comparison, Figure 4.4(b) shows the variation of maximum load and yield strength at 0.2% offset value. It is observed that for 5 % and 10 % cement particles filled gear materials,

maximum increase in load remains relatively constant to 7.35%, while further increase in fillers to 15% reduces 18% of the maximum load. Similar characteristics are also observed as the yield strength increases to 24.8% and 29% when filler loading varies from 5% to 10% with 0.2% offset.

Thus, the results show significant improvement in mechanical properties as the filler loading percentages go up to 10%. It is anticipated that good interfacial bonding between polypropylene matrix and cement particles and better distribution of the fillers results in easy transfer of load from matrix to reinforcing element. The tensile modulus of the composite gear materials increases with an increase of cement particles loading (%wt) in polypropylene matrix. In the case of ultimate tensile strength (UTS), the trend is also increasing when the loading percentage of cement particles increased but up to a certain amount. The composite material of 10% of cement fillers is showing the highest value. Hence; further addition of loading up to 15% is showing the negative trends for ultimate tensile strength.

Materials and geometry of the composite gear significantly influence energy storage and gear performance. To imply appropriate material for the gear, specific strain energy of the cement particles filled polypropylene composite materials are considered. According to Yu and Kim, (*1988*), amount of specific elastic strain energy stored in a system is given as in the eqn. (4.2).

$$\gamma_{se} = \frac{\sigma_{max}^2}{2\rho E} \tag{4.2}$$

where, E denotes the modulus of elasticity of the material, ρ refers the density of the material and σ_{max} is the maximum allowable stress of the material. The above equation depicts that most appropriate material for the gear application must have maximum strength with reasonable modulus of elasticity. As shown in the Figure 4.5, the 10% cement particles filled composite gear material gives high specific elastic strain energy; make it suitable as a potential gear material for lightweight application. Hence, it is anticipated that, in dynamic loading, due to high specific strain energy of the specified material, the fatigue characteristics will be enhanced.

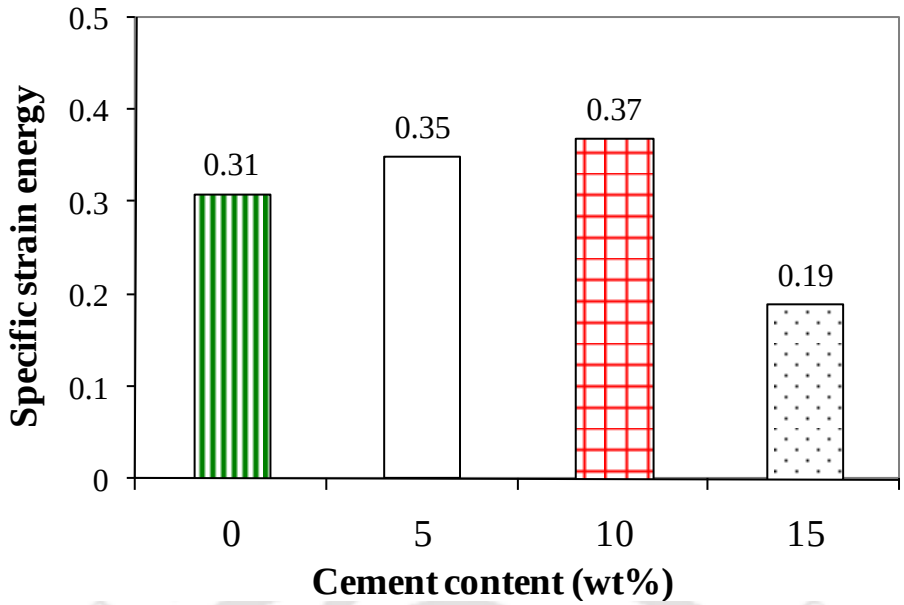

Figure 4.5 Variation of specific strain energy of composite materials with percentage cement loading

4.3.2 Morphological Analysis of Fractured Surface of Gear Materials

Morphological analysis of fractured surface of the gear materials is essential to understand the homogeneity of dispersion of fillers and the presence of defects that may results under loading, contribute to the failure of the gear.

The test is conducted under LEO 1430 VP scanning electron microscope (SEM) supplied by LEO Electron Microscopy Inc. Fractured surface of the specimen is prepared by gold coating (as the composite is non-conductive) and examined under high voltage (15kV) with 1000 X magnification. Figure 4.6 (a), (b) and (c) illustrate the SEM micrograph of the fractured surface of 5%, 10% and 15% cement particles filled polypropylene gear materials respectively. The result shows adequate dispersion of cement particles in the polypropylene matrix, validate the fair bonding between the matrix and filler material. The results show the change in microstructure of the composites when it undergoes fatigue failure under dynamic loading condition. It is further expected that the bonding is improved and enhanced due to the presence of grafted polypropylene. Figure 4.7 shows the corresponding EDX (energy-dispersive X-ray) graph of the fractured surface of the 15% cement particles filled gear material, which reveals the presence of the amount of cement particles constituents (Table 4.2). These morphological features of composite determine the behavior of the fabricated spur gears during fatigue or fracture failure when it runs under dynamic loading.

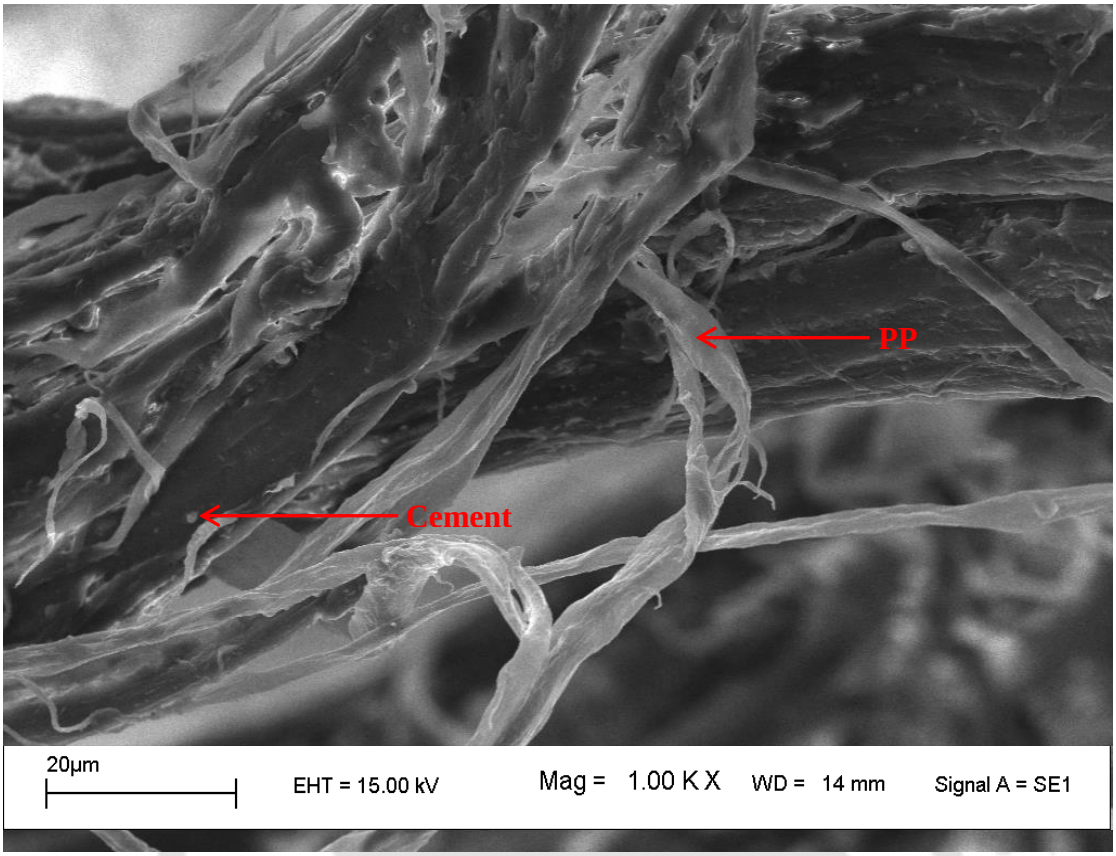
PP
Cement
20µm
EHT = 15.00 kV
Mag = 1.00 K X
WD = 14 mm
Signal A = SE1

(a)

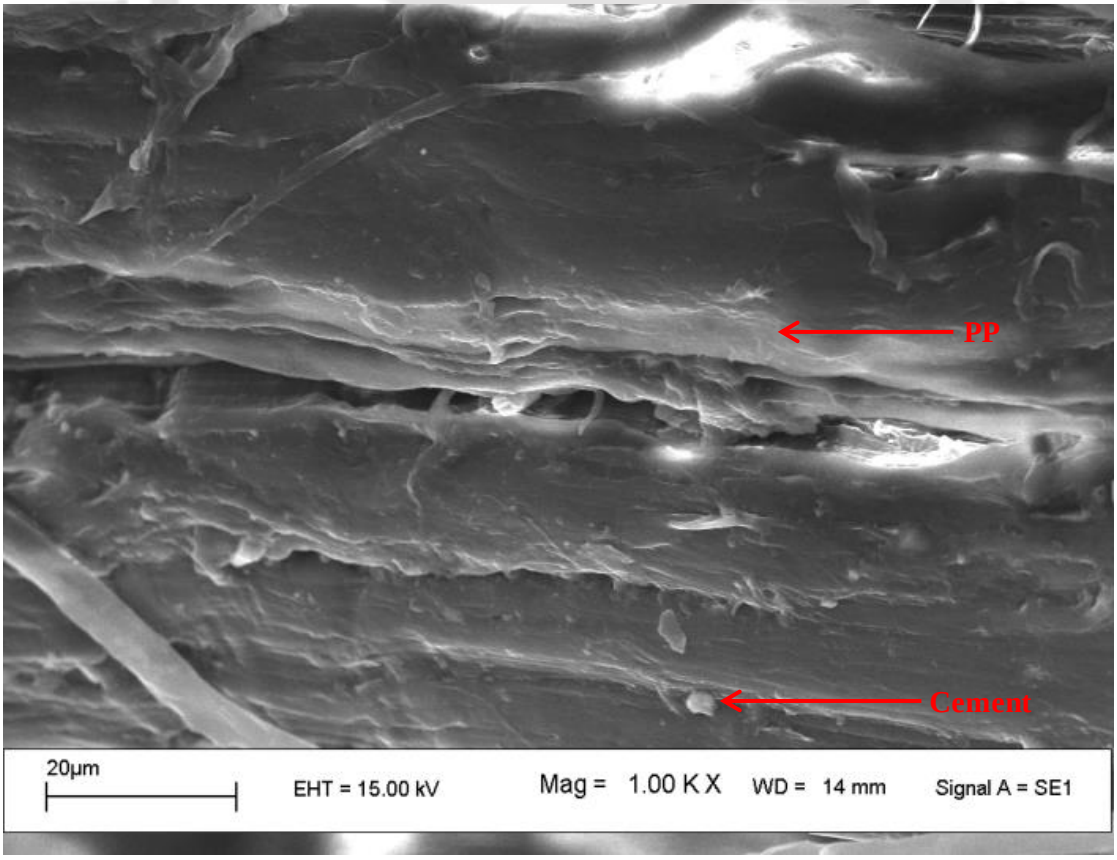
PP
Cement
20µm
EHT = 15.00 kV
Mag = 1.00 K X
WD = 14 mm
Signal A = SE1

(b)

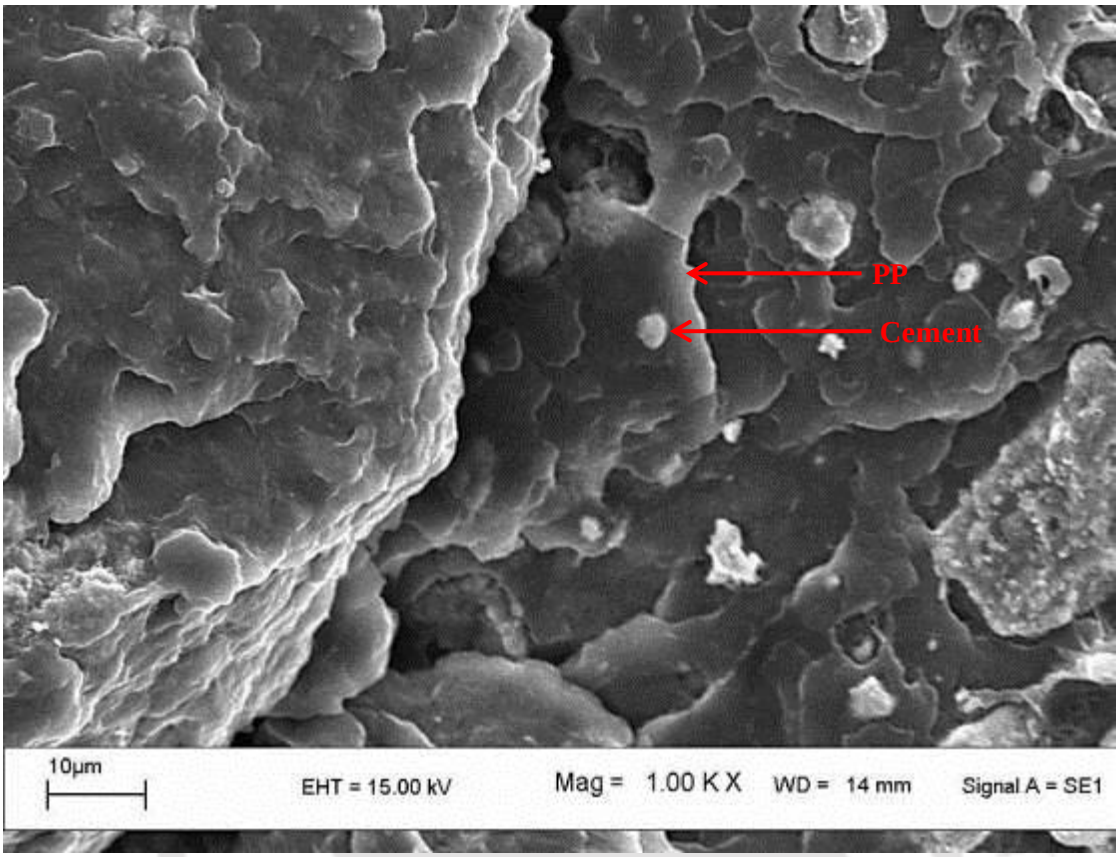

(c)

Figure 4.6 SEM image of the fractured surface of (a) 5%, (b) 10% and (c) 15% cement filled composite materials

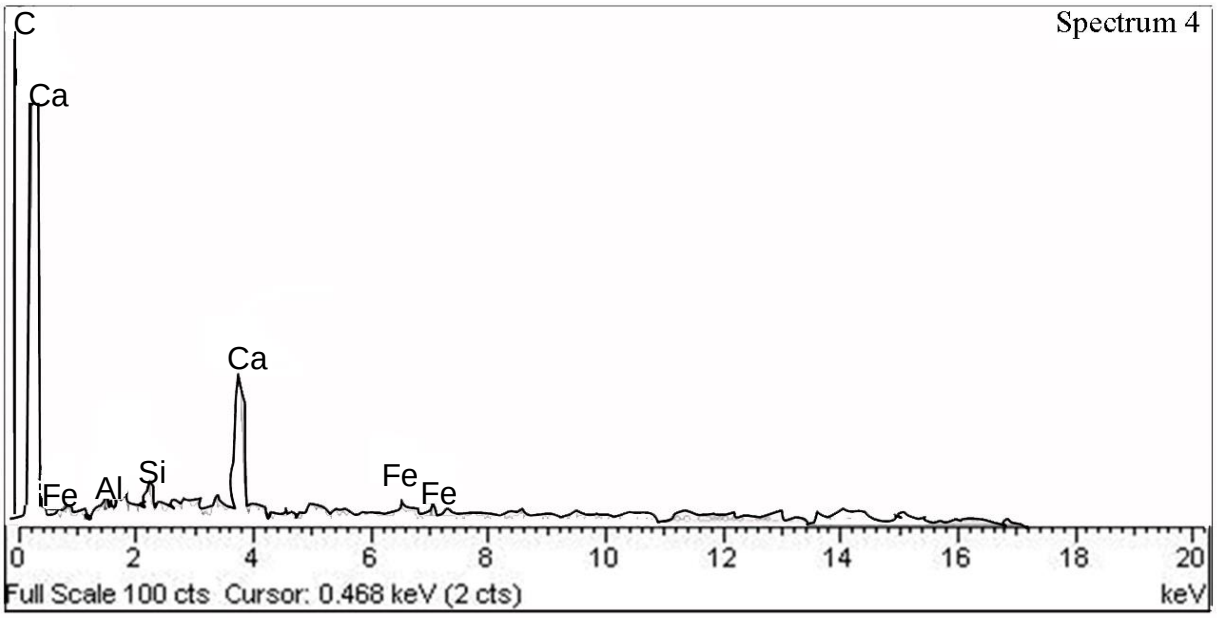

Figure 4.7 EDX graph of the fractured surface corresponding to Fig. 4.6(c) i.e. 15% cement filled composite gear material

Table 4.2 Amount of constituents present in the fractured surface of 15% cement filled composite material

Element	CaCO3	Al2O3	SiO2	Ca (Wollastonite)	Fe
Weight (%)	56.3	0.06	1.41	39.25	3.21
Atomic (%)	80.84	0.04	1.06	16.31	2.01

It is clearly observed that the mechanical properties show significant improvement with increment of cement loading percentages up to 15 %. It is anticipated that good interfacial bonding between polypropylene matrix and cement particles and better distribution of the same filler results in easy transfer of load from matrix to reinforcing element. Hence, the study of mechanical properties of composites reveal that the change in particular properties is observed remarkably for 10% of cement loading.

4.3.3 Prediction of Mechanical Properties Materials Based on Experimental Results

The tensile modulus of the composites increased with an increase of cement loading (% wt) in polypropylene matrix as illustrated in the Figure 4.4(a). In the case of ultimate tensile strength (UTS), the trend is also increasing when the loading percentage of cement increased but up to a certain amount. Up to 10% of cement loading, tensile strength of the composite is showing the highest value. Further, with increment of loading percentage i.e. 15% is showing the negative trend for ultimate tensile strength. Thus, it is essential to establish a relationship with the wt% of cement loading and with other mechanical properties such as elastic modulus, ultimate tensile and yield strength that helps to find out the suitable composition for development of composite materials. Second order polynomial curves have been fitted to get the approximate relation between elastic modulus (Y), ultimate tensile strength (σ_{uts}) and 0.2% yield strength ($\sigma_{0.2\%ys}$) with loading percentage of cement (% wt) which are given in the eqn. (4.3), (4.4) and (4.5) respectively.

$$Y = -0.1629W_c^2 + 22.894W_c + 1324 \qquad R^2 = 0.99 \qquad (4.3)$$

$$\sigma_{uts} = -0.0866W_c^2 + 0.9942W_c + 29.041 \qquad R^2 = 0.98 \qquad (4.4)$$

$$\sigma_{0.2\%ys} = -0.0496W_c^2 + 0.865W_c + 12.612 \qquad R^2 = 0.98 \qquad (4.5)$$

where, R^2 is the quality factor of the curve fit. The unit of Y, σ_{uts} and $\sigma_{0.2\%ys}$ is in MPa. These theoretical relationships are essential to find out the approximate change of the mechanical

properties with respect to the cement loading percentage without the need of experimental study. Thus, obtained results based on the relationship as in eqn. (4.3), (4.4) and (4.5) provide the measure of the cement loading for obtaining optimal mechanical properties of the composite as shown in the Figure 4.8. It is further observed that the maximum cement loading can be made up to 23%. Beyond which, the UTS of composite material is leaser than the 0.2% yield strength, subjected to the condition is that the elastic modulus increases with cement loading.

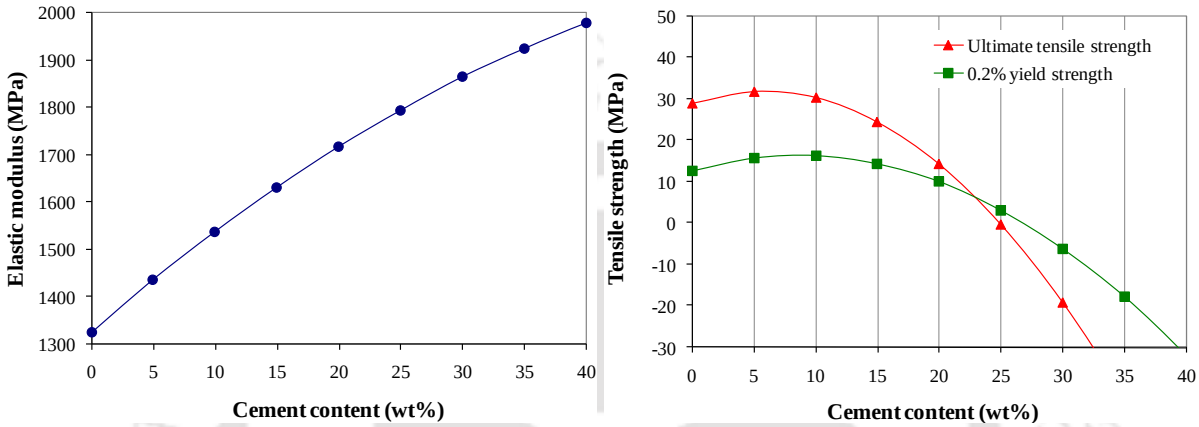

Figure 4.8 (a) Graphical representation of eqn. (4.3) and (b) Graphical representation of eqn. (4.4, 4.5)

It is anticipated that improper bonding between polypropylene matrix and cement particles due to the agglomeration of the filler causes the severe fall in composite tensile strength, maximum load carrying capacity and also the yield strength beyond 15% cement loading. Only increase of the elastic modulus is attributed due to the brittleness of the sample at highest loading (15%) of cement particles in the polypropylene matrix. It is further anticipated that poor interfacial adhesion enhances the debonding between polymer and filler material as the percentage of cement loading increased led to large agglomeration of filler materials into the polymer matrix system. Comparing with experimental results, 10% cement filled composite properties give close agreement with the theoretical results.

4.3.4 Dynamic Mechanical Analysis (DMA) of Gear Materials

It is essential to know the dynamic mechanical properties of the viscoelastic composite material before its application in vibration prone dynamic condition. This consequence leads to understand the storage and loss modulus of the material and it can be attributed implying specific vibration as well as thermal mode. Dynamic modulus can be defined as the ratio of stress to strain in vibration system. The storage modulus can be measured as the stored

energy, representing the elastic portion, whereas loss modulus is measured as the dissipated heat energy, representing the viscous portion. DMA is carried out on gear composite materials in dry condition. The test is conducted in open environment in tensile mode with 10 mm span length. Dynamic force of magnitude 100 mN is applied over a temperature range of 15-90ºC in EXSTAR TMA/SS 6000 instrument. The stress frequency is taken as 0.02 Hz while the heating rate is kept constant at 5°C min^{-1}. Figure 4.9 shows the specimens prepared for the DMA test.

Trend of loss factors of all the specimens are found to be increasing with the increase in temperature and this behavior is due to the matrix softening which results in increased molecular mobility at elevated temperature as shown in the Figure 4.10(c). The change in storage modulus with temperature is demonstrated in the Figure 4.10(a), while, Figure 4.10(b) demonstrates the dynamic loss modulus for both polypropylene and other gear materials with temperature. These results suggest that composite gear materials having improved stiffness and better thermal stability than pure polypropylene which validates the suitability of the gear application under dynamic loading condition with fluctuating temperature.

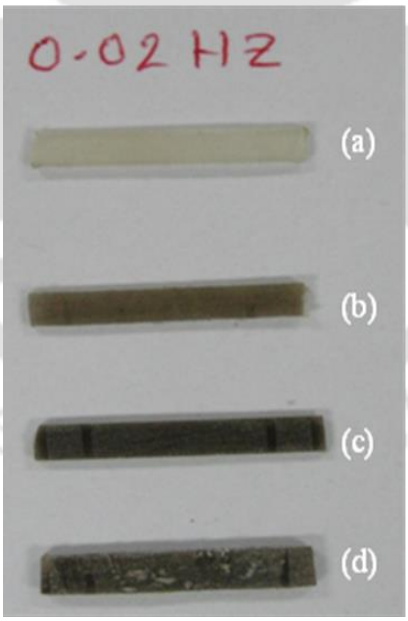

Figure 4.9 DMA test composite samples, (a) polypropylene, (b) 5%, (c) 10% and (d) 15% cement filled composites

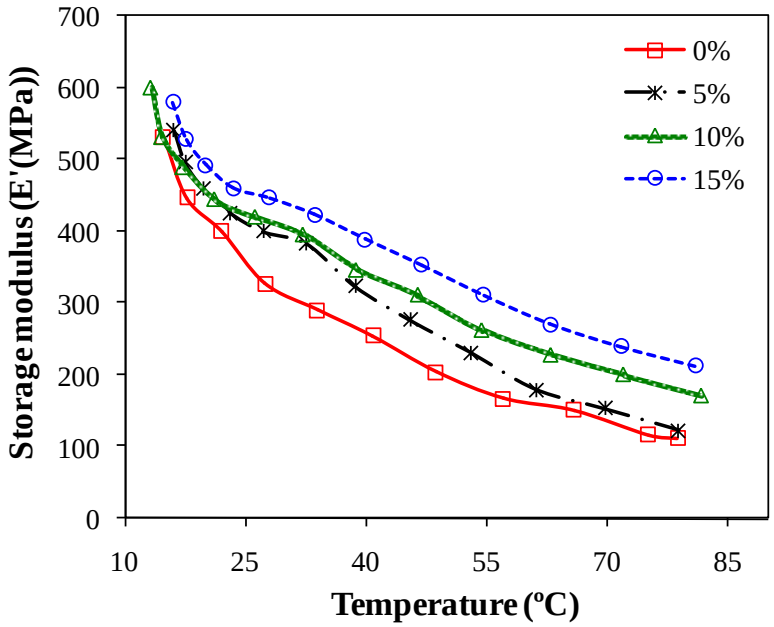
Storage modulus (E'(MPa))
700
600
500
400
300
200
100
0
10
25
40
55
70
85
Temperature (ºC)
0%
5%
10%
15%

(a)

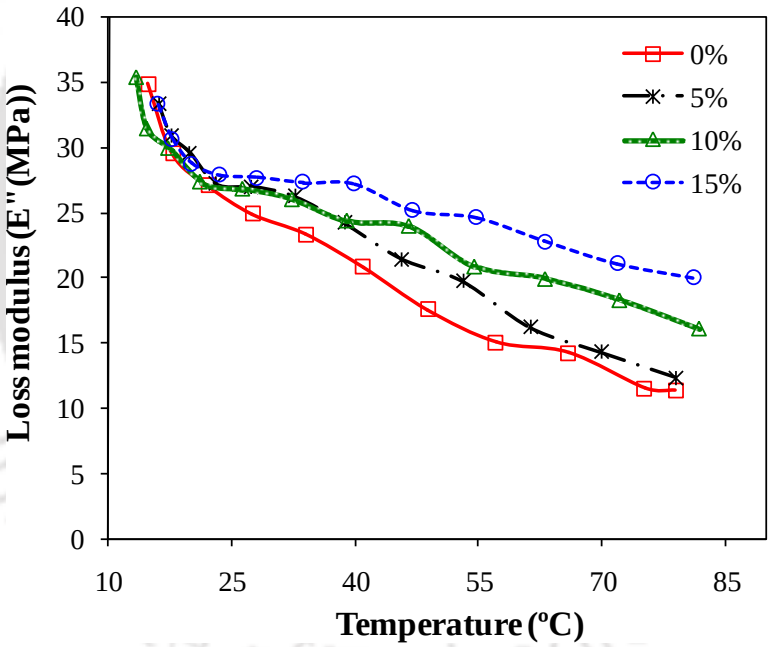
Loss modulus (E''(MPa))
40
35
30
25
20
15
10
5
0
10
25
40
55
70
85
Temperature (ºC)
0%
5%
10%
15%

(b)

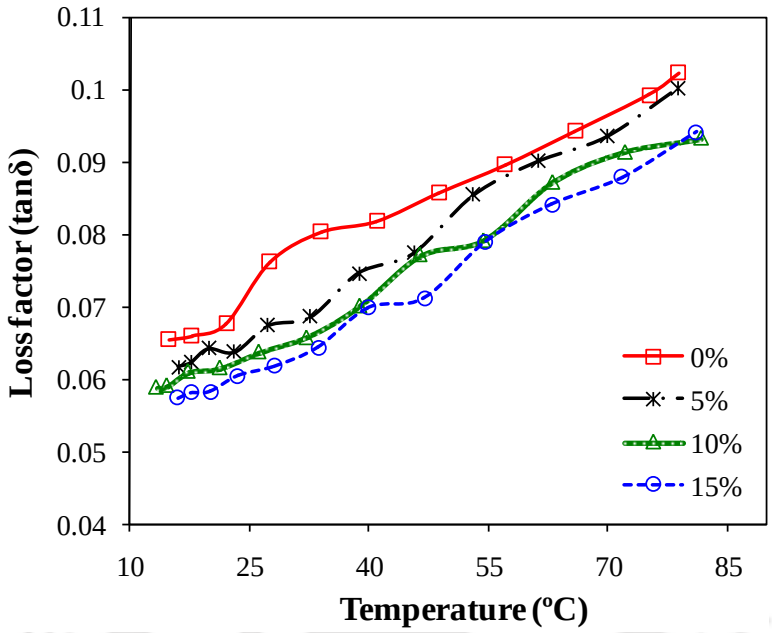

(c)

Figure 4.10 (a) Change in storage modulus of the materials, (b) Loss modulus of composite materials at various temperatures and (c) Variation of loss factor of composite gear materials with temperatures

Thus; from the experimental results i.e. mechanical properties, morphology of the fractured surface and the dynamic-mechanical analysis of the gear materials, it is observed that the 10% cement particles filled composite material shows optimal characteristics. Hence, 10% cement particles filled composite material is chosen to fabricate the composite spur gears.

4.4 Gear Tooth Performance under Loading

Detail schematic configurations and specifications of the fabricated composite spur gears are shown in the Figure 4.11 and Table 4.3 respectively. The fabricated composite gear samples are shown in the Figure 4.12(a) to Figure 4.12(d).

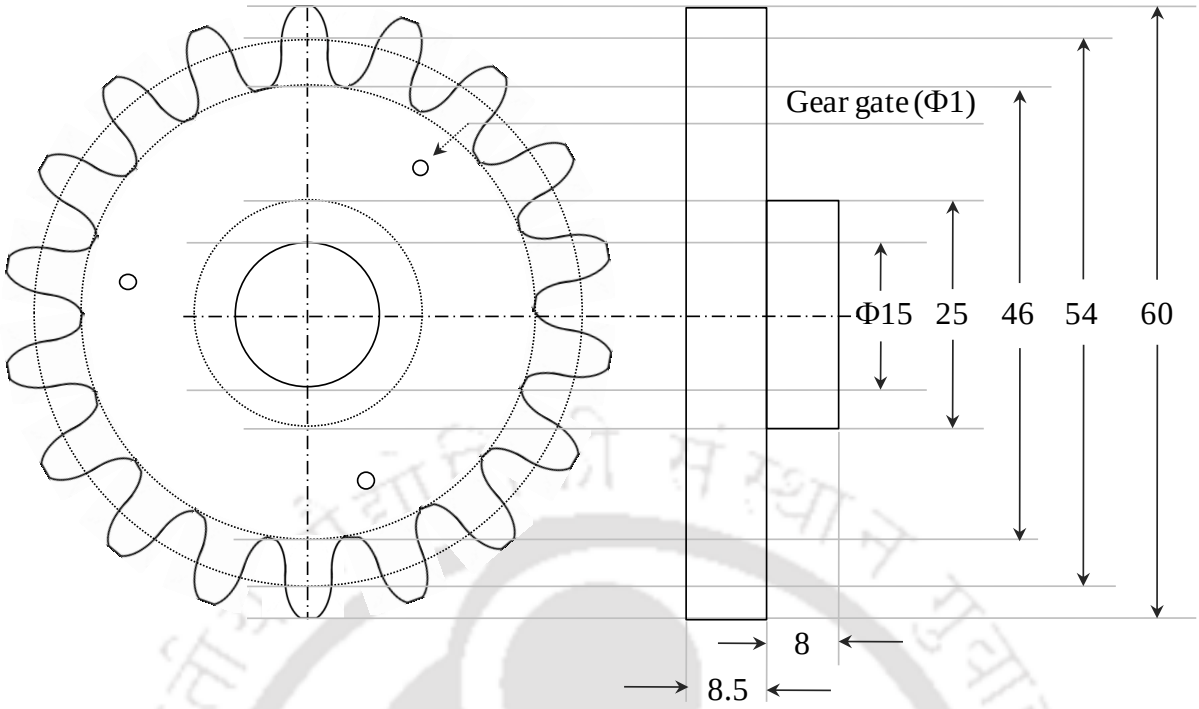

Figure 4.11 Schematic configurations of fabricated spur gear

Table 4.3 Parameters of the fabricated gear

Specification	Value and unit
Number of teeth	18
Module	3 mm
Face width	8.5 mm
Base circle diameter	46 mm
pitch circle diameter	54 mm
Outer tooth diameter	60 mm

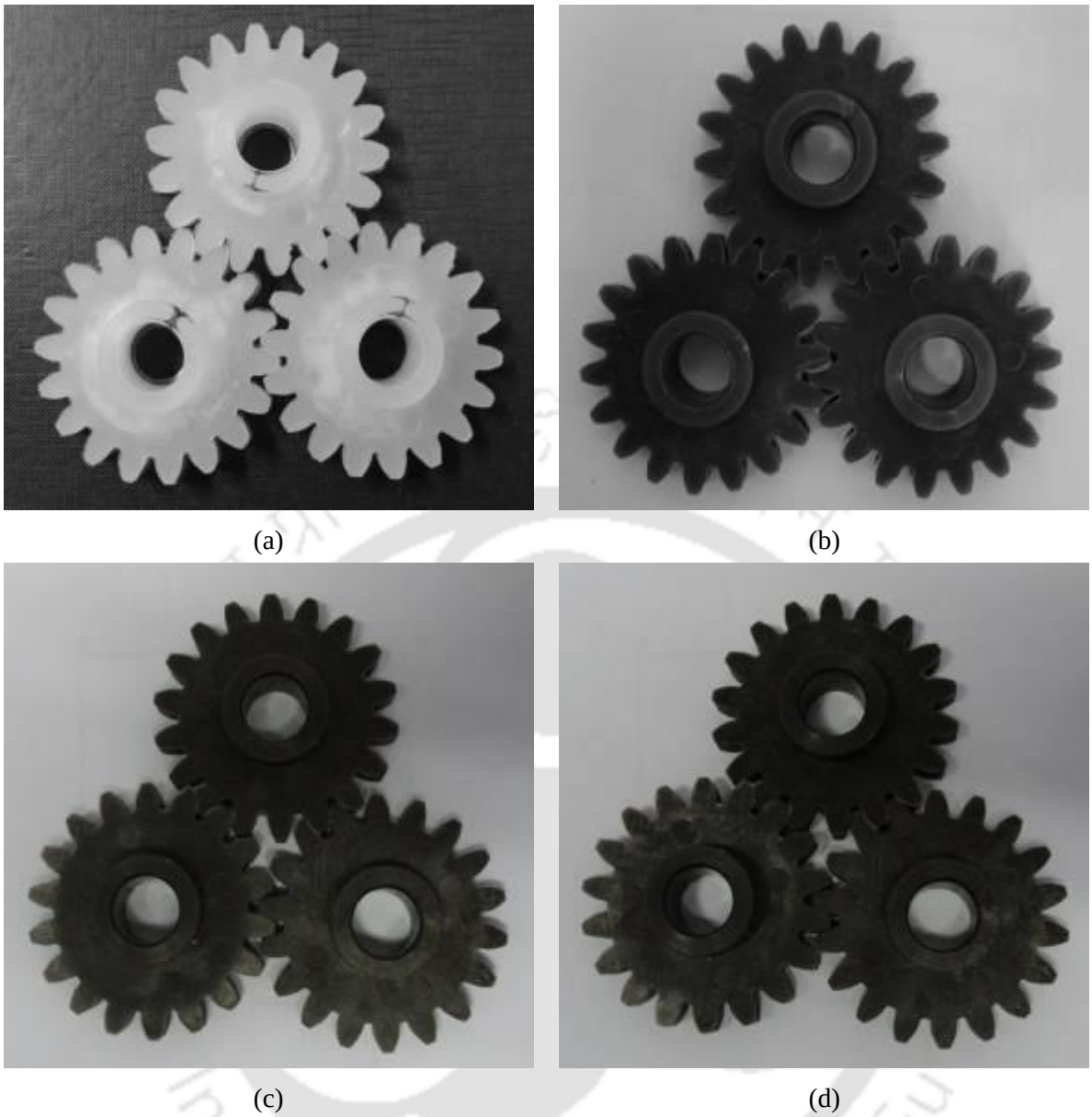

(a) (b)

(c) (d)

Figure 4.12 (a) Pure polypropylene, (b) 5%, (c) 10% and (d) 15% cement reinforced composite spur gears

4.4.1 Bending Deformation Analysis

Several experiments have been conducted to evaluate gear-tooth performance under various loading condition. A single tooth is selected for this experiments on which constant compressive load is applied at a constant rate of elongation i.e. 1 mm/min using Instron universal testing machine. Load is applied to the direction of 20º at the contact point i.e. line of action in dynamic condition of the spur gear which is shown in the Figure 4.13(a) and (b).

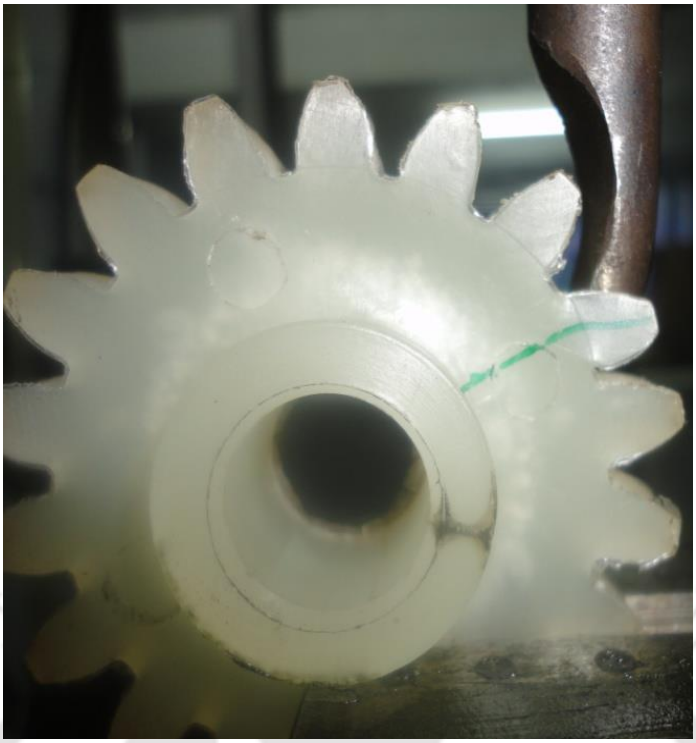

(a)

(b)

Figure 4.13 Compressive load applied to (a) pure polypropylene spur gear and (b) 10% cement reinforced composite spur gear at an angle of 20º

The compression resilience of the tooth is higher when the filler percentage is higher within the ductile limit, since, brittle composite does not show good flexibility as well as resiliency.

The deteriorated tooth profile after failure is shown in the Figure 4.14 (a) to Figure 4.14 (b). The experimental results are shown in the Figure 4.15 and Table 4.4. The average maximum load bearing capacity of a single tooth of 10% cement reinforced composite spur gear is showing approximately 1000N whereas, pure polypropylene and 5% cement reinforced composite spur gears show 915N and 931N respectively. It is also observed that 15% cement reinforced composite gear shows highest load bearing capacity, approximately 1111N, due to the higher elastic modulus of the material.

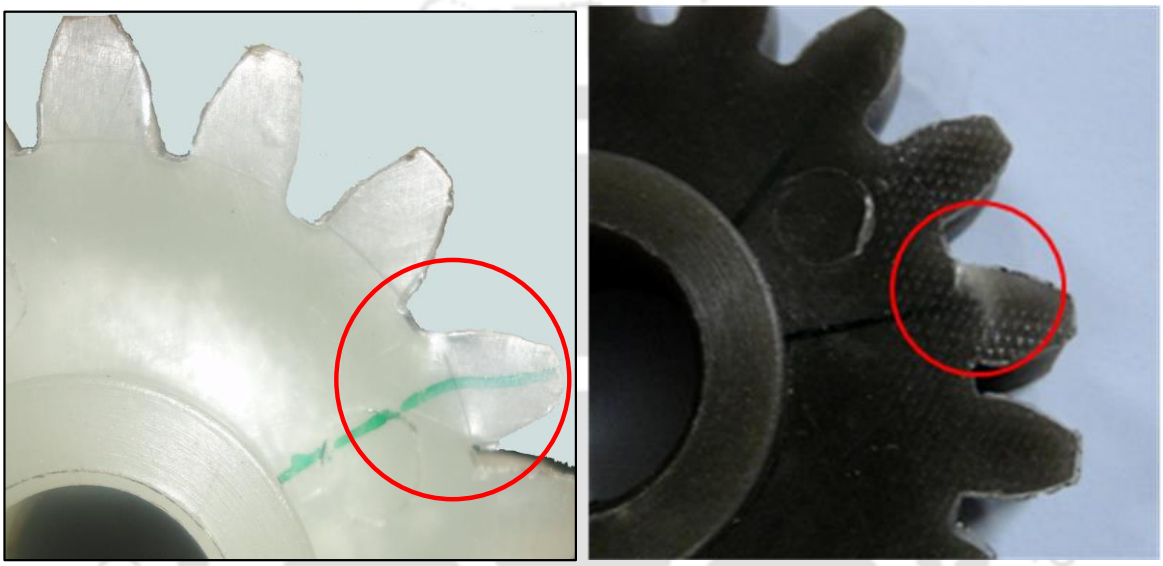

(a) (b)

Figure 4.14 Damaged tooth after failure (a) pure polypropylene and (b) 10% cement reinforced composite gear

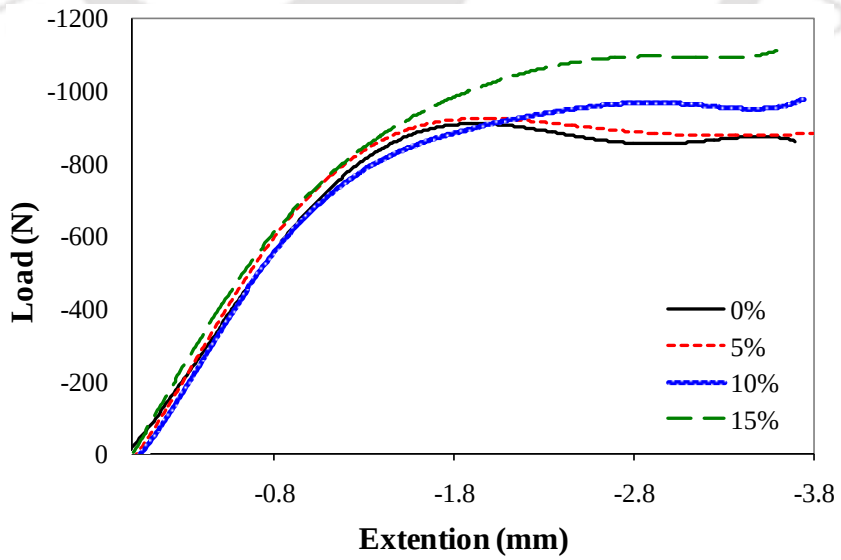

Figure 4.15 Variation of load bearing capacity of single tooth of cement reinforced composite gears at 20º load acting angle

Table 4.4 Experimental results of the gears

Sample	Max load (N)	SD	Max extension (mm)	SD
0%	915.60	3.74	3.7	1.89
5%	930.95	2.82	4.13	1.56
10%	998.75	3.18	3.52	2.12
15%	1111.36	3.56	3.60	2.34

It is clearly observed significant improvement of load bearing capacity of the gear tooth due to incorporation of the cement particles. The load bearing capacity of the gear depends on the load acting angle at the tooth contact point, homogeneity of dispersion of fillers material, fillers percentage and the filler-matrix bonding within the material.

Further, fabricated composite gears have also undergone testing at continuous loading condition show crack formation at the tooth root region. This is because of the fact that high shear stress concentration in the tooth root region leads to crack formation similar to other polymeric and metallic gears (*Walton and Shi, 1989*). Subsequently, nucleated crack grows due to repeated gear tooth loading which leads to total gear tooth failure. The representation of crack formation due to fatigue loading near the gear root region is shown in the Figure 4.14. The gear tooth root cracks are observed for pure polypropylene and 10% cement reinforced gear under 1 kN compression load respectively. The surface morphology of the deformed zone of the gear tooth is studied using ΣIGMA field emission scanning electron microscope (FE-SEM) (maker: Carl Zeiss NTS GmbH). A sample specimen of fractured gear tooth is examined under 3 kV with 500X magnification. Figure 4.16 illustrates morphological structure of the fractured surface of the deformed tooth of 10% cement reinforced gear. Micro cracks have also been observed on the fractured surface of gear tooth, which is developed due to continuous loading.

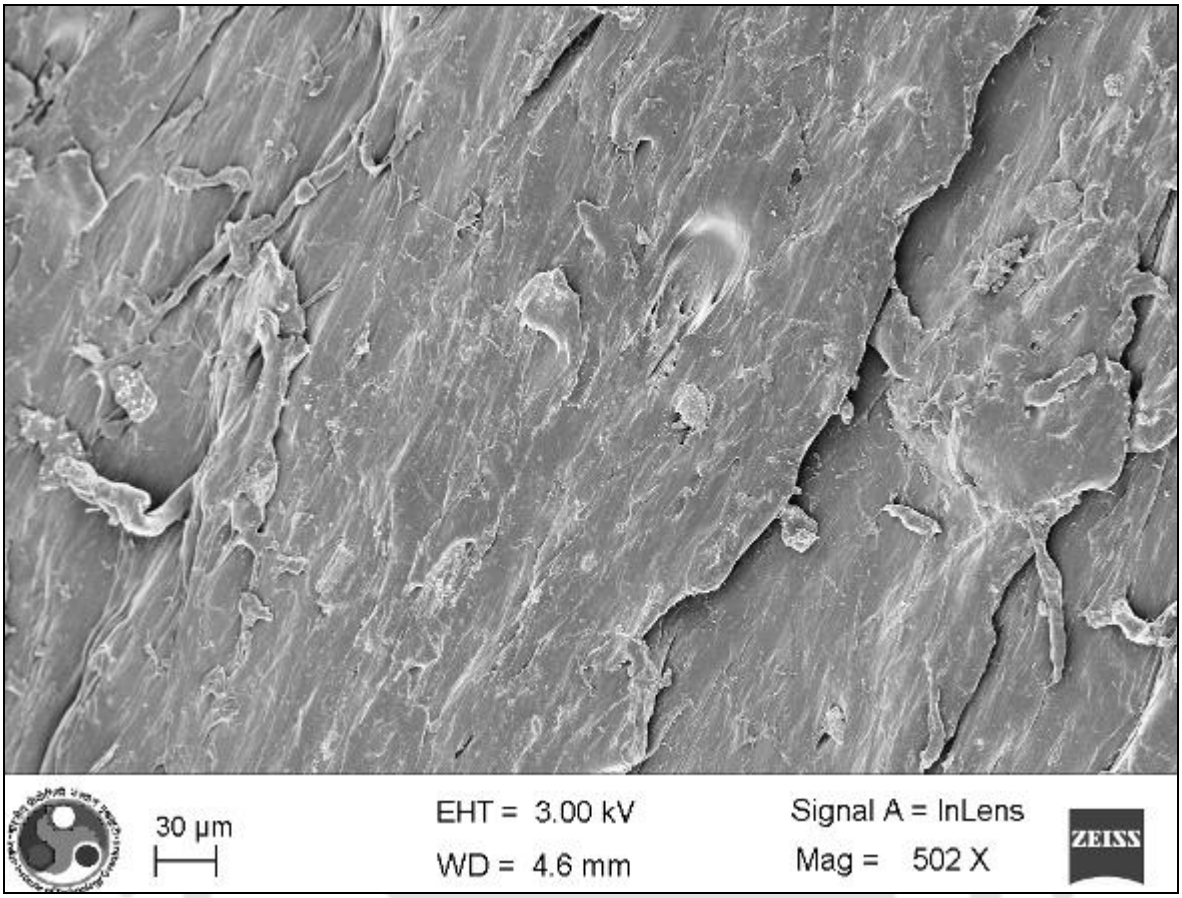

Figure 4.16 FE-SEM images of damaged tooth of fractured area of 10% cement reinforced composite gears

4.4.2 Fatigue Analysis of Gear Tooth

Fabricated spur gears have undergone short-term fatigue test to evaluate and study the short-term (5000 cycles) fatigue characteristics. The test is conducted in the Instron Universal testing machine (100 kN, maker, Instron, model no. 8801) keeping initial load 0.5 kN, test frequency 1 Hz and deflection amplitude 0.1 mm. The experiment is conducted after making a metallic test rig as shown in the Figure 4.17.

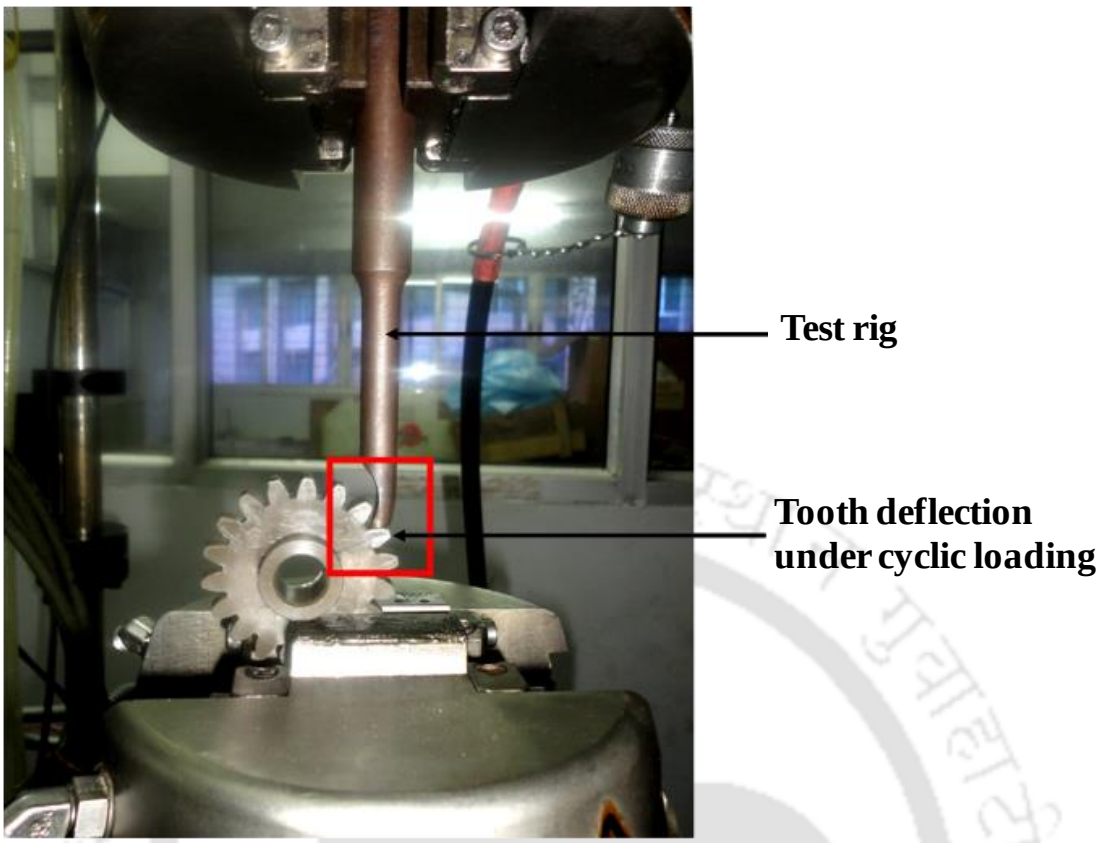

Figure 4.17 Gear tooth fatigue test setup

Figure 4.18 shows the hysteresis loop of the load-deflection relationship is obtained during each loading cycle. A hysteresis loop consists of a loading and unloading path as shown in the Figure 4.18. The results show the deformation characteristics of the composite gear tooth under cyclic tension-compression across thickness of the gear tooth.

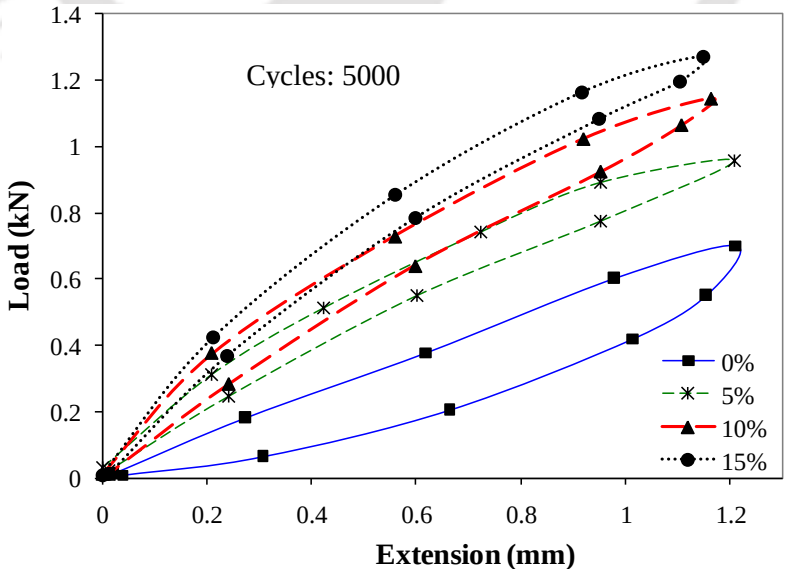

Figure 4.18 Cyclic load-deflection curve for composite spur gears

The results established the fact that the fatigue life of the composite specimen is highly dependent on the loading conditions. This also infer that not only the stress level but also the strain should be taken into consideration to explicate the fatigue behavior of specimens under various loading conditions (*Sugimoto and Sasaki, 2007*).

The area enclosed by the loading and unloading path quantifies the hysteresis loss of the tested gear. Figure 4.19 shows the average hysteresis loss of the 0%, 5%, 10% and 15% cement reinforced gear. It is observed that the 10% cement reinforced gear exhibit much less hysteresis loss compared to pure polypropylene gear. This eventually makes the gear better thermally stable and improved fatigue life during service of the composite gear.

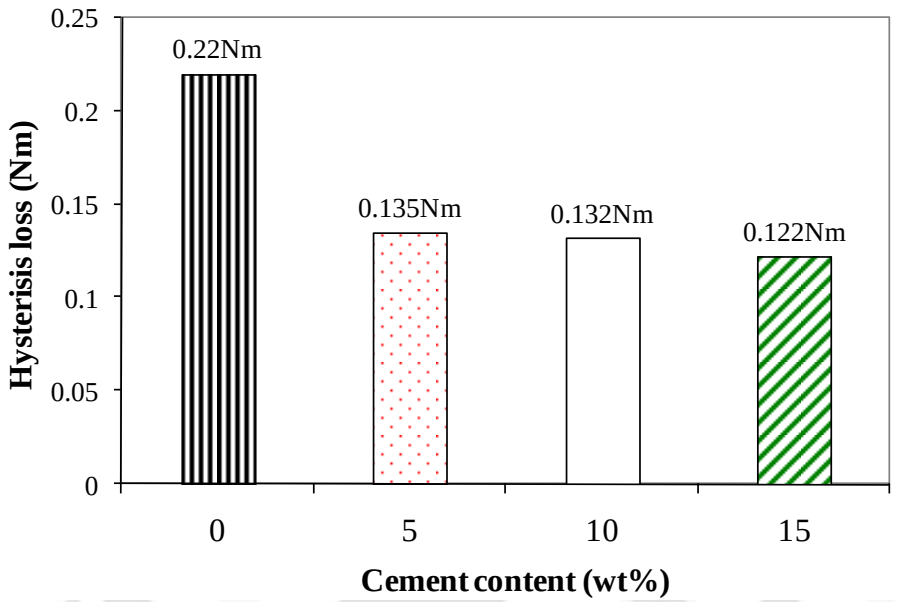

Figure 4.19 Variation of hysteresis loss of composite gears

4.5 Impact Test and Evaluation of Toughness

The pendulum Impact Tester, model IT-30 is used for conducting charpy impact test of the composite spur gears. The experimental setup is shown in the Figure 4.20.

Figure 4.20 Pendulum Impact Tester, (IT-30)

Schematic representation of the test mechanism with gear specimen of 10% cement reinforced composite spur gear are shown in the Figure 4.21(a), (b) and Figure 4.22 (a), (b) respectively. Two experimental procedures have been followed to evaluate the impact strength and toughness of the composite material spur gear. As shown in the Figure 4.21, direct impact load is applied on the spur gear tooth to assess the impact strength. On the other hand, impact load is applied on the gear base as shown in the Figure 4.22. The absorbed impact energy gives measure of the toughness of the fabricated gear.

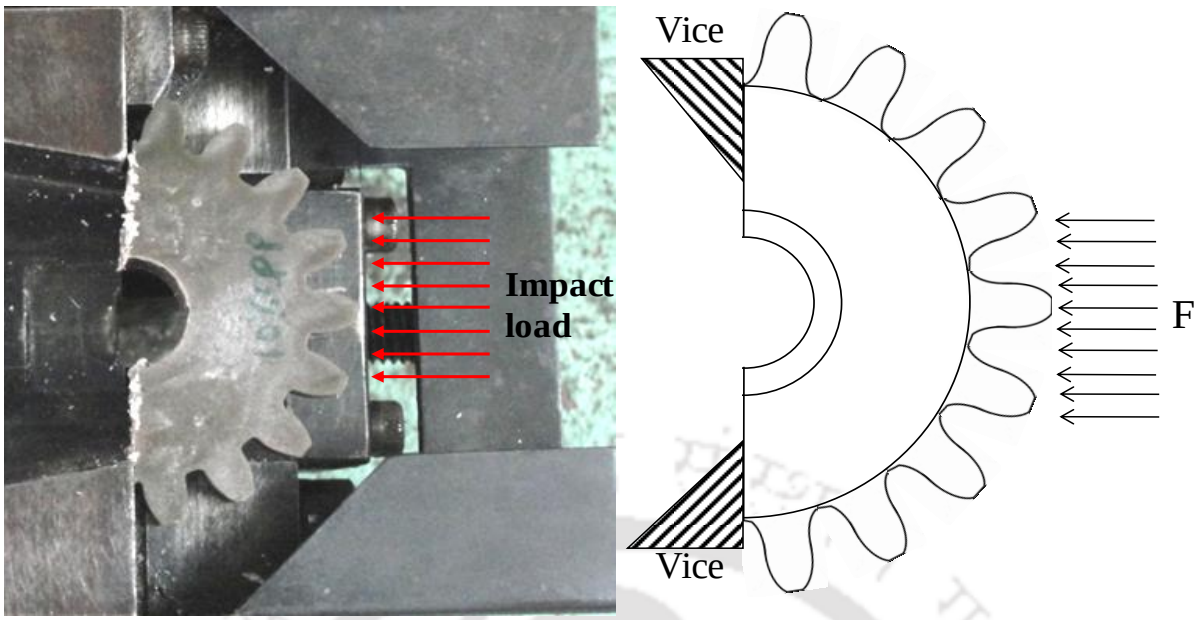

(a) (b)

Figure 4.21 Charpy impact mechanism of (a) 10% cement reinforced composite spur gear and (b) direction along which load is applied on the tooth

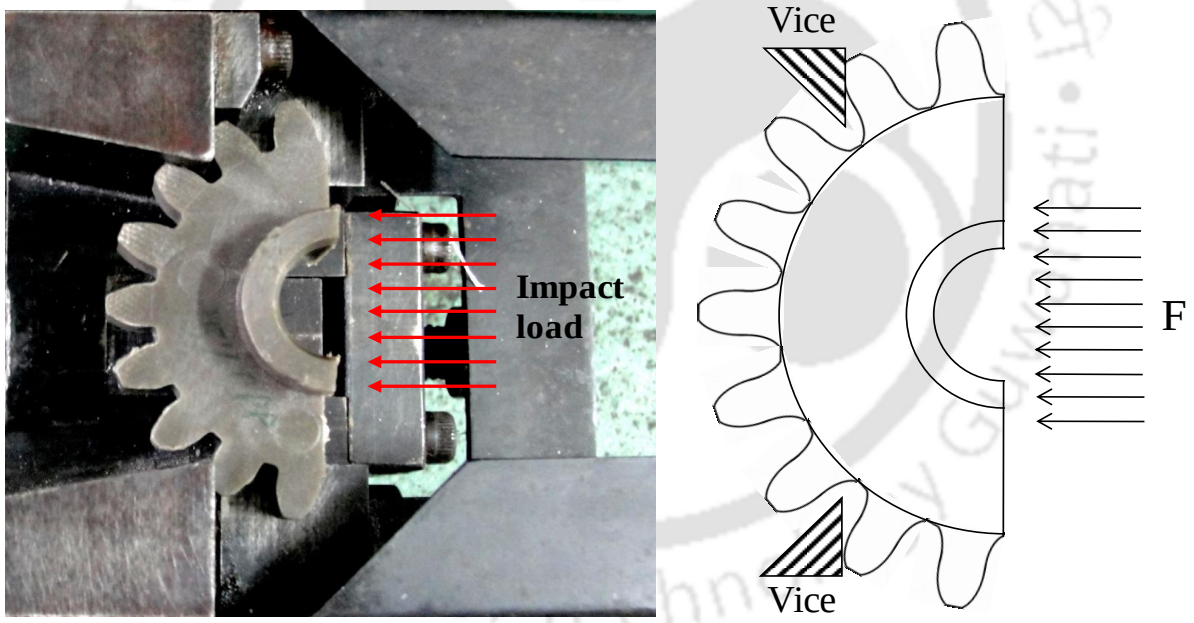

(a) (b)

Figure 4.22 Charpy impact mechanism (reverse side) of (a) 10% cement reinforced composite spur gear and (b) direction along which load is applied on the gear base

The energy absorption by the spur gears corresponding to the Figure 4.21 has shown in the Figure 4.23. Similarly, impact energy absorbed by various gears corresponding to the mechanism as shown in the Figure 4.22, are illustrated in the Figure 4.24. Comparative study reveals that during impact failure, 15% cement reinforced gear absorbed higher energy, compared to 5% and 10% cement filled gear whereas, pure polypropylene gear shows

minimum energy absorption. The anticipated reason is that the cement reinforced composite materials exhibit higher modulus as well as work-of-rupture as seen in the previous section. Further, as shown in the Figure 4.24, the impact energy absorption by the gear tooth (corresponding to the Figure 4.22) is observed to be less, approximately 2J for pure polypropylene and maximum energy absorption about 8.1J for 15% cement filled gear tooth. Although, it is observed that impact energy absorption by the gear **base** is much higher as compared to gear tooth due to its thin structure as shown in the Figure 4.23. Thus, impact strength of gear base is much higher compared to the gear tooth.

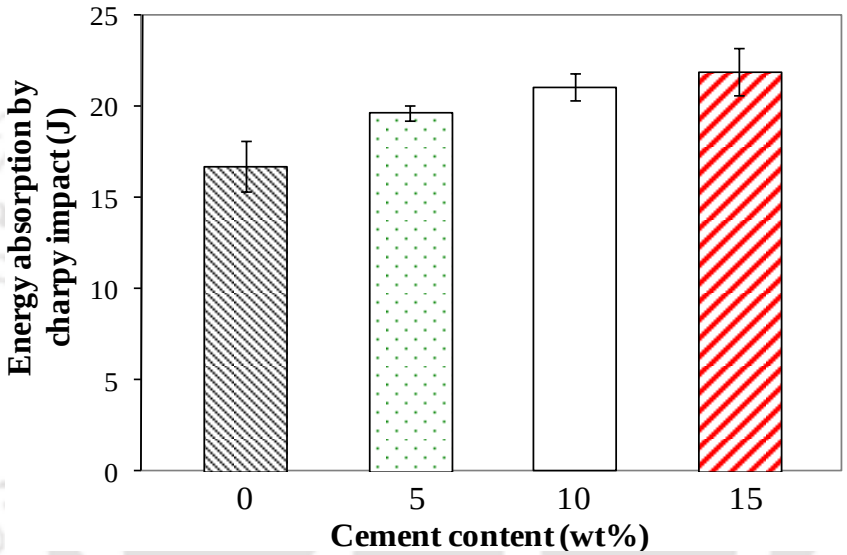

Figure 4.23 Energy absorption spur gear base during charpy impact test

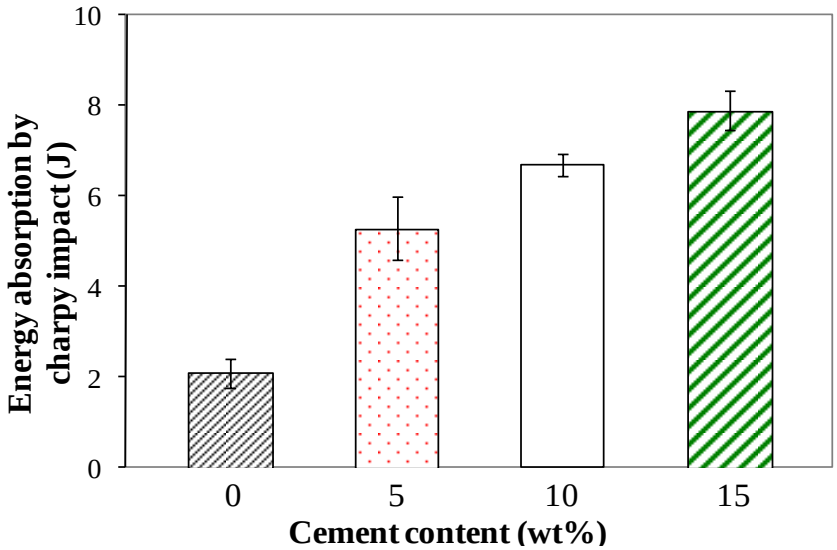

Figure 4.24 Energy absorption by spur gear tooth during charpy impact test

A comparative study between polypropylene gear with other gear materials have been presented in the Table 4.5. After careful market survey, it is found that cheapest polymer for gear material is polypropylene. Various other aspect of materials are taken into consideration before selecting the suitable composite gear material for industrial applications.

Table 4.5 Comparative study of various gears with respect to fabricated cement reinforced polypropylene composite gear [187-202]

Parameters	**Polypropylene**	**Nylon/PEEK/PE**	**Acetal/PMMA**	**Polyester**	**Metal (Steel)**
Matrix cost (Rs./kg)	100-125/	190-250/	200-350/	>200	46-50/
Cost of reinforcement	Nominal (cement) (Rs. 450/50 kg)	E-Glass fibre (Rs. 100-150/kg) Carbon fibre/ (Rs. 180-200/kg), Nanomaterials (CNTs, and other) (Rs. 100-250/g)			-
Density (g/cc)	0.9	1.3/1.32/0.98	1.41/1.18	1.4-1.6	7.8
Chemical Resistance (oils, lubricant, acid/base solvent)	inactive	reactive	reactive	reactive	reactive
Processing (melting temperature)	170ºC	270ºC/ 343ºC(PA/PEEK)	175ºC	260ºC	1500ºC
Max. surface temperature during operation (ºC)	35ºC (at 1800 rpm/ load 13.5N) and 52ºC (at 2500 rpm/ load 13.5N)	61ºC-74ºC (at 4.5 Nm, 257-494 rpm)	140ºC (at 2500 rpm/ torque 10Nm)	-	93ºC
Quantities of gears per kg material	52-55 (proposed gear)	-	-	-	5 (maintaining the same dimension as of composite material gear)
Cost of a single spur gear (as per the dimensions)	Rs. 3-3.5/piece (including all processing and labor cost)	-	-	-	Rs. 200-250/ (approx.)

Thus, comparative study indicate that polypropylene as matrix material and cement as filler material are the most suitable for fabrication of low cost composite gear in automotive light-scale applications. Further, employing the injection molding technique the gear can be fabricated in batch, results in saving of huge labor cost.

4.6 Theoretical Model of Stress Distribution along the Mating Surface of Gear Tooth

It is essential to understand the stress profile along the tooth mating contact surface when it is in work, as it directly influences performance and durability of the gear. A number of literatures have been reviewed, where, results indicated that significant enhancement of mechanical properties can be achieved by varying small amount of filler particles concentration. Thus, stress distribution along the contact surface and performance of the gear depend on the mechanical properties of the material directly. However, it is observed that metallic gear can be replaced by non-metallic gear up to a certain limit of yield strength above which metallic gear cannot be substituted (*Mahebub and Kevin, 2014*).

Several researchers have proposed and developed polymeric composite gear as an alternative to metallic gear (*Deo et al., 2001, Düzcükoglu, 2009, Endo et al., 2006*). Till date, various modeling technique have been developed so far to study the dynamic behavior of gear with respect to various factors such as quasi-static surface wear, wear depth, stress analysis and nonlinear contact deformation etc (*Ivana et al., 2009; Sunil et al., 2010; Savage et al., 1986; Abbes et al., 2011; Ding, 2007; Draˇca, 2006*). For composite material gear, reinforcement significantly influence the residual compressive stress in the tooth profile proves to be effective in increasing the fatigue strength (*Mendi et al., 2006*). Further, performance of the composite gear depends on various parameters such as fiber length, gear tooth fillet radius, topography, fatigue and failure, tooth deflection, friction and wear etc. (*Mao, 2007, Senthilvelan and Gnanamoorthy, 2004*).

However, past literatures indicate that few works concerned and addressed about the variation of stresses along the gear tooth contact region under dynamic loading condition. In general, developing a theoretical model that describes the principal stress distribution based on experimental result is still limited. This motivates to develop a theoretical model using Hertz's contact theorem, anticipating high interest to model the stress profile of a gear during running condition.

In this work, a low cost spur gear is fabricated using fly ash based Portland pozzolana cement as filler material into the polypropylene matrix followed by Injection molding process. Detail fabrication procedure can be found in the literature (*Sardar and Bandopadhya, 2014*). The fabricated composite material gear has been studied both experimentally and theoretically. Primarily, research has been focused on investigation of the stress distribution along the contact surface using Hertz's contact theorem. It is observed that, maximum stress variation

occurs at the dedendum region for both the driver and driven gears owing to sliding action along the contact area (*Draˇca, 2006*) while the tooth deformation depends on factors like loading condition and the modulus of the gear materials. This theoretical model would benefit the study of the variation of stress-distribution along tooth contact region of the composite material spur gear without the need of experimental study.

Hence, the main objectives of this work are as follows:

- Development of an analytical stress model following the Hertz's contact theorem based on experimental results.
- Comparative analysis of theoretical results with the experimental data

To achieve these objectives, a theoretical investigation on stress distribution has been carried out on the mating surface of the gear tooth following the Hertz's cylinder contact model. The cylinder contact model has been modified that describes the stress-distribution along the tooth contact surface under applied load. To compare and validate the theoretical results, some experimental procedures are intended and conducted for the correlation with the model. It is observed that the experimental results are closely matched with the theoretical results.

4.6.1 Experimental Analysis under Applied Load

A pair of pure polypropylene and composite material spur gears have been chosen for experimental investigation of stress distribution along the line of action. The experiment is conducted under Instron universal testing machine. The instrument, 100kN dynamic testing machine, (maker: INSTRON, model no. 8801) was digitally controlled and aided by the closed loop servo hydraulic system and the corresponding gear testing setup is shown in the Figure 4.25. Two conjugated teeth of upper test gear on a single tooth of the bottom test gear are selected for this experiment as shown in the Figure 4.25(a). Compressive load is applied at a constant rate of elongation i.e. 0.5 mm/min using Instron universal testing machine. The meshing teeth of the gear have been shown in the highlighted circle in the Figure 4.25(a). The schematic of the experiment has been shown in the Figure 4.25(b).

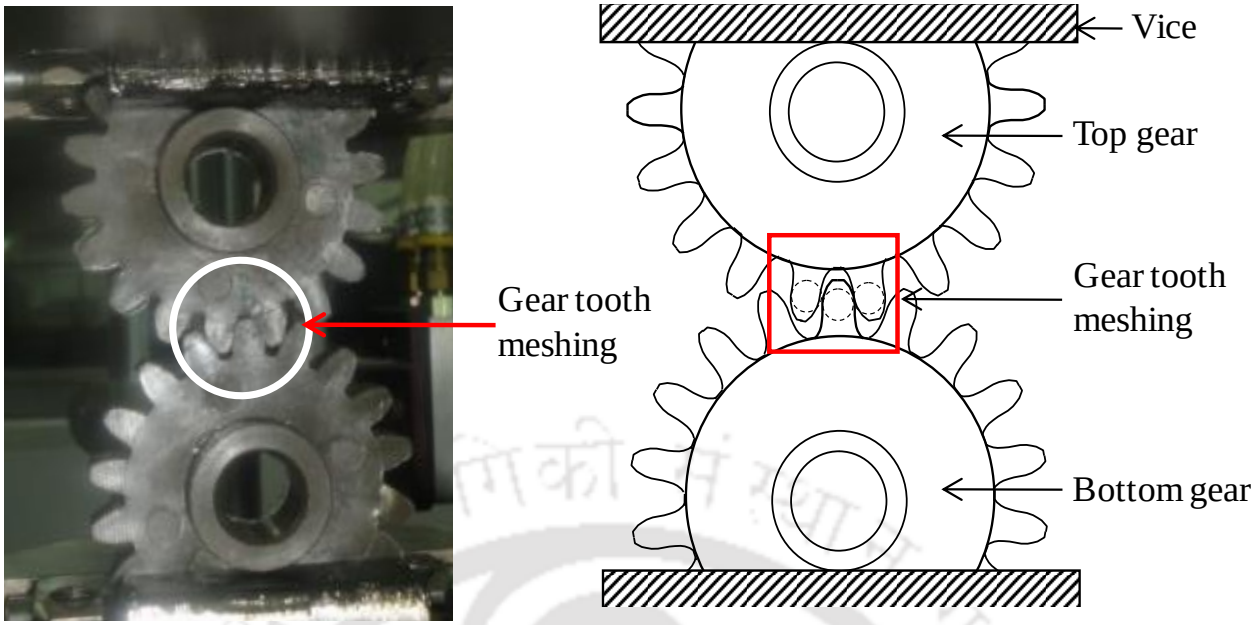

(a) (b)

Figure 4.25 (a) Gear-to-Gear meshing under compressive load at pressure angle of 20º: white circle shows the teeth meshing during experiment (b) corresponding, schematic representation of the setup

Gear to gear compressive load bearing capacity up to 6 mm extension are given in the Table 4.6. The comparative study between pure polypropylene spur gear and other cement filled spur gears results reveal that with the percentage increase of cement fillers, the compressive load bearing capacity of the gears increases maintaining the same extension of gear tooth. It is clearly observed that the 15% cement filled composite gear exhibits much better results due to higher percentage of cement fillers, results in higher modulus. However, 15% cement filled composite material proves to be inferior because its brittleness compared to 10% cement filled composite material.

Table 4.6 Experimental results of load bearing capacity of gear-to-gear compression

Sample	Max. com. extension (mm)	SD	Max. load (N)	SD
0%	-5.86	1.56	-2017.25	3.05
5%	-5.81	1.23	-2225.12	2.56
10%	-5.75	1.62	-2523.51	2.32
15%	-4.89	1.45	-2587.88	2.67

4.6.2 Derivation of the Model

Past literatures indicate that a theoretical model is in demand that describes the stress distribution along the tooth contact region of the mating gears. It is expected that with increase in loading and running speeds, the teeth of the driver and driven gears experience change in stress level and further increase in load and speed, this stress distribution aids the failure of the gear. As shown in the Figure 4.26(a), two gear teeth are engaged together under compressive load results in variation of stress profile along the tooth contact region. The loading direction of principal axis has been shown in the Figure 4.26(b). The primary objective is to model the stress-distribution using Hertz's contact theorem to validate and correlate the experimental results.

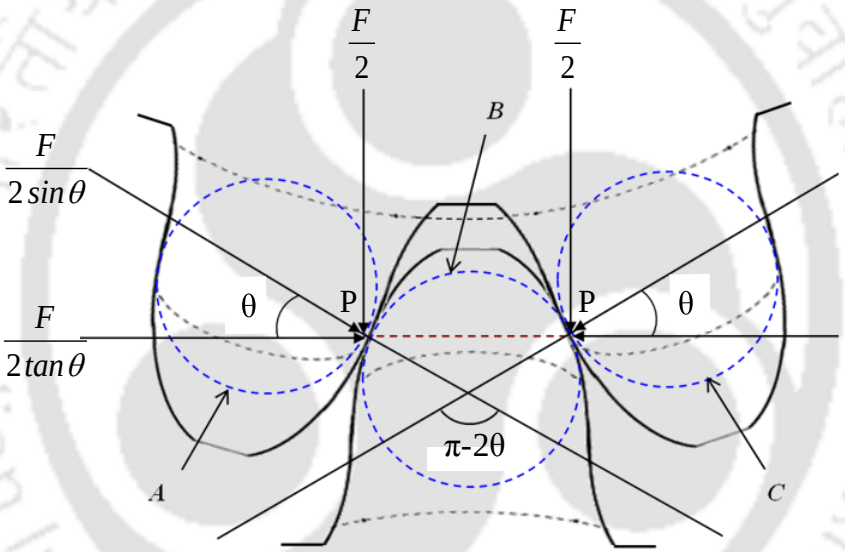

(a)

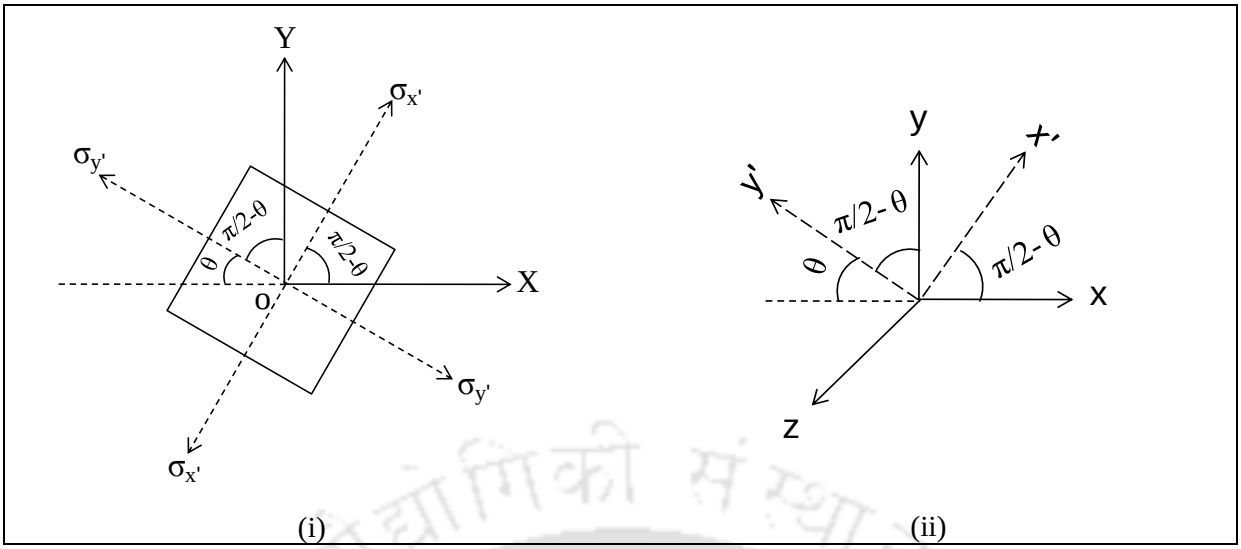

(b)

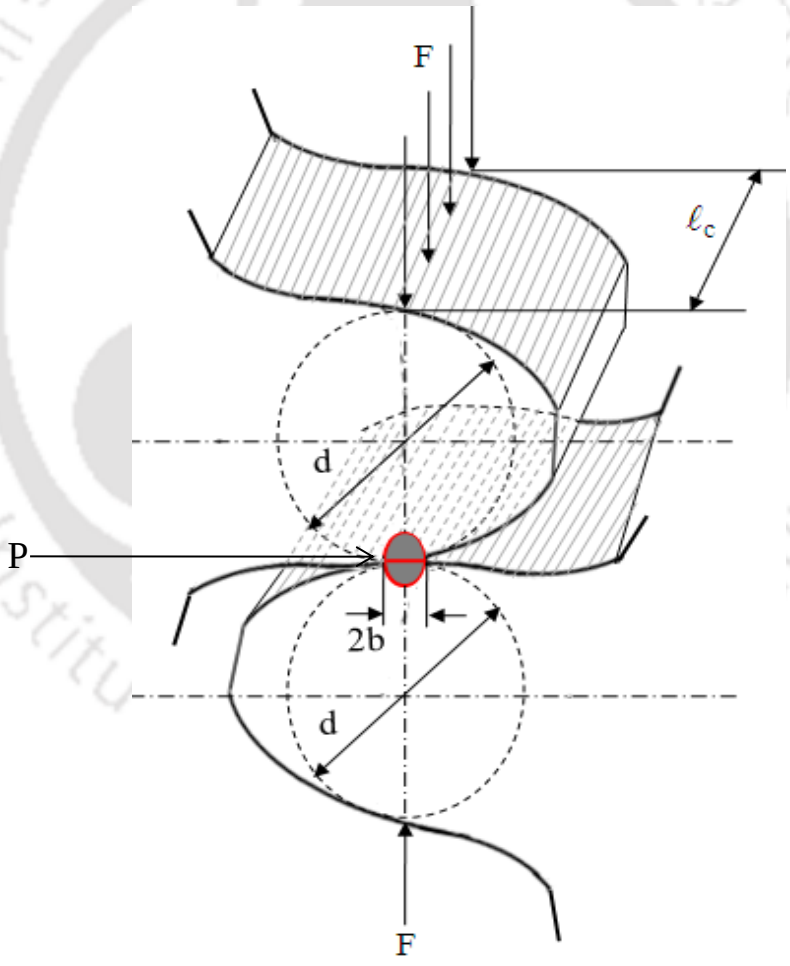

(c)

Figure 4.26 Active tooth profile (a) under vertical compressive load, (b) Principal stresses along the direction of θ and (c) contact area half width 'b' and cylinder length 'ℓ_x' and cylinder diameter '*d*'

As shown in the Figure 4.26, three imaginary cylinders (A, B, C) are drawn inside of the active tooth maximizing by the tooth width and thickness. Further, these consecutive cylinders (A, B) and (B, C) contact each other at the addendum part denoted by point P. According to Hertz' contact theorem, when a pair of cylinders comes together in line contact, under load, local deformation occurs (*Draˇca, 2006*). From the direct cylinder-to-cylinder contact principle, the contact half width is given as:

$$b = \sqrt{\frac{2F}{\pi l_x} \frac{\frac{\left(1-\nu_1^2\right)}{E_1} + \frac{\left(1-\nu_2^2\right)}{E_2}}{\frac{1}{d_1} + \frac{1}{d_2}}} \tag{4.6}$$

b denotes contact area half-width, ℓ_x denotes cylinder length and d refers diameter of cylinders, F denotes applied compressive load, ν is the Poisson's ratio of cylinder material and E is the modulus of elasticity of cylinders material. The subscript 1 and 2 denote the properties of the 1st cylinder and 2nd cylinder respectively.

The maximum pressure (P_{max}) is obtained as:

$$P_{max} = \frac{2F}{\pi b l_x} \tag{4.7}$$

And the stress along y axis can be expressed as (*Hassan, 2009; Draˇca, 2006*):

$$\sigma_y = -P_{max} \frac{1}{\sqrt{1+\left(\frac{y}{b}\right)^2}} \tag{4.8}$$

Assuming, properties of gear materials remain same for the entire tooth. As the model illustrated in the Figure 4.26(a), where load-acting angle is referred to θ, according to the Hertz's cylinder contact theorem, contact half width has been modified and expressed in the eqn. (4.9):

$$b = \sqrt{\frac{F\left(1-\upsilon^2\right)d}{\pi E l_x \sin\theta}} \tag{4.9}$$

and P_{max} can be expressed as eqn. 4.10:

$$P_{max} = \frac{F}{\pi b l_x \sin\theta} \tag{4.10}$$

The cylinder diameter does not remain constant due to applied load and it varies with the load amplitude. An empirical analysis is carried out with the experimental results and it is found that the cylinder diameter *d* varies with the applied load by a power regression function. This power regression function can be expressed as:

$$d = 6.66 \times 10^{-3}\ F^{-0.6423} \tag{4.11}$$

Therefore,
$$F = e^{\frac{\ln(d)+5}{-0.6423}} \tag{4.12}$$

Thus, the modified half width can be expressed with the help of eqn. 4.11, in eqn. 4.9 as:

$$b = 0.0816\sqrt{\frac{\left(1-\upsilon^2\right)F^{0.3577}}{\pi E l_x \sin\theta}} \tag{4.13}$$

Similarly, the maximum pressure (P_{max}) is obtained with the help of eqn. 4.12 in eqn. 4.10 as:

$$P_{max} = \frac{e^{\frac{\ln(d)+5}{-0.6423}}}{\pi b l_x \sin\theta} \tag{4.14}$$

and the stress along pressure angle i. e. y' direction can be expressed as:

$$\sigma_{y'} = -P_{max}\frac{1}{\sqrt{1+\left(\frac{y\sin\theta}{b}\right)^2}} \tag{4.15}$$

where, $y' = y\ sin\theta$ and $\sigma_{y'}$ = stress in y' directions. According to the theory of principal stresses, the principal stress is dependent to shear stress and has close relation with the direction of the applied load. Here, the stresses along y' axis has been calculated with the help of the direction of applied load (θ) and contact half width (b).

4.6.3 Results and Discussions

In the Figure 4.27(a) and (b), both theoretical and experimental compressive stresses are plotted along y'-axis while Figure 4.28(a) shows the stress distribution along y-axis. The principal stresses along y'-axis and stresses along y-axis is observed to exhibit linear variation

with load amplitude. Both theoretical and experimental results show close agreement, this in turns validate the assumption made and correction factor incorporated.

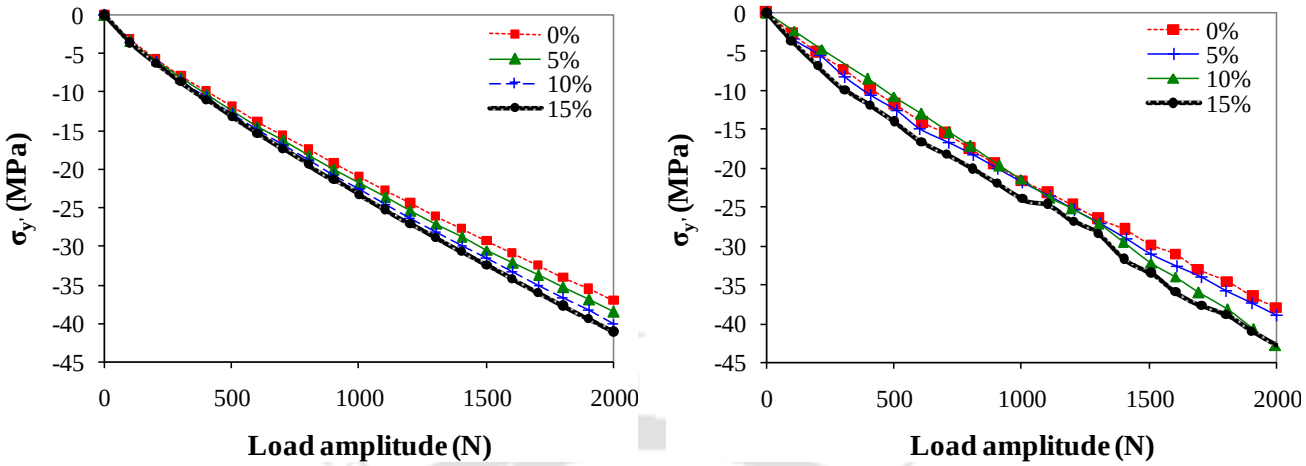

(a) (b)

Figure 4.27 Principal stress distribution of pure polypropylene and other composite spur gear along *y'* direction (a) theoretical and (b) experimental

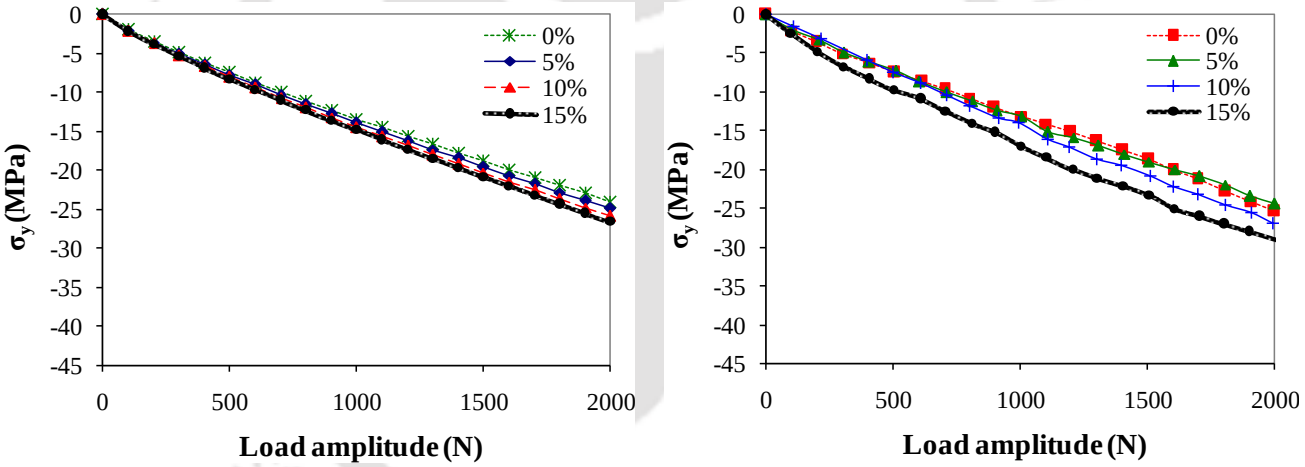

(a) (b)

Figure 4.28 Principal stresses distribution of pure polypropylene and other composite spur gear along *y* direction (a) theoretical and (b) experimental

Further, theoretical distribution of principal stress with respect to the distance away from contact point has been shown in the Figure 4.29. Applied load is varied from 100N to 2000N with an increment of 100N in each step. In the Figures 4.29(a) to (d) and Figures 4.30(a) to (d), the distribution of principal stresses of pure polypropylene and other composite spur gears are shown along the *y'*-axis and *y*-axis under variable loads.

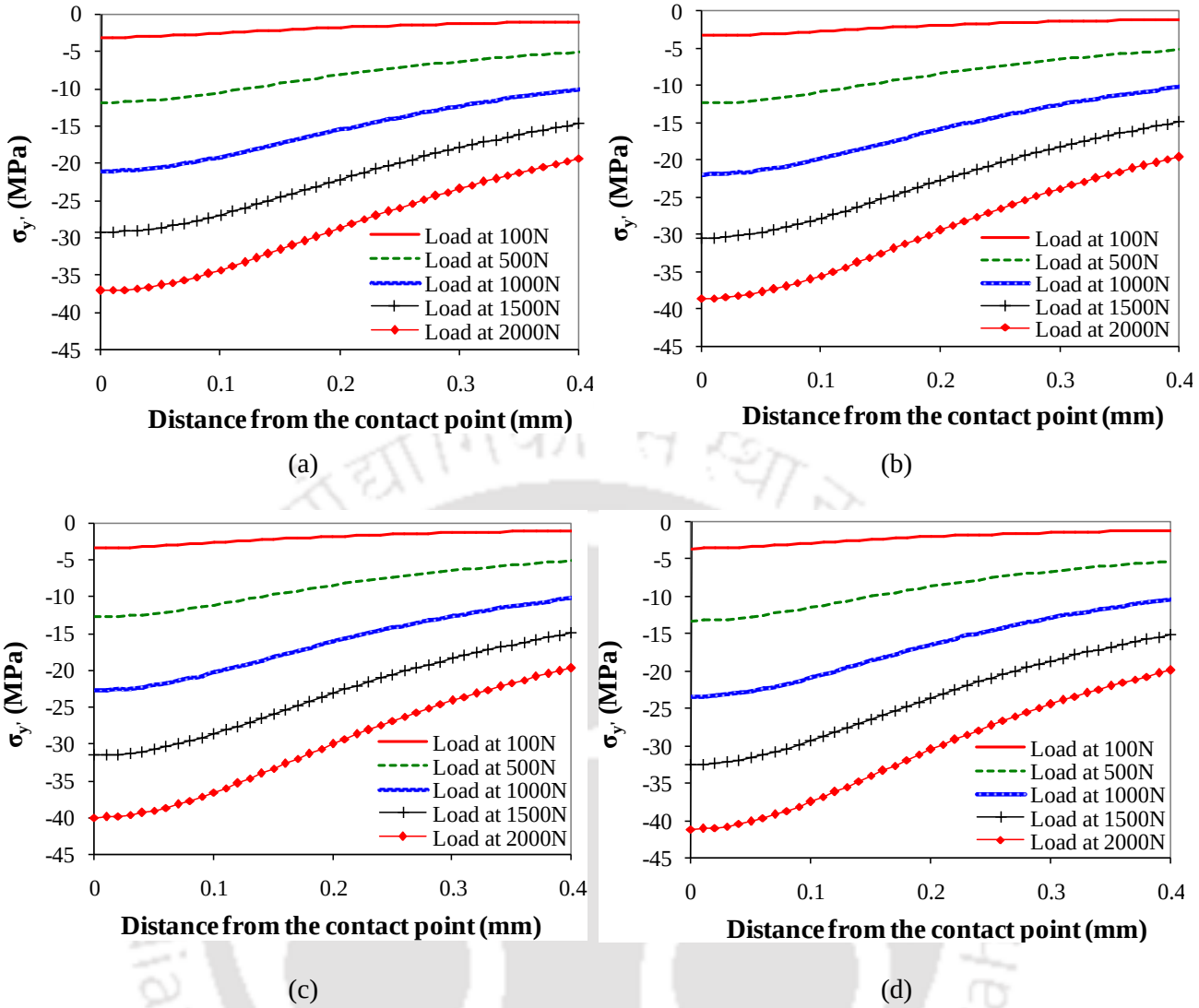

Figure 4.29 The distribution of principal stress variation of (a) pure polypropylene, (b) 5% composite, (c) 10% composite and (d) 15% composite spur gear along *y'* direction

It is observed that variation of principal stress profile remain similar with the percentage change of cement loading. However, as the cement loading increases, the magnitude of stress distribution increases. Thus, it is anticipated that as the running speed with load increases; the tooth of the gear may undergo wear loss results in backlash and may ultimately lead to failure of the gear. Further, at a particular distance away from the contact point the stress concentration saturated, but could vary with different angle of contact.

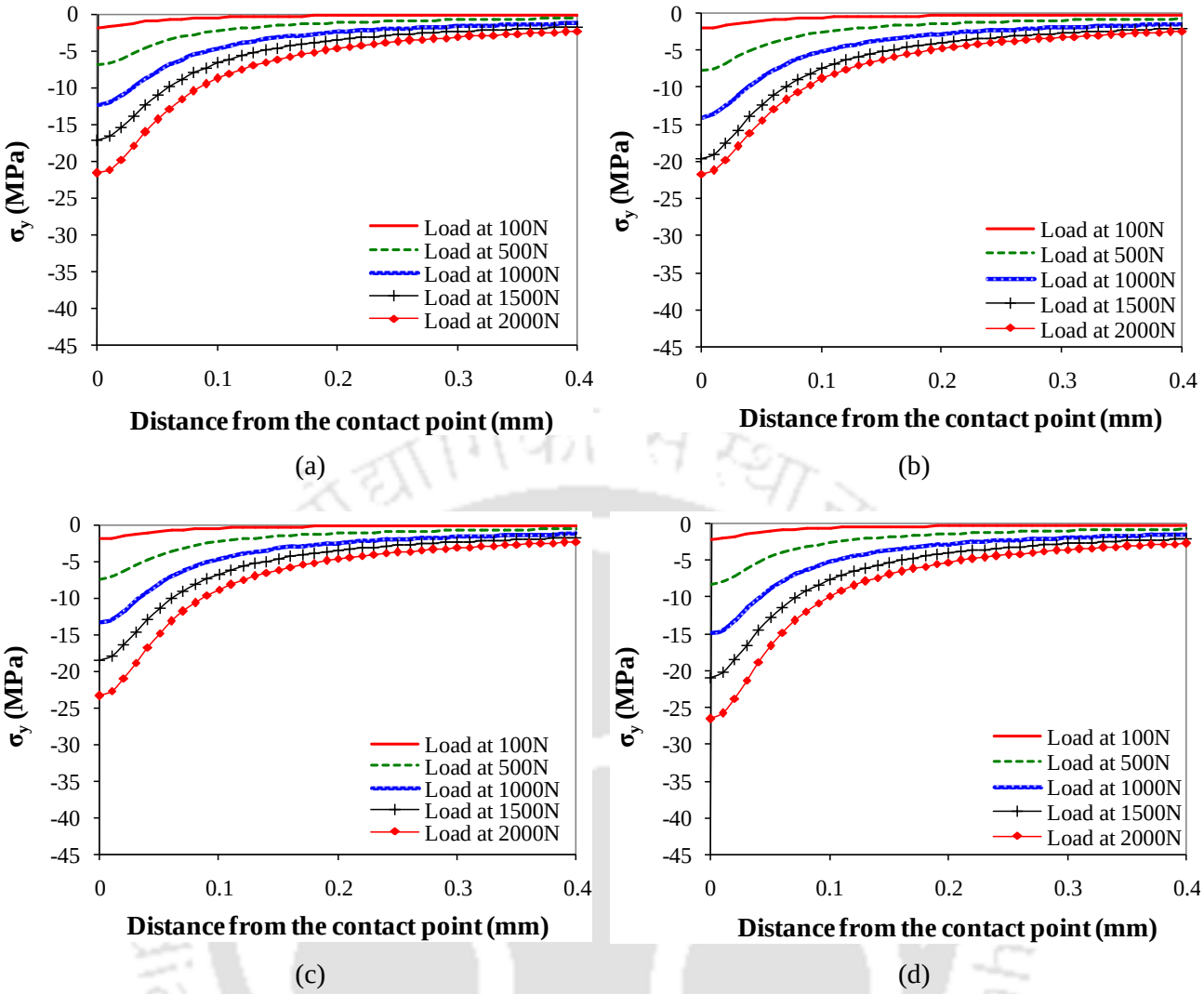

Figure 4.30 The distribution of principal stress variation of (a) pure polypropylene, (b) 5% composite, (c) 10% composite and (d) 15% composite spur gear along *y* direction

Figure 4.31 shows the variation of principal stresses ($\sigma_{y'}$ and σ_y) of spur gears for an applied load of 1000N. It is observed that even with the percentage increase of cement materials the spur gears do not exhibit significant changes both in experimental and theoretical results. Thus, the theoretical model developed using Hertz's contact theorem, based on experimental data suitable to study the stress-distribution along the tooth contact region during running condition without the need of experimental study.

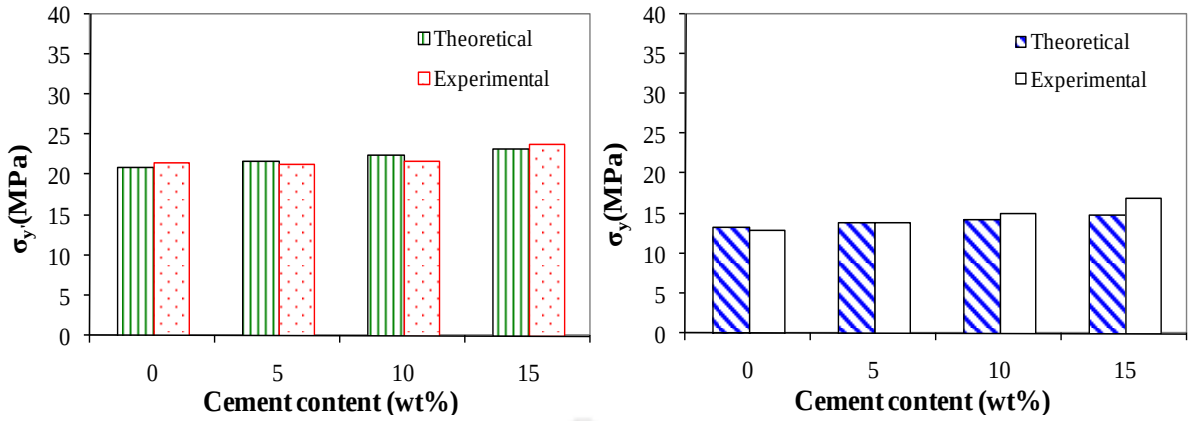

(a) (b)

Figure 4.31 Variation of experimental and theoretical distribution of principal stresses (a) $\sigma_{y'}$ and (b) σ_y of polypropylene and cement reinforced composite spur gears at constant load of 1000N

Another experimental procedure has been chosen to study the performance of the gears, where the load is applied at an angle 20º with respect to vertical axis.

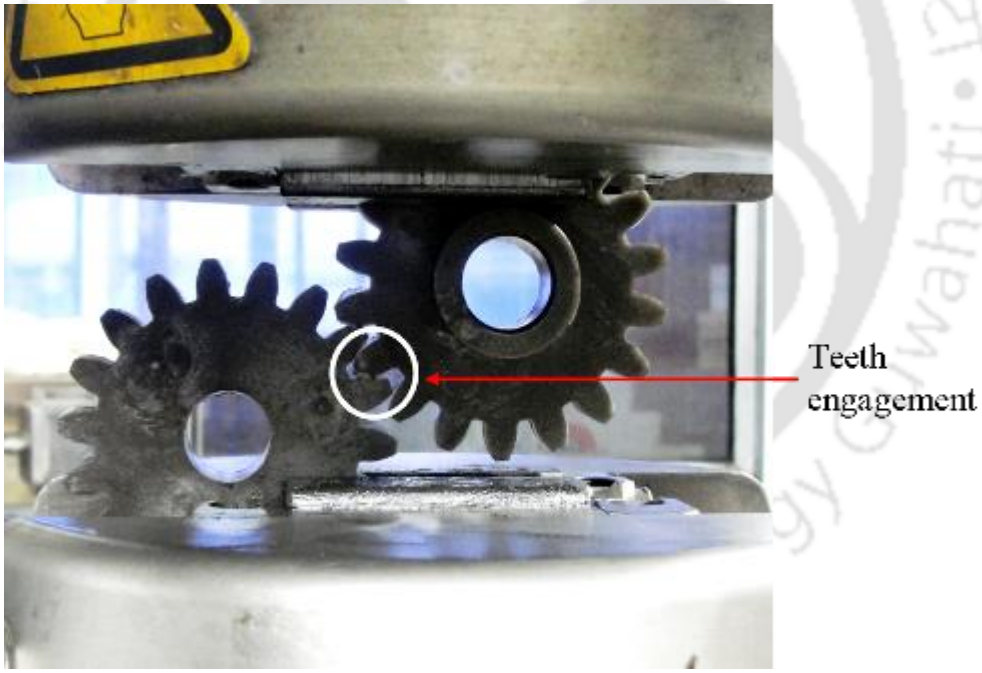

(a)

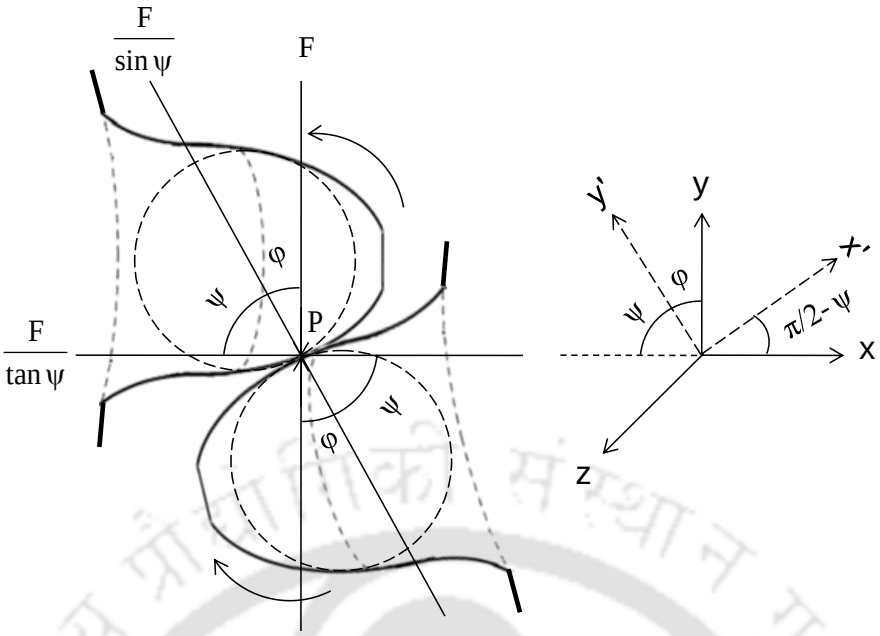

(b)

Figure 4.32 Tooth to tooth compressive load applied to composite gear at the pressure angle of 20º: (a) white circle shows the teeth contact during experiment and (b) applied load along the angle

The experimental results have been given in the Table 4.7. The experimental results reveal that 10% cement reinforced composite spur gear retains higher dynamic load bearing capacity even with the same deflection. Root failure region of 10% cement filled composite spur gear after testing has shown in the Figure 4.33(a) and highlighted by a circle. The corresponding FE-SEM micrograph of the failure region of 10% and 15% composite spur gear have also been shown in the Figure 4.33(b) and Figure 4.33(c) respectively. Both the micrographs show the failure mechanism of the gear tooth under loading. It is anticipated that due to the high stress concentration developed at the root of the gear tooth, the matrix flow has taken place during failure of 10% cement filled composite spur gear. Further, it is observed, that brittle fracture has been taken place for 15% cement filled composite spur gear as this also validates that with percentage increase of cement loading, **increases** brittleness of the material.

Table 4.7 Experimental results of load bearing capacity of gear-to-gear compression indicate uniqueness i.e., contact

Sample	Max. tooth deflection (mm)	SD	Max. load (N)	SD
0%	-3.72	1.23	-915.60	2.12
5%	-3.68	1.15	-938.56	1.86
10%	-3.70	1.10	-1031.42	2.04
15%	-3.02	1.45	-1135.58	2.68

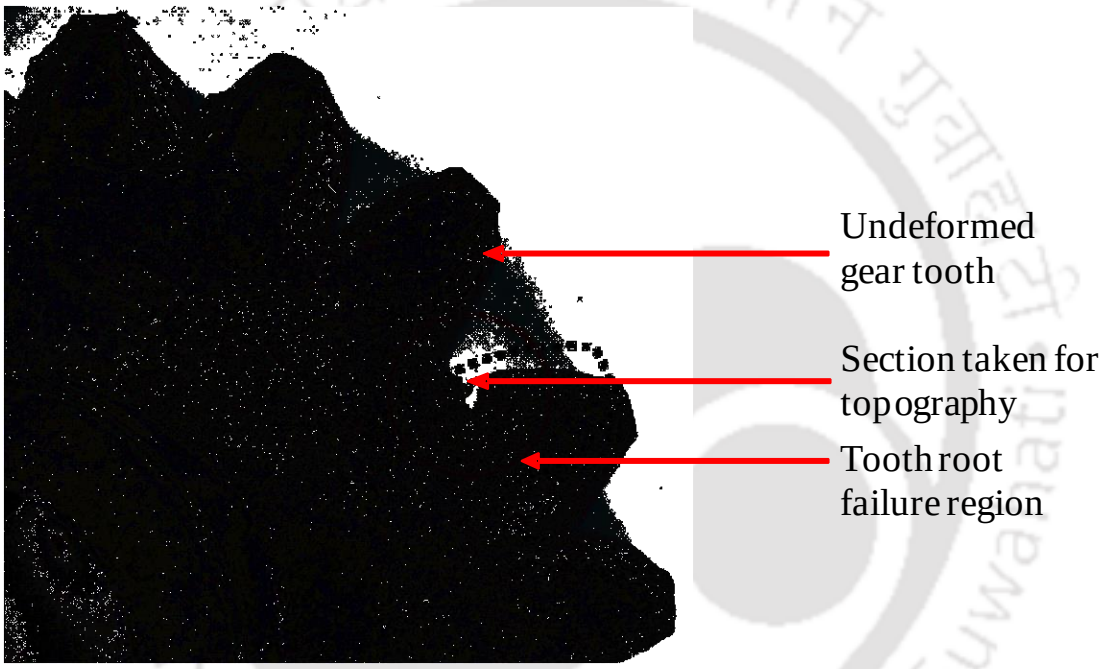

(a)

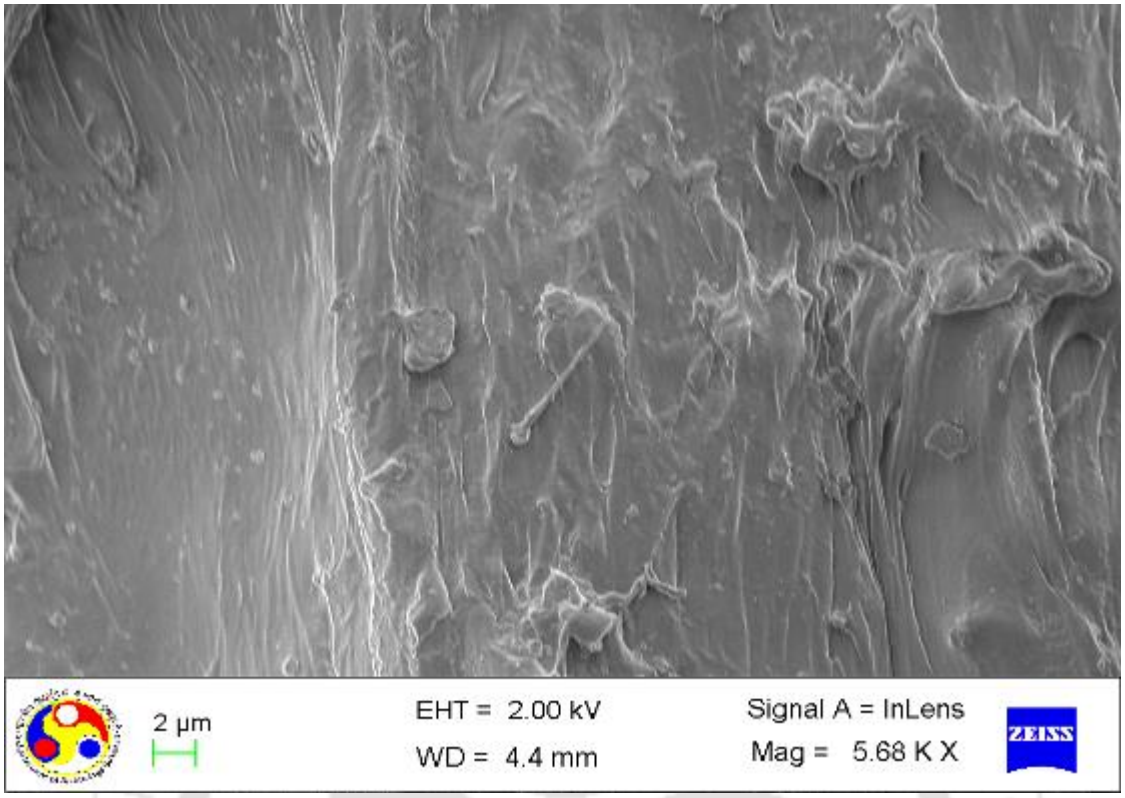

(b)

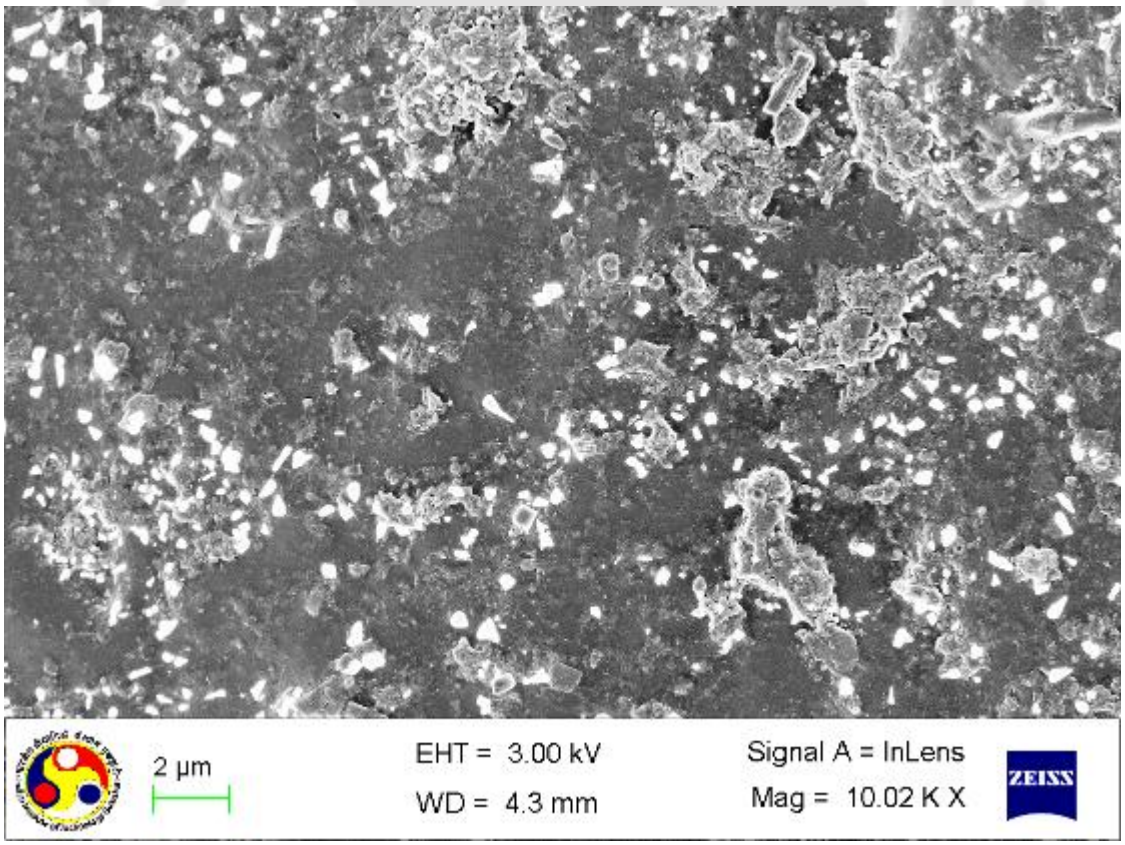

(c)

Figure 4.33 (a) 10% composite spur gear root failure with dislocation, (b) FE-SEM micrograph of (b) 10% and (c) 15% cement reinforced composite gear at fracture region

4.7 Summary

A low cost polymeric composite material spur gear has been fabricated following the injection molding technique. Polypropylene is chosen as matrix material while the low cost cement particles as reinforcement. 5%, 10% and 15% in weight fraction of cement particles are taken to fabricate and optimize the gear material. Numerous experiments such as dynamic mechanical analysis (DMA), tensile tests, morphological analysis is conducted and it is observed that 10 w% cement particles filled composite gear material exhibits better mechanical properties and performance to fabricate the gear. The developed inexpensive composite material gear is suitable in industrial application as an alternative to metallic gear. In addition, the gear material exhibits insulating properties thus could also act as thermal and electric insulator.

The specific conclusion and contribution can be summarized as:

- A technology demonstration is carried out successfully employing injection molding technique for fabrication of complex shaped damage tolerant composite material gear for light to medium duty device application. The fabricated composite material gears possess excellent corrosion and fatigue resistant characteristics.
- 100% polypropylene gears exhibit much hysteresis loss compared to 10% fillers composite gear material and thus yields better performance and higher fatigue life. Further, significant improvement of load bearing capacity of the gear tooth is achieved due to incorporation of the cement particles. The compression resilience of the gear tooth is higher when cement particles percentages are higher within the ductile limit.
- The primary benefit of using this low cost cement based composites instead of metals is that large weight saving can be obtained. Further, on selecting large series production of these gears, large cost saving seem also feasible.

Using Hertz's contact theorem the fabricated cement filled composite spur gears are analyzed to assess the stress distribution along tooth contact region and to predict the failure criterion owing to the load applied. It is observed that the stress concentration saturated after a certain distance away from the contact surface. Further, maintaining the contact surface pressure angle of action to 20º, with the percentage increase of cement loading both tooth displacement and principal stress ($\sigma_{y'}$) decreases. The theoretical stress distribution profile of

the mating surface of the tooth contact region closely validate the experimental results. Thus, the theoretical model developed is useful to study the stress distribution without the needs of experimental study.

Chapter 5

Dynamic Performance Evaluation and Assessment of Wear Characteristics of Composite Material Spur Gear

5.1 Introduction

The heat loss during running of the gear is a matter of concern as it severely affects the dynamic performance and influences the product life. Further, heat dissipation is directly related to the power consumption as well as the degradation of the gear material. Taking into account of these factors, one of the preliminary areas that can be controlled is to reduce the heat loss and enhance the product life. In general, metallic gear experience much friction at high speed leading to more heat loss during working compared to the composite material gear. Thus, to reduce the heat loss and to control wear loss sometimes lubricant is used for metallic gear. These disadvantages pave the way for replacing the metallic gear by a non-metallic gear, which proves to be more effective and beneficial for lightweight application. In addition, polymeric composite gears have some advantages, such as low noise level during operation, sustainability against corrosion, low weight, easy to batch production, and workability without lubrication. However, few limitations such as sustainability under low operational temperature and load limit the composite material gear for heavy-duty application. It is sometime observed that poor heat conductance of polymeric gear material results in accumulation of localized heat and softens the material quickly. In addition, at high speed, the plastic gear-contact-surface temperature rises to local softening and scales up the surface wear.

In practical application, the heat loss is observed to be very high for metallic gears, for which polymeric composite gear comes in core interest to replace the metallic gears. In addition, geometrical structure of the product depends on the parameters like loading-unloading condition and temperature fluctuation and that severely affects the material performance and shortens the product life. The main objectives of this work are as follows:

- Modification of a gear test-rig to investigate the performance of the spur gear at different speed and loading conditions
- Investigation and evaluation of heat loss in terms of temperature during running condition

- Measurement and quantification of wear rate of the gear materials and calculation of wear volume of gear tooth for different operating speed.

The dynamic performance of the gear is tested under variable loads and speeds and the effect of temperature is ascertained. Further, the composite material spur gear was tested to evaluate its friction and wear characteristics in both adhesive and abrasive wear modes. Weight loss due to wear of the composite gear is evaluated through direct measurement under a specific load and running condition. It is observed that the adhesive wear rate significantly reduced when the cement filler loading increases. This is because shear strength and surface energy of the composite material changes while toughness and hardness of the material improve due to strengthening by cement fillers.

5.2 Modification of Gear Test-rig and its Accessories

The purpose of the dynamic test of the gear is to identify and assess the effect of temperature on the gear performance. The rise of temperature and its subsequent effect directly involves with the material performance and hence influences the working life. Because of this, it is necessary to quantify the heat loss in terms of temperature during running of the gear pair. The gears setup with metallic bush has been shown in the Figure 5.1. Several experiments are conducted and the dynamic performance of the gear is evaluated under various loading and running conditions. Initially, a dynamic gear test-rig is modified for the experimental procedure suitable to comprehend the performance during running of the gears. The test-rig, equipped with two parallel shafts adjusted by a high-speed AC motor. The parallel shafts are then fixed by two movable self-lubricated bearing housing that allow the free rotation subjected to minimal frictional loss of the shafts. Two load cells of 13.5N and 8.5N of mild steels are employed as per the features of the test gear, gear dimensions and mechanical properties of the gear materials are shown in the Figure 5.2(a) and (b) respectively.

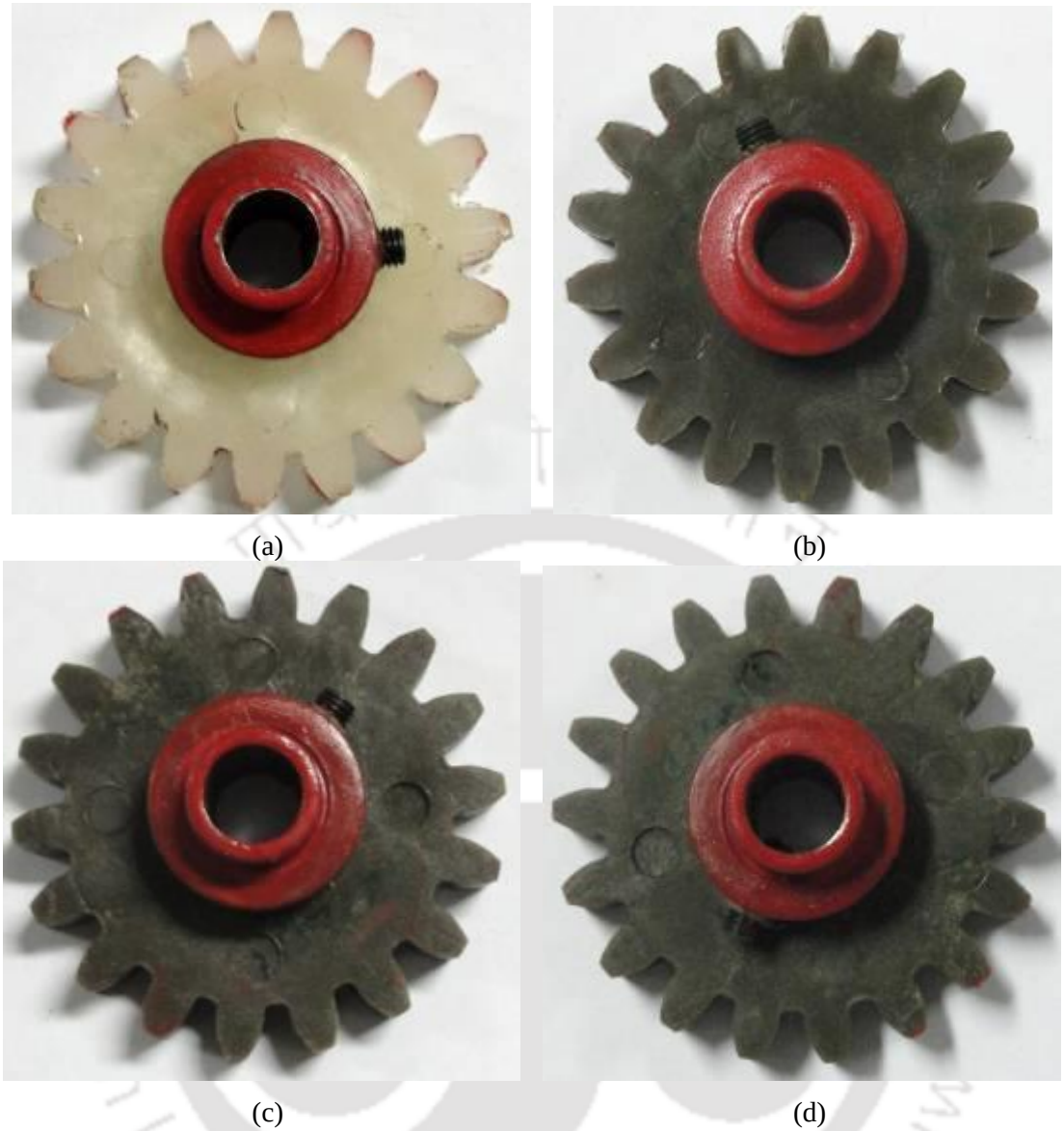

Figure 5.1 Fabricated composite gears with bush (a) pure polypropylene, (b) 5%, (c) 10% and (d) 15% cement reinforced composite spur gears

Four variable speeds are selected in order to investigate the heat loss due to friction in terms of temperature between the gear pair during working condition. Evaluation of surface temperature in dynamic condition is aided, in line, by an Infra-Red assisted camera, IR-TCM 384. In addition, the composite spur gear material was tested to evaluate its friction and wear characteristics in both adhesive and abrasive wear modes. In dynamic condition, the gear pair runs at desired speeds with preset loading condition. Owing to the high speeds, teeth flanks i.e., surface of both the driver and driven gears come into contact very frequently, eventually, high friction takes place, results in increase of flash temperature. This induced temperature of the gear amount to fall of the performance and results in shortening of the gear life.

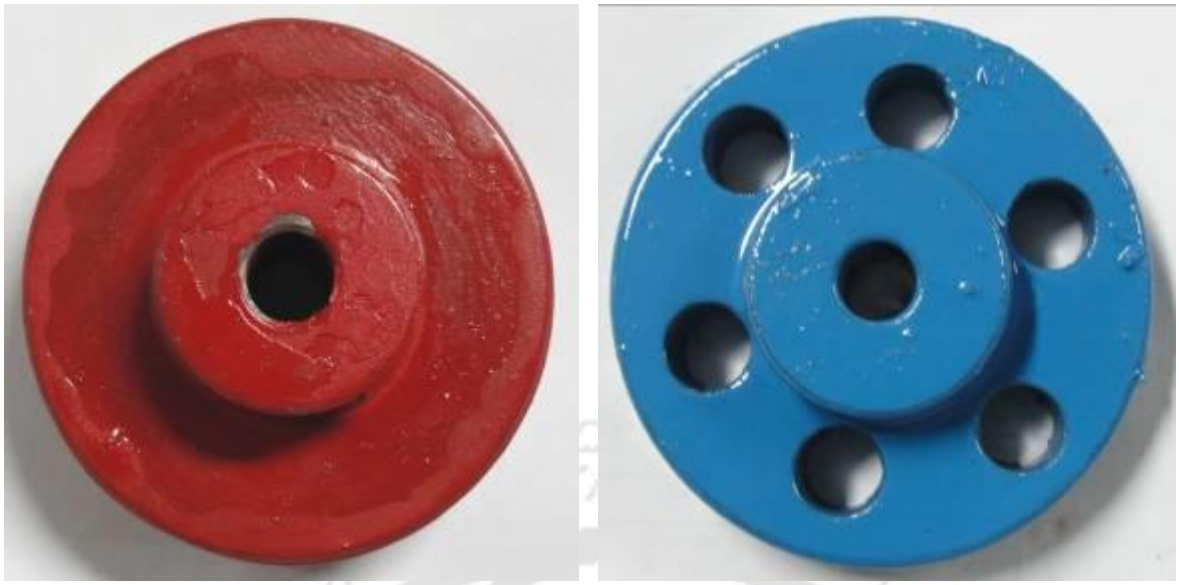

(a) (b)

Figure 5.2 Loading condition during gear running (a) 13.5N and (b) 8.5N

A high-speed AC motor (SAGAR, S.M. motor- Sl. No. 202758, type- AC/DC-CONT/ACW) of 6500 rpm, 1/12 HP capacity, 0.75 AMPs, 220 V, is used to run the gear pair as shown in the Figure 5.3(a). A rheostat (DIMMERSTAT, Sl. No. 701/9277417, input-240 V, output-0-270 V, 2 A, Type- 2D-1P) is used to control the gear speed of the motor as shown in the Figure 5.3(b). During the test, the speed is measured using a digital non-contact tachometer (maker: Digital Promoters India Private Limited, model: DT-2001B, range: 1 to 99999 rpm).

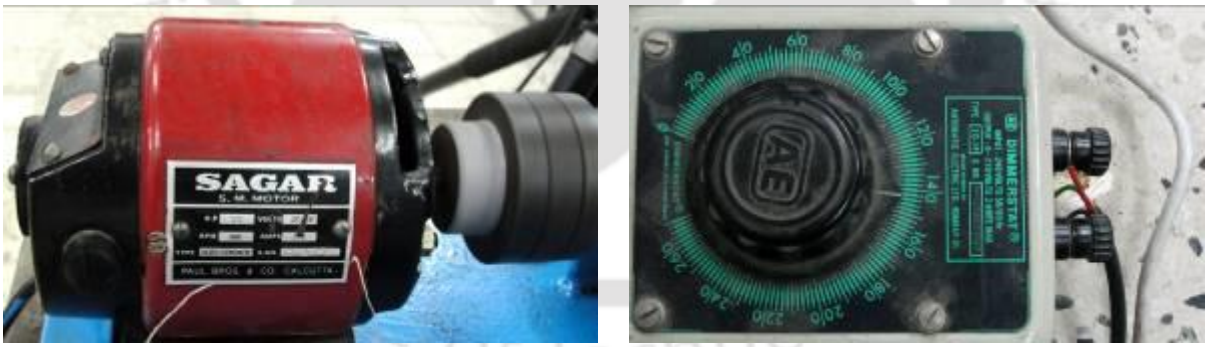

(a) (b)

Figure 5.3 (a) AC motor used in the experiment and (b) the Rheostat

The experimental dynamic gear test-rig setup is shown in the Figure 5.4. Two parallel shafts are used and the gear meshing is supported by four bearing houses. Motor yields clockwise rotation to the driver shaft attached with the gear and corresponds to power transfer to the parallel-driven-shaft results in anti-clockwise rotation. The rheostat controls the preset motor speed for the test.

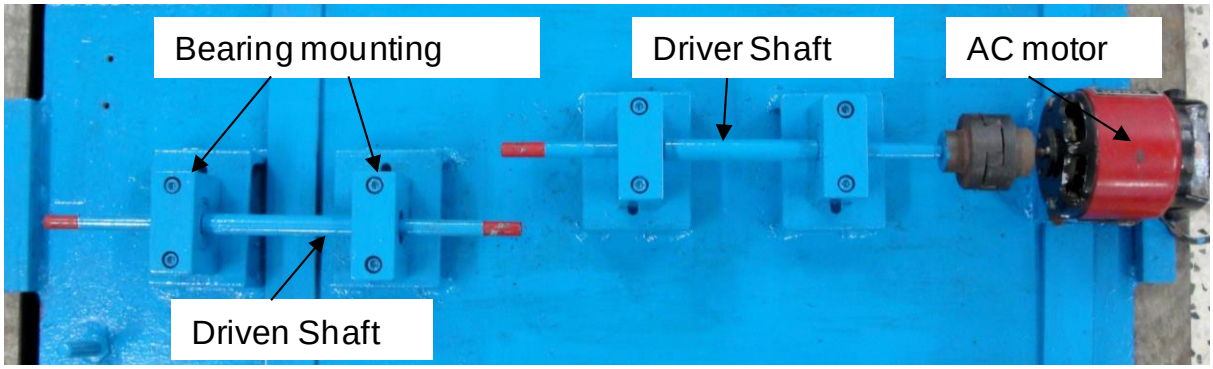

Figure 5.4 Modified gear testing setup used in the experiments

In the Figure 5.5(a) and (b), pure polypropylene and 10 wt% cement reinforced composite gear pair meshing have been illustrated. Initially, the gear pair meshing is done with the shafts using bush and set-screw arrangement.

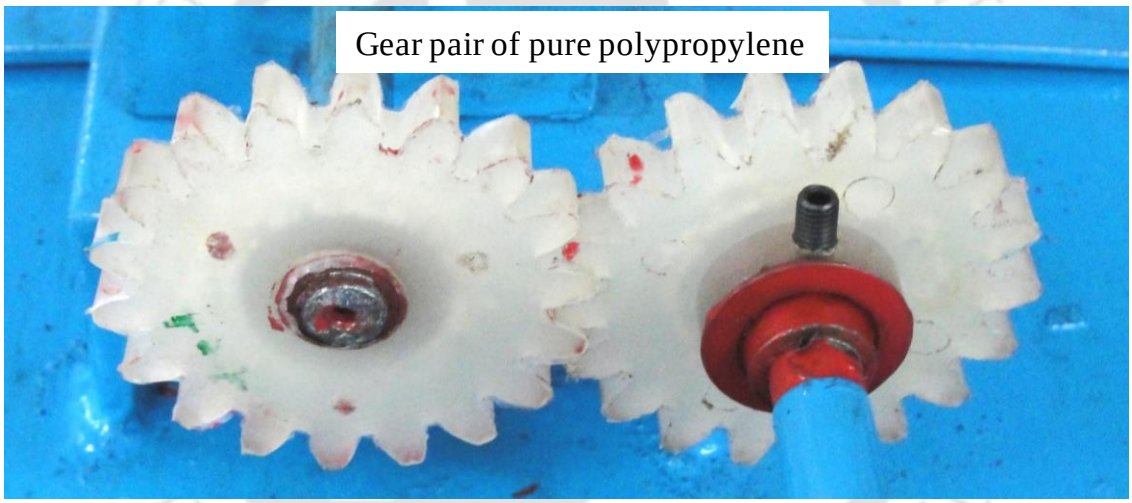

(a)

(b)

Figure 5.5 (a) Pure polypropylene and (b) 10% cement filled composite test gear mesh

During experimentation, the IR assisted camera is fixed at two different directions along (a) transverse and (b) longitudinal direction. The ambient temperature of the laboratory remains to be 27ºC (room temperature) during experimentation. During running of the gear pair, the surface temperature rises and reaches an optimal value and this gives direct measures of the heat loss. The camera senses the emitted heat loss in terms of temperature, greater than ambient temperature and analyzed the data in accordance with the principle of infrared emissivity. The dynamic experimental conditions in different positions are shown in the Figure 5.6(a) and (b).

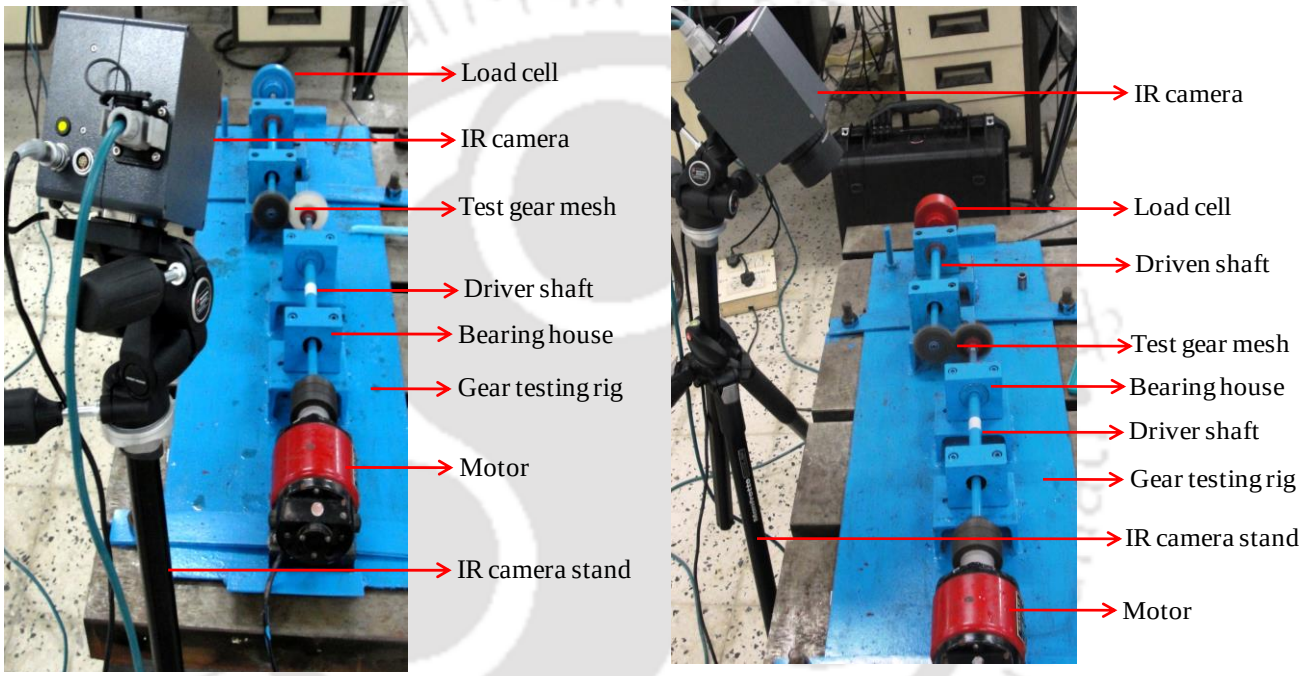

(a) (b)

Figure 5.6 Dynamic gear test rig setup with accessories (a) along transverse direction and (b) longitudinal direction

The gear pair teeth meshing is an elliptical shape in dynamic condition signifies the teeth contact region where the friction wear takes place. The gear teeth meshing have been illustrated in the Figure 5.7.

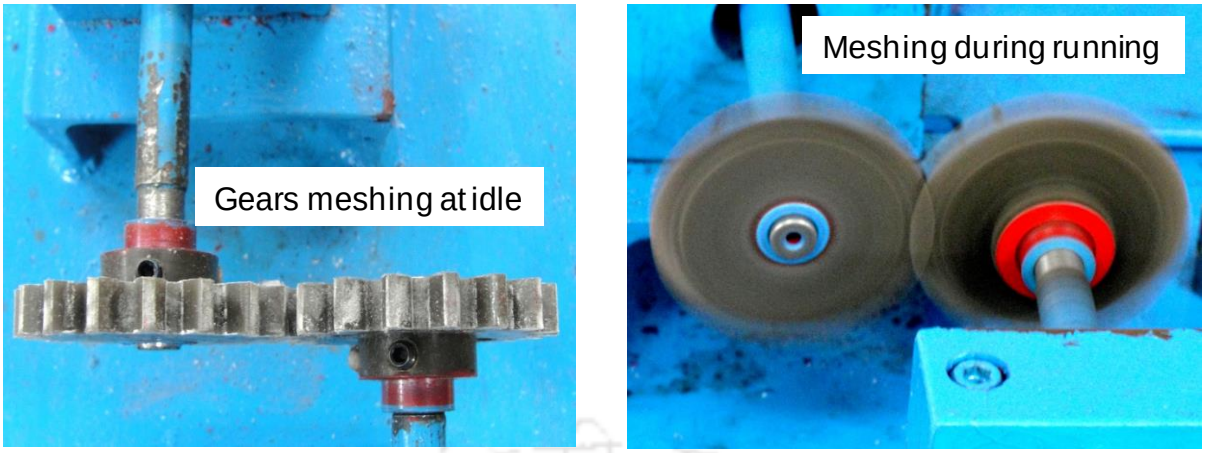

(a) (b)

Figure 5.7 Gear pair meshing (10% cement filled composite) (a) idle longitudinal position (b) transverse position at dynamic condition

5.3 Effect of Heat and Performance Analysis

In this section, the effect of heat in terms of temperature on the performance of the gear is investigated as it directly influences the service life. The surface temperature during running of the pair gear has been measured and quantified and analyzed by IRBIS 3 PLUS software. Figures 5.8(a) to 5.11(a) are showing the maximum and minimum temperature variation with time for 10% cement reinforced composite gear pair during running under 13.5 N load with speed of 600, 1200, 1800 and 2500 rpm respectively. While in meshing, along the teeth of the gear pair, a rectangular section is selected through software and all the results are obtained in that region as shown in the Figures 5.8(b) to 5.11(b). It is observed that the maximum surface temperature of gear tooth flaks to be around 29ºC, 30.5ºC, 34ºC for 600, 1200 and 1800 rpm respectively, while at 2500 rpm, the maximum temperature is recorded to be around 52ºC which is 53% higher than the surface temperature of the gear pair when the speed is 1800 rpm. This variation of heat loss anticipated because of temperature rise owing to the high friction takes place at high speed. The maximum and minimum temperature graphs indicate that the variation of highest temperature and lowest temperature at the selected rectangular section throughout the experimental time span.

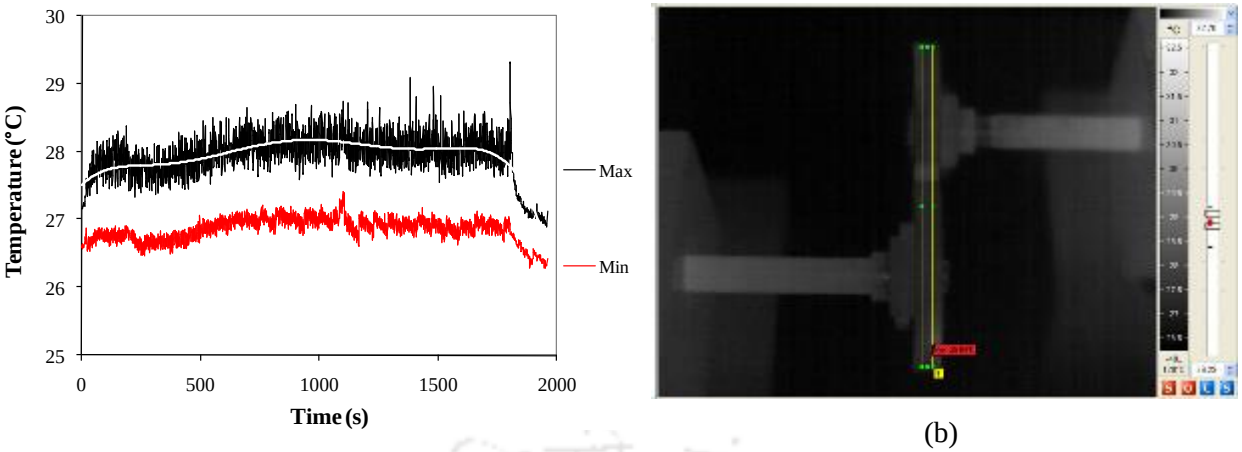

(a) (b)

Figure 5.8 10% cement reinforced composite driver-and driven intact gear at 600 rpm: (a) max. and min. surface temperature vs. time (b) selected region for evaluation of temperature

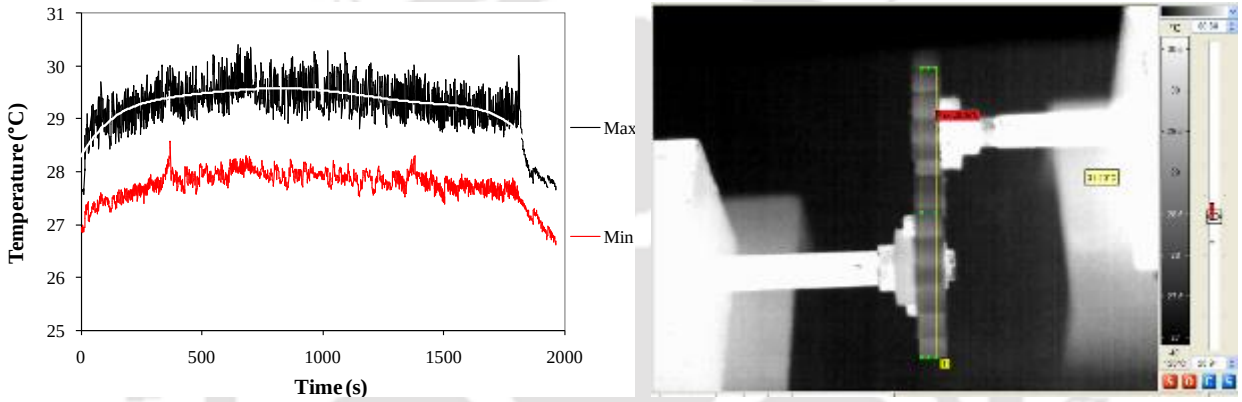

(a) (b)

Figure 5.9 10% cement reinforced composite driver-and driven intact gear at 1200 rpm: (a) max. and min. surface temperature vs. time (b) selected region for measuring the temperature

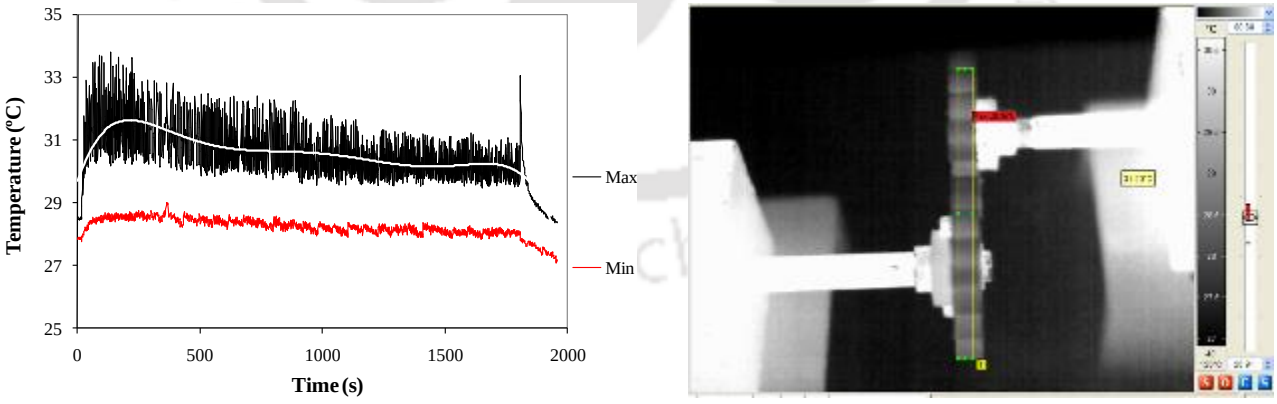

(a) (b)

Figure 5.10 10% cement filled driver-and driven composite gear at 1800 rpm: (a) max. and min. surface temperature vs. time (b) selected region for temperature evaluation

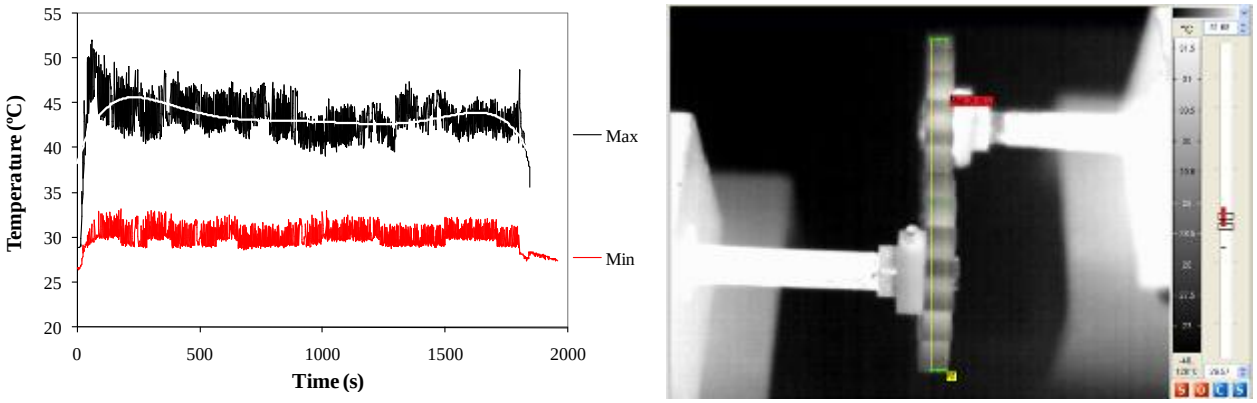

(a) (b)

Figure 5.11 10% cement filled driver-and driven gear at 2500 rpm: (a) max. and min. surface temperature vs. time (b) selected region for measuring the temperature

For all the cases, the power transfer takes place through the metallic gear shaft, located along at the centre of the gear and attached with its collar. As the metallic shaft passes through the collar of the gears, higher temperature rise is observed at the gear collar section. The corresponding thermographs have been shown in the Figures 5.12 to 5.15 with respect to time where preset speeds are 600, 1200, 1800 and 2500 rpm respectively. It is observed that temperature rise with time depends on the speed and as well as the load applied. In this work an elevated load of magnitude 13.5 N is selected for the experimentation.

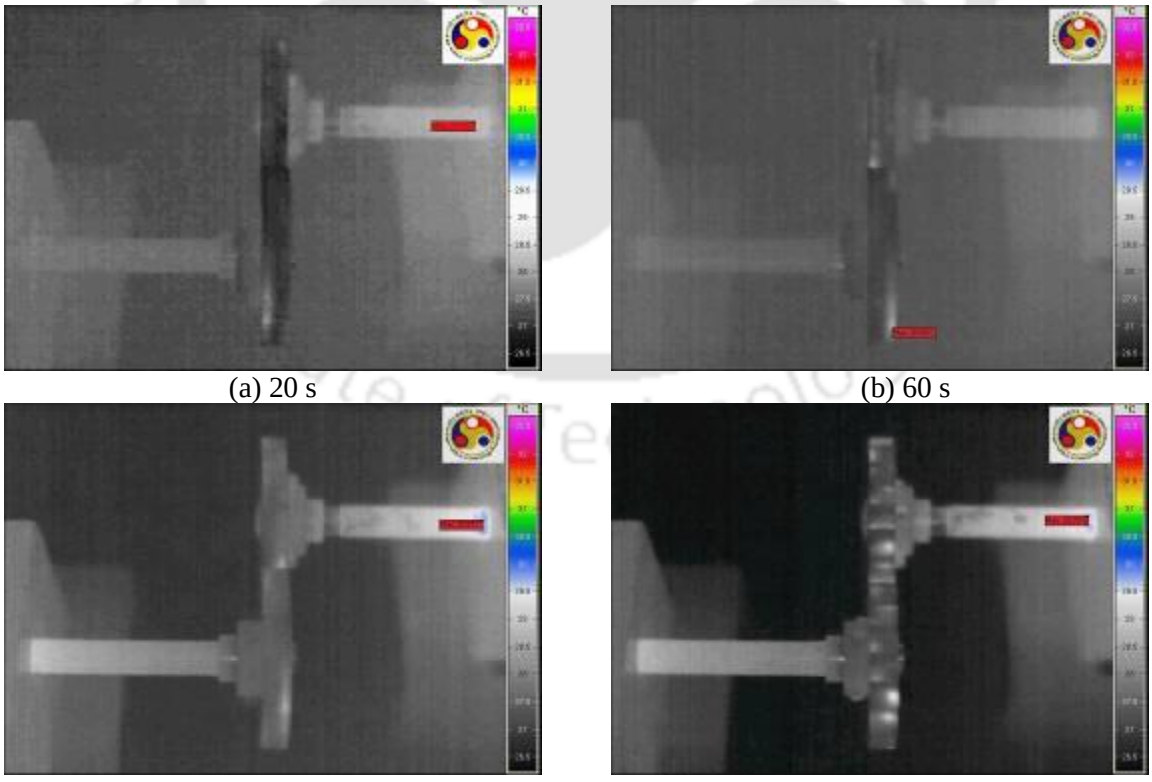

(a) 20 s (b) 60 s

(c) 1000 s (d) just stop

Figure 5.12 The contour of thermograph of the gear pair after running for (a) 20 s, (b) 60 s, (c) 1000 s and (d) just brought to rest, speed 600 rpm

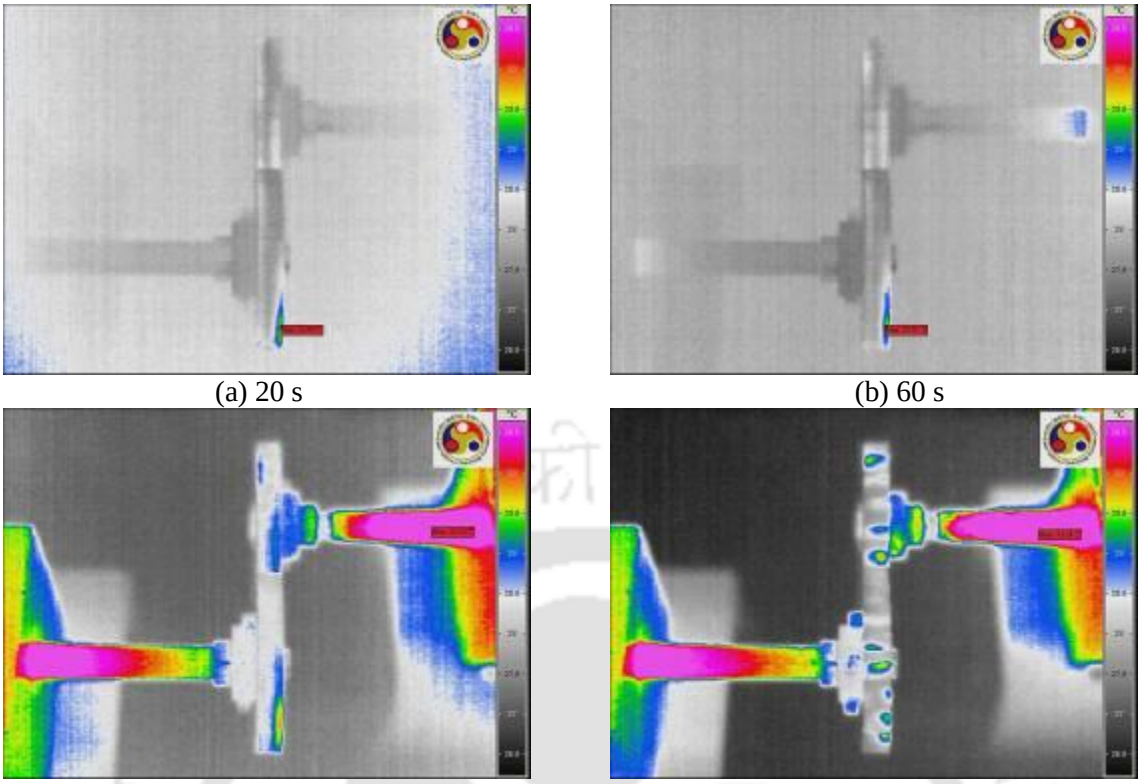

(a) 20 s (b) 60 s

(c) 1000 s (d) just stop

Figure 5.13 The contour of thermograph of the gear pair after running for (a) 20 s, (b) 60 s, (c) 1000 s and (d) just brought to rest, speed 1200 rpm

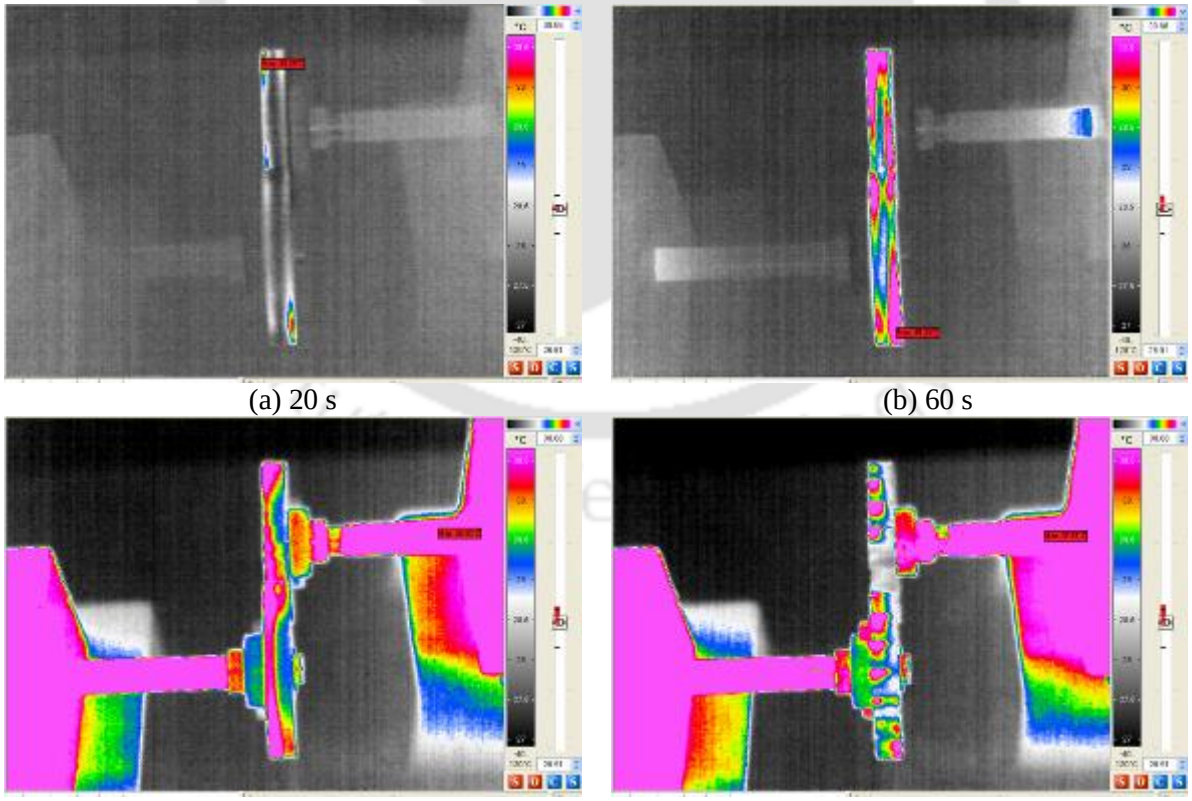

(a) 20 s (b) 60 s

(c) 1000 s (d) just stop

Figure 5.14 The contour of thermograph of the gear pair after running for (a) 20 s, (b) 60 s, (c) 1000 s and (d) just brought to rest, speed 1800 rpm

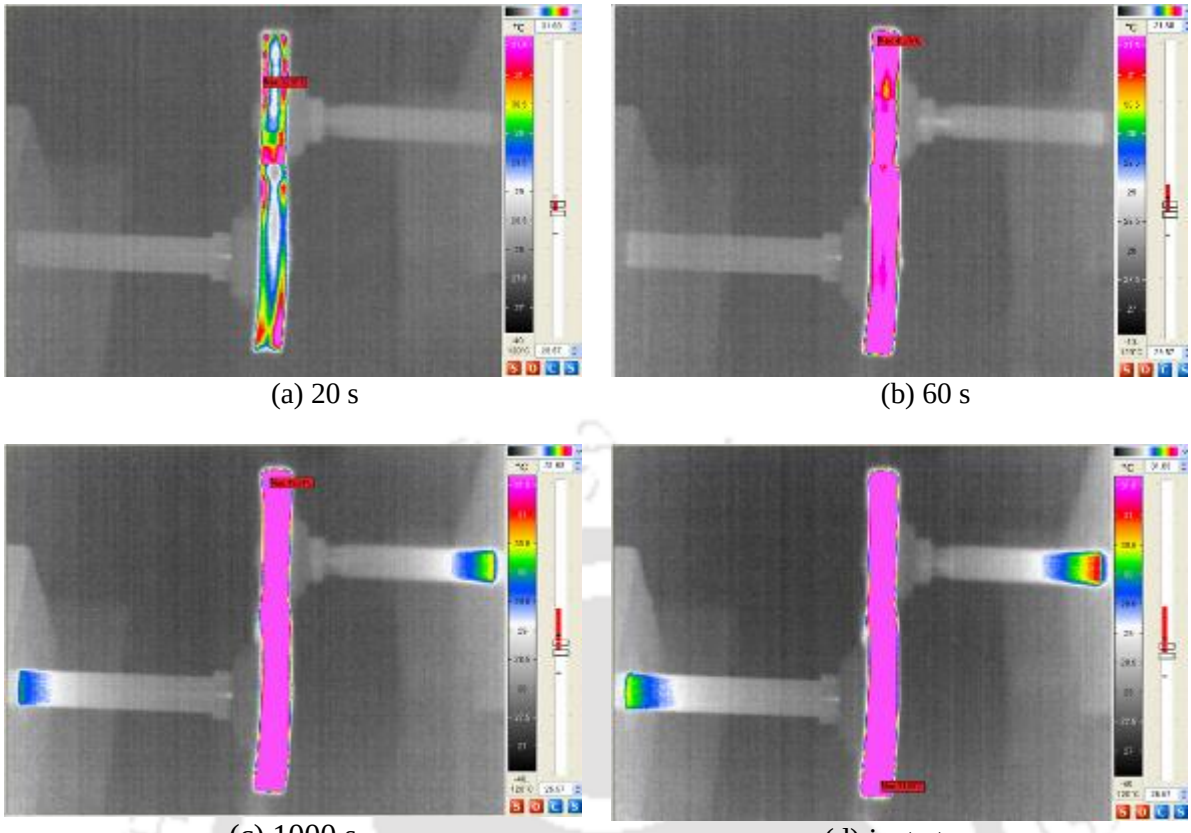

(a) 20 s (b) 60 s

(c) 1000 s (d) just stop

Figure 5.15 The contour of thermograph of the gear pair after running for 2500 rpm after (a) 20 s, (b) 60 s, (c) 1000 s, (d) just brought to rest, speed 2500 rpm

5.4 Dynamic Performance Test of Gear with Single Crack

It is essential to investigate the gear performance with inherent manufacturing defects or deformities developed during operation under a certain speed and loading condition. Thus, it is anticipated that the presence of cracks or deformities may be one of the reasons that governs the fall of performance of the gears during working condition. Hence, taking into account this consideration that tooth root regions are vulnerable to deformations, experiments are conducted to study the effect of deformities on the gear performance. Further, 1 mm crack has been generated manually at the tooth root region for both the driver and driven gear and the effect of cracks on the surface temperature has been investigated.

Similar to the intact gear tooth configuration, experiments are conducted on single crack for both driver and driven gears and the results are comparatively discussed. The experimental condition and the procedure are maintained same as for defect free gears. It is observed that maximum and minimum temperature rise up to 29.5ºC, 31ºC, 34.6ºC and 52ºC for 600, 1200, 1800 and 2500 rpm respectively. The results have been shown in the Figures 5.16(a) to 5.16 (d) respectively. It is observed that maximum temperature change with single cracked gear

pair is trivial compared to the intact gear pair. It is further noticed that surface temperature change shoots up to 50% high at the speed of 2500 rpm compared to the surface temperature with speed of 1800 rpm as shown in the Figure 5.16(d).

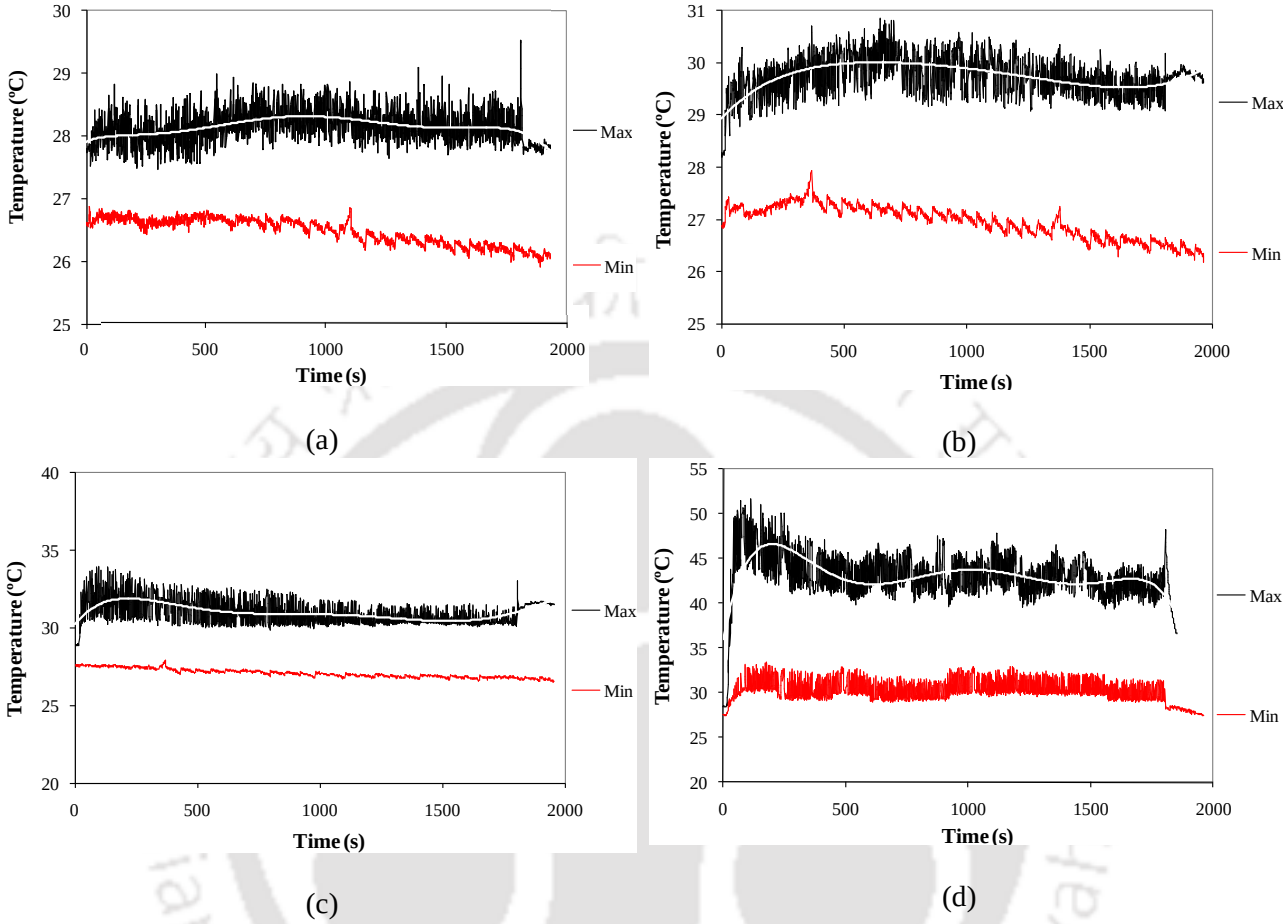

Figure 5.16 10% cement reinforced composite driver-single cracked driven gear at (a) 600, (b) 1200, (c) 1800 and (d) 2500 rpm

The contour of thermographs of single cracked gear pair have been shown in the Figure 5.17 with respect to time with a speed of 1800 rpm. The results further indicate that the temperature rising rate is higher at teeth meshing region during initial stage, owing to the higher friction in the region.

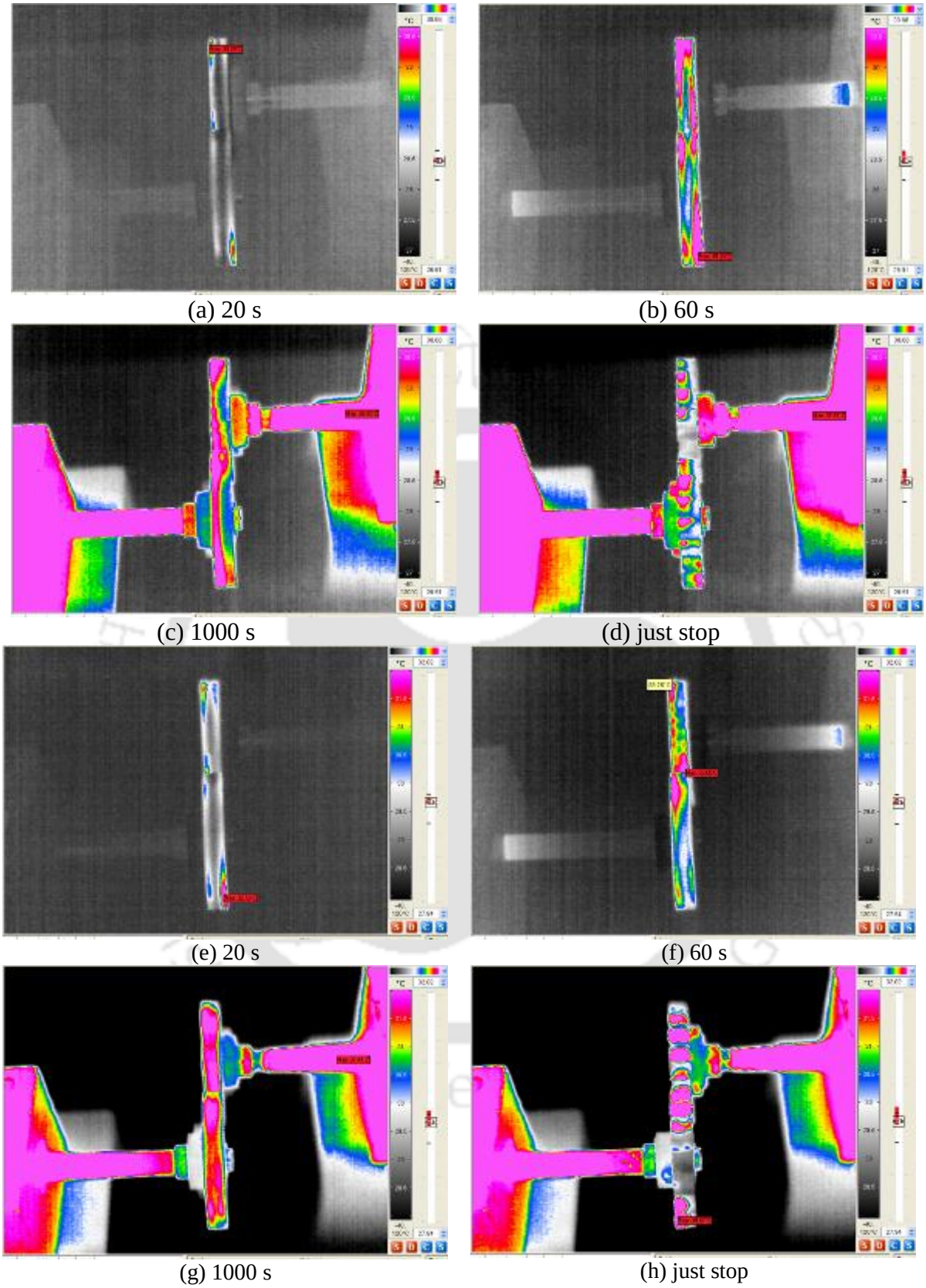

(a) 20 s (b) 60 s

(c) 1000 s (d) just stop

(e) 20 s (f) 60 s

(g) 1000 s (h) just stop

Figure 5.17 The contour of thermograph of the intact gear pair after (a) 20 s, (b) 60 s, (c) 1000 s and (d) just brought to rest, similarly, for single crack gear pair after (e) 20 s, (f) 60 s, (g) 1000 s and (h) just brought to rest with the speed of 1800 rpm

5.5 Dynamic Performance of Multi Crack Gear

Similar to single crack experimentation, gears with multiple cracks have been experimented. For this purpose, three cracks of 1 mm depth are manually implemented on the three adjacent teeth root of the driver and driven gear. For this, three cracks have been created manually on the three teeth roots. For the 10% cement reinforced composite spur gears with multiple cracks, experiments are conducted at elevated speeds. At high speed, the gear pair shows significant change in temperature level from its ambient condition. With gear speed of 2500 rpm and after time interval of 900s, the surface temperature change is observed to be little more than 52.8ºC which is approximately 45% higher than the surface temperature at the speed of 1800 rpm as shown in the Figure 5.18 (d). Another important observation is made when the gear is set to stop, the maximum temperature get stimulated. The anticipated reason is that at idle condition (just stop) the cracked section does not transfer the heat to the next conjugated tooth. The contour of thermograph of multiple cracked gear pair have been shown in the Figures 5.19 and 5.20 for 1800 and 2500 rpm respectively. It is observed that after 1000s, the thermograph contour shows high temperature rise along the teeth engagement location.

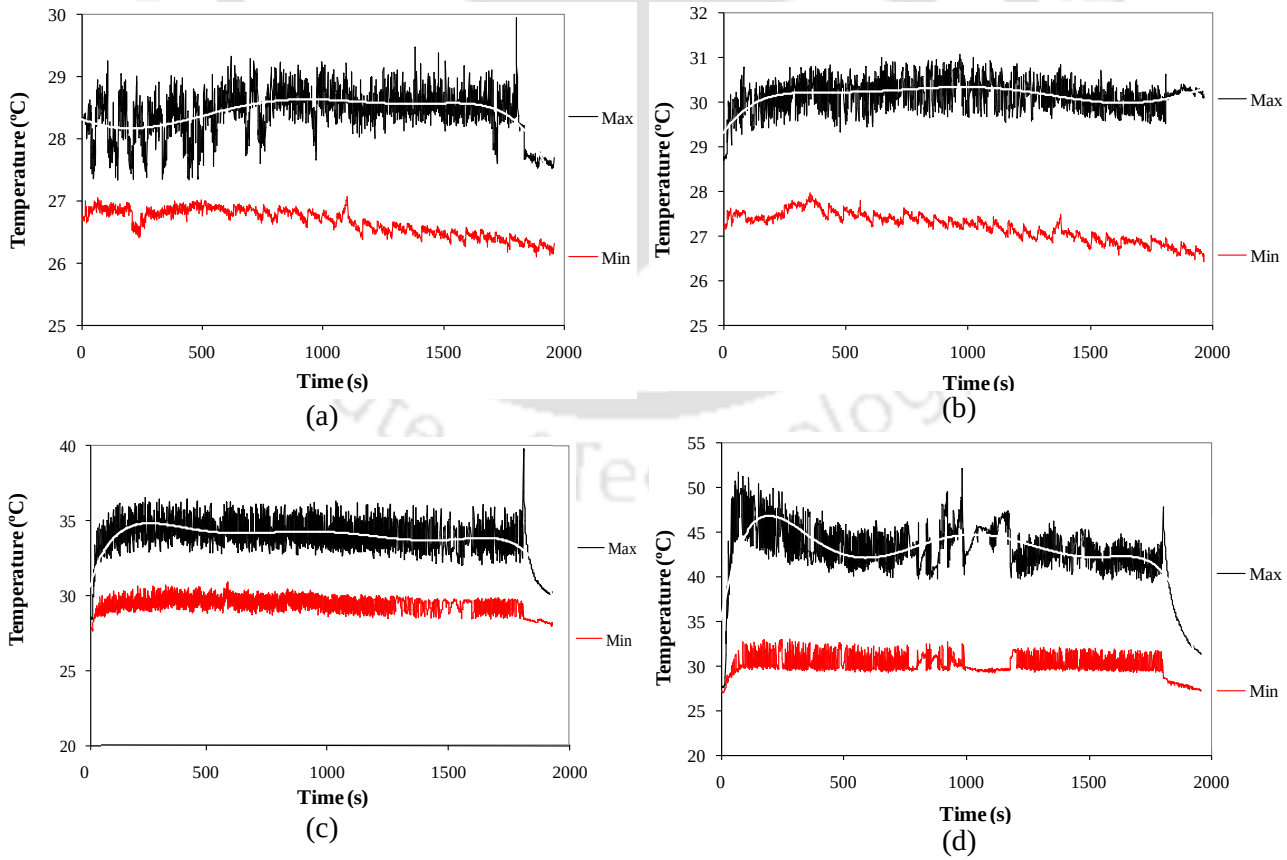

Figure 5.18 10% cement reinforced composite driver-10% cement reinforced composite multi cracked gear at (a) 600, (b) 1200, (c) 1800 and (d) 2500 rpm

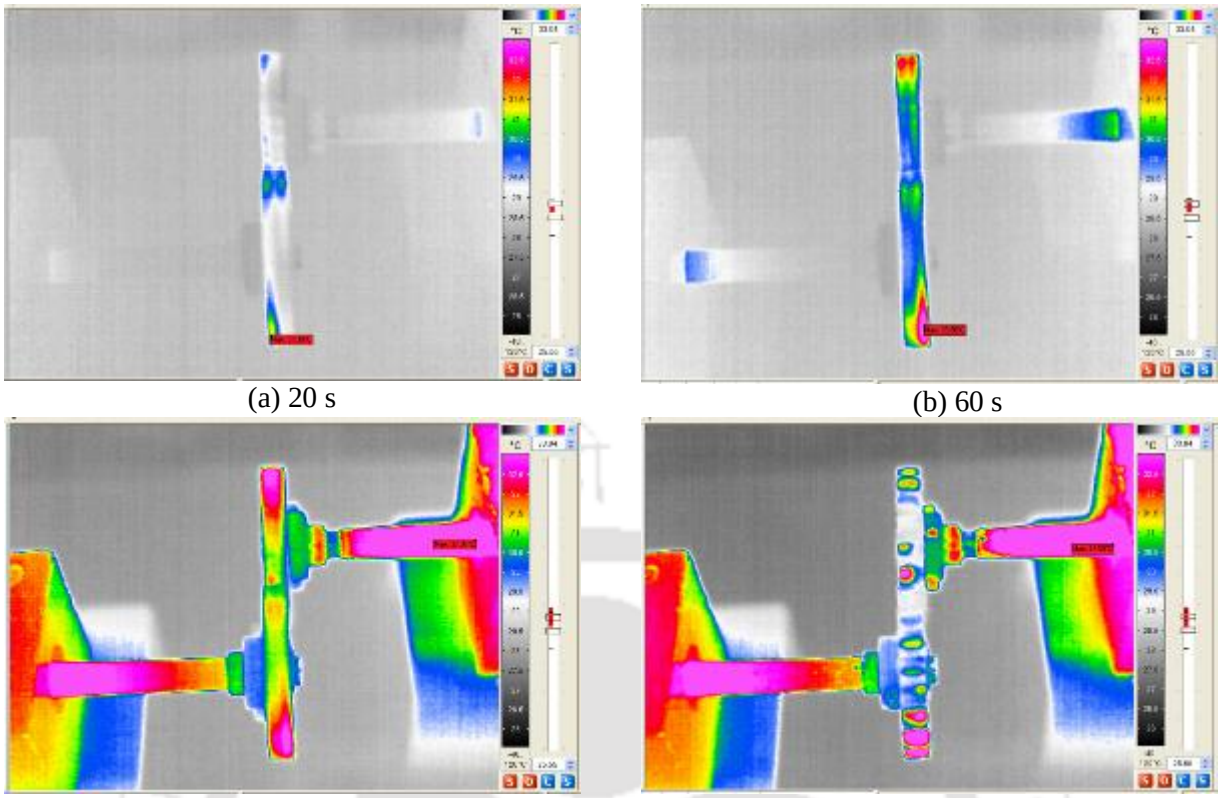

(a) 20 s (b) 60 s

(c) 1000 s (d) just stop

Figure 5.19 The contour of thermograph of the multiple (3) crack gear pair after (a) 20 s, (b) 60 s, (c) 1000 s and (d) just brought to rest, speed 1800 rpm

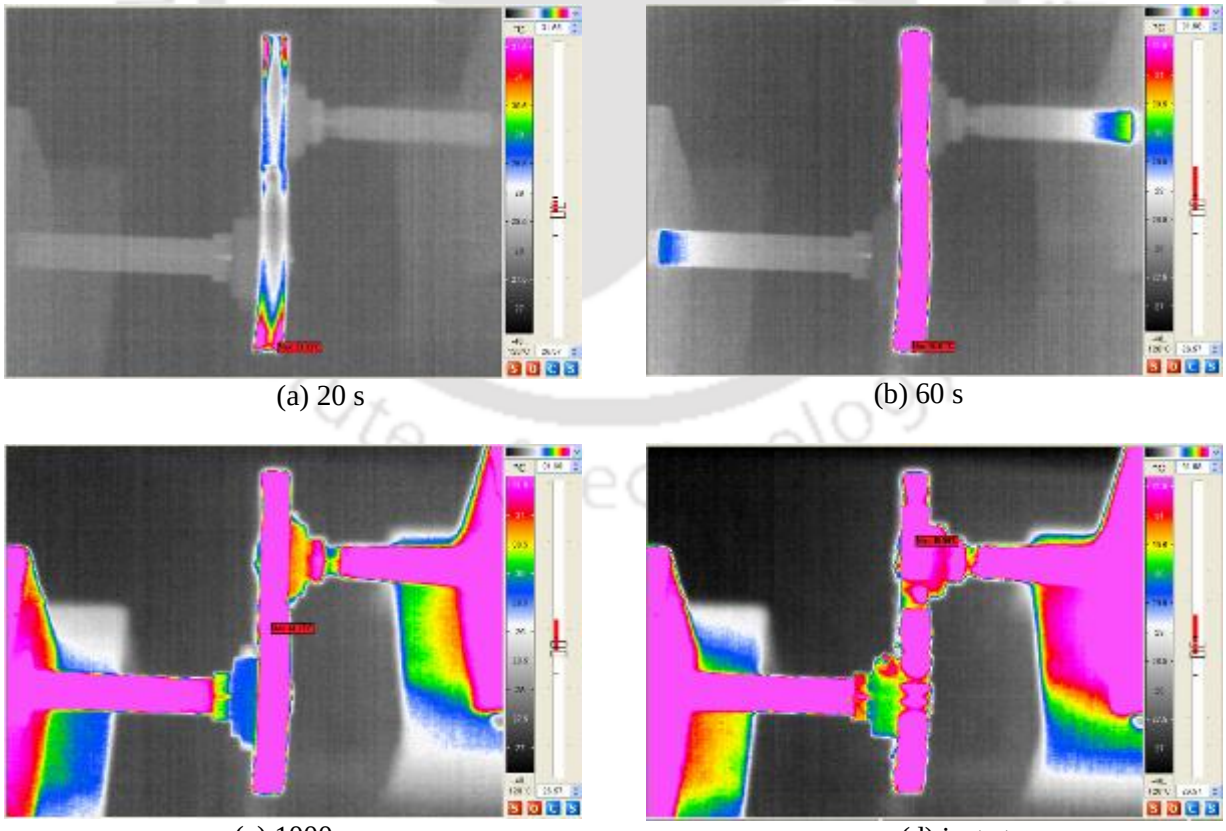

(a) 20 s (b) 60 s

(c) 1000 s (d) just stop

Figure 5.20 The contour of thermograph of the multiple (3) cracks gear pair for 2500 rpm after (a) 20 s, (b) 60 s, (c) 1000 s, (d) just brought to rest, speed 2500 rpm

It is observed that the induced crack does not affect significantly in variation of flank surface temperature of the test gears.

5.5.1 Performance Analysis along Transverse Direction

Similar results are also obtained along the transverse direction of the gear pair during running where data are accumulated at tooth meshing region. The test results with a speed of 1800 rpm are shown in the Figure 5.21. The contours of thermograph of the corresponding experiment have been shown in the Figures 5.22 to 5.24. It is clearly to be observed that the minimum and maximum temperature rise is close to each other. The reason behind this is the small mesh region of the gear pair selected, where in longitudinal direction, the temperature is measured throughout the gear tooth taking a comparatively bigger rectangular region. It is, further, to be noticed that the rectangular region is selected in the meshing region, exhibits uniform temperature variation. As shown in the previous results, it is found that the threshold speed of the gear is 1800 rpm when load is applied 13.5N and surface temperature raised approximately 34ºC. Beyond this speed, the surface temperature of the gear is increased dramatically, and observed to be around 52ºC for test speed of 2500 rpm.

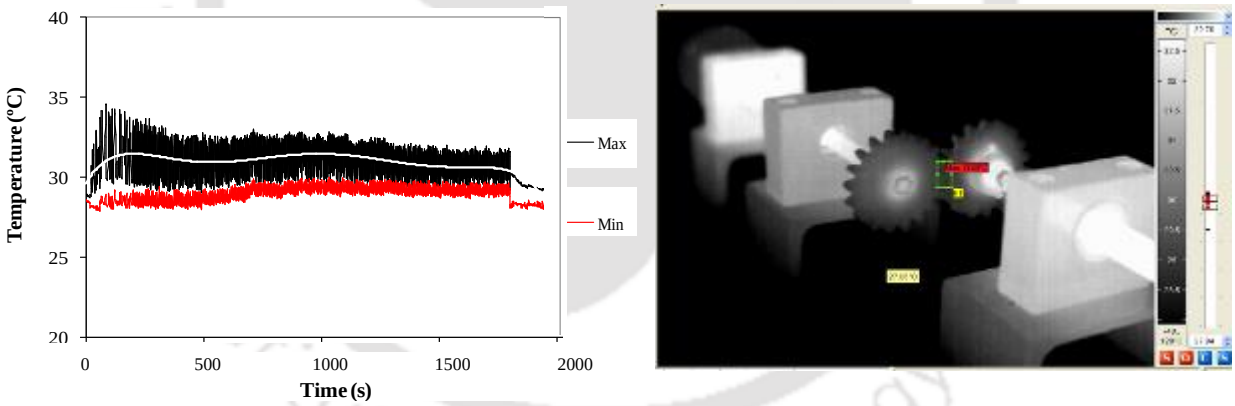

Figure 5.21 10% cement reinforced composite driver-and driven intact gear teeth mesh along transverse direction with 1800 rpm

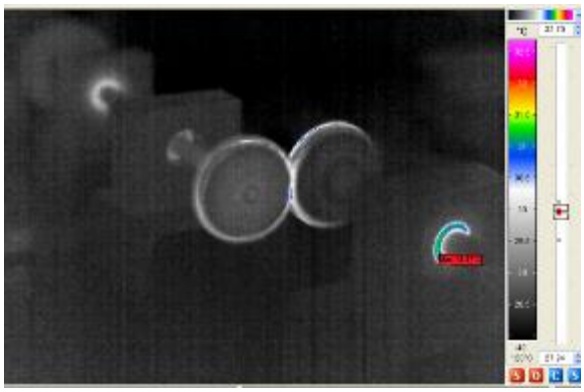

(a) 20 s

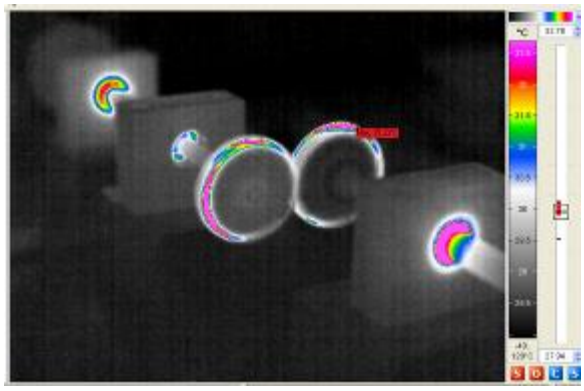

(b) 60 s

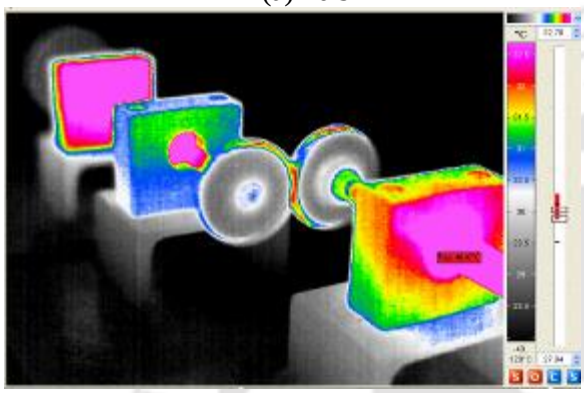

(c) 1000 s

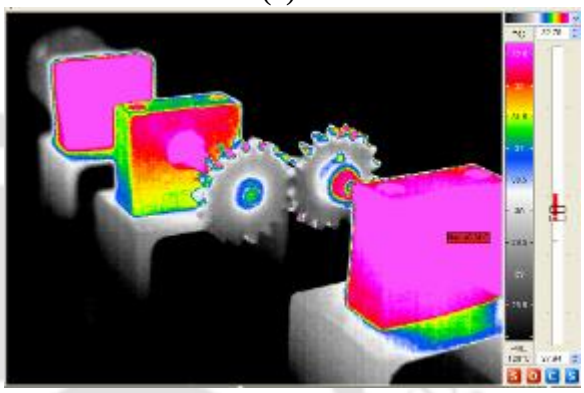

(d) just stop

Figure 5.22 The contour of thermograph of the intact gear pair after (a) 20 s, (b) 60 s, (c) 1000 s and (d) just brought to rest, speed 1800 rpm

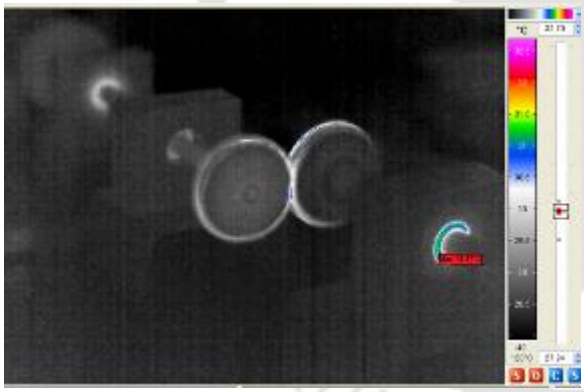

(a) 20 s

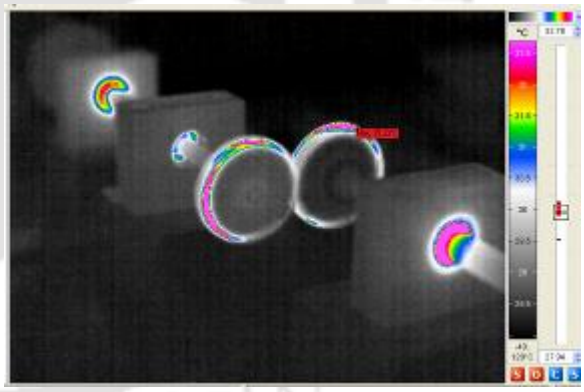

(b) 60 s

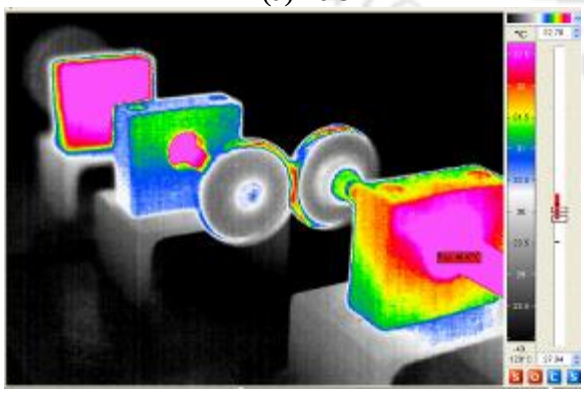

(c) 1000 s

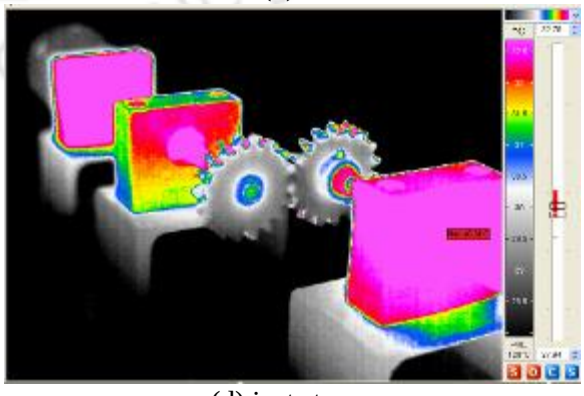

(d) just stop

Figure 5.23 The contour of thermograph of the single crack gear pair after (a) 20 s, (b) 60 s, (c) 1000 s and (d) just stop at 1800 rpm

The highest and lowest surface temperature of the gear pair for a single revolution is occurred across the face width of the gear during the test. In the Figure 5.24(e), corresponding to the revolution of the gear, highest and lowest surface temperature can be found. The experimental results are shown for the 10% cement reinforced gear under a load of 13.5N and speed of 1800 rpm. The right one is driver gear that runs clockwise and left one is the driven gear runs in anticlockwise. Referring, 0º is the mesh point of the gear pair, the contact flanks surfaces of the driver and driven gears, measurements are taken at a location of 180º on the driven gear after mesh point and 0º for both driver and driven gear. Similarly, for non-contacting flanks surfaces, measurements are taken at a location of 270º after the mesh point for the driven and 90º for the driver gear. The surface temperature of non-contacting gear flank is measured to be around 28.8ºC (i.e. corresponding to 270º revolution for driven gear and 90º for driver gear after the reference mesh point) which is 5.2ºC lower than the contact flank surface temperature i.e. 34ºC (corresponding to 180º revolution for driven and 0º revolution for both the driver and driven gear). This surface temperature can be found little different when the cracks takes place at the root of the gear tooth. However, huge difference can be observed when the speed of the gear pair is higher as example, 2500 rpm. This analysis has been quantified as per the literature reported by Mao, (*2007*).

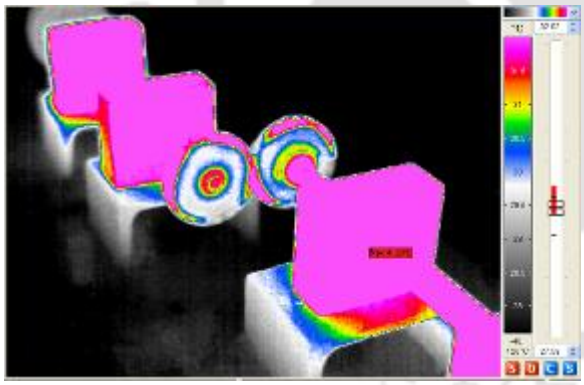

(a) 20 s

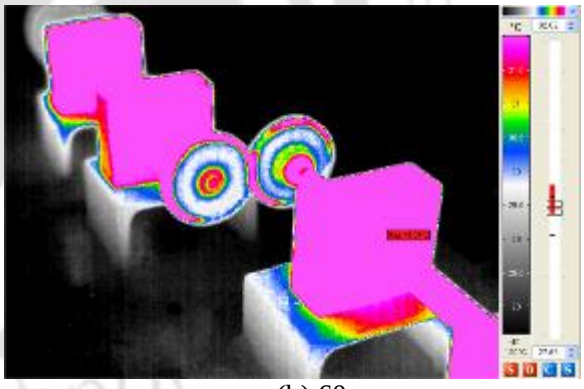

(b) 60 s

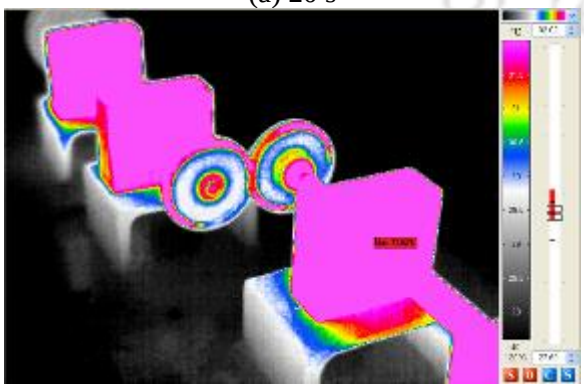

(c) 1000 s

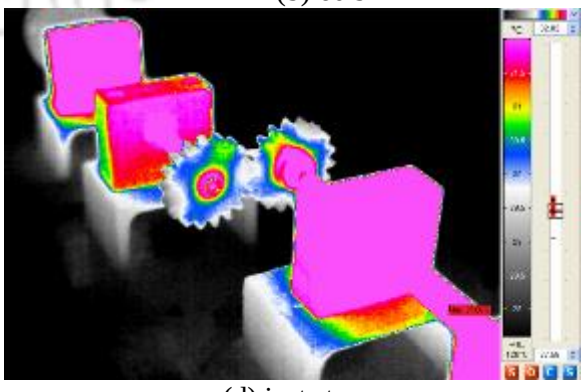

(d) just stop

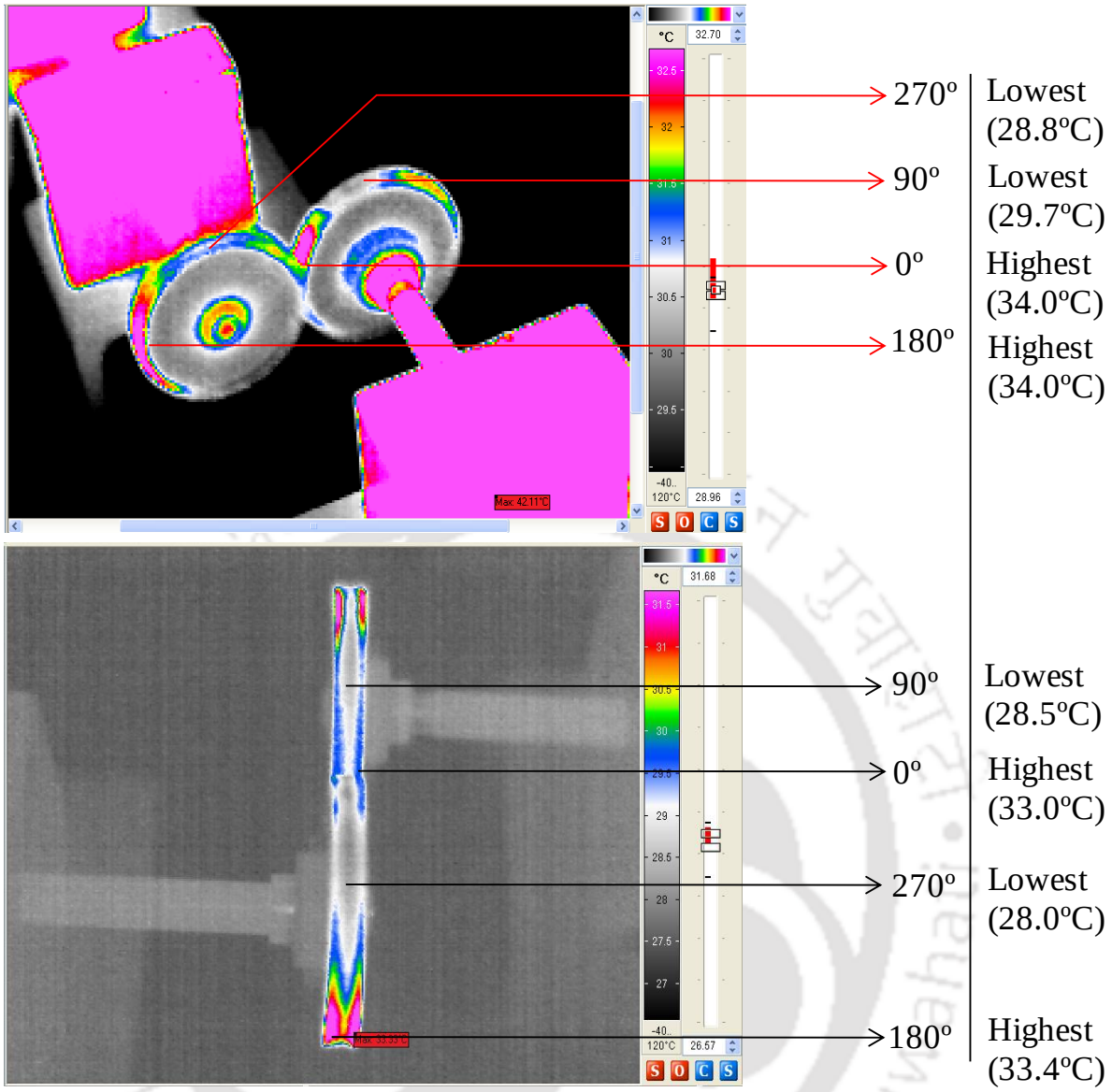

(e)

Figure 5.24 The contour of thermograph of the multiple crack gear pair after (a) 20s, (b) 60 s, (c) 1000 s,(d) just stop at 1800 rpm and (e) highest and lowest temperature position

Table 5.1 shows the surface temperature rise under variable speeds and loads with inbuilt cracks. It is observed that average surface temperature increases with load and speed. In the present study, it is observed that the location and depth of cracks on the driver and driven gears do not have significant affect on the gear performance compared with the intact gear. However, it is expected that multiple cracks of variable depths and locations on gear tooth could affect the material performance and further with associated heat emission rise, owing to high speed and loading condition may ultimately lead to failure of the gear. It is also observed that the surface temperature rises more prominently at the flanks surface of the gear

tooth. The reason behind this is more friction takes place at the flanks surface due to its bulging of the flanks compared to the edge of the tooth.

Table 5.1 Maximum surface temperature in different variables and comparison

Speeds (rpm)	8.5N			13.5N		
	Intact	Single crack	Multiple crack	Intact	Single crack	Multiple crack
600	29.0ºC	29.0ºC	29.0ºC	29.0ºC	29.5ºC	30.0ºC
1200	29.5ºC	29.5ºC	30.0ºC	30.5ºC	31.0ºC	31.0ºC
1800	31.2ºC	31.5ºC	31.5ºC	34.0ºC	34.6ºC	36.5ºC
2500	45.8ºC	46.1ºC	46.3ºC	52.0ºC	52.0ºC	52.8ºC

The surface temperature of the cement reinforced polypropylene composite material gear and other gears have been compared and tabulated in the chapter 4. As the results presented and discussed in the Table 4.5 in chapter 4, and correlating with the results given in the Table 5.1, it is observed that the polypropylene and Portland pozzolana cement particles are the cheapest matrix and reinforcing material respectively. In addition, the other advantages of this material such as low melting temperature of the matrix, reasonable mechanical properties, low density, recyclability and other superior characteristics conglomerate core interest in lieu of the metallic gears. Hence, 10 wt% cement filled composite gear is suggested for automotive industrial application and is suitable within the operating speed of 1800 rpm and applied load up to 13.5N.

5.6 Evaluation of Wear Characteristics

Past researchers have proposed and developed non-metallic gear as an alternative to metallic gear because of their acceptable advantages on wear and fatigue characteristics (*Düzcükoglu et al, 2009; Hoskins et al., 2011; Kirupasankar et al., 2012*). Mao, (*2007*), discussed the detail fabrication of polymeric composite gears using various materials such as glass and carbon fiber reinforced Nylon 66 and Acetal. Research emphasized on the effect of various parameters on the performance of the composite gear such as fiber length, gear tooth fillet radius, topography, fatigue and failure, tooth deflection, friction and wear etc. Few researchers evaluated the polymeric composite gear wear with respect to metallic gear by either bending strength or surface durability (*Chauhan et al., 2010*). Wright and Kukureka, (2001) have also exhibited similar type works. Their work mostly encompasses the performance of the fibre-reinforced polyamide-66 composite gear and detailing on the wear

performance. However, the work remains untouched on influence of filler percentages as well as filler aspect ratio on the tensile properties. These parameters significantly influence the mechanical properties of the composite materials for gear fabrication and its performance. Further, these composite materials not only weight effective but also possess exceptional corrosion and fatigue resistant properties. However, significant contribution can be achieved by designing composite materials which proves superior cost-effectiveness compared to conventional metals (*Deo et al., 2001; Breeds et al., 1993*). A number of literatures have been reviewed; however, very few literatures have shown the direct evaluation of wear characteristics of polymeric composite gear. Further, past researches indicate that, none of the procedures highlighted well with the experimental results. Thus, a detailed scientific investigation is in demand to evaluate the wear characteristics of the material to achieve optimal performance of the spur gear by minimizing the losses and thus improving the service life.

Fabricated composite material underwent several experiments to evaluate wear characteristics under Tribometer and employing wear & friction monitor (TR- 201, DUCOM) following both adhesive and abrasive friction wear mode with different loading conditions. Direct gear wear characteristics have been evaluated by weight reduction process after a certain run of a gear pair under 13.5 N and 8.5 N loads. Few rotational speeds have been selected for this experiment and the final weight loss has been measured by Analytical Balance. It is observed that out of three variations, 10 wt% PPC composite gear material exhibits optimal wear properties compared to other percentage selected.

5.6.1 Experimental Evaluation of Wear

Tribometer, wear & friction monitor – TR- 201, DUCOM is shown in the Figure 5.25 (pin-on-disc type) is used to investigate the adhesive and abrasive friction wear characteristics of the gear materials. The counter body of the instrument is a disc made of stainless steel (AISI 316 L stainless steel, hardened to 55 HRc). The specimen is held stationary and the disc is rotated while a normal force is applied through a lever mechanism. Testing is carried out as per ASTM G99 standard. The experimental setup is shown in the Figure 5.25.

Figure 5.25 Pin-on-disc type Tribometer (TR- 201)

5.6.2 Adhesive Wear

The friction force is measured with the force transducer fixed on the loading lever arm. Both the friction & wear testing are conducted at a constant load of 2 kgf (19.6 N) and 3 kgf (29.4 N) with a constant sliding velocity of 0.5 m/s at room temperature. Wear tests are conducted up to a sliding distance of 1000 m. The material loss from the composite surface is measured using a precision electronic balance with an accuracy of ± 0.01 mg. The specific wear rate (m^3/Nm) is then expressed on 'volume loss' basis as given in the eqn. (1) (*Bahadur and Polineni, 1996*):

$$K_w = \frac{\Delta m}{S_d \rho_c F_n} \times 1000 \tag{5.1}$$

where, K_w denotes the specific wear rate (mm^3/Nm), Δm indicates the mass loss (g) within the test duration, ρ_c denotes the density of the composite (g/cm^3), F_n refers the applied normal load (N), S_d denotes the sliding distance (m). The variation of coefficient of friction (μ) of the pure polypropylene and its composites with sliding distance is shown in Figure 5.26 (a) and (b). Similar effect can be observed in case of abrasive wear as shown in the Figure 5.27 (a) and (b). The coefficient of friction values are continuously recorded and the output is obtained during the entire rotation cycle of the disc. Initially an increase in coefficient of friction is observed. This is due to the anchoring between micro projections present on the

substrate and disc surface and subsequently this is worn out. Further, it is observed that coefficient of friction is found to be constant after a certain sliding distance. The coefficient of friction is in the range 0.2-0.3 in all the cases matching with the results of earlier researchers (*Ferreira et al., 2001*). Thus, it is anticipated that transfer film on the counter material plays a significant role in influencing wear mechanism (*Myshkin et al., 2005*). After the formation of transfer film on the counter face material, coefficient of friction reached steady state. As the sliding distance increases, the real area of contact increases as close as to apparent area of contact due to the asperities deformation. When two surfaces approach each other, initially their opposing asperities with maximum height come into contact. As the time increases, new pairs of asperities with lesser height make contact forming individual spots (*Sugimoto et al., 2007*).

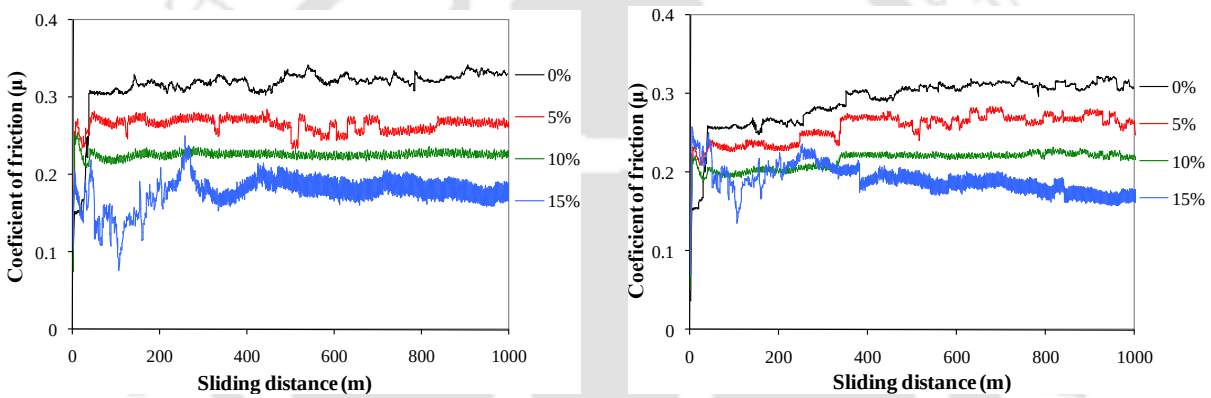

(a) (b)

Figure 5.26 Coefficient of friction evaluated for an applied load (a) 19.6N and (b) 29.4N

5.6.3 Abrasive Friction Wear

Silica carbide abrasive emery paper of 320 grit size is used for this test. The emery paper is firmly attached on the stainless steel (AISI 316 L stainless steel) disc to alter from adhesive to abrasive counter surface condition. The abrasive wear tests are conducted under 9.8 and 19.6 N normal loads at 0.5m/s sliding velocity. The laboratory condition remains to be normal room temperature and 60% relative humidity for the experiment. The experiment is conducted up to a sliding distance of 1000 m. The volumetric wear rate is quantified by mass loss as stated in the eqn. (1).

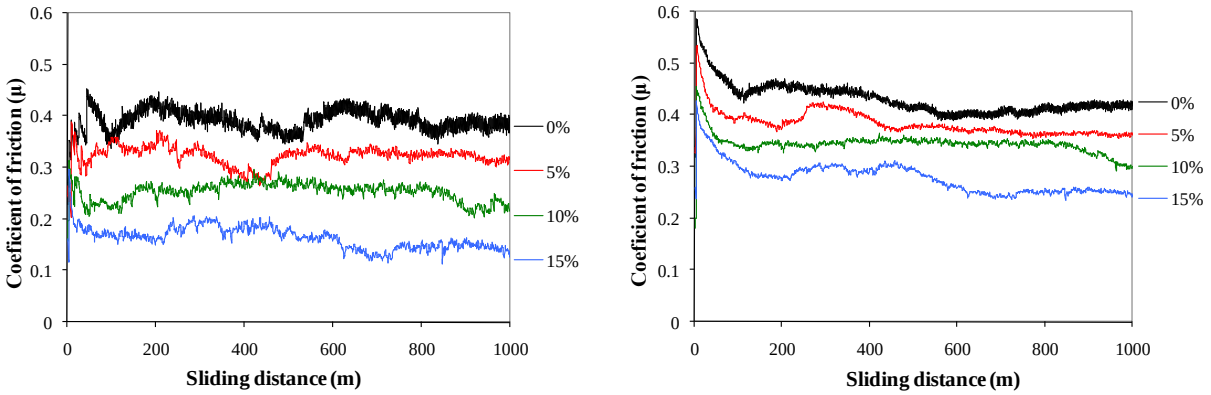

Figure 5.27 Coefficient of friction on abrasive mode under applied load (a) 9.8N and (b) 19.6N

5.6.4 Influence of Loading Conditions on Specific Wear Rate

In order to understand the influence of normal load and sliding velocity, coefficient of friction and specific wear rate are plotted against two different applied normal loads during wear test. The coefficient of friction, of all the gear materials for adhesive and abrasive wear properties, decreased with increase in normal load (Figure 5.28 and Figure 5.29). This behavior is due to the low sliding resistance offered by the specimen asperities at higher normal load. In spite of decrease in friction coefficient, specific wear rate of all the test gear materials increased with increase of normal load as shown in the Figure 5.28 and Figure 5.29. Further, it is observed that under same loading conditions, PPC reinforced composite gear materials exhibit less specific wear rate than unreinforced polypropylene, comparable to abrasive wear as well. The same trend has also demonstrated in the Figure 5.29. It is observed that 10% cement filled composite material exhibits optimal wear characteristics compared to pure polypropylene and other composite materials.

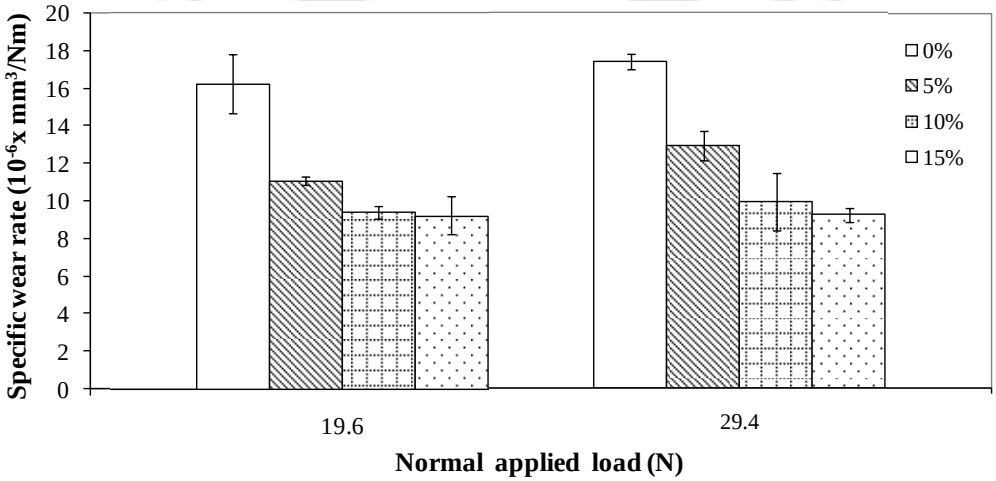

Figure 5.28 Variation of specific wear rate with applied normal load in adhesive wear

However, one can observe from the Figure 5.29 that 15% cement filled composite exhibits little more specific wear rate compared to 10% cement filled composite gear material. It is anticipated, this could be due to removal of PPC particles during running condition, as loading % of PPC is higher when emery paper is used.

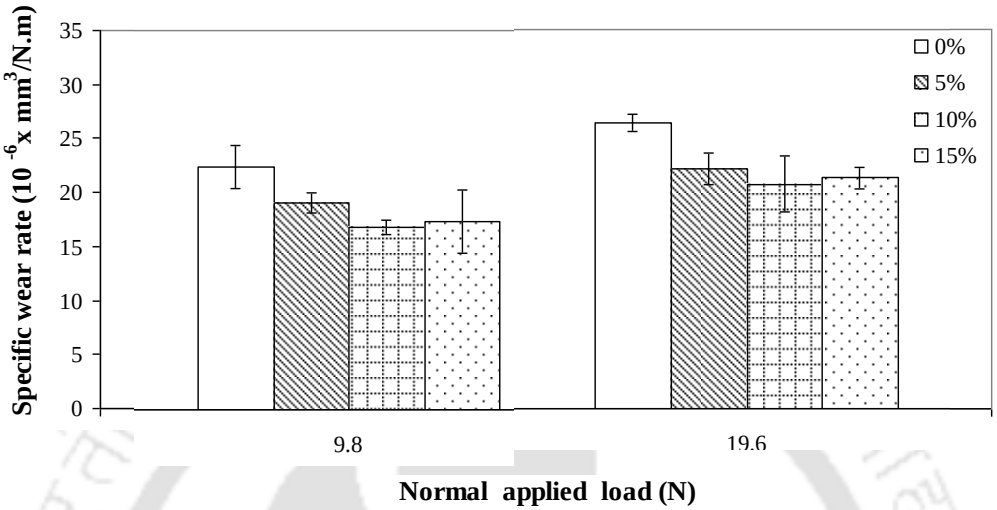

Figure 5.29 Variation of specific wear rate with applied normal load in abrasive wear

However, this is not observed for adhesive wear as shown in the Figure 5.28, it is observed that the specific wear volume decreases with increase of loading of filler materials in polypropylene. Further, specific wear rate is increased when the applied normal load increases.

5.6.5 Evaluation of Gear Wear: Direct from the Tooth Profile

For evaluation and measurement of wear due to friction in dynamic condition, a setup is developed equipped with an Infra-Red assisted camera, IR-TCM 384. The gear pair meshing in dynamic condition is shown in the Figure 5.7. The composite spur gears are subjected to the dynamic test and wear loss is evaluated by weight loss measurement after 156×10^5 cycles run for each gear pair. In dynamic condition, the gear pair runs at high speed, results in high friction between the gear pair at the tooth contact point, leads to wear of the material. These wear characteristics further aided by temperature rising, as a result, the gear performance starts to fall, which results in shortening of the gear life. This pros and cons are more applicable to the metallic gears. To remediate this problem, polymeric composite gears come in core interest to replace the metallic gears as well. The photographs of intact tooth profile and tooth profile after test have been given in the Figure 5.30. In the Figures 5.31(a) and (b)

show the worn-out of flank surface of polypropylene gear tooth and 10% cement reinforced composite gear tooth after test respectively.

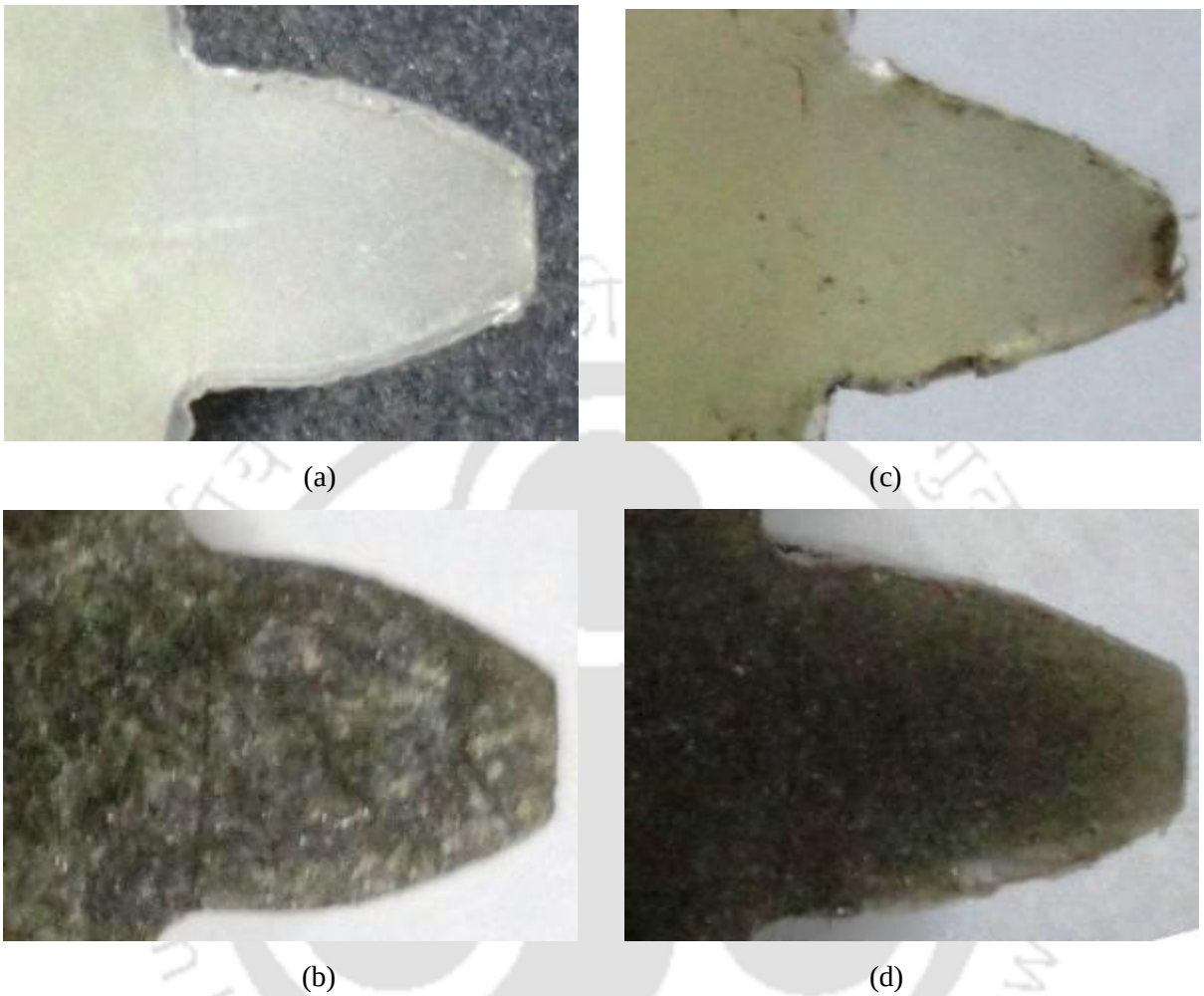

(a) (c)

(b) (d)

Figure 5.30 Intact tooth profile of (a) pure polypropylene, (b)10% cement filled composite and tooth profile after test (c) pure polypropylene, (d) 10% cement filled composite gears

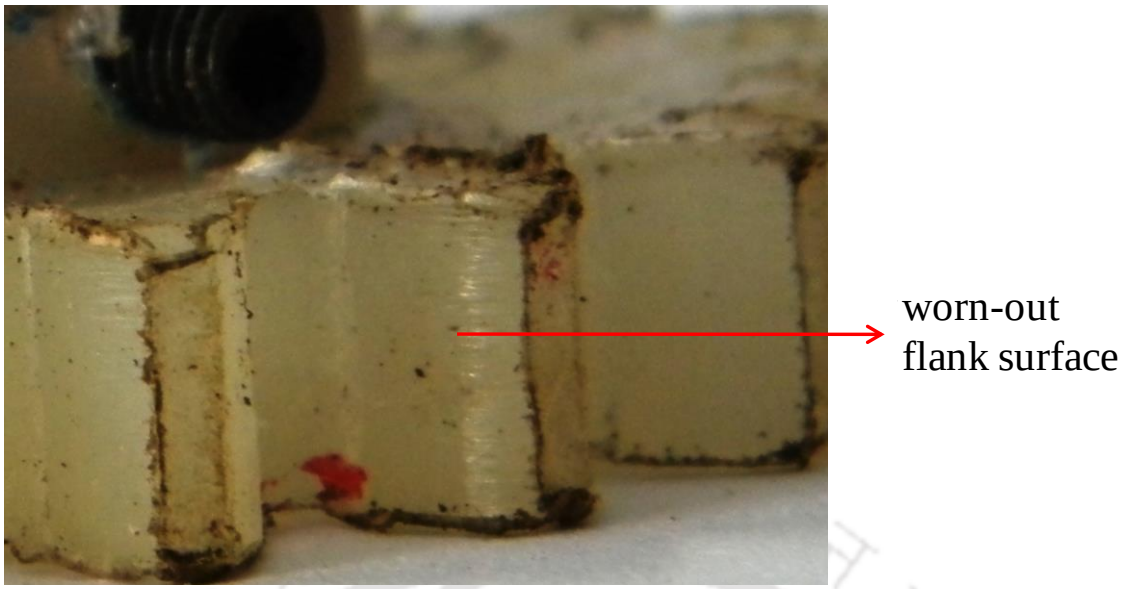

(a)

(b)

Figure 5.31 Warned out flank surface of (a) pure polypropylene and (b)10% cement filled composite gear tooth profile after test

5.6.6 Results and Discussions

Both intact edge profile and profile after test, are taken into account and the weight loss due to wear and wear volume have been calculated for all the samples with respect to loading conditions i.e., under 13.5N and 8.5N. The graphical expressions for both the cases are highlighted in the Figures 5.32-5.33 and Figures 5.34-5.35 respectively. Weight loss due to wear and wear volume of pure polypropylene gear is showing the highest value at elevated

rpm. At 2500 rpm, both the parameters, weight loss due to wear and wear volume are highest in comparison with other running speeds with the percentage increase of cement fillers.

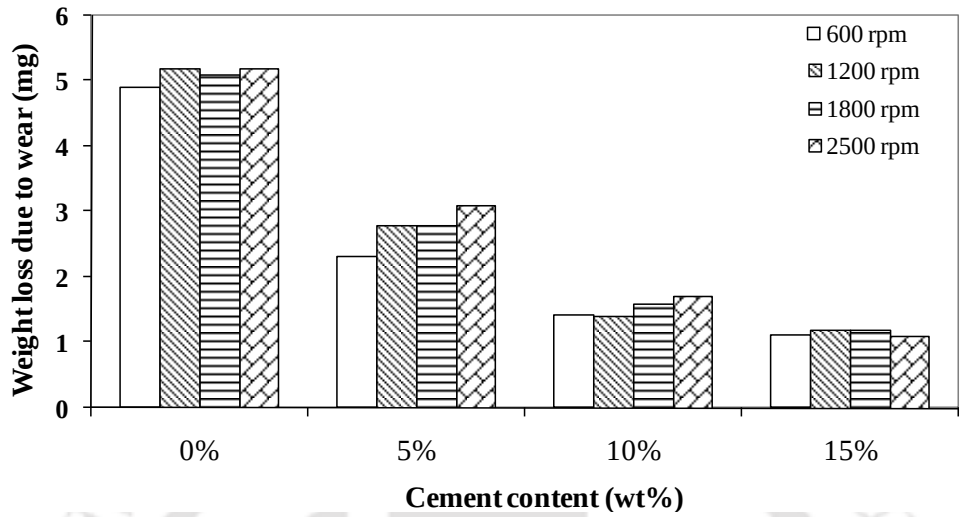

Figure 5.32 Weight losses due to wear at different rpm with 13.5N load

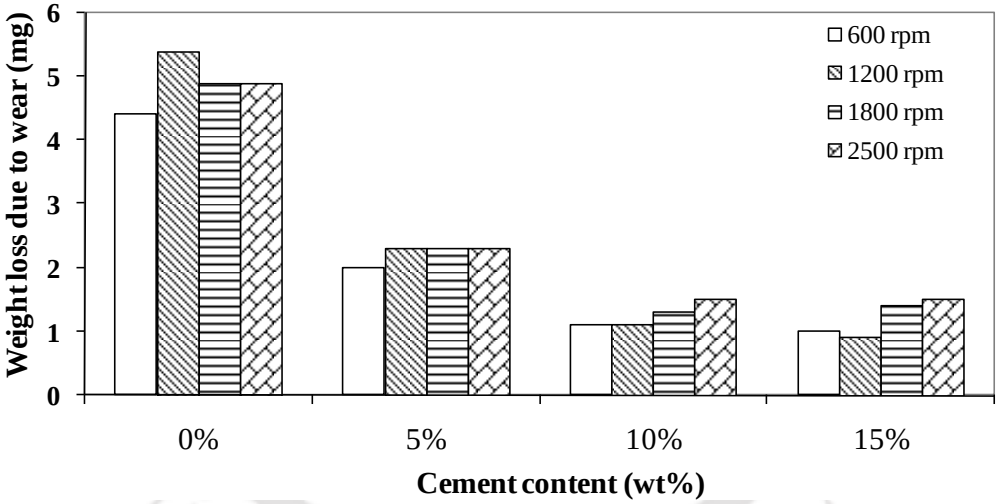

Figure 5.33 Weight losses due to wear at different rpm with 8.5N load

The reason is that the engaged tooth pair comes in contact more frequently when the running speed is 2500 rpm as compared to other variable speeds. Due to repeated contact, more friction takes place between the common tooth pair with less time as compared to other speeds. One can notice that, the 10% and 15% cement filled composite gears are giving relatively same results when running speeds are 1200, 1800 and 2500 rpm. However, when the running speed is 600 rpm, 15% cement filled composite gear gives lowest weight loss due to its significant higher stiffness and shear modulus compared to other materials.

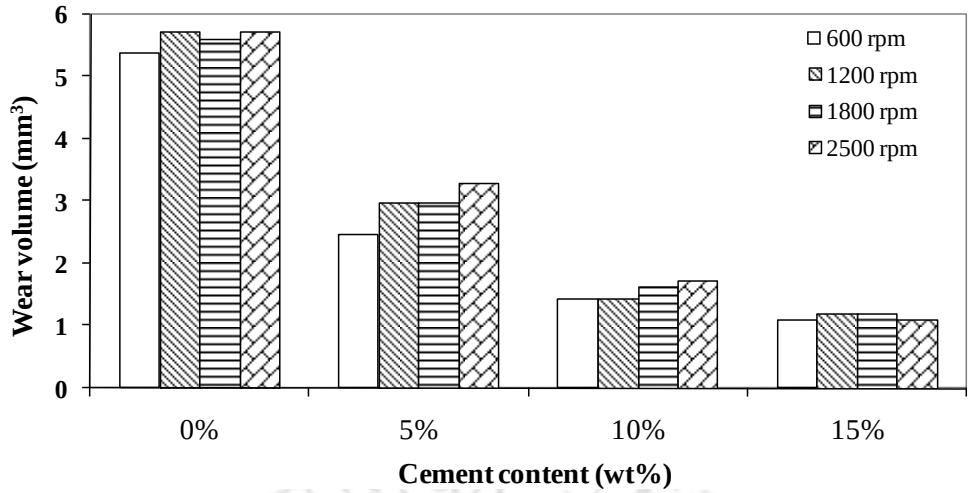

Figure 5.34 Wear volume at different rpm with 13.5N load

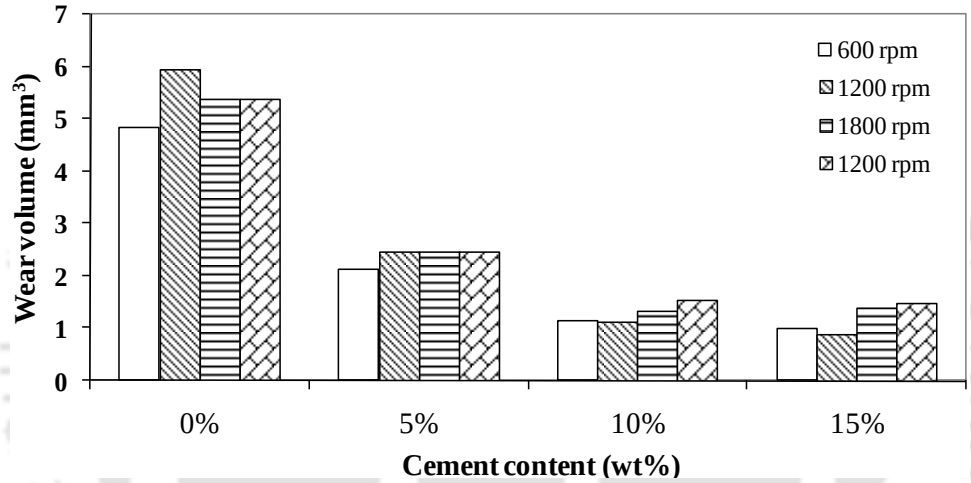

Figure 5.35 Wear volume at different rpm with 8.5N load

The weight loss i.e. volumetric wear of 10% cement filled composite gear is significantly less as compared to pure polypropylene and 5% and nearly equal to the 15% cement filled composite gear. This is because of comparatively lower coefficient of friction of 10% and 15% cement filled composite as compared to the other materials reported in this work.

5.7 Summary

The dynamic performance of the gear has been evaluated under loading conditions subjected to variable speeds. A unique test-rig, which allows free runs of gear pair has been modified and applied in evaluating polymer composite gear performance by an Infra-Red camera. Surface temperature rise and corresponding heat emission has been estimated on the performance of the gear under variable speeds and loading conditions. It is observed that, as the test speed increases the surface temperature of test gear increases leading to more

frictional loss of the gear material. It is also observed that gear is suitable to run at moderate speeds under moderate loading condition. Further, it is observed that the surface temperature of the gear pair is less as compared to the results indicated in the past researches for other composite and metallic gears as well.

Besides this, the spur gear material is tested to evaluate its friction and wear characteristics in adhesive and abrasive wear modes. Weight loss due to wear of the composite gear is evaluated through direct measurement under a specific load and running condition. It is observed that the adhesive wear rate significantly reduced when the cement filler loading increases. This is because shear strength and surface energy of the composite material changes while toughness and hardness of the material improves due to strengthening by cement fillers. It is observed that the 10% cement reinforced composite material gives optimum wear and fatigue performance because of its high stiffness ratio compared to pure polypropylene and 5% cement reinforced composite, though inferior to 15% cement reinforced composite. The weight loss due to wear and wear volume have been calculated directly by weighing after running the gears at elevated speed under variable loading conditions. It is found that 10% cement reinforced composite spur gear shows less weight loss due to wear friction during running. It is observed that out of three variations, 10 % PPC composite gear material exhibits optimal wear properties compared to other percentage selected. Thus, 10% cement filled composite material gear is better suitable to fabricate the non-metallic spur gear for industrial application.

Chapter 6

Studies on Vibration and Mechanical Properties of the Composite Materials and its Sandwich Panels

6.1 Introduction

Mechanical properties, fatigue resistance and outstanding inherent damping behavior are the most enviable characteristics of the composite materials for structural application. The fabricated composites are suitable for application in wide range of vibration prone structural components such as building shades, automobile body parts, propeller blades, suspension spring for automobile applications etc. Besides this, the composite can be used for door panels and interior furniture as well. In this context, the proposed thermoplastic composite materials make high interest as efficient vibration attenuator not only for their competence to absorb vibration energy but also for low density, high stiffness, easy processing capability and low cost. Further, in industry, the attenuation of vibration for mechanical parts get importance as unexpected vibration of the machine parts take place due to mass imbalance and improper centering. Thus, complete and systematic understanding of all the damping properties of reinforced polymeric composite materials is necessary for designing this class of material for structural applications. Cracks pose a severe menace to proper functioning of composite materials and eventually shorten working life of structural components made of it. Most of the failures of presently used equipment are observed to be due to material fatigue. For this reason, methods making early detection and localization of possible cracks have been the subject of many investigations. In structural element cracks causes some local variations in its stiffness and other mechanical properties, which affects the dynamics of the whole structure to a considerable measure.

The frequencies of natural vibrations, amplitudes of forced vibrations and areas of dynamic stability change due to the existence of such cracks. The effect of cracks on the damping performance of the composite material is necessitated when it is intended to apply for structural applications. However, very limited works in the past, emphasized on the effect of cracks for reinforced polymeric composite materials for its structural applications.

Nowadays Sandwich panels and beams of composite and metallic materials are increasingly getting recognition in various applications such as facades, partition walls and ceilings used

in sports hall and commercial building, naval and submarine structures, aircraft structures, and many more such applications (*Steeves and Fleck, 2004; Mitra, 2010; Mouritz et al., 2001*). The area of applications requiring high bending stiffness and strength along with required damping properties combined with specific gravity. The sandwich concept is that mostly rigid metallic skins suitable to carry axial and bending loads of the beam, separated by a low density core material that can carry the shear loads (*Steeves and Fleck, 2004*). The purpose of this study is to design a light-weight sandwich panels suitable for specific industrial application.

In this chapter, the Portland pozzolana cement (PPC) reinforced polypropylene composite materials are taken into account to evaluate the damping properties subjected to free vibration tests. The experiments are conducted using the laser assisted vibrometer (LAV) to evaluate and characterize the damping at low frequency. The time response and Fast Fourier Transform (FFT) analysis have been carried out and subsequently the damping and loss factor of the materials are obtained. The effects of cracks on the material performance with respect to its position and depth on the composite beams are also investigated vastly subjected to experimental analysis and the results are validated and comparatively studied and discussed.

Sandwich panel of the composite material is manufactured where aluminum and galvanized iron (GI) sheets are used as skin materials and cement reinforced polypropylene based composite material is used as core material. The proposed sandwich panel is similar to the GI skinned face sandwich panel used in automobile structural components, marine and in aircraft structures etc. These arrangements prove to be much more beneficial as it reduces the overall weight of the vehicle suitable to ply on in trailer, road train and other road transports. Further, damping characteristics of composite cantilever beams and metal skinned composite core sandwich panels have also been studied under forced vibration and the results are discussed.

6.2 Evaluation of Damping Properties

Geometrical structure of the end product, presence of any crack or any kind of deformations severely affect the material performance and ultimately leads to material failure. In this study thus efforts have been given to investigate and study the materials performance with cracks and deformities. For this, circular notch of various sizes are fabricated and vibration characteristics of the composite is investigated. Various circular holes of size 2 mm, 3.5 mm, 5 mm and 6.5 mm at the mid-section of the samples are prepared as shown in the Figure

6.1(a). In order to evaluate the damping characteristics, a composite sample of size 130×13×3.5 (mm^3) has been tested in cantilever mode using Laser Vibrometer (maker: Bruel Kjaer) as shown in the Figure 6.1(b). Low magnitude force is applied on end-tip of the specimen and allowed it to vibrate for a time span before it comes to its initial condition. Free vibration response is then measured using PULSE LabShop Version 13.1.0 software with respect to time. Vibration response of the 10% and 15% cement filled composite samples are measured and the experimental results are used to evaluate the damping characteristics of the proposed composites samples.

(a)

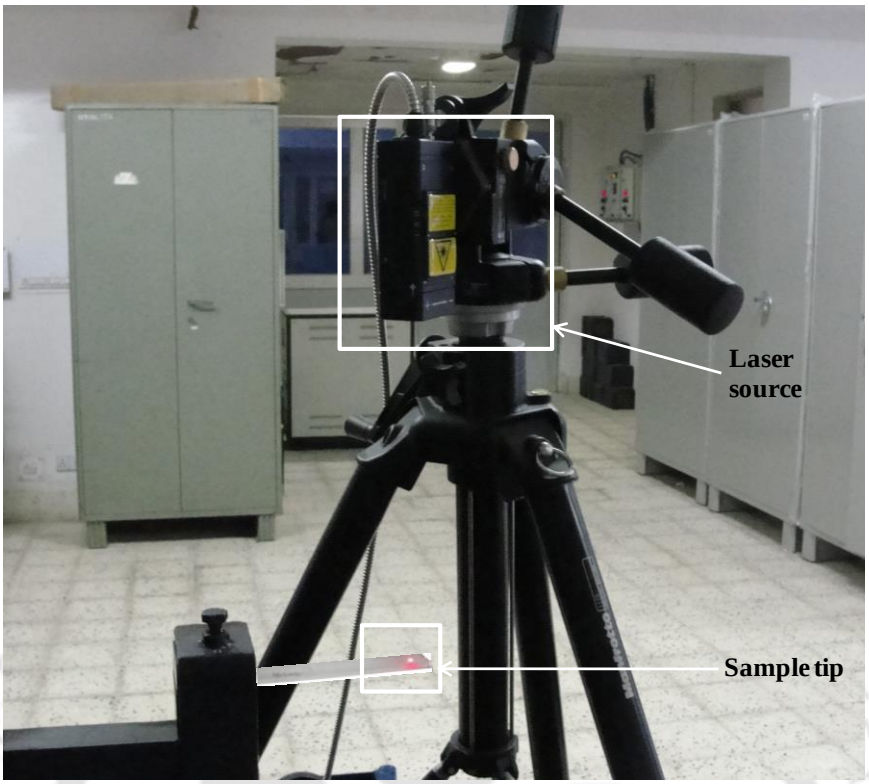

(b)

Figure 6.1 (a) Composite samples with various notches (b) experimental setup for vibration test with the Laser Vibrometer

In vibration engineering, the damping ratio (ξ) (*Gu (1997)*) is expressed as a dimensionless measure that describes how oscillations in a system decay after a disturbance. The logarithmic decrement is the natural log of the amplitudes of any two successive peaks. Loss factor (η) (*Landro and Lorenzi, 2009*) of the composites is measured as function of frequency, ranging from 0.01 to 140 Hz (*Sardar and Bandopadhya, 2010*). The logarithmic decrement for vibration can be expressed as,

$$\delta_n = \frac{1}{n}\ln\left(\frac{x_0}{x_n}\right) = \frac{2\pi\xi}{\sqrt{1-\xi^2}} \quad (n \neq 0) \tag{6.1}$$

where, x_0 denotes the 1st and x_n denotes the nth no. amplitude; ξ is the damping ratio. For small value of ξ, the above eqn. (6.1) can be approximated by neglecting the denominator part as:

$$\delta_n = 2\pi\xi \tag{6.2}$$

10% and 15% composite samples are chosen and the logarithmic decrement (δ_n) value is calculated taking into account of the experimental data. Thus, subsequently ξ and η is

calculated from the obtained results. Loss factor (η) of the material is calculated using the eqn. (6.3) and is expressed as (*Landro and Lorenzi, 2009; Gibson, 1992*):

$$\eta = \frac{\delta_n}{\pi} = 2\xi \tag{6.3}$$

6.2.1 Results and Discussions

Experimental data are taken into account, subsequently damping ratio (ξ) and loss factor (η) and quality factor (Q) of pure polypropylene and 5%, 10% and 15% cement filled composite material are calculated and given in the Table 6.1 and 6.2. Table 6.3 respectively shows the damping properties of various undeformed composite samples.

Table 6.1 Damping ratio of pure polypropylene, 5%, 10% and 15% cement reinforced composites

	Damping Ratio (ξ)			
Notch	**0%**	**5%**	**10%**	**15%**
Intact	0.027	0.025	0.026	0.023
2 mm	0.026	0.025	0.025	0.024
3.5 mm	0.024	0.023	0.023	0.022
5 mm	0.026	0.024	0.027	0.027
6.5 mm	0.029	0.027	0.027	0.030

Table 6.2 Loss factor of pure polypropylene, 5%, 10% and 15% PPC filled polypropylene composite

	Loss Factor (η)			
Notch	**0%**	**5%**	**10%**	**15%**
Intact	0.054	0.05	0.052	0.046
2 mm	0.052	0.0496	0.050	0.048
3.5 mm	0.048	0.046	0.047	0.043
5 mm	0.052	0.049	0.054	0.053
6.5 mm	0.058	0.053	0.054	0.060

The damping analysis reveals that the 15% cement filled composite material provides highest loss factor with 6.5 mm notch compared to other variants. It is further observed that the 3.5 mm notch gives the minimum loss factor as well as the damping ratio (Table 6.1). It is anticipated that this happens due to the optimum air-drag-force acts along the notch position while 2 mm notch does not experience sufficient air drag owing to its small size effect.

While, in the case of 5 mm and 6.5 mm notches, the drag force acts across the notches results in more air friction, in addition, mass of the samples also decreases with notch size.

Table 6.3 Experimental results of pure polypropylene and PPC filled polypropylene composites (intact beam)

Samples	**0%**	**5%**	**10%**	**15%**
Damping Ratio (ξ)	0.027	0.025	0.026	0.023
Loss factor (η)	0.054	0.05	0.052	0.046
Natural Frequency (Hz)	42.12	44.20	44.32	45.02
Quality Factor (Q)	18.52	20	19.23	21.74

The vibration response results of various composite samples are shown in the Figure 6.2(a), (b), (c) and (d). The corresponding FFT curves are also shown in the Figures 6.3(a), (b), (c) and (d) for 0%, 5%, 10% and 15% cement reinforced composites respectively.

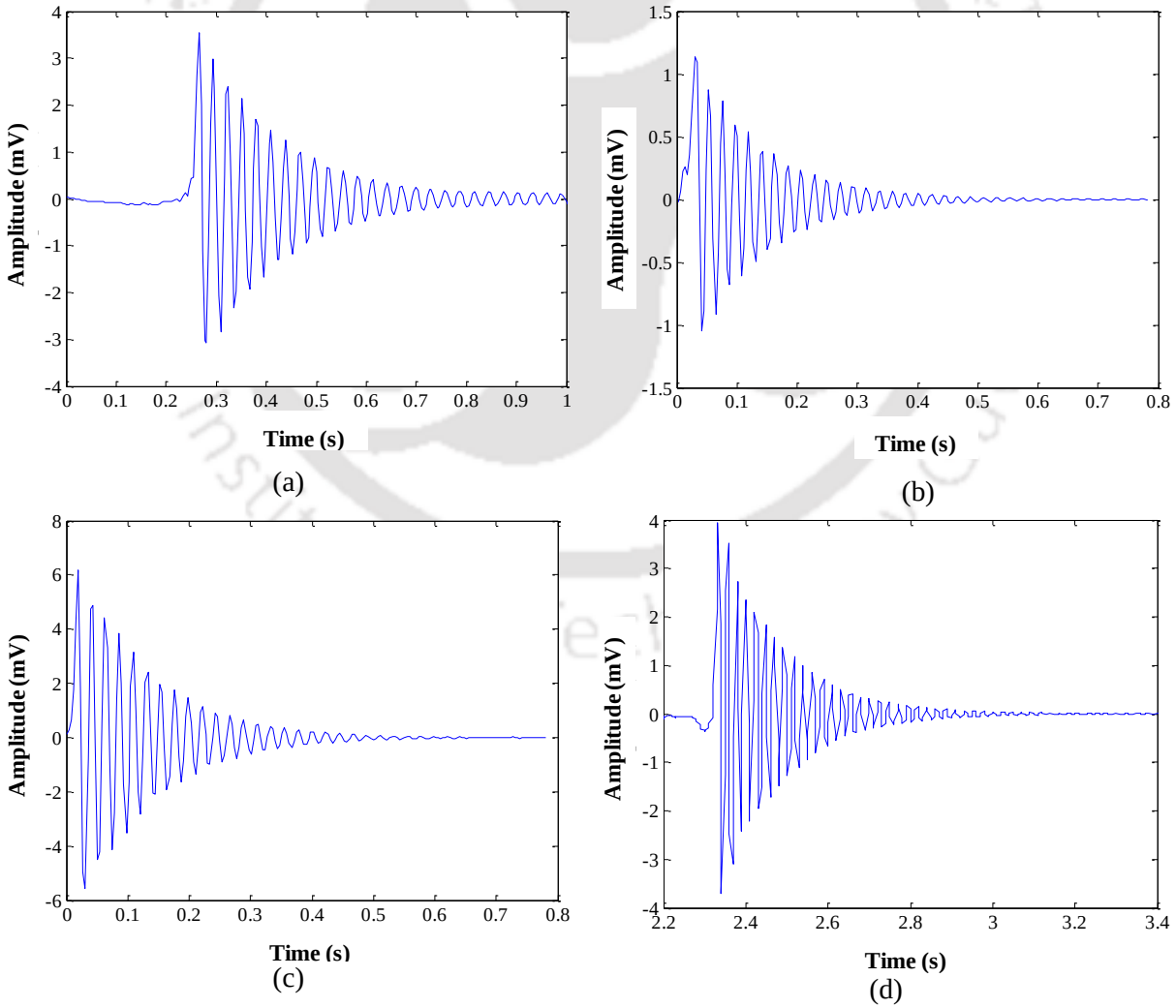

Figure 6.2 Free vibration response of (a) pure polypropylene, (b) 5% (c) 10% and (d) 15% cement filled composites

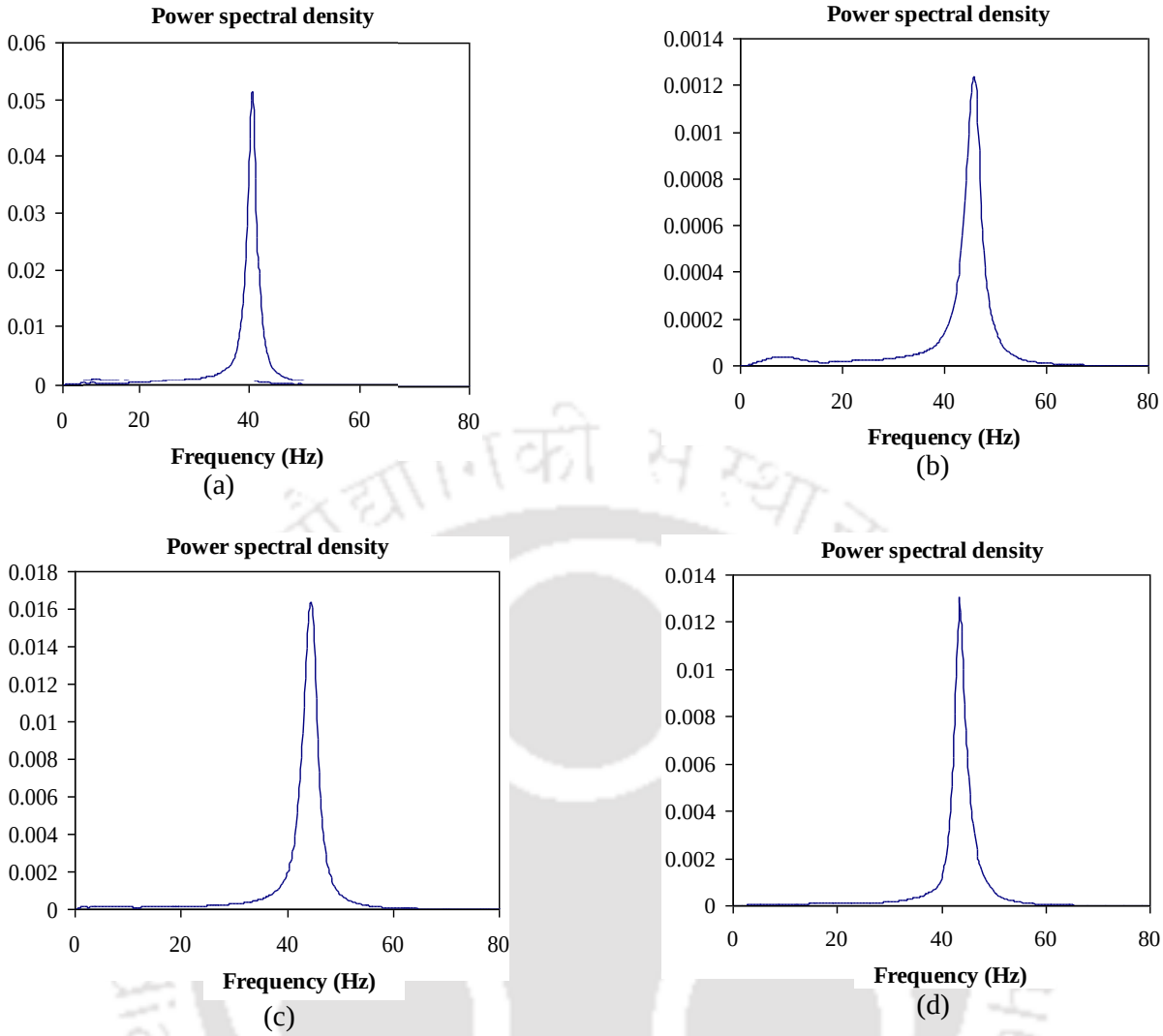

Figure 6.3 Corresponding FFT graphs of (a) pure polypropylene, (b) 5% (c) 10% and (d) 15% cement filled composites

It is observed that with the percentage increase of cement materials, the loss factor of the material show abrupt changes, while exhibiting good damping characteristics for industrial applications.

6.2.2 Experimental Investigation on Effect of Crack

In this work, the effect of cracks in the structural cantilever beams has been thoroughly investigated under a laser vibrometer. The experimental procedure remains the same as discussed in the previous sections 6.2. The schematic of cracks that have been made on the specimens are illustrated in the Figure 6.4, while Figure 6.5 shows the samples with the cracks. The specimen dimension is kept as 120mm×13mm×3.2mm. The relative crack position (ℓ_c/ℓ) is selected to be 0.1 and 0.8 whereas; the relative crack depth (a/H) is taken as

0.4 for all the specimens. Where, 'ℓ_c' denotes the crack position from the fixed end and 'ℓ' denotes the total length of the beam. '*a*' denotes crack depth and '*H*' denotes thickness of the beam.

Table 6.4 and 6.5 present the comparative study on experimental results for relative crack position of 0.1 and 0.8 respectively where the relative crack depth is kept 0.4 constant. The results clearly indicate that the presence of crack significantly influenced the natural frequencies of the structural elements although the effect is insignificant whether the crack is single sided or double sided. In addition, it is further observed that relative crack position significantly influence the natural frequencies with decrease in relative crack position from the fixed end and with increase of relative crack depth, the natural frequency decreases.

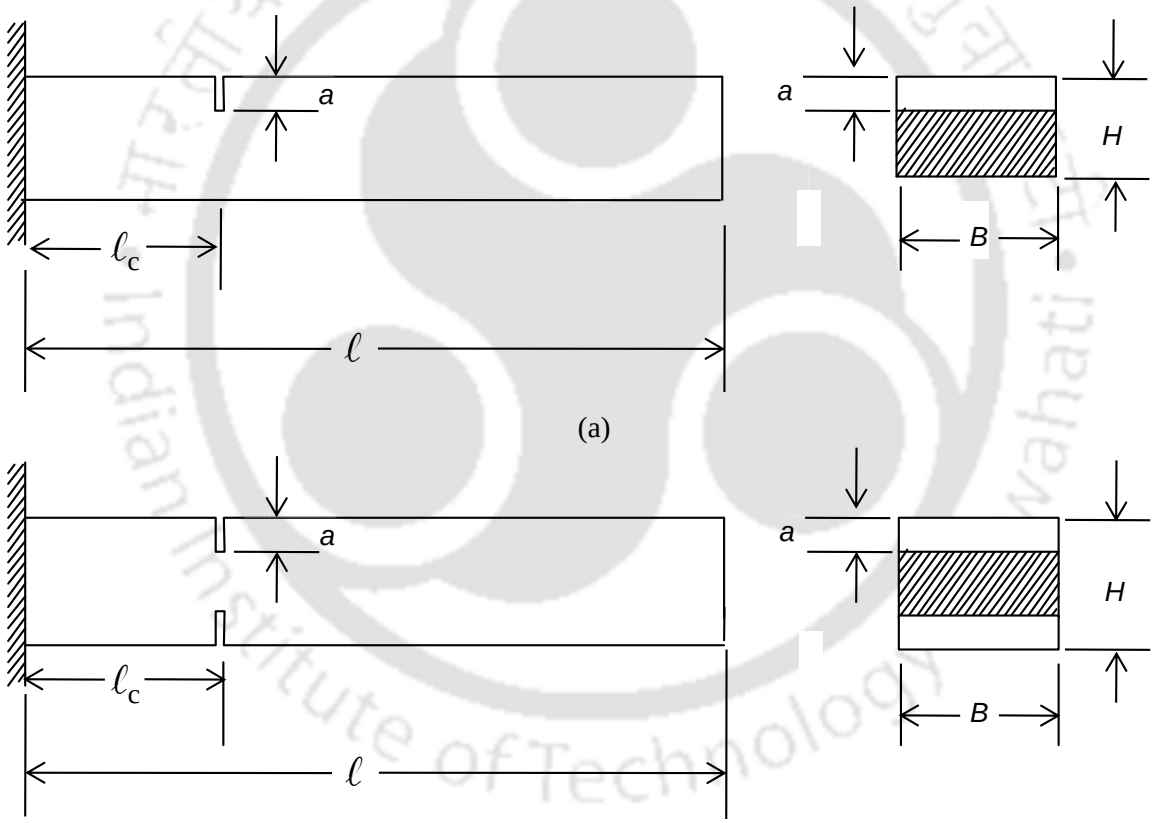

Figure 6.4 Schematic of (a) single sided and (b) double-sided crack

(a)

(b)

Figure 6.5 10% cement reinforced polypropylene composite beams (a) $\ell_c/\ell=0.1$, (b) $\ell_c/\ell=0.8$

Table 6.4 Variation of natural frequencies with cracks at relative position ($\ell_c/\ell = 0.1$) and relative depth ($a/H = 0.4$)

Filler (%)	Intact beam	Single sided crack	Double sided crack
	Natural Frequency (Hz)	Natural Frequency (Hz)	Natural Frequency (Hz)
0	42.12	33.00	32.00
5	44.20	37.50	34.00
10	44.32	40.00	38.50
15	45.02	41.50	40.50

Table 6.5 Damping properties of the material with cracks at relative position ($\ell_c/\ell = 0.1$) and relative depth ($a/H = 0.4$)

	0%		5%		10%		15%	
Factor	Single	double	Single	double	Single	double	Single	double
δ_n	0.188	0.191	0.176	0.185	0.178	0.182	0.187	0.192
ξ	0.028	0.026	0.032	0.030	0.032	0.029	0.028	0.028
η	0.060	0.052	0.056	0.053	0.054	0.051	0.054	0.054

The free vibration response and corresponding FFT curves with 80 Hz bandwidth of single sided crack composite beams have been illustrated in the Figures 6.6 and 6.7 respectively. Similarly, the free vibration response and corresponding FFT curves of double sided cracked composite beams are shown in the Figure 6.8 and 6.9 respectively. The experimental test results and the obtained damping properties of the material are represented in the Table 6.6 and 6.7.

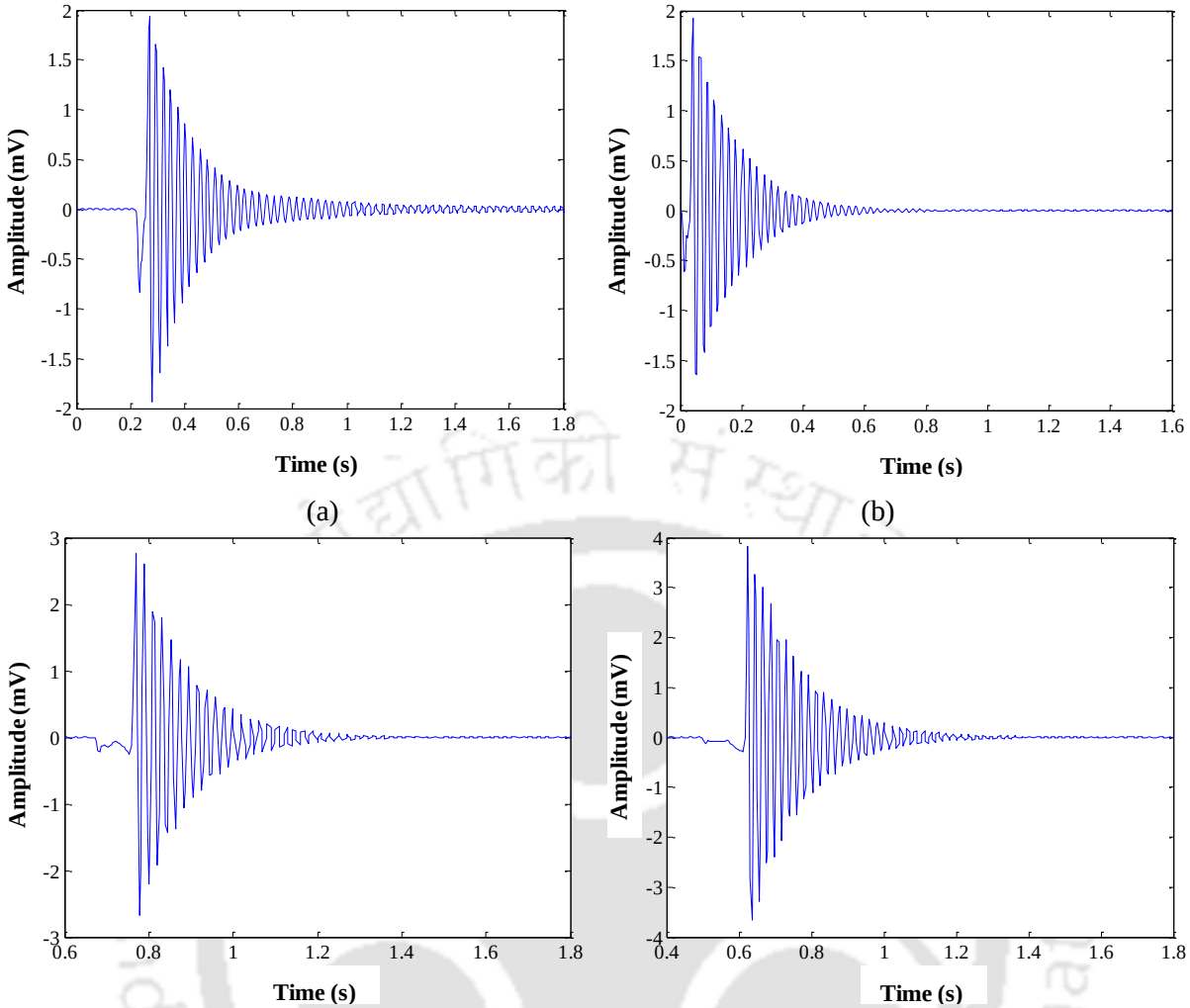

Figure 6.6 Free vibration responses with respect to time of (a) 0%, (b) 5%, (c) 10% and (d) 15% cement reinforced polypropylene composites cracked beams (single sided crack, $\ell_c/\ell = 0.1$)

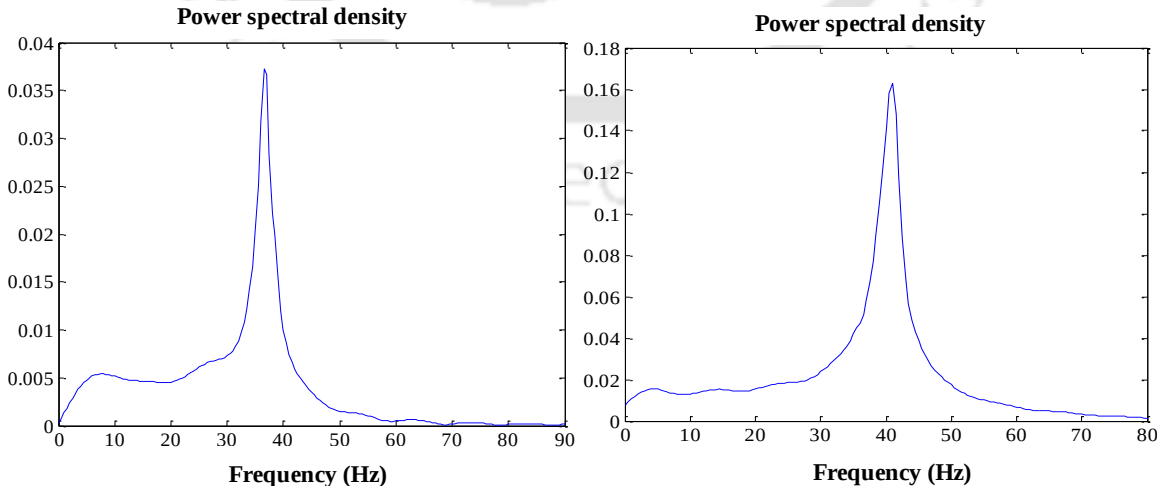

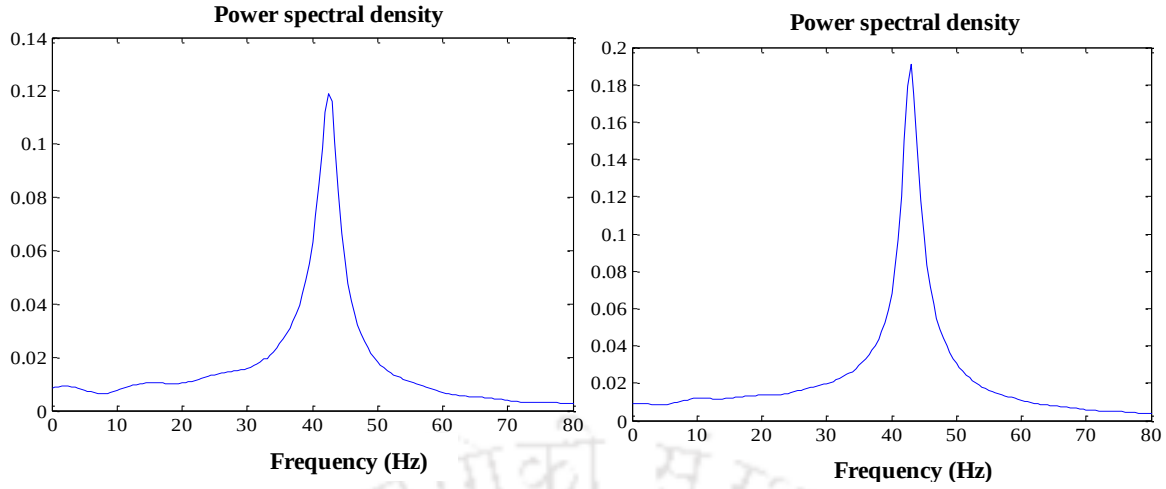

(c) (d)

Figure 6.7 Corresponding FFT signals of (a) 0%, (b) 5%, (c) 10% and (d) 15% cement reinforced polypropylene composites (single sided crack, $\ell_c/\ell = 0.1$)

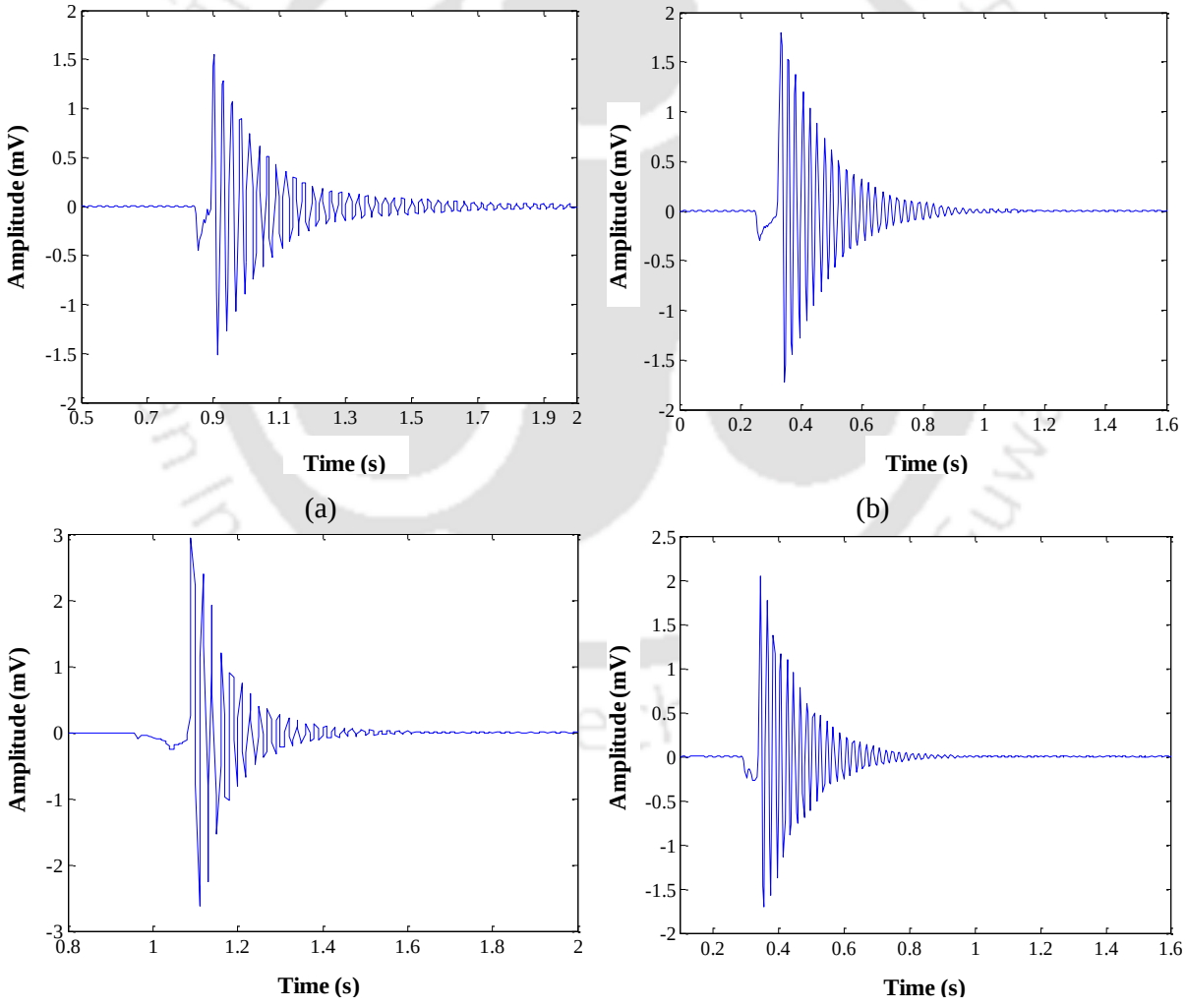

(a) (b)

(c) (d)

Figure 6.8 Free vibration response with respect to time of (a) 0%, (b) 5%, (c) 10% and (d) 15% cement reinforced polypropylene composites cracked beams (double sided crack, $\ell_c/\ell = 0.1$)

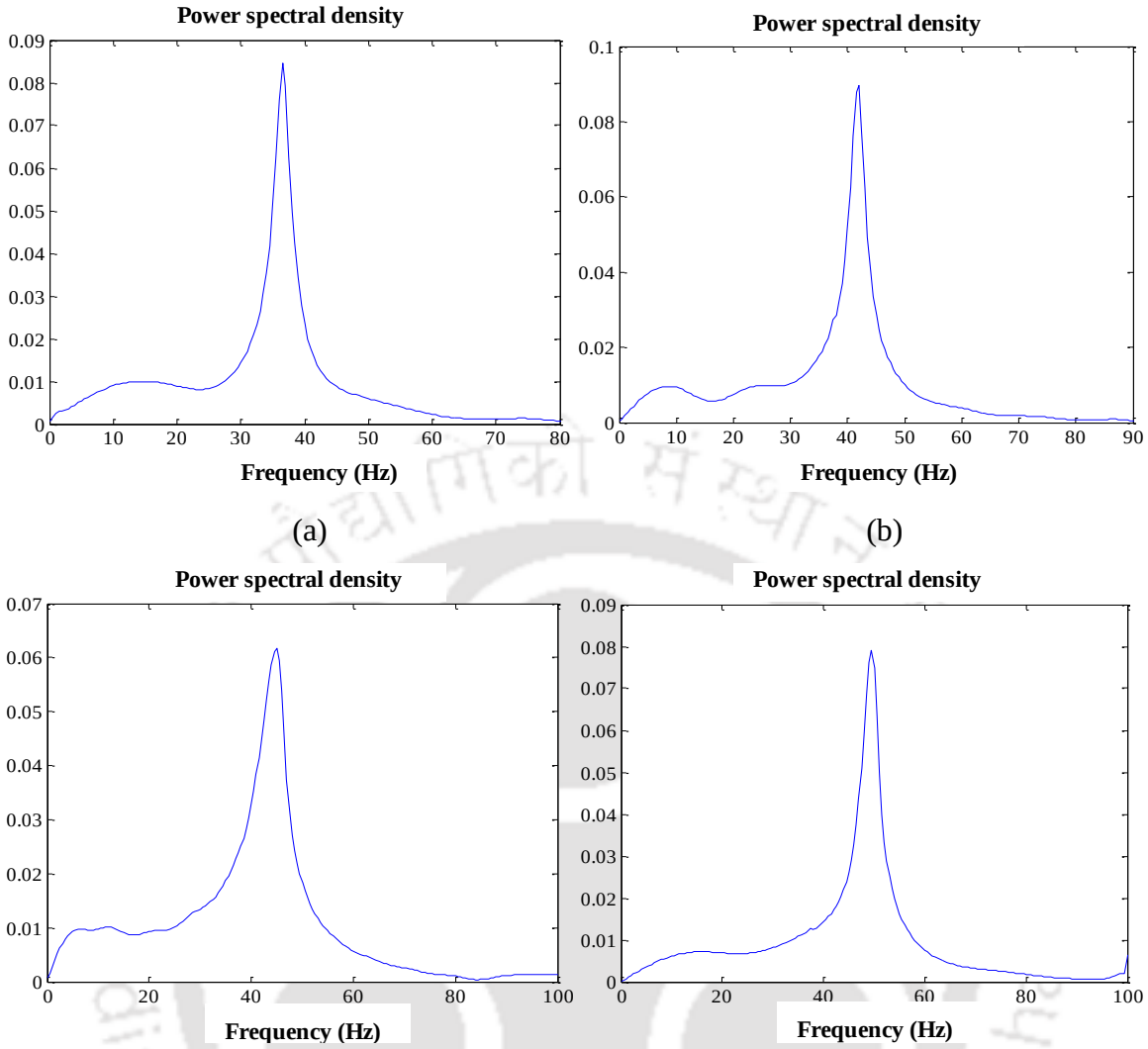

Figure 6.9 Corresponding FFT signals of (1) 0%, (2) 5%, (3) 10% and (4) 15% cement reinforced polypropylene composites (double sided crack, $\ell_c/\ell = 0.1$)

Table 6.6 Variation of natural frequencies with cracks at relative position ($\ell_c/\ell = 0.8$) and relative depth ($a/H = 0.4$)

Filler (%)	Single sided crack	Double sided crack
	Natural Frequency (Hz)	Natural Frequency (Hz)
0	35.00	34.00
5	42.00	40.50
10	43.00	42.0
15	43.50	43.00

Table 6.7 Variation of free vibration parameters with cracks at relative position $\ell_c/\ell = 0.8$) and relative depth ($a/H = 0.4$)

	0%		5%		10%		15%	
Factor	**Single**	**Double**	**Single**	**Double**	**Single**	**Double**	**Single**	**Double**
δ_n	0.181	0.188	0.168	0.187	0.181	0.188	0.185	0.188
ξ	0.028	0.025	0.030	0.027	0.030	0.028	0.029	0.028
η	0.058	0.051	0.052	0.057	0.058	0.060	0.058	0.062

After vibration test, the cracked surface morphology of the composite beam is studied using ΣIGMA field emission scanning electron microscope (FE-SEM) (maker: Carl Zeiss NTS GmbH). The specimens are prepared by gold coating on the cracked surface area (as the composite is non-conductive) and examined under high voltage field emission electrons with 1000× magnification. Micrograph of crack induced 10% and 15% reinforced polypropylene composite materials are shown in the Figure 6.10(a) and (b) respectively.

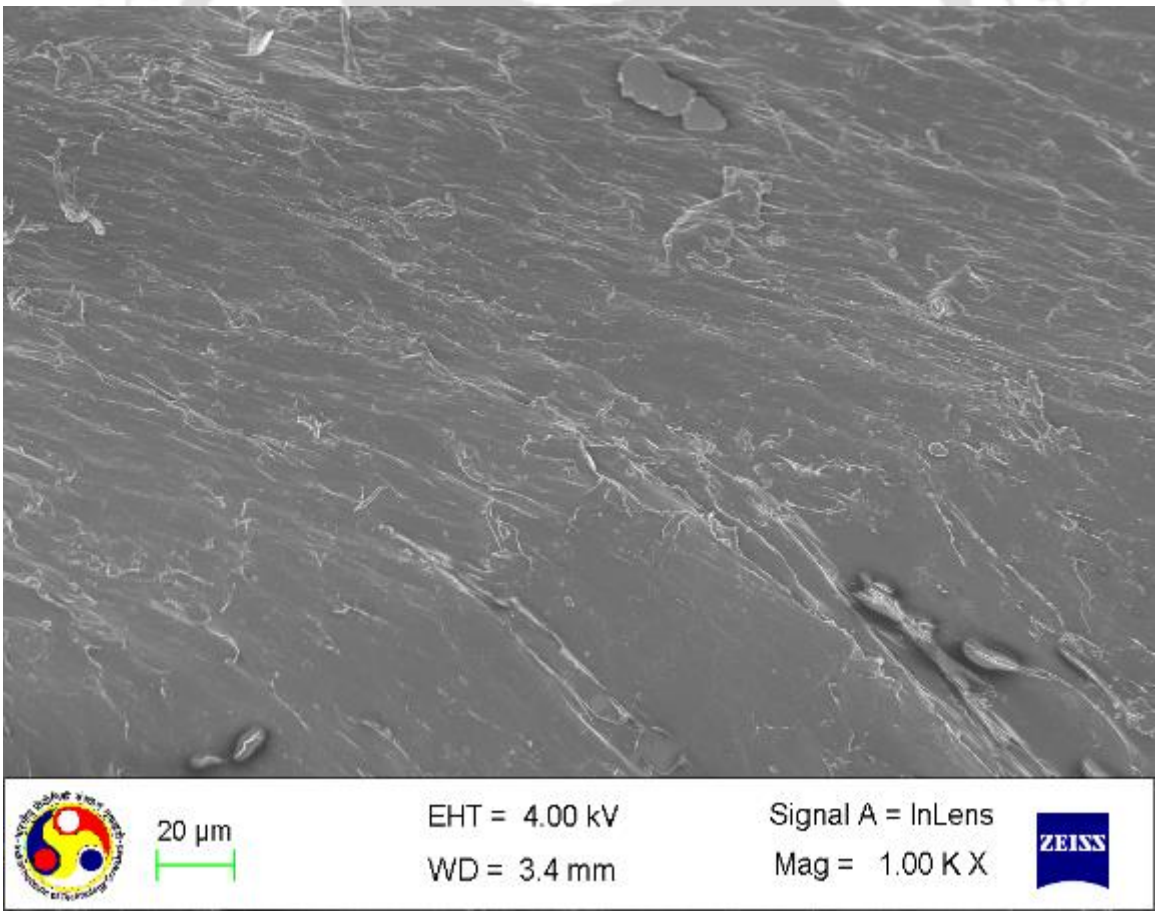

(a)

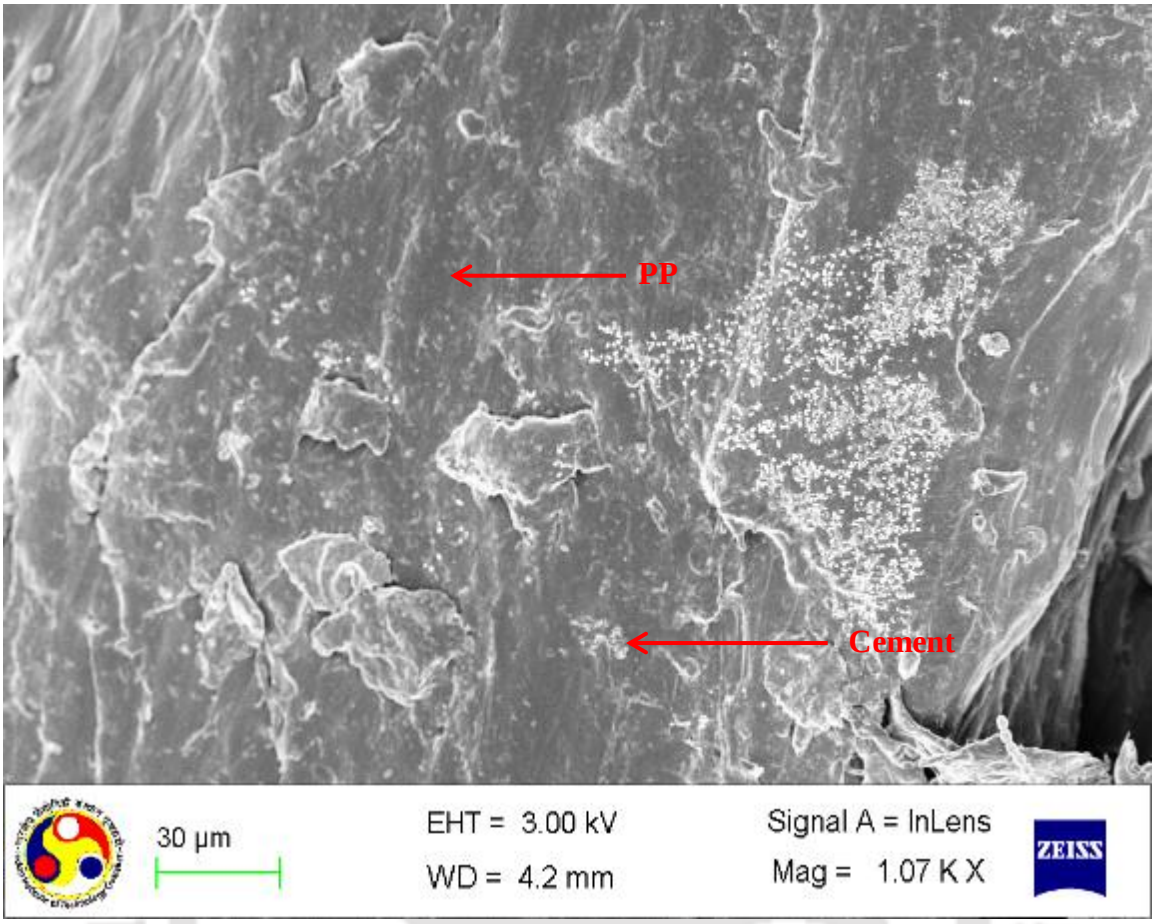

(b)

Figure 6.10 FE-SEM photomicrograph of fractured surface of (a) 5% and (b) 10% cement filled composite at 1000×

Figure 6.10(b) illustrates morphological structure of the fractured surface of the crack zone of 15% PPC reinforced composite beam. Micro cracks have also been observed on the cracked surface of the 15% cement filled composite beam material, owing to the compression and tensile effect during vibration, while remains absent in the other composites.

6.3 Damping and Forced Vibration Characteristics of Sandwich Panels

Sandwich panels are fabricated using two different metal skins. Initially, the metal sheet is cut in the same shape and size using Laser cutting machine (2.5 kW CO2 Laser Cutting Machine, Make: LVD Company n.v., SIRIUS 3015 Plus]. The metal skins are then fixed at each side of the composite sample using plastic adhesive. The detail manufacturing process of sandwich panel is given in the Figure 6.23 (b). Sandwich panels are manufactured using aluminum (Al) and galvanized iron (GI) as skin materials and cement filled polymeric composite as core materials. It is anticipated that during forced vibration, energy dissipation

is due to the plastic deformation of the material, although in the present study, the effect is neglected considering the low amplitude force excitation. The specimens (130mm×13mm×3.5mm) are shown in the Figure 6.11(a)-(c). Schematic and the corresponding experimental setup for the forced transverse vibration analysis of composite beams are shown in the Figure 6.12(a)-(b).

(a)

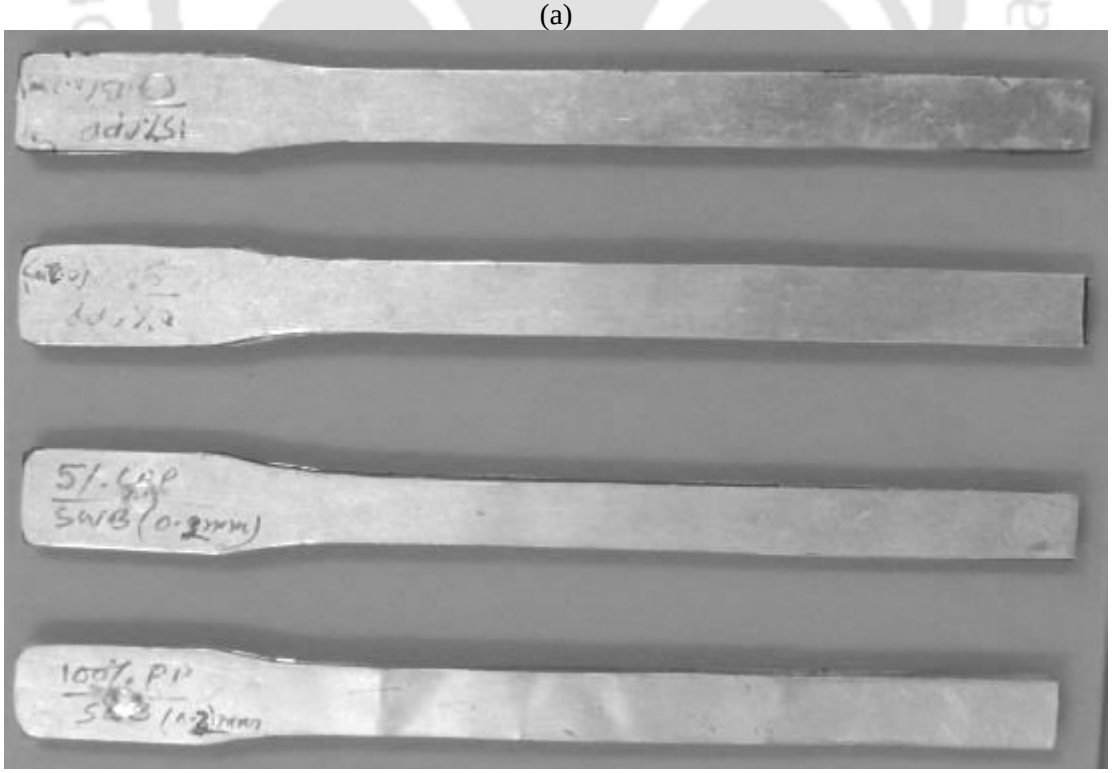

(b)

(c)

Figure 6.11 Forced vibration samples (a) composite beam (b) Aluminum skinned sandwich beams and (c) GI skinned sandwich beams

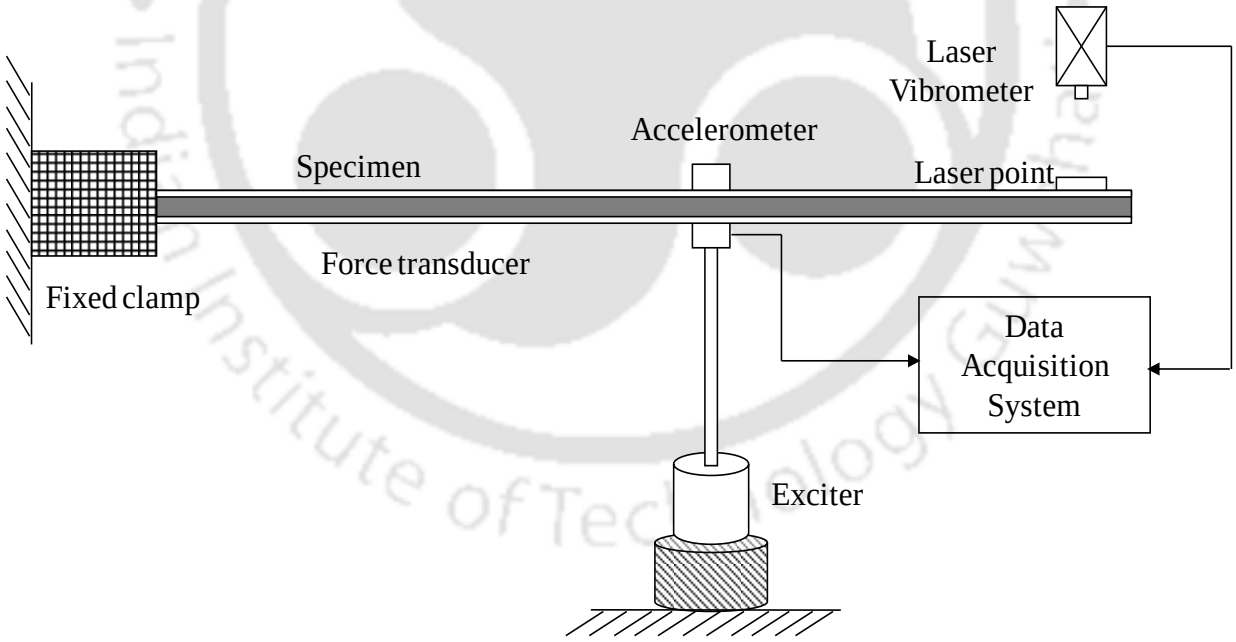

(a)

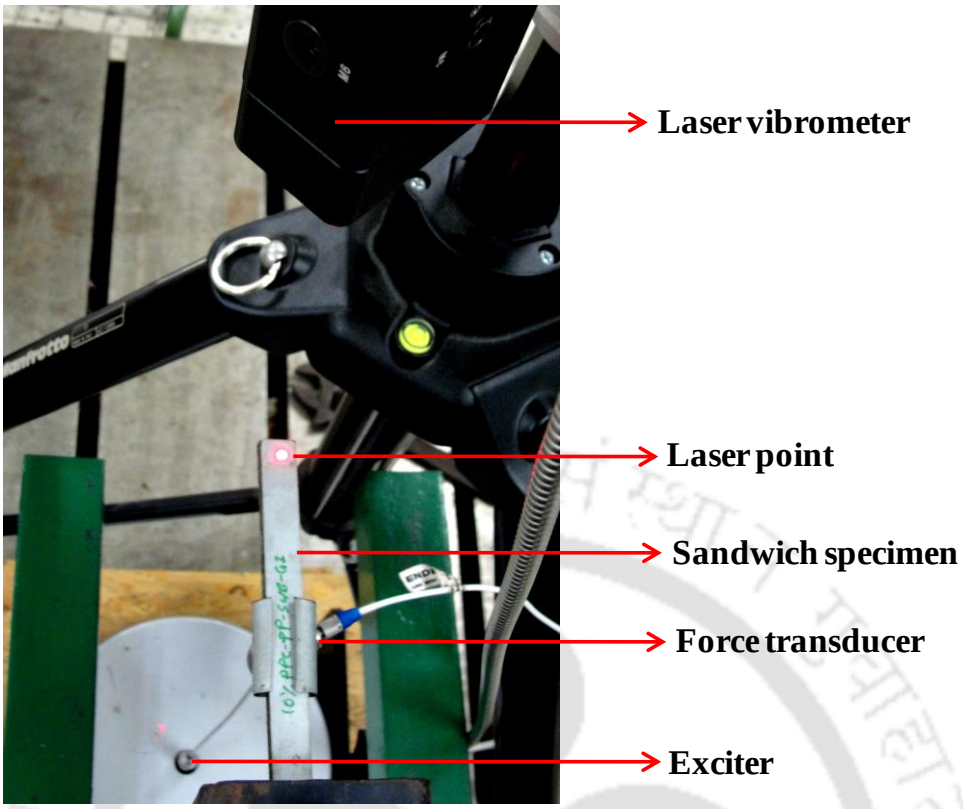

(b)

Figure 6.12 Forced vibration accessories (a) Schematic diagram of experimental setup for forced vibration and (b) actual experimental setup

The test specimen is clamped at one end, a force transducer (Endevco type 2311- force transducer) equipped with a Modal Exciter Type 4824 (maker: Bruel Kjaer) is fixed at the middle position of the samples as shown in the schematic diagram Figure 6.12(a). A LASER assisted vibrometer (maker: Bruel Kjaer) is used to acquire the vibration response data through laser beam, pointed at the end of the specimen as depicted schematically. The exciter is vibrated with sinusoidal exciting frequency maintained at 40 Hz for all the specimens. Using LABSHOP- Pulse 7700 software, the experimental data are analyzed. The phase difference (φ) is calculated using the relation (*Subramanian et al, 2011*) as:

$$\varphi = \frac{\tau}{T} \times 360^0 \tag{6.4}$$

where, T denotes the time period for one cycle and τ refers the time (s) difference between exciting force and the LASER acquisition response. Phase difference is the time by which the response lags behind the exciting force and the material response and this gives measure of the damping. Further, for a material, phase difference is directly proportional to the damping (*Aberg and Widell, 2004*) where, damping factor for forced vibration is calculated using the relationship (Genta, 1999) as:

$$tan(\varphi) = \frac{2\xi\left(\frac{f}{f_n}\right)}{1-\left(\frac{f}{f_n}\right)^2} \tag{6.5}$$

where, φ denotes the mean phase difference in degree, f denotes the forced frequency (maintained 40 Hz for all the cases) and f_n is the natural frequency; obtained from the free vibration FFT analysis while, forced excitation frequency is taken 80 Hz for sandwich beam experimentation.

6.3.1 Results and Discussions

The phase difference obtained experimentally taking into account of all the composite samples under forced vibration responses are shown in the Figure 6.13. Mean phase difference and damping ratio of all the composite specimens are illustrated in the Figure 6.14(a) and (b) along with pure polypropylene respectively. Mean phase difference of 0%, 5%, 10% and 15% cement reinforced composite materials are found to be 30.15º, 18.77º, 19.28º and 16.9º respectively. It is observed that addition of cement fillers into the pure polypropylene matrix significantly limits elastic deformation of the material and results in falling of phase difference between the excitation force and the corresponding material response captured by the Laser vibrometer.

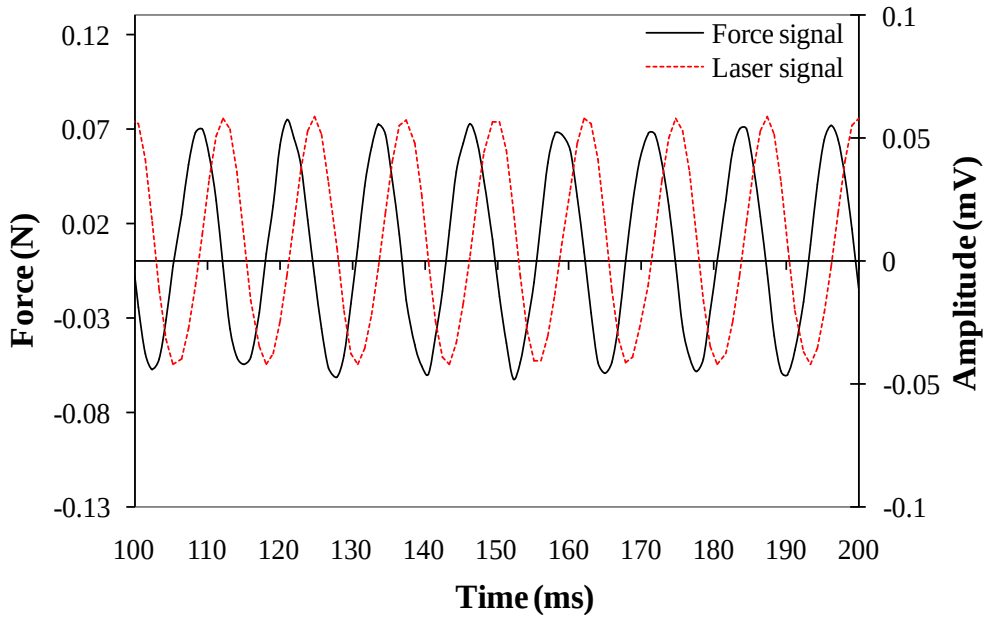

(a)

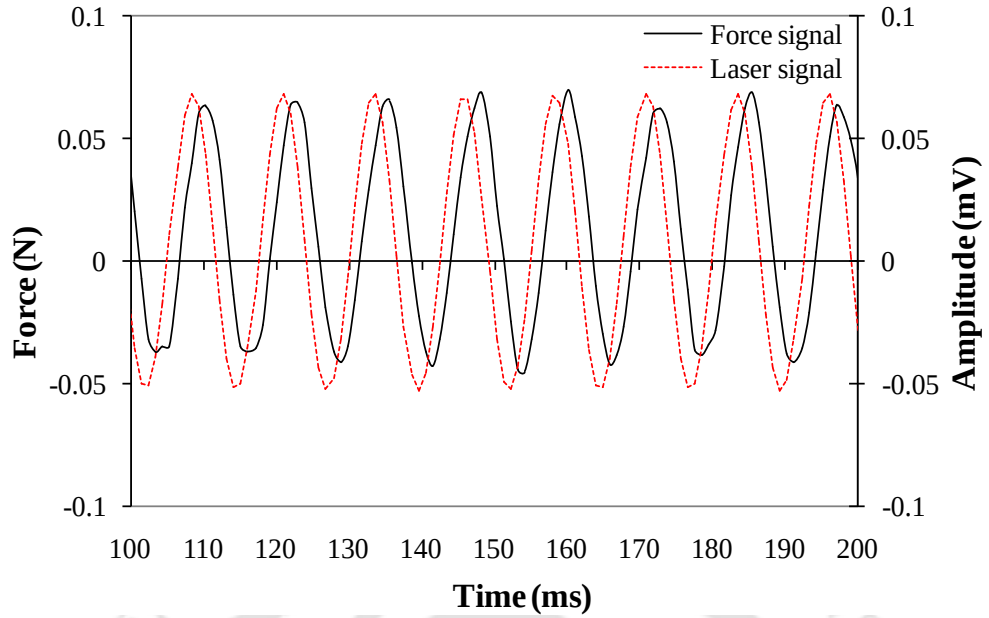
Force signal
Laser signal
Force (N)
Amplitude (mV)
Time (ms)
0.1
0.05
0
-0.05
-0.1
100
110
120
130
140
150
160
170
180
190
200

(b)

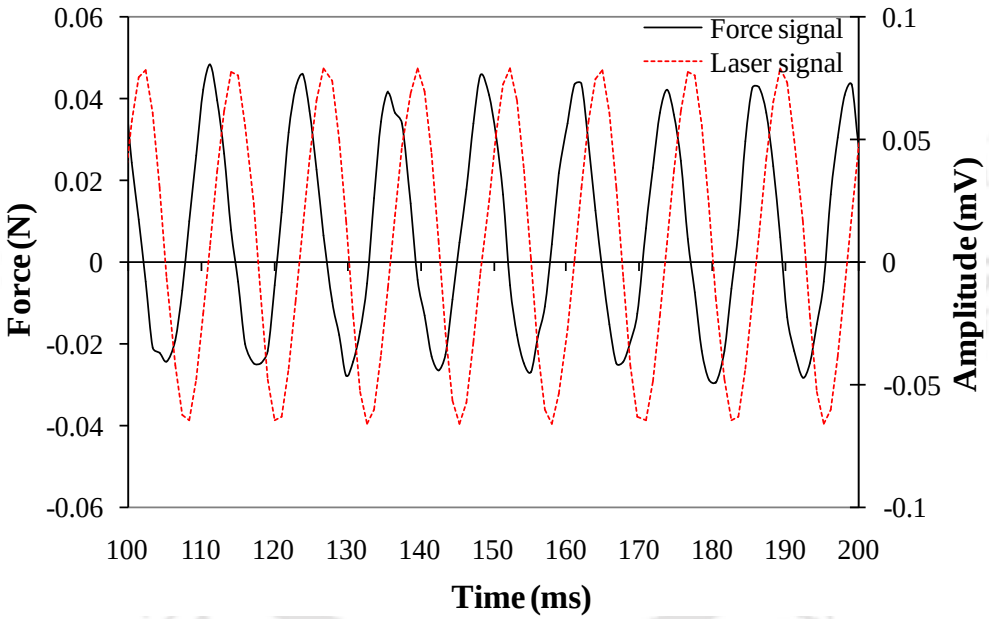
Force signal
Laser signal
Force (N)
Amplitude (mV)
Time (ms)
0.06
0.04
0.02
0
-0.02
-0.04
-0.06
0.1
0.05
0
-0.05
-0.1
100
110
120
130
140
150
160
170
180
190
200

(c)

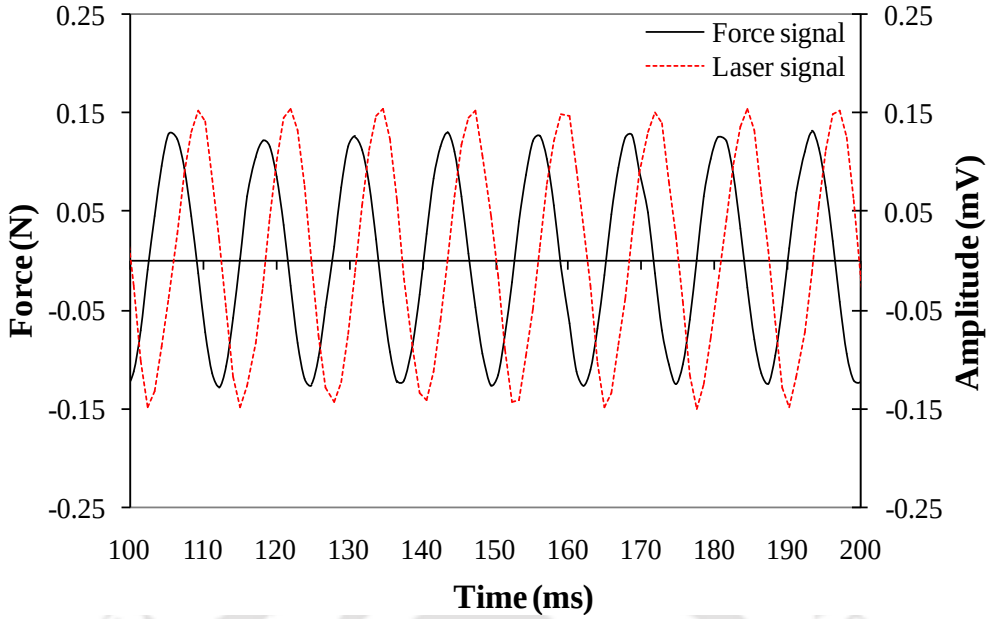

(d)

Figure 6.13 Forced vibration response of (a) 0%, (b) 5%, (c) 10% and (d) 15% cement reinforced polypropylene

Among the other cement reinforced composite materials, 15% cement reinforced composite depicts lower phase difference compared to 10% and 5% cement reinforced composites owing to filler matrix interface, which, eventually, caused delayed response of the specimens. Experimentally obtained forced vibration data are taken into consideration and the damping ratio of the composite materials (0%, 5%, 10% and 15% fillers) are obtained as, 0.031, 0.034, 0.036 and 0.036 respectively. It is observed that as the filler loading increases, results in minute increase of loss factors of the composites.

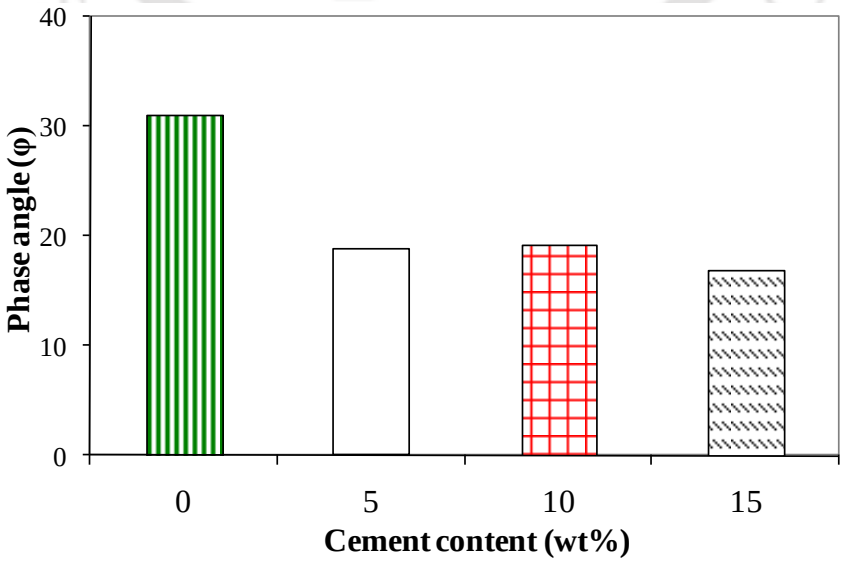

(a)

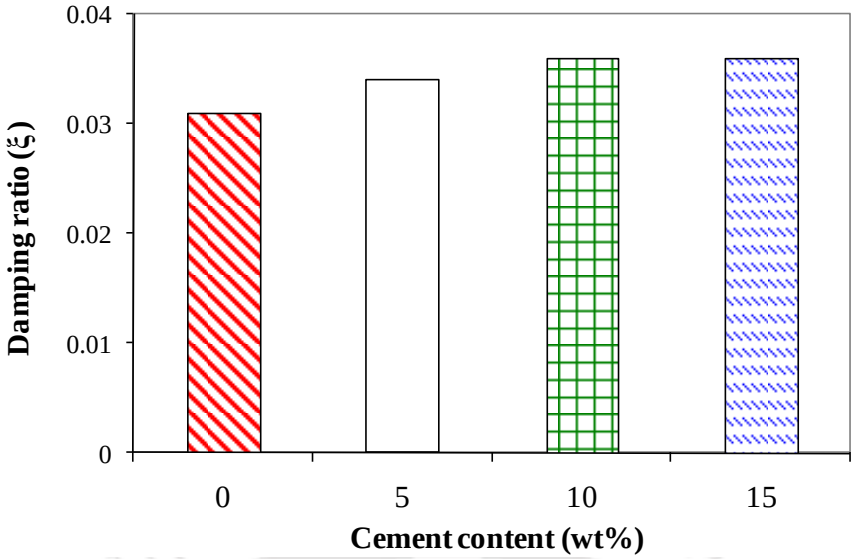

(b)

Figure 6.14 Forced vibration response results of composite specimens (a) mean phase angle (φ) and (b) damping ratio (ξ)

Similar results have also been obtained for Aluminum (Al) and Galvanized iron (GI) skinned sandwich panel with cement reinforced composite as core material. The forced vibration response of Al and GI skinned sandwich composite beams are illustrated in the Figure 6.15 and Figure 6.17 respectively. Figure 6.16 and Figure 6.18 show the variation of phase difference and damping ratio of Al and GI skinned sandwich composite panels respectively. As expected, high stiffness metal skin for sandwich composite panels, significantly limits the materials elastic deformation and decrease the phase angle (φ) between the excitation force and the corresponding material response captured by LASER vibrometer. The damping ratio for aluminum skinned sandwich panels are obtained as 0.061, 0.069, 0.074 and 0.080 with pure polypropylene, 5%, 10% and 15% cement reinforced composite materials as core materials. Similarly, for GI skinned sandwich panels, the damping ratio obtained from the forced vibration test are 0.082, 0.086, 0.091 and 0.093 respectively. It is observed that 10% cement reinforced composite core material with both aluminum and galvanized iron skinned sandwich panels give optimal damping ratio compared to other sandwich panels. It is anticipated that incorporation of cement materials aided the resistance to mobility of the materials and subsequently results in fall in elastic deformation. However, it is observed that 15% cement reinforced composite materials offer more resistance to mobility and elastic deformation although enhances the brittle characteristics simultaneously as compared to other core materials.

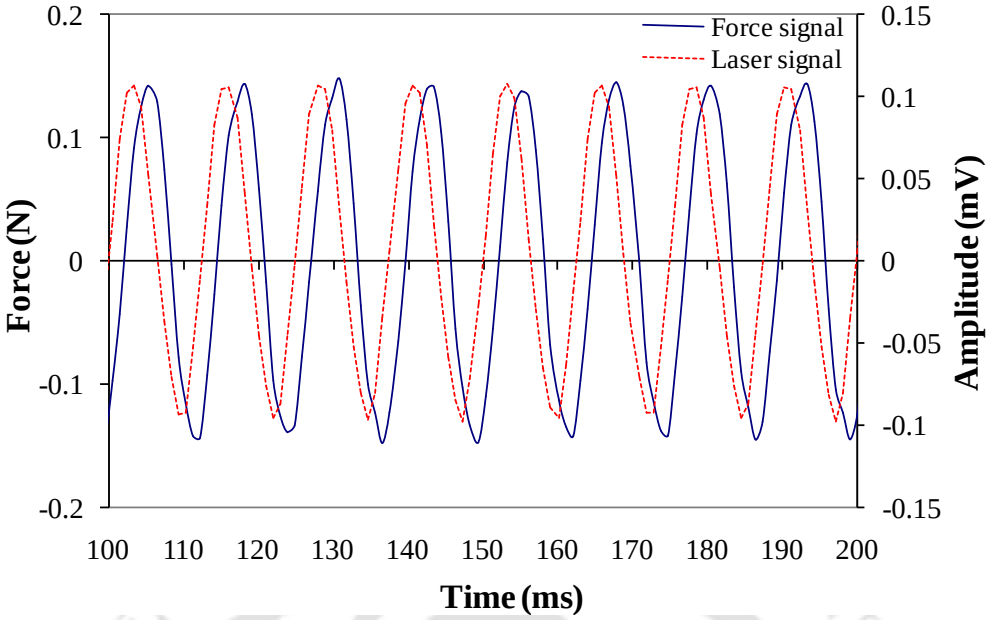
Force signal
Laser signal
Force (N)
Amplitude (mV)
Time (ms)
0.2
0.1
0
-0.1
-0.2
0.15
0.1
0.05
0
-0.05
-0.1
-0.15
100 110 120 130 140 150 160 170 180 190 200

(a)

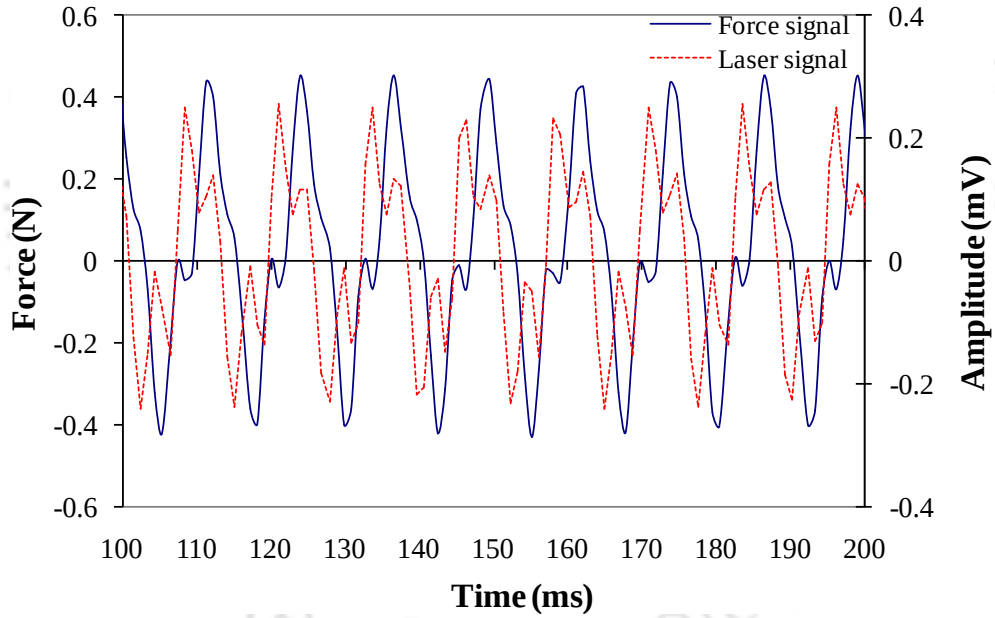
Force signal
Laser signal
Force (N)
Amplitude (mV)
Time (ms)
0.6
0.4
0.2
0
-0.2
-0.4
-0.6
0.4
0.2
0
-0.2
-0.4
100 110 120 130 140 150 160 170 180 190 200

(b)

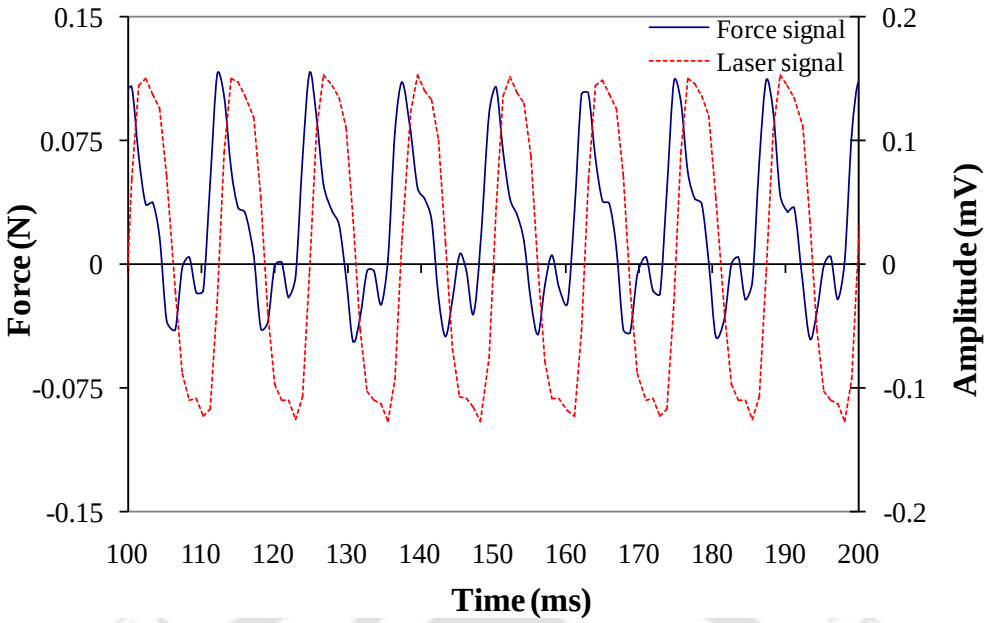

(c)

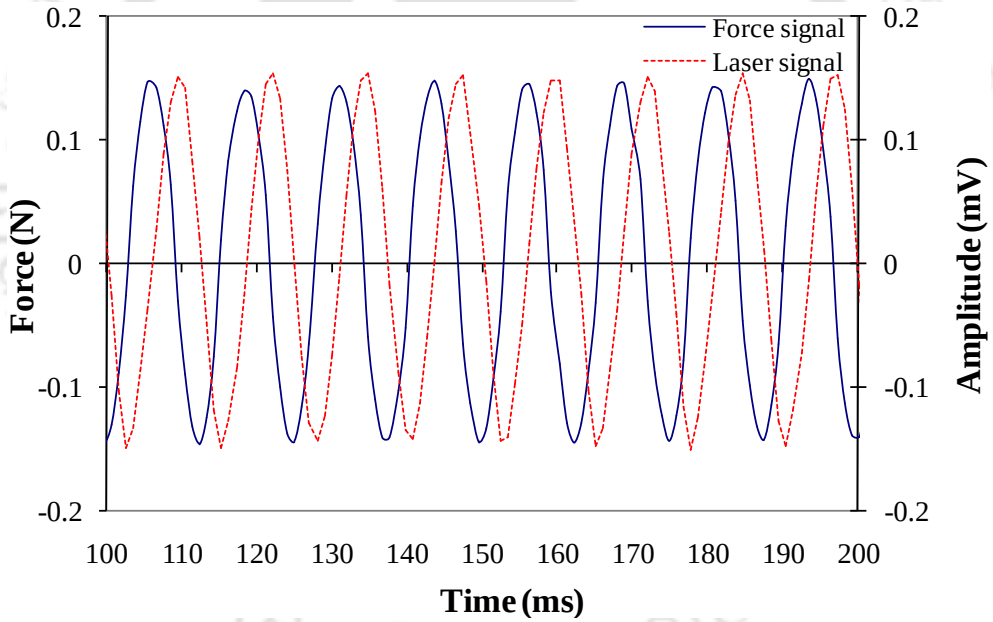

(d)

Figure 6.15 Forced vibration response of Aluminum skinned sandwich panels of core (a) 0%, (b) 5%, (c) 10% and (d) 15% cement reinforced polypropylene

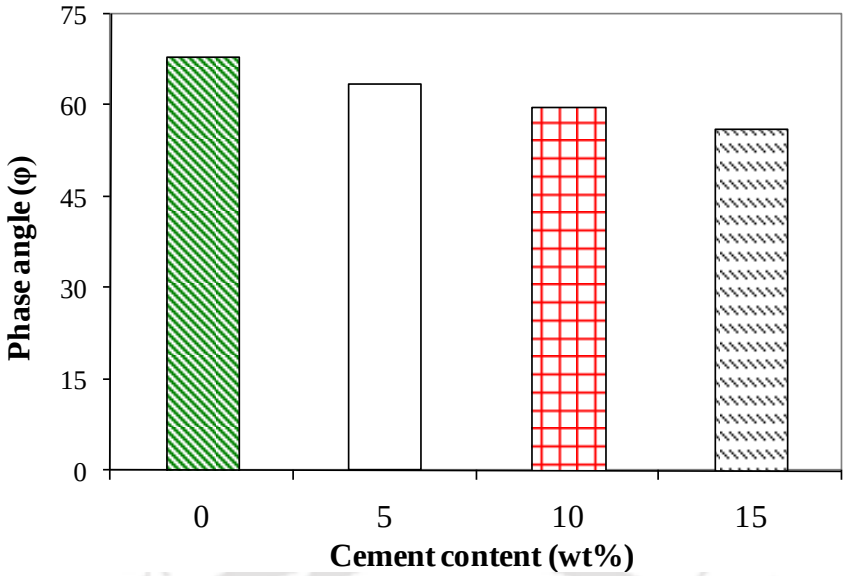

(a)

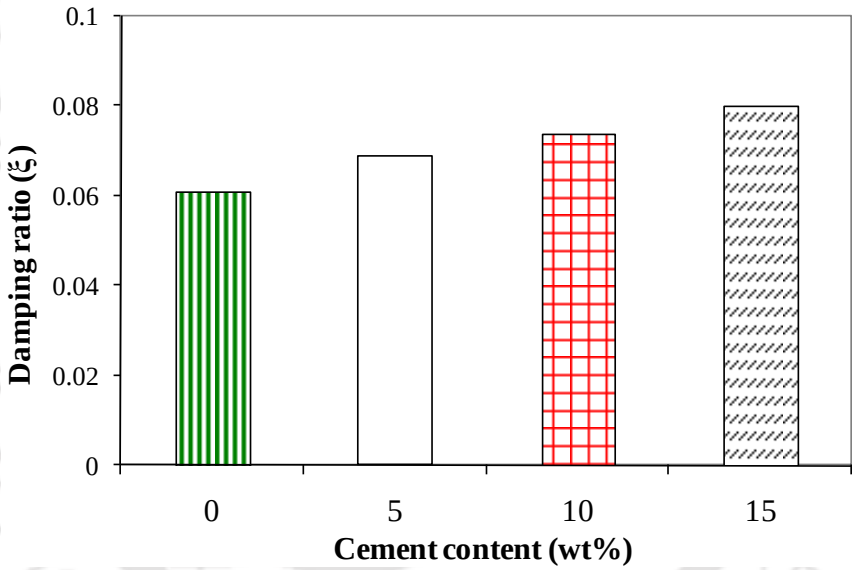

(b)

Figure 6.16 Forced vibration response results of Aluminum skinned sandwich panels (a) phase angle (φ) and (b) damping ratio (ξ)

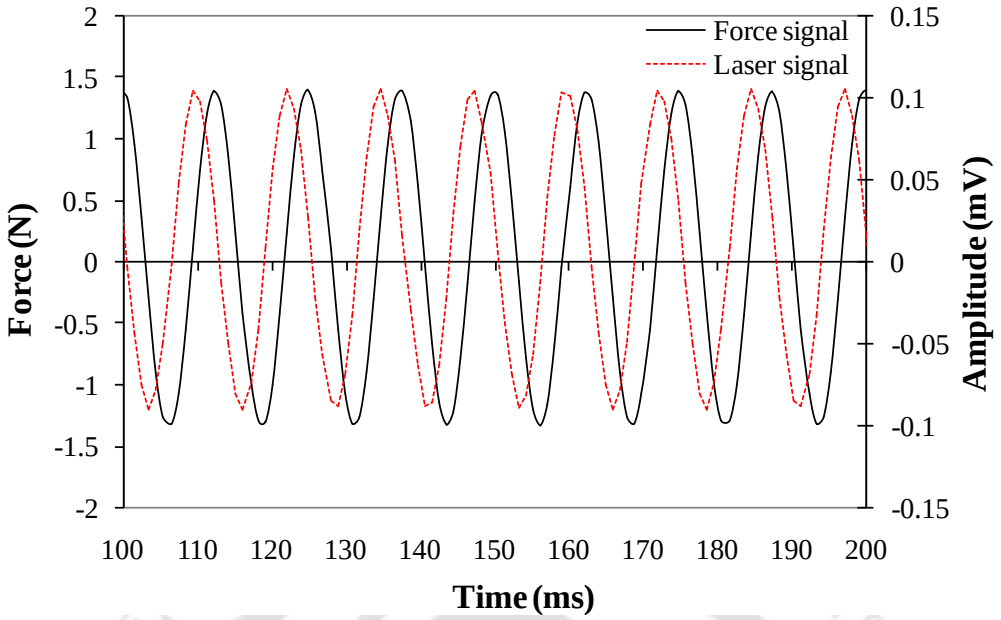
Force signal
Laser signal
Force (N)
Amplitude (mV)
Time (ms)
2
1.5
1
0.5
0
-0.5
-1
-1.5
-2
0.15
0.1
0.05
0
-0.05
-0.1
-0.15
100
110
120
130
140
150
160
170
180
190
200

(a)

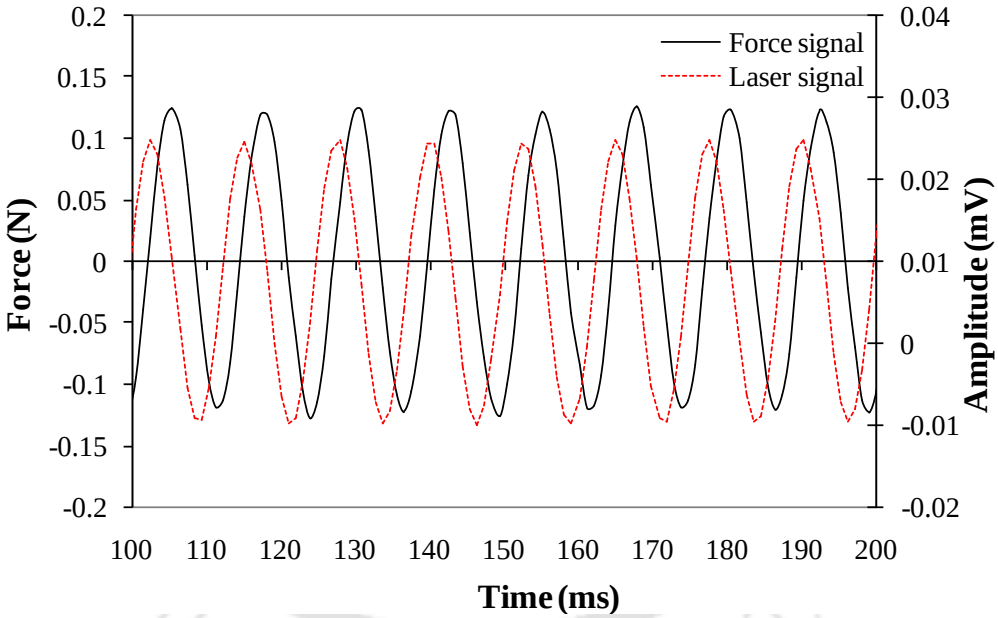
Force signal
Laser signal
Force (N)
Amplitude (mV)
Time (ms)
0.2
0.15
0.1
0.05
0
-0.05
-0.1
-0.15
-0.2
0.04
0.03
0.02
0.01
0
-0.01
-0.02
100
110
120
130
140
150
160
170
180
190
200

(b)

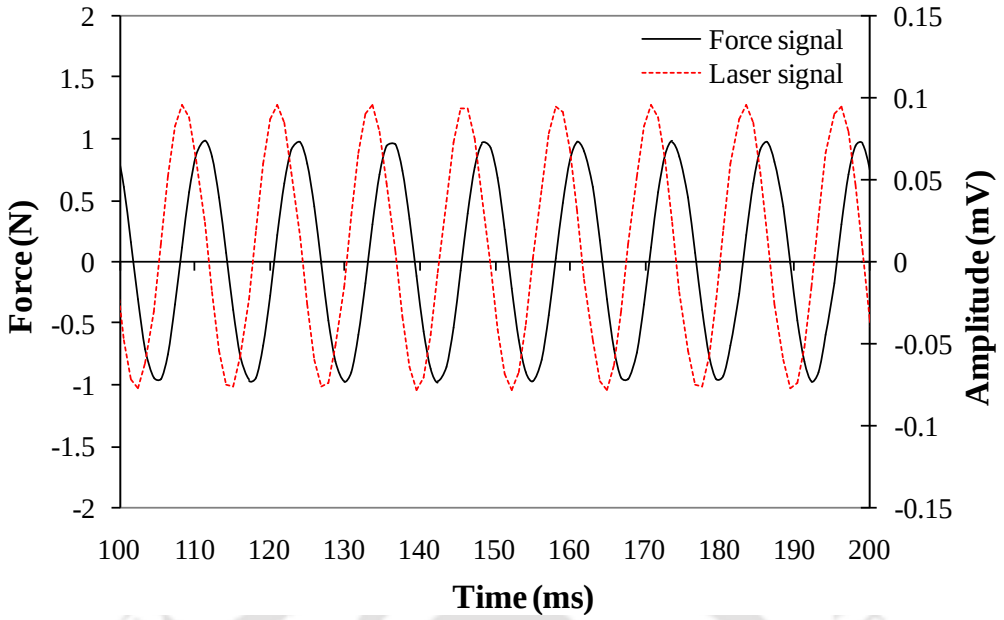

(c)

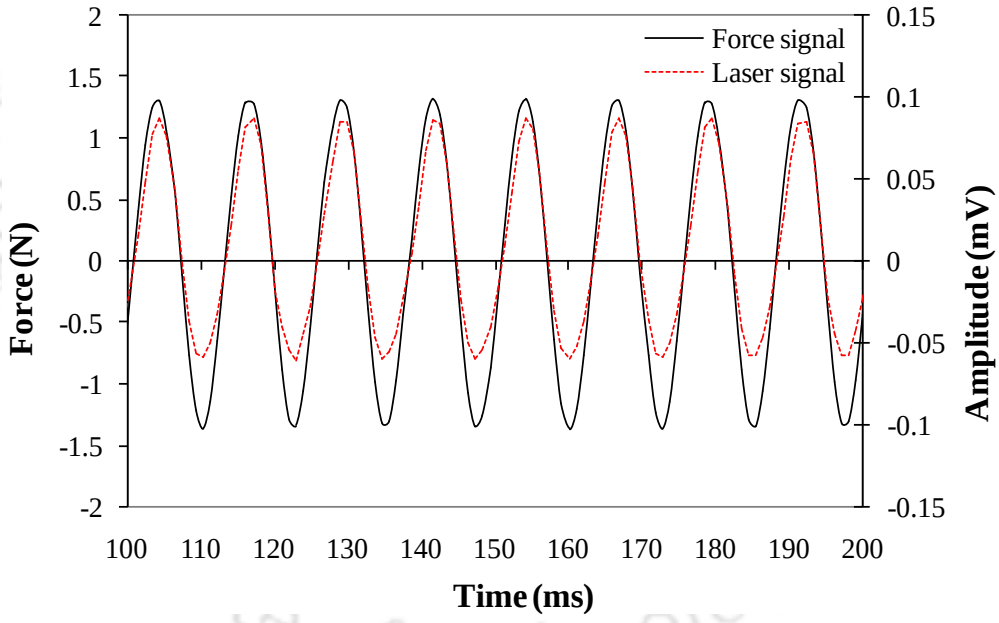

(d)

Figure 6.17 Forced vibration response of GI skinned sandwich panels of core (a) 0%, (b) 5%, (c) 10% and (d) 15% cement reinforced polypropylene

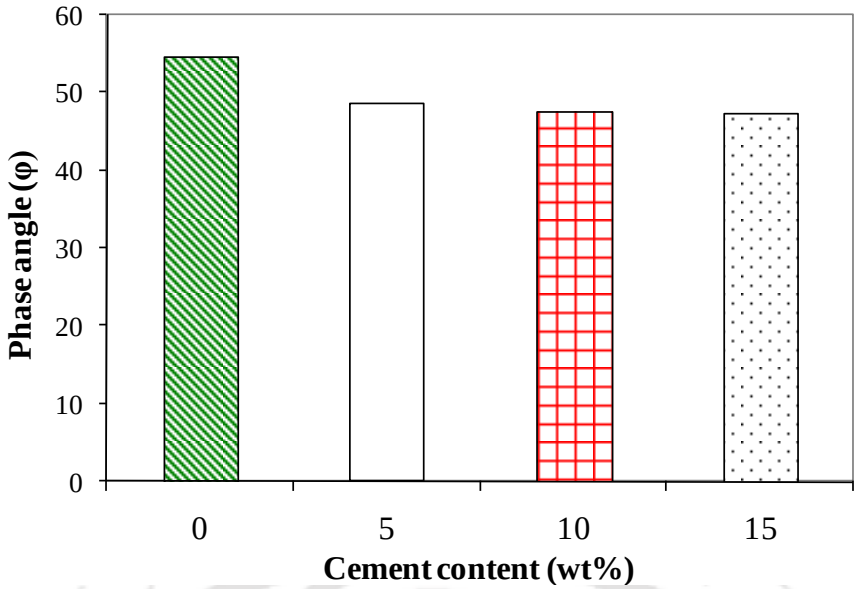

(a)

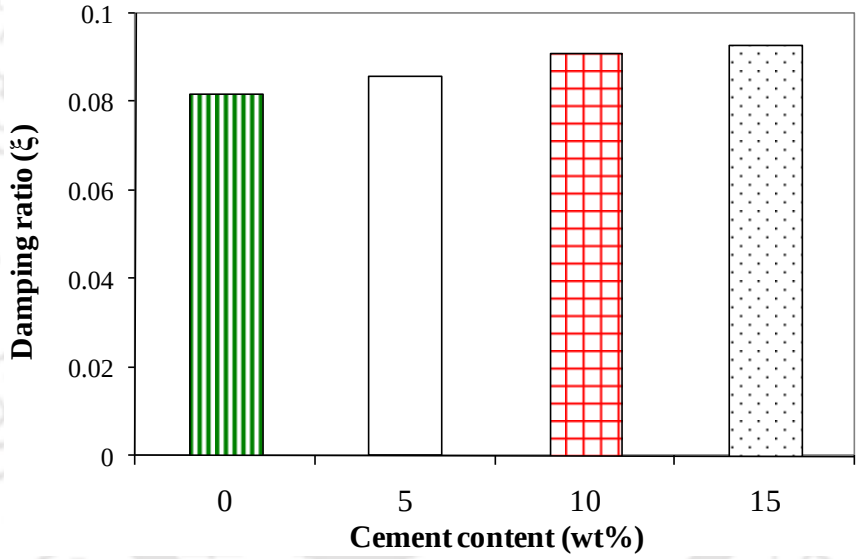

(b)

Figure 6.18 Forced vibration response results of GI skinned sandwich panels (a) phase angle (φ) and (b) damping ratio (ξ)

6.4 Mechanical Characterizations of Composite Sandwich Panels

6.4.1 Bending Deformation Analysis of Sandwich Panels

It is essential to know the mechanical behaviors of the sandwich panels before applications. These typical engineered materials have peculiar mechanical properties over conventional metals as well as polymeric composite materials because of its complex structures. In this complex structure, the core material is a viscoelastic material and skinned material is metal. Due to this, the elongation, bending as well as other mechanical behavior differs from the

conventional materials. In this consequences, 3-point bending tests of sandwich composite structures of Aluminum and GI as skin materials are conducted under Universal Testing Machine (INSTRON- 8801) followed by the ASTM standard D790. The load-deflection graph of the test results are represented in the Figure 6.19. At the same time, the tensile behaviors of these complex materials are also studied and discussed in the section 6.4.2.

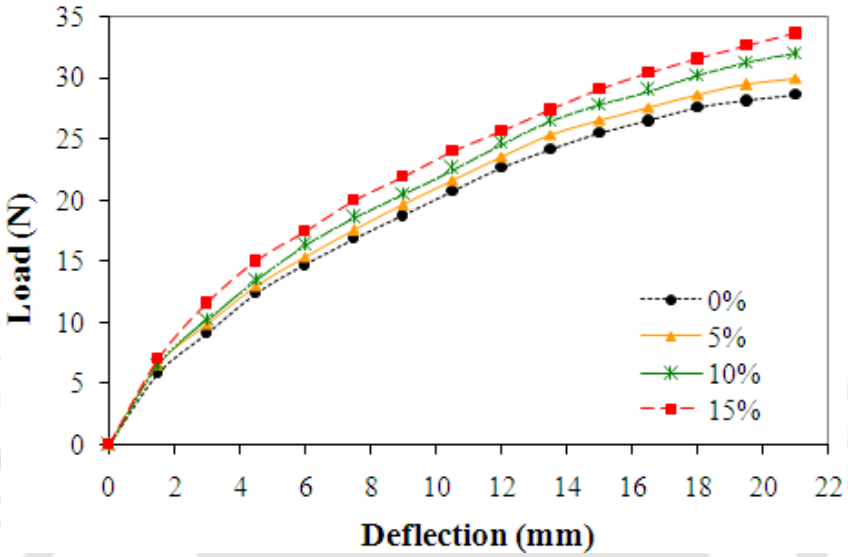

Figure 6.19 Load-deflection behavior of Al skinned sandwich panel

The tensile stress and the shear stress for the composite (where it is maximum) are given by the following expressions (*Christiansen et. al., 1972*):

$$\sigma = \frac{3P}{2BD}\left(\frac{L}{D}\right) \tag{6.6}$$

$$\tau = \frac{3P}{4BD} \tag{6.7}$$

where, τ denotes the inter-laminar shear stress along the neutral axis, P refers the load, L, B and D denotes the length, width and thickness of the specimen respectively. The load is measured at the first major maximum in the load deflection curve shown in Figure 6.19. The results obtained for complete range of the composite samples using the load deflection results and are illustrated in Figure 6.20.

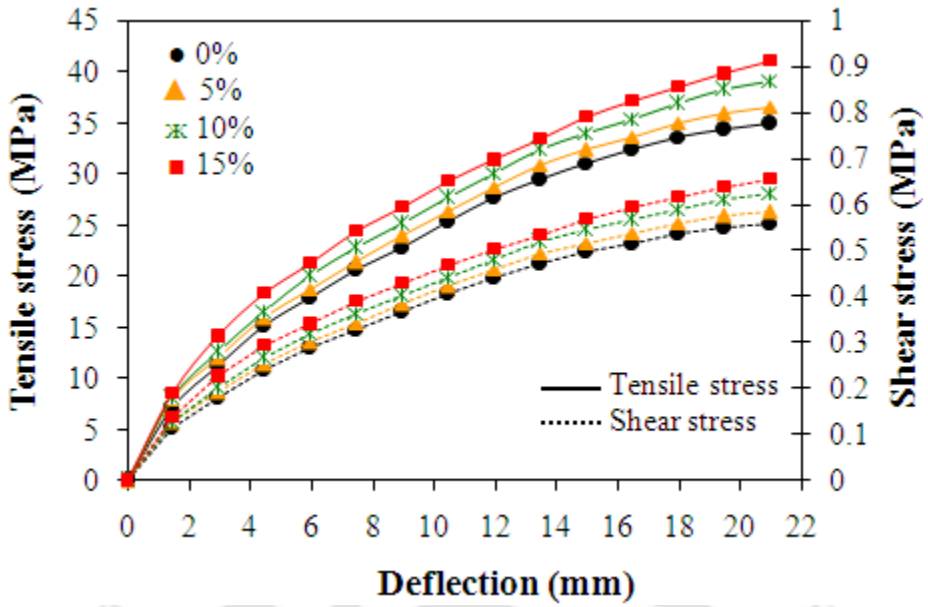

Figure 6.20 Variation of tensile stress and shear stress vs. deflection of the composite materials of Al-skinned sandwich specimens

Similarly, Figure 6.21 and Figure 6.22 show the bending behaviors of GI skinned sandwich composite specimens. It is observed that with the percentage increase of cement fillers and using the composite as core materials, bending characteristics of the sandwich panel improved. It is further observed that GI skinned sandwich panels give better results compared to aluminum skinned sandwich panel.

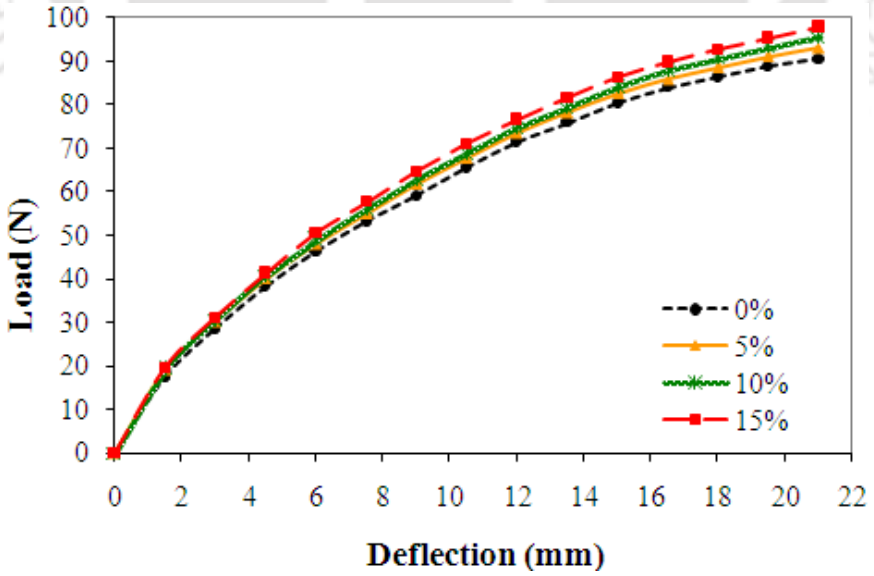

Figure 6.21 Load-deflection behavior of GI skinned sandwich specimens

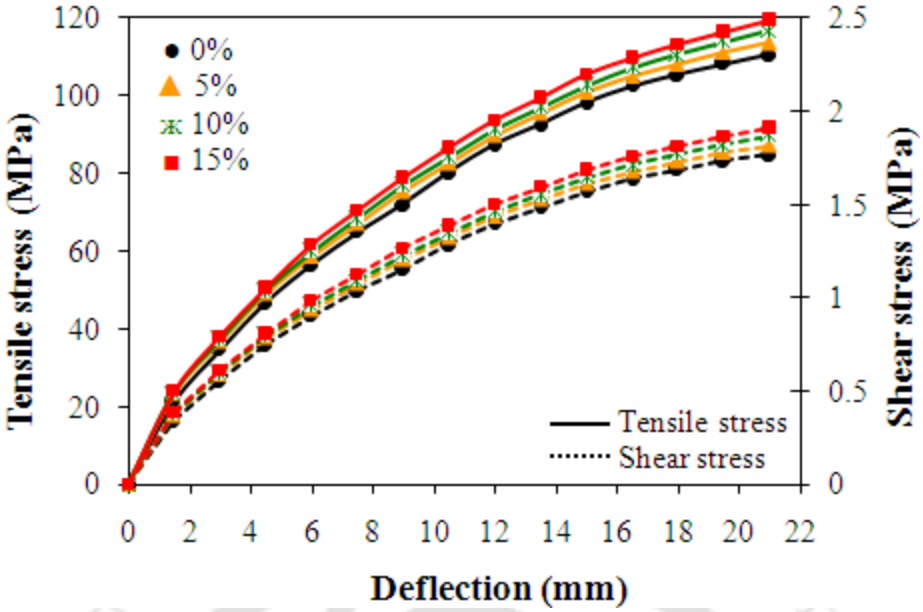

Figure 6.22 Variation of tensile stress and shear stress vs. deflection of the composite materials of GI skinned sandwich specimens

6.4.2 Evaluation of Tensile Properties of Sandwich Panels

The tensile mechanical properties of cement filled sandwich (Aluminum and GI skinned) composite specimens (dog bone shaped) are obtained followed by the ASTM standard D638 using Universal Testing Machine (Instron Tensile Tester), digitally controlled by the closed loop Servo Hydraulic 100 kN dynamic testing machine (maker: INSTRON, Model no. 8801). The tests are carried out at a crosshead speed of 2 mm/min at room temperature. Figure 6.23(a) and (b) represent the GI-skinned sandwich panels and schematic of sandwich panel respectively where, the Figure 6.24(a) and (b) illustrate the tensile test setup and the corresponding fractured sample images after testing of 10% cement reinforced-GI- sandwich panel respectively. Similar images for 10% cement reinforced composite-Al skinned- sandwich panel has also been shown in the Figure 6.25. The mechanical properties of the sandwich panels have been evaluated experimentally and true tensile stress-strain graph is shown in the Figure 6.26. It is observed that aluminum skinned sandwich panel failed within 3% strain because of its low thickness and less modulus of elasticity.

(i)

(ii)

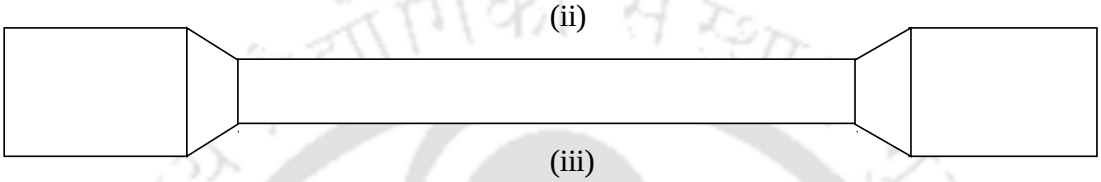

(iii)

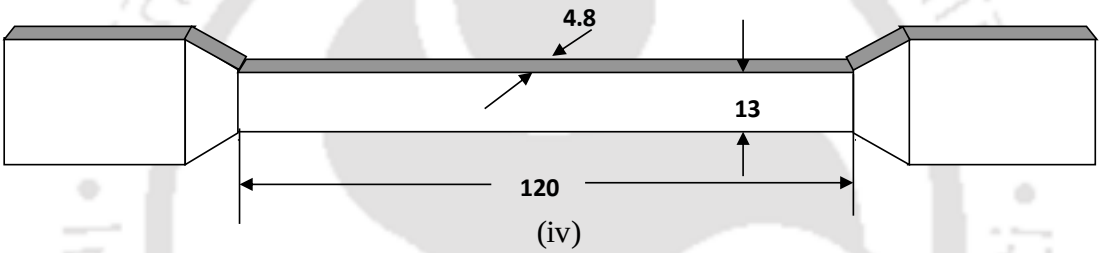

(iv)

(v)

(b)

Figure 6.23 (i) Schematic of core material, (ii) Fabricated core material, (iii) Skin material (Thickness 0.5 mm for GI and 0.3mm for Al), (iv) Schematic of sandwich sample and (v) Fabricated sandwich sample

(a)

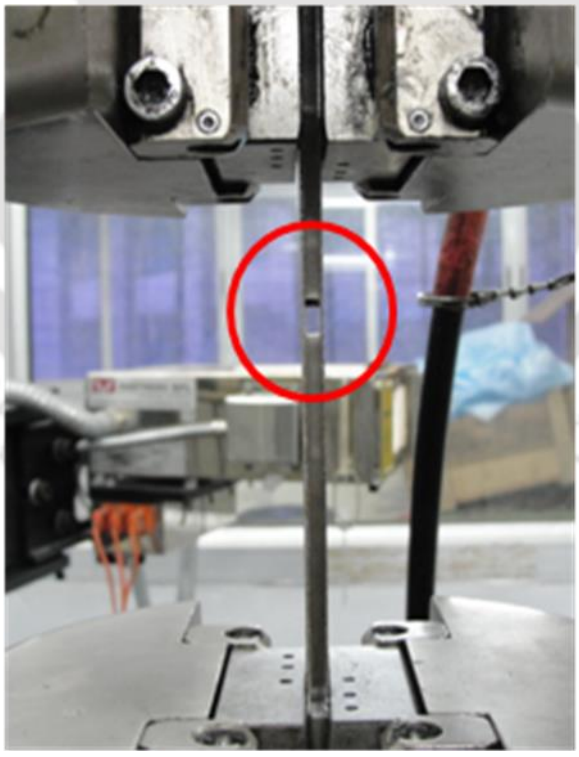

(b)

Figure 6.24 (a) Tensile test of 10% cement reinforced composite-GI skinned- sandwich panel and (b) corresponding fractured of the 10% cement reinforced composite-GI skinned sandwich composite

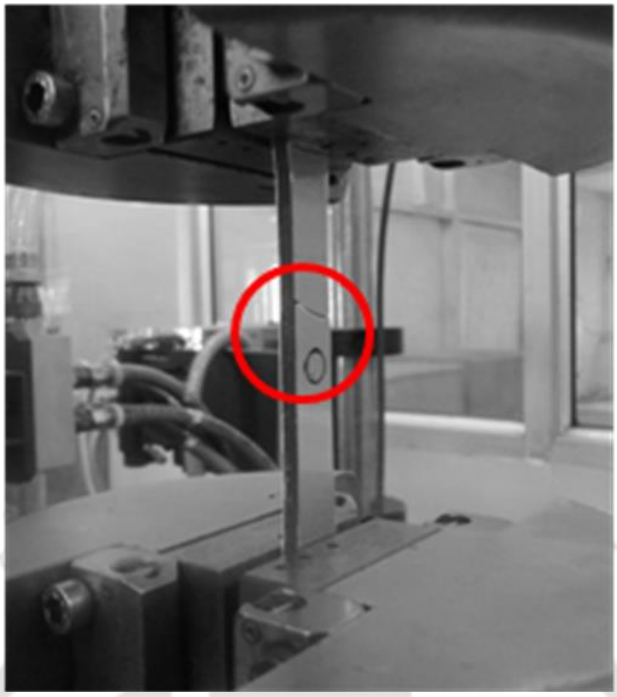

Figure 6.25 Corresponding skin failure of 10% cement reinforced composite-Al skinned sandwich specimen

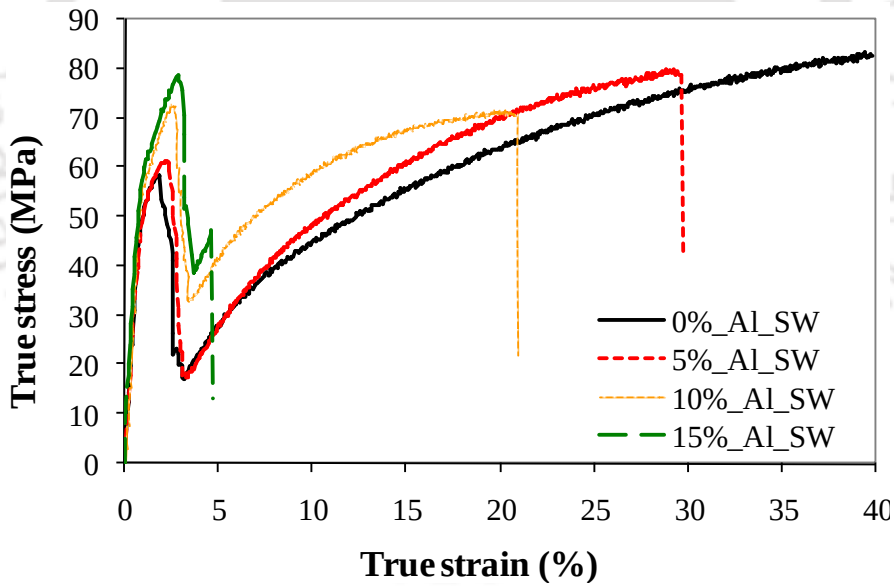

Figure 6.26 True stress-true strain behavior of aluminum skinned sandwich panels

Further, it is observed that the core composites withstand and hold the load that significantly delayed to failure especially for 5% and 10% cement filled composite core materials. The study of mechanical properties of cement reinforced polypropylene composite as core materials for Al skinned sandwich panel, reveals that the significant change in the respective properties is observed for 10% of cement loading in the polypropylene matrix. Figure 6.27(a) illustrates the variation of ultimate tensile strength and elastic modulus with cement content (wt%). The tensile test results are given in

the Table 6.8. For cement filled composite materials, it is observed that the ultimate tensile strength increased by 6.05% for 5%, 25.86% for 10% and 32.75% for 15% of cement contents. Further, significant change in elastic modulus values have been observed for higher loading of cement materials in polypropylene matrix. With an increase of 5%, 10% and 15% of cement loading, an increase of 3.32%, 10.55% and 26.50% of elastic modulus is observed compared to pure polypropylene. Figure 6.27(b) represents maximum load values and yield strength at 0.2% offset with cement loading percentages. In case of load bearing capacity, it is observed that with 5%, 10% and 15% cement loading, load bearing capacity improves by 3.20%, 13.38% and 7.70% respectively.

A comparative study of available sandwich panels is given in the table 6.9.

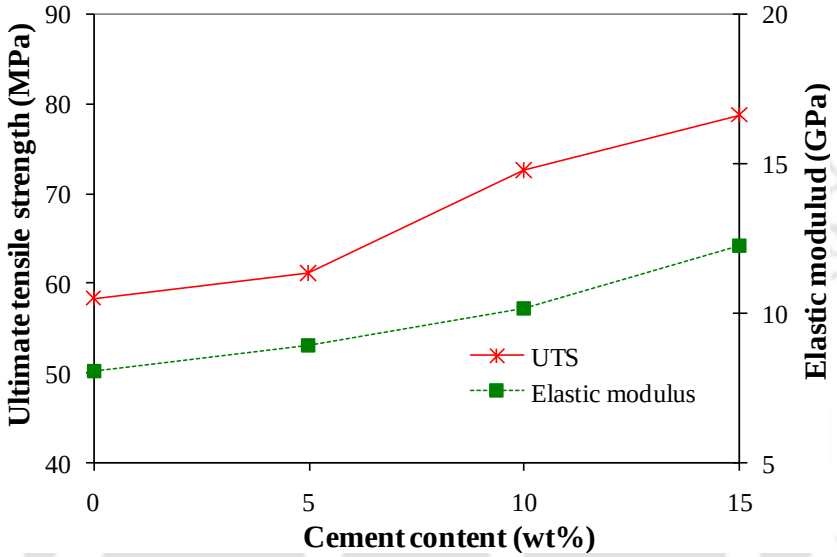

(a)

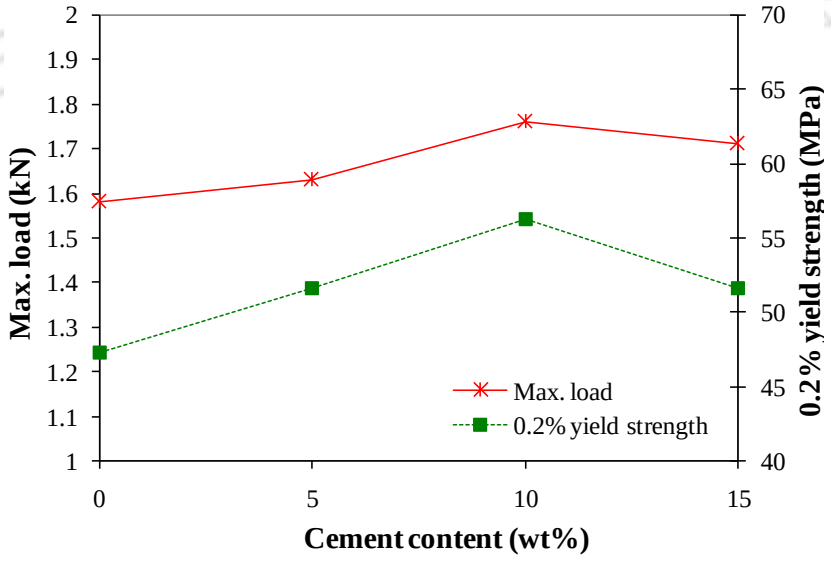

(b)

Figure 6.27 (a) Ultimate tensile strength and elastic modulus variation with the % of cement reinforced composite-Al skinned sandwich composite, (b) variation of maximum load and yield strength at 0.2% offset with the % of cement reinforced composite-Al skinned sandwich composite

Similar trend is observed in the yield strength value, where an increase in yield strength value at 0.2% offset is about 11.54% more than pure polypropylene with 5% of cement content and about 21.53% for 10% cement loading and 12.80% for 15% cement loading for aluminum sandwich panel.

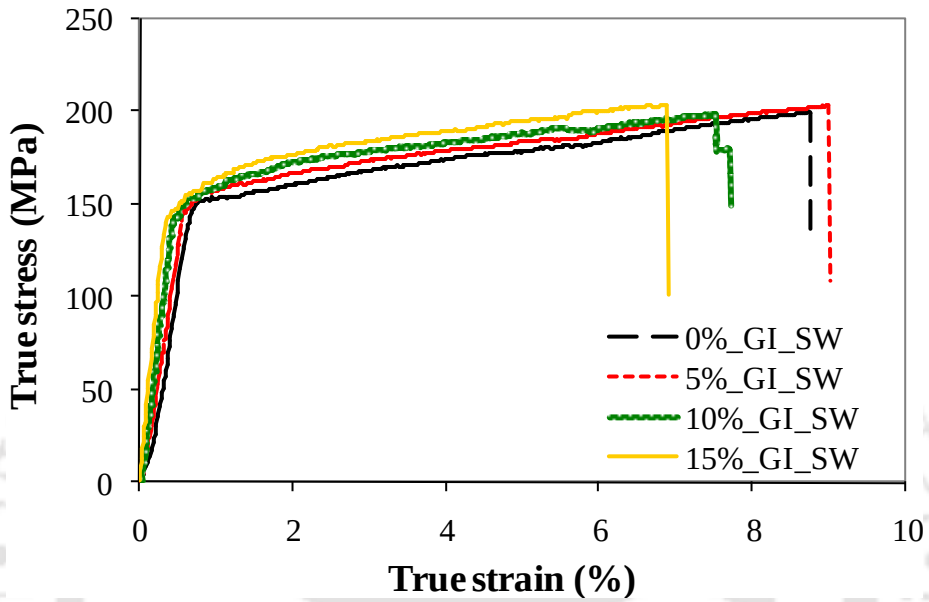

Figure 6.28 True stress-true strain behaviors of GI skin sandwich composites

As discussed earlier section, compared to Aluminum skinned sandwich panels, however, the GI skinned sandwich panels show significant deviation in the tensile behavior of the composites [Figure 6.28 and 6.29(a), (b)]. In this case, it is observed that the sandwich structures i.e. the core materials fail earlier than the metallic skin. It is further observed that the skinned material, i.e., GI withstand and holds the load even after failure of the core composite. This is due to the higher thickness (0.50 mm) with elastic modulus of 200 GPa (*Coni et al., 2009*) of GI skin compared to Aluminum skin (0.33 mm) with elastic modulus of 68.9 GPa (*Seli et al., 2013;*) [203]

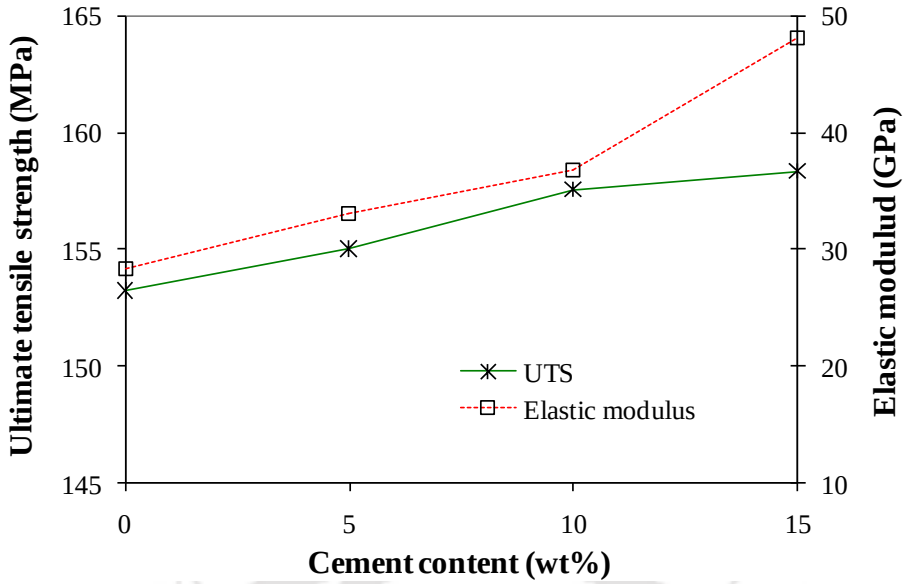

(a)

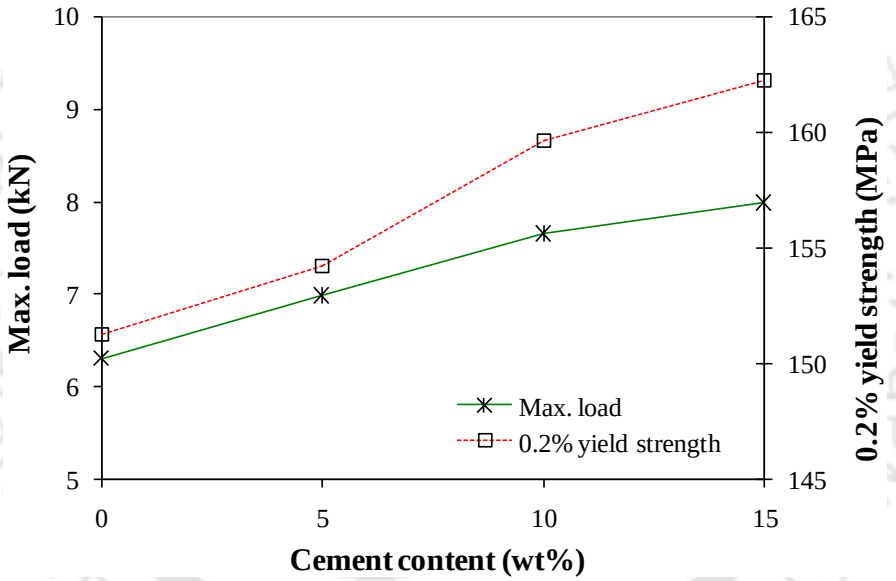

(b)

Figure 6.29 (a) Ultimate tensile strength and elastic modulus variation with the cement % of composite-GI sandwich panels, (b) variation of maximum load and yield strength at 0.2% offset with the cement % of composite-GI sandwich panel

The tensile test results can be interpreted such that the mechanical properties show significant enhancement with increase of cement loading percentages less than 15 % with the metallic skin sandwich structures. These results are believed to be due to good interfacial bonding between polypropylene matrix and cement particles as well as metallic skins and better distribution of cement particles throughout the polymer matrix thus enables easy transfers of load from polypropylene to skin materials. Hence, the study of mechanical properties of cement filled composites with metallic skin materials for sandwich structures reveal that the

change in the particular properties is observed optimal for 10 % of cement loading composite as core material for the proposed sandwich components.

Table 6.8 Tensile test results of sandwich specimens (*Seli et al., 2013; Coni et al., 2009*) [203-204]

Sample	UTS (MPa)	SD	Elastic modulus (MPa)	SD	Max. load (kN)	SD	0.2% Yield strength (MPa)	SD
0%	29.44	1.40	1325.28	2.25	1.22	1.85	12.60	1.64
5%	30.65	2.02	1430.56	3.05	1.28	2.12	15.73	1.52
10%	31.52	1.58	1540.50	2.12	1.31	1.78	14.27	2.03
15%	24.07	2.11	1629.48	2.23	1.00	1.88	14.46	1.97
Al sheet- 6061	310		68900		-		276-277	
GI sheet	700		200000		-		600	
Al-0%-Al*	58.37	1.82	8092.66	1.23	1.58	2.11	47.28	1.84
Al -5% -Al	61.13	1.13	8916.39	1.57	1.63	2.05	51.58	2.42
Al -10% -Al	72.55	1.53	10160.48	1.08	1.76	1.65	56.26	1.56
Al -15% -Al	78.75	1.08	12256.85	1.67	1.71	1.78	51.62	1.78
GI -0% -GI*	153.24	2.02	28305.87	1.56	6.30	2.25	151.27	1.24
GI -5% -GI	155.03	2.13	33138.93	1.38	6.98	1.64	154.23	1.84
GI -10% -GI	157.55	1.64	39800.88	2.03	7.65	1.66	159.65	2.23
GI -15% -GI	158.36	1.39	47084.17	1.88	7.98	1.89	162.23	1.09

**Al-SW- Aluminum skinned sandwich panel and GI-SW- Aluminum skinned sandwich panel*

The fabricated sandwich panels can be utilized in various applications listed below:

1. Decorative Building Panels
2. Insulated Building Panels
3. Panel Sealing
4. Structural Assembly
5. Roof Panels
6. Door Panels and
7. Marine sandwich panels

Table 6.9 Comparative study of the fabricated sandwich panels and available sandwich panels

Sample	Market Price/m^2 (approx.) (Rs.)*
0% _Al-SW	180
5% _Al-SW	180
10% _Al-SW	180
15% _Al-SW	180
0% _GI-SW	200
5% _GI-SW	200
10% _GI-SW	200
15% _GI-SW	200
PVC sandwich panel	300
Heat insulation polyurethane sandwich panel	450
Insulated eps sandwich panel	1200
Aluminum honeycomb sandwich panel	3500
Rock wool sandwich panel	1500
FRP sandwich wall panels	6500

(http://www.alibaba.com/showroom/sandwich-panel-price.html)

As per the market survey, it is observed that the price of the fabricated sandwich panel is cheaper than the available sandwich panels (*http://www.alibaba.com/showroom/sandwich-panel-price.html: date: 18.05.2014).*

6.5 Summary

An in-depth investigation and understanding of damping properties of materials are essential before fabrication of mechanical components for industrial application. For this, cement filled polymeric composite materials underwent free and forced vibration tests for evaluation of the damping properties and vibration characteristics. Experiments are conducted using the laser assisted vibrometer (LAV) to evaluate and characterize the damping properties of the materials at low frequency. Besides this, the time response and Fast Fourier Transform (FFT) analysis have been carried out and subsequently the damping ratio and loss factor of the materials are obtained. The effects of crack on the material performance with respect to its position and depth are evaluated on a composite beam experimentally and the results are validated comparatively with respect to different percentage of cement fillers. Sandwich panel of the composite material is manufactured where aluminum and galvanized iron (GI) sheets are used as skin materials and cement reinforced polypropylene based composite material is used as core material. Damping characteristics and mechanical properties of the sandwich panels are also investigated vastly. The proposed sandwich panels proved to be much more beneficial as it reduces the overall weight of the structural component suitable to various automotive industrial applications.

Chapter 7

Conclusions and Future Scopes

7.1 General Conclusions

A new type of polypropylene (PP) based composite material has been developed using Portland Pozzolanic cement (PPC) particles as filler material for industrial applications. The morphological study of the composite shows adequate bonding between the PP matrix and the PPC particles. It is observed that no crystallographic changes occur in the matrix with the incorporation of PPC particles at high loading rate. Further, the absence of major peaks is understood to have the possible exfoliation of the cement particles into the polymer matrix.

Damping analysis of the composites shows that the percentage increase of cement materials, the loss factor of the material varies. It is also observed that the damping properties of the composite materials depend not only on the filler material's properties but also on the notch size. According to the ASTM D638 standard, tensile tests are carried out to investigate the mechanical properties of the material in the Instron Universal testing machine. The experimental results reveal that the elastic modulus increases with increase of the cement percentages. Although, ultimate tensile strength and 0.2% yield strength decreases beyond 10% cement loading.

Several experiments are conducted such as TGA, DSC and TMA and thermal characteristics of the composite have been evaluated. From the experimental results, it is observed that the composites show better thermal stability when the percentages of filler loading increases. It is further concluded that the thermal stability and fire retardant property of the composite are also improved with the percentage increase of PPC particles. It is also observed that the composite retains its crystallinity even with the incorporation of varying percentage of cement particles.

The fabricated composites are also characterized using various other techniques such as nanoindentation, Raman spectroscopy and FT-IR analysis. Mechanical performance analysis like, 3-point bending, short run cyclic fatigue, notchtensile, dynamic mechanical behavior have also been carried out for the composite materials. The characterizations analysis of the composite materials and its fillers show adequate bonding between the PP matrix and the PPC particles. Nanoindentation test reveals the localized mechanical behaviors of the

composite materials which correlate the global properties of the said materials. From the Raman spectroscopy and FT-IR analysis, it is attributed that the band peaks of the filler materials do not mingle with the composites materials which validates the adequate bonding between fillers with matrix.

Mechanical characterizations of the composite materials show that the percentage increase of cement materials, the mechanical properties enhanced up to a certain percentage of filler material. It is also observed that presence of deformation onto samples significantly affects the mechanical performance of the materials. Based on the modified Halpin-Tsai and modified rule-of-mixing series model, the results are analyzed. And it is observed that the elastic modulus depends on the filler loading as well as the aspect ratio. DMA results show that storage modulus and loss modulus increases with cement loading percentage, and eventually, loss factor decreases.

Polypropylene is chosen as matrix material whereas the low cost PPC particles as reinforcement. 5%, 10% and 15% in weight fraction of PPC particles are taken to fabricate and optimize the gear material. Numerous experiments such as dynamic mechanical analysis (DMA), tensile tests, morphological analysis is conducted and it is observed that 10 wt% PPC particles filled composite gear material exhibits better mechanical properties and performance to fabricate the gear. Reduction of the viscous properties due to incorporation of the cement materials causes a reduction of material resilience. 100% PP gears exhibit more hysteresis loss compared to 10% PPC particles filled composite gear material results in better performance and higher relative life. The heat emission in dynamic condition due to gear-to-gear friction subjected to the applied load and variable speeds on material performance are studied and demonstrated with extensive discussions.

Mechanical characterizations of the sandwich panels show that the mechanical properties depends on the enhanced properties of viscoelastic core materials as well as skin material's thickness and properties. Free and Forced vibration behaviors of the fabricated composite materials as well as its sandwich structures show significant results for structural applications. The influence of cracks on the natural frequencies are evaluated experimentally and compared with the theoretical results. It is observed that the computational results are in good agreement with the experimental results.

7.2 Specific Conclusions

Some of the important contributions of the present thesis are outlined as follows:

- A new type of polypropylene based composite materials has been designed and developed using Portland pozzolanic cement (PPC) particles as filler material for industrial applications. The work boasts the idea to use PPC as a cheaper, though effective, strengthening polymeric material without any significant chemical and physical modifications.

- Several characterization techniques are employed and numerous mechanical and thermal properties have been evaluated. The morphological study of the composite shows adequate bonding between the polypropylene matrix and the PPC particles. Several experiments such as TGA, DSC, and TMA are conducted and thermal characteristics of the composite are evaluated. The experimental results indicate better thermal stability when the percentage of filler loading increases. In addition, composites underwent several characterization tests such as rheology studies to understand the viscoelastic behavior and damping properties of the material in thermal condition. XRD analysis carried out to investigate possible exfoliation and crystallographic analysis of filler particles into the matrix material. Nanoindentation test has been conducted for evaluation of localized mechanical properties of the composite materials. Further, Raman spectroscopy and FT-IR analysis have also been carried out to identify the organic and inorganic molecules presence in the composite materials with its excitation vibrational bands.

- According to the ASTM D638 standard, tensile tests are conducted to investigate the mechanical properties in the Instron Universal testing machine. The experimental results reveal that the elastic modulus increases with increase of the cement percentages. Although, ultimate tensile strength and 0.2% yield strength decreases beyond 10% cement loading. Mechanical characterization of the composites indicated that the mechanical properties enhanced when filler material incorporated up to a certain percentage into polymer. In addition, Halpin-Tsai principle and rule-of-mixing series model are modified and applied to analyze the mechanical properties of composite materials.

- A new type, low cost, recyclable polymeric composite material spur gear has been fabricated following the injection molding technique. Polypropylene is chosen as matrix

material whiles the low cost PPC particles as reinforcement. 5%, 10% and 15% in weight fraction of cement particles are taken to fabricate and optimize the gear material. Numerous experiments such as dynamic mechanical analysis (DMA), tensile tests, morphological analysis is conducted and it is observed that 10 wt% cement particles filled composite gear material exhibits better mechanical properties and performance to fabricate the gear. It is also observed that, the elastic modulus depends on the filler loading as well as the aspect ratio. The DMA test shows that the storage modulus and loss modulus increases with PPC loading percentage although material loss factor decreases. The developed inexpensive composite material gear is suitable for industrial application as an alternative to metallic gear. In addition, the gear material exhibits insulating properties thus could also act as thermal and electric insulator.

- A technology demonstration is carried out successfully employing the injection molding technique for fabrication of complex shaped damage tolerant composite material gear for light-to-medium duty device application. The fabricated composite material gears possess excellent wear and fatigue resistant characteristics.

- 10% fillers composite gear material exhibit much less hysteresis loss compared to 100% PP gears and thus yields better performance and higher fatigue life. Further, significant improvement of load bearing capacity of the gear tooth is achieved due to incorporation of the cement particles. The compression resilience of the gear tooth is higher when PPC particles percentages are higher within the ductile limit.

- The primary benefit of using this low cost cement based composites instead of metals is that large weight saving can be obtained. Further, on selecting large series production of these gears, large cost saving seem also feasible.

- The dynamic performance of the gear has been evaluated under loading conditions subjected to variable speeds. It is observed that, as the test speed increases the temperature of test gear increases leading to more frictional loss of the gear material. It is also observed that gear is suitable to run at moderate speeds under moderate loading condition. Besides this, the spur gear material is tested to evaluate its friction and wear characteristics in adhesive and abrasive wear modes. Weight loss due to wear is evaluated through direct measurement under a specific load and running condition. It is observed that the adhesive wear rate significantly reduced when the cement filler loading increases.

This is because shear strength and surface energy of the composite material changes while toughness and hardness of the material improves due to strengthening by cement fillers. Further, emission of heat resulted from the gear pair during running is observed to be less compared to the results indicated in the past researches for other metallic and non-metallic gears.

- Sandwich panel of the composite material is manufactured where aluminum and galvanized iron (GI) sheets are used as skin materials and cement reinforced polypropylene based composite material is used as core material. The proposed sandwich panels proved to be much more beneficial as it reduces the overall weight of the structural body suitable to various automotive industrial applications.

Thus, the results and performance of the composite gear materials as well as test gears and hybrid sandwich composite panels validate the usefulness of the material for industrial applications as an alternative to metallic material.

7.3 Future Scope of Work

Few scopes on the composite material for future works towards design and development and application are outlined below:

- The composite can be manufactured by further reinforcement of polypropylene with Multi-walled/single-walled carbon nanotubes.
- Using the same composite material, different grade of gears can be manufactured and analyzed. The performance test can also be evaluated by standard gear testing machine.
- Identification and quantification of crack propagation at the gear tooth root region can be investigated experimentally and computationally.
- Vibration analysis can be performed during gear running condition followed by finite element method.
- The flash temperature from tooth root-to-tip via pitch point can be calculated. Quantification of noise emission of test gear pair and its control can also be performed.

References

1. **Abbes, M. S.**, Hentati, T., Maatar, M., Fakhfakh, T. and Haddar, M., (2011), 'Dynamic analysis of helical gears supported by rolling element bearings', Journal of Theoretical and Applied Mechanics, Vol. 41 (1), pp. 33–50.

2. **Aberg, J.** and Widell, B., (2004), 'Uniaxial material damping measurements using a fiber optic lattice: a discussion of its performance envelope, Experimental Mechanics, Vol. 44, pp. 33–36.

3. **Adams, R.D.** and Maheri, M. R., (2003), 'Damping in advanced polymer–matrix composites', Journal of Alloys and Compounds, Vol. 355, pp. 126–130.

4. **Allaoui, A.**, Bai, S., Cheng, H. M. and Bai, J. B., (2002), 'Mechanical and electrical properties of a MWNT/epoxy composite', Composites Science and Technology, Vol. 62 (15), pp. 1993-1998.

5. **Andrzej, K.** and Marek M., (1984), 'Waste cement dusts as fillers for rubber compounds', Cement and Concrete Research. Vol. 14, pp. 776-784.

5. **Ahmed, S. F.**, Rho, G. H., Lee, J. Y., Kim, S. J., Kim, H. Y., Jang, Y. J., Moon, M. W. and Lee, K. R., (2010), 'Nano-embossed structure on polypropylene induced by low energy Ar ion beam irradiation', Surface & Coatings Technology, Vol. 205, pp. 104-108.

8. **Andrzej, K.** and Marek M., (1984), 'Waste cement dusts as fillers for rubber compounds', Cement and Concrete Research. Vol. 14, pp. 776-784.

8. **Anon**, (March/April 1999) 'A Brief Look at Composite Materials in Airbus Commercial Aircraft, High Performance Composites', pp. 32-36.

9 **Arruebarrena, M. B.**, Hendra, P. J. and Judkins, M., (1995), 'The Raman spectra of oriented isotactic polypropylene', Spectrochimica Acta Part A, Vol. 51, pp. 2117-2124.

10. **Ashby, M. F.**, (1987), 'Technology of 1990s: advanced materials and predictive design', Philosophy Transactions of the Royal Society London, Series A, Vol. 322, pp. 393-407.

11. **Ataeefard, M.** and Moradian, S., (2011), 'Surface properties of polypropylene/organoclay nanocomposites', Applied Surface Science, Vol. 257, pp. 2320–2326.

12. **Auad, M. L.**, Mosiewicki, M., A., Uzunpinar, C. and Williams, R. J. J., (2009), 'Single-wall carbon nanotubes/epoxy elastomers exhibiting high damping capacity in an extended temperature range', Composites Science and Technology, Vol. 69, pp.1088–1092.

13. **Bahadur, S.** and Polineni, V. K., (1996), 'Tribological studies of glass fabric-reinforced polyamide compositesfilled with CuO and PTFE**',** Wear, Vol. 200 (1), pp. 95-104.

14. **Bao, S. P.** and Tjong, S. C., (2008), 'Mechanical behaviors of polypropylene/carbon nanotube nanocomposites: The effects of loading rate and temperature', Materials Science and Engineering A, Vol. 485, pp. 508–516.

15. **Barron, A. R.**, (2010), 'Chemical composition of portland cement', Connexions module: m16445, Version 1.9: Jan 4, 6:47 pm US/Central.

16. **Bentz, D. P.** and Haecker, Claus J., (1999) 'An argument for using coarse cements in high performance concretes', Cement and Concrete Research, Vol. 29, pp. 615-618.

17. **Bhattacharyyaa, A. R.**, Sreekumar, T. V., Liu, T., Kumar, S., Ericson, L. M., Hauge, R. H. and Smalley, R. E., (2003), 'Crystallization and orientation studies in polypropylene/single wall carbon nanotube composite', Polymer, Vol. 44, pp. 2373–2377.

18. **Bikiaris, D.**, Vassiliou, A., Chrissafis, K., Paraskevopoulos, K. M., Jannakoudakis, A. and Docoslis, A., (2008), 'Effect of acid treated multi-walled carbon nanotubes on the mechanical, permeability, thermal properties and thermo-oxidative stability of isotactic polypropylene', Polymer Degradation and Stability, Vol. 93, pp. 952-967.

19. **Bishop, M.**, Bott, S. G. and Barron, A. R., (2003), 'A New Mechanism for Cement Hydration Inhibition: Solid-State Chemistry of Calcium Nitrilotris (methylene) triphosphonate', Chemistry of Materials, Vol. 15 (16), pp. 3074-3088.

20. **Breeds, A. R.**, Kukureka, S. N., Mao, K., Walton, D. and Hooke, C. J., (1993), 'Wear behaviour of acetal gears', Wear, Vol. 166, pp.85–91.

21. **Burgt, F. P.**, (2002),' Crystallization of isotactic polypropylene,' A PhD Thesis, Dutch Polymer Institute, Eindhoven University of Technology.

22. **Cai, L.F.**, Mai, Y.L., Rong, M.Z., Ruan, W.H., Zhang, M.Q., (2007), 'Interfacial Effects in Nano-Silica/Polypropylene Composites Fabricated by In-Situ Chemical Blowing', eXPRESS Polymer Letters 1(1), pp. 2–7.

23. **Chabert, E.**, Gauthier, C., Dendievel, R., Chazeau, L. and Cavaillé, J. Y., (2003), 'Mechanical Behavior of Polymer Nanocomposites : a discrete simulation approach', Materials Research. Society Proceedings, Vol. 740, pp. 16.1.1-16.1.6.

24. **Chandra, R.**, Singh, S.P. and Gupta, K., (1999), 'Damping studies in fiber-reinforced composites -a review', Composite Structures, Vol. 46, pp. 41-51.

25. **Charles, D. F.**, Gnanamoorthy, R. and Ravindran, P., (2010), 'Rolling contact fatigue behavior of polyamide clay reinforced nanocomposite—Effect of load and speed, Wear, Vol. 269, pp. 565–571.

26. **Chauhan, S. R.**, Kumara, A. Singh, I. and Kumar, P., (2010), 'Effect of Fly Ash

Content on Friction and Dry Sliding Wear Behavior of Glass Fiber Reinforced Polymer Composites - A Taguchi Approach', Journal of Minerals & Materials Characterization & Engineering, Vol. 9 (4), pp. 365-387.

27. **Chen, G. X.**, Kim, H.S., Park, B. H. and Yoon, J. S., (2006), 'Multi-walled carbon nanotubes reinforced nylon 6 composites', Polymer, Vol. 47, pp. 4760–4767.

28. **Cheng, L. P.**, Lin, D. J. and Yang, K. C., (2000), 'Formation of mica-intercalated-Nylon 6 nanocomposite membranes by phase inversion method', Journal of Membrane Science, Vol. 172, pp. 157–166.

29. **Choi, J. H.**, Jegal, J. and Kim, W. N., (2006), 'Fabrication and characterization of multi-walled carbon nanotubes/polymer blend membranes', Journal of Membrane Science, Vol. 284, pp. 406–415.

30. **Christiansen, A. W.**, Lilley, J. and Shortall, J. B., (1972), 'A three point bend test for fibre reinforced composites', Fibre Science and Technology, Vol. 7, pp. 1-13.

31. **Clorius, C. O.**, Pedersen, M. U., Hoffmeyer, P. and Damkilde, L., (2000), 'Compressive fatigue in wood', Wood Science and Technology, Vol. 34, pp. 21-37.

32. **Coni, N.**, Gipiela, M. L., D'Oliveira A. S. C. M. and Marcondes, P. V. P., (2009), 'Study of the Mechanical Properties of the Hot Dip Galvanized Steel and Galvalume', Journal of the Brazilian Society of Mechanical Sciences and Engineering, Vol. XXXI (4), pp. 319-326

33. **Cox, H. L.**, (1952), 'The elasticity and strength of paper and other fibrous materials', British Journal of Applied Physics 3, pp. 72–9.

34. **Daniels, B. K.**, Harakas, N. K. and Jackson, R. C., (1971), 'Short beam shear tests of graphite fiber composites', Fibre Science and Technology 3, pp. 187-208.

35. **Deo, R. B.**, Starnes, J. H. and Holzwarth, R. C., (May-2001), 'Low-cost composite materials and structures for aircraft applications', Technical Meeting, Leon, Norway, published in RTO-MP 069-II.

36. **Dickson, R. F.**, Fernando. G., Adam. T., Reiter. H. and Harris. B., (1989), 'Fatigue Behaviour of Hybrid Composites', Journal of Materials Science, Vol. 24, pp. 227-233.

37. **Dieter, G. E.**, (1961), 'Mechanical Metallurgy', McGraw-Hill Book Company, New York.

38. **Dighe, A. D.**, Mishra, A. K. and Wakchaure, V. D., (2014) 'Investigation of Wear Resistance and Torque Transmission Capacity of Glass Filled Polyamide and PEEK Composite Spur Gears', International Journal of Engineering and Advanced Technology, Vol. 3(3), pp. 299-303.

39 **Dikobe, D. G.** and Luyt, A. S., (2009), 'Morphology and properties of polypropylene/ethylene vinyl acetate copolymer/wood powder blend composites',

eXPRESS Polymer Letters, Vol.3(3), pp. 190–199.

40. **Ding, H.**, (2007), 'Dynamic wear models for gear systems', PhD thesis, The Ohio State University.

41. **Dong, Y.**, Bhattacharyya, D. and Hunter, P. J., (2008), 'Experimental characterisation and object-oriented finite element modelling of polypropylene/organoclay nanocomposites', Composites Science and Technology, Vol. 68, pp. 2864–2875.

42. **Draˇca, S.**, (2006), 'Finite element model of a double-stage helical gear reduction', Thesis, Degree of Master of Applied Science, University of Windsor.

43. **Düzcükoglu, H.**, (2009), 'PA 66 spur gear durability improvement with tooth width modification', Materials and Design, Vol. 30, pp. 1060–1067.

44. **Endo, M.**, Hayashi, T., and Kim, Y. A., (2006), 'Large-scale production of carbon nanotubes and their applications', Pure Applied Chemistry, Vol. 78 (9), pp. 1703–1713.

45. **Fang, T. H.** and Chang, W. J., (2004), 'Nanoindentation characteristics on polycarbonate polymer film', Microelectronics Journal, Vol. 35, pp. 595–599.

46. **Fang, T. H.**, Chang, W. J. and Tsai, S. L., (2005), 'Nanomechanical characterization of polymer using atomic force microscopy and nanoindentation', Microelectronics Journal, Vol. 36, pp. 55–59.

47. **Felekoglu, S. B.** and Dulluc, S., (2007), 'Influence of various acids on the physic-mechanical properties of pozzolanic cement mortars', Sadhana, Vol. 32(6), pp. 683-691.

48. **Ferreira, E. C.**, Neves, N. M., Muschalle, R. and Pouzada, A. S., (2001), 'Friction properties of thermoplastics in injection molding', Innovation and technology from Portugal, Portuguese proceedings at SPE ANTEC conferences.

49. **Finegan, I. C.,** Tibbetts, G. G. and Gibson, R. F., (2003), 'Modeling and characterization of damping in carbon nanofiber/polypropylene composites', Composites Science and Technology, Vol. 63, pp.1629–1635.

50. **Fortunati, E.**, Armentano, I., Iannoni, A. and Kenny, J. M., (2010), 'Development and thermal behaviour of ternary PLA matrix composites', Polymer Degradation and Stability, Vol. 95, pp. 2200-2206.

51. **Friswell, M. I.** and Penny, J. E. T., (2002), 'Crack Modeling for Structural Health Monitoring', Structural Health Monitoring, Vol. 1(2), pp. 139-148.

52. **Fung, K. L.**, Xing, X. S., Li, R. K. Y., Tjong, S. C. and Mai, Y. W., (2003), 'An investigation on the processing of sisal fibre reinforced polypropylene composites', Composites Science and Technology, Vol. 63, pp.1255–1258.

53. **García, M.**, (2004), 'Polymer - inorganic nanocomposites: Influence of colloidal

silica', PhD Thesis, University of Twente.

54. **García, M.**, Van Vliet, G., Jain, S. B., Chrauwen, A. G. S., Sarkissov, A., VanZyl, W. E. and Boukamp, B., (2004), 'Polypropylene/SiO_2 Nanocomposites With Improved Mechanical Properties', Reviews on Advanced Materials Science, Vol. 6, pp. 169-175.

55. **Gassan, J**. and Bledzki, A. K., (2000), 'Possibilities to Improve the Properties of Natural Fiber Reinforced Plastics by Fiber Modification – Jute Polypropylene Composites', Applied Composite Materials, Vol. 7, pp. 373–385.

56. **Gauvin, R.**, Girard, P. and Yelle, H., (1984), 'Maximum Surface 'Temperature of the Thermoplastic Gear in a Non-Lubricated Plastic/Steel Gear Pair', Gear Technology, August-September, pp. 20-46.

57. **Genta, G.**, (1999), 'Vibration of Structures and Machines', Springer Verlag, New York, USA.

58. **Gibson, R. F.**, (1992), 'Damping Characteristics of Composite Materials and Structures', Journal of Materials Engineering and Performance, Vol. 1(1), pp. 11-20.

59. **Goh, H. W.**, Goh, S. H., Xu, G. Q., Pramoda, K. P. and Zhang, W. D., (2003), 'Dynamic mechanical behavior of in situ functionalized multi-walled carbon nanotube/phenoxy resin composite', Chemical Physics Letters, Vol. 373, pp. 277–283.

60. **Golebiewski, J.**, Galeski, A., (2007), 'Thermal stability of nanoclay polypropylene composites by simultaneous DSC and TGA', Composites Science and Technology, Vol. 67, pp. 3442–3447.

61. **Groner, M. D.**, George, S.M., Mclean, R.S., Carcia, P.F., (2006), 'Gas Diffusion Barriers on Polymers using Al_2O_3 Atomic Layer Deposition'. Applied Physics Letter, Vol. 88, pp. 051907.

62 **Gu, W.**, (1997), 'Interfacial Adhesion Evaluation of Uniaxial Fiber-Reinforced-Polymer Composites by Vibration Damping of Cantilever Beam', Thesis of Doctor of Philosophy, Virginia Polytechnic Institute and State University.

63 **Gupta, M.**, Lin, Y., Deans, T., Baer, E., Hiltner, A. and David, A. S., (2010), 'Structure and Gas Barrier Properties of Poly(propylene-graft-maleic anhydride)/Phosphate Glass Composites Prepared by Microlayer Coextrusion', Macromolecules, Vol. 43(9), pp. 4230–4239.

64. **Gutiérrez, G.**, Fayolle, F., Régnier, G. and Medina, J., (2010), 'Thermal oxidation of clay-nanoreinforced polypropylene', Polymer Degradation and Stability, Vol. 95, pp. 1708-1715.

65. **Hakimian E.** and Sulong, A. B., (2012), 'Analysis of warpage and shrinkage properties of injection-molded micro gears polymer composites using numerical simulations assisted by the Taguchi method', Materials and Design, Vol. 42, pp. 62–

71.

66. **Haecker, C.J.,** Bentz D.P., Feng X.P. and Stutzman, P.E., (2003), 'Prediction of cement physical properties by virtual testing', Reprinted from Cement International, Vol. 1, No. 3, pp. 86-92.

67. **Haisty, B. S.** and Springer, W. Z., (1991), 'A general beam element for use in damage assessment of complex structures', Trans. ASME/J. Vibration, Acoustics, Stress and Reliability in Design, Vol. 110**,** pp. 389-394, 1988.

68. **Halpin J. C.**, Kardos, J. L., (1976), 'The Halpin-Tsai Equations: A Review', Polymer Engineering And Science, Vol. 16, (5), pp. 344-352.

69. **Harper, C. A.**, (1999), 'Modern plastics handbook', McGraw-Hill, New York.

70. **Hassan, A. R.**, (2009), 'Contact Stress Analysis of Spur Gear Teeth Pair', World Academy of Science, Engineering and Technology, Vol. 3, pp. 10-20.

71. **Holzer, L.**, Flatt, R. J., Erdog˘an, S. T., Bullard, J. W. and Garboczi, E. J., (2010), 'Shape Comparison between 0.4–2.0 and 20–60 lm Cement Particles', Journal of the American Ceramic Society, Vol. 93(6), pp. 1626–1633.

72. **Hooke, C. J.**, Mao, K., Walton, D., Breeds, A. R. and Kukureka, S. N., (1993), 'Measurement and prediction of the surface temperature in polymer gears and its relation to surface wear', Journal of Tribology, Vol. 115, pp. 119–124.

73. **Hoskins, T. J.**, Dearn, K. D., Kukureka, S. N. and Walton, D., (2011), Acoustic noise from polymer gears – A tribological investigation, Materials and Design, Vol. 32(6), p 3509-3515.

74. **Hussain, F.** and Hojjati, M., (2006), 'Review article: Polymer-matrix nanocomposites, processing, manufacturing, and application: an overview', Journal of Composite Materials, Vol. 40, pp. 1511-1575.

75. **Idrus, M. A. M.**, Hamdan, S., Rahman, M. R. and Islam, M. S., (2011), 'Treated Tropical Wood Sawdust-Polypropylene Polymer Composite: Mechanical and Morphological Study', Journal of Biomaterials and Nanobiotechnology, Vol. 2, pp. 435-444.

76. **Ivana, A.**, Vera, N. S., Dejan, D. and Dejan, M., (2009), 'Finite element model for stress analysis and nonlinear contact analysis of helical gears', Scientific Technical Review, Vol. LVIX (1), pp. 61-68.

77. **Jie, P.**, Shaojun, L. and Xiaozhou, H., (2013), 'The Bulk Temperature Analysis of the Involute Spur Gear Based on Parameterized Modeling of APDL', Fifth Conference on Measuring Technology and Mechatronics Automation, IEEE Computer Society, pp. 1146-1149.

78. **Jin, Z.**, Pramoda, K.P., Xu, G. and Goh, S. H., (2001), 'Dynamic mechanical behaviour of melt-processed multi-walled carbon nanotube/Poly(methyl

methacrylate) composites', Chemical Physics Letter, Vol. 337, pp. 43-47.

79. **Johnson, T.,** http://composite.about.com/od/aboutcompositesplastics/a/History of Composites. 10/08/2013.

80. **Jonathan, N. C.**, Khan, U., Werner J. B., Yurii, K. G., (2006), 'Small but strong: A review of the mechanical properties of carbon nanotube–polymer composites', Carbon, Vol. 44, pp. 1624–1652.

81. **Jose, J. P.**, Malhotra, S. K., Thomas, S., Joseph, K., Goda, K. and Sreekala, M. S., (2012), 'Advances in Polymer Composites: Macro- and Microcomposites – State of the Art, New Challenges, and Opportunities', Introduction to Polymer Composites Part one, First Edition, Wiley-VCH Verlag GmbH & Co. KGaA, Vol. 1, pp. 1-16.

82. **Jose, S.**, Thomas, S., Biju, P.K., Koshy, P. J. and Kocsis, K., (2008), 'Thermal degradation and crystallisation studies of reactively compatibilised polymer blends', Polymer Degradation and Stability, Vol. 93, pp. 1176–1187.

83. **Kanagaraj, S.**, Varanda, F.R., Tatiana, V.Z., Mo´Nica, S.A.O., Jose, A.O.S., (2007), 'Mechanical Properties of High Density Polyethylene/Carbon Nanotube Composites', Composites Science and Technology, Vol. 67, pp. 3071–3077.

84. **Kanny, K.**, Jawahar, P., Moodley, V. K ., (2008), 'Mechanical and tribological behavior of clay–polypropyleneNanocomposites', Journal of Materials Science, Vol. 43, pp.7230–7238.

85. **Kashiwagi, T.**, Grulke, E., Hilding, J., Groth, K., Harris, R., Butler, K., Shields, J., Kharchenko, S., Douglas, J., (2004), 'Thermal and flammability properties of polypropylene/carbon nanotube nanocomposites', Polymer, Vol. 45, pp. 4227–4239.

86. **Katsioti, M.**, Tsakiridis, P. E., Giannatos, P., Tsibouki, Z. and Marinos, J., (2009), 'Characterization of various cement grinding aids and their impact on grindability and cement performance', Construction and Building Materials, Vol. 23, pp. 1954–1959.

87. **Kirupasankar, S.**, Gurunathan, C. and Gnanamoorthy, R., (2012), 'Transmission efficiency of polyamide nanocomposite spur gears', Materials and Design, Vol. 39, pp. 338-343.

88. **Kordani, N.**, Fereidoon, A. and Ashoori, M., (2010), 'Effect of Carbon Nanotube on Damping Properties of Epoxy', Journal of Electronic Science And Technology, Vol. 8, (1), pp. 25-30.

89. **Krawczuk, M.** and Ostachowicz, W. M., (1992), 'Parametric Vibrations of beam with crack', Archive of Applied Mechanics, Vol. 62, pp. 463-473.

90. **Krawczuk, M.**, Zak, A., and Ostachowicz, W., (2000), 'Elastic beam finite element with a transverse crack', Finite Elements in Analysis and Design, Vol. 34, pp. 61-73.

91. **Kultural, S. E.** and Eryurek, I. B., (2007), 'Fatigue behavior of calcium carbonate filled polypropylene under high frequency loading', Materials and Design, Vol. 28,

pp. 816–823.

92. **Lackhoff, M.**, Prieto, X., Nestle, N., Dehn, F., Niessner, R., (2003), 'Photocatalytic activity of semiconductor-modified cement—influence of semiconductor type and cement ageing', Applied Catalysis B: Environmental, Vol. 43(3), pp. 205–216.

93. **Landro, L. D.** and Lorenzi, W., (2009), 'Mechanical Properties and Dynamic Mechanical Analysis of Thermoplastic-Natural Fiber/Glass Reinforced Composites', Macromolecular Symposia, Vol. 286, pp. 145-155.

94. **Lee, S. H.**, Wang, S., Pharr, G. M. and Xu, H., (2007), 'Evaluation of interphase properties in a cellulose fiber-reinforced polypropylene composite by nanoindentation and finite element analysis', Composites: Part A, Vol. 38, pp. 1517–1524.

95. **Lertwimolnun, W.** and Vergnes, B., (2005), 'Influence of compatibilizer and processing conditions on the dispersion of nanoclay in a polypropylene matrix', Polymer, Vol. 46, pp. 3462-3471.

96. **Li, C.** and Cho, T. W., (2003), 'Elastic moduli of multi-walled carbon nanotubes and the effect of van der Waals forces', Composites Science and Technology, Vol. 63, pp. 1517–1524.

97. **Ling, Y.**, (1996), 'Uniaxial True Stress-Strain after Necking,' AMP Journal of Technology, Vol. 5, pp. 37-48.

Lothenbach, B., Saout, G. L., Gallucci, E. and Scrivener, K., (2008), 'Influence of limestone on the hydration of Portland cements', Cement and Concrete Research, Vol. 38, pp. 848-860.

98. **Luo, J. J.**, and Daniel, I. M., (2003), 'Characterization and modeling of mechanical behavior of polymer/clay nanocomposites', Composites Science and Technology, Vol. 63, pp. 1607–1616.

99. **Mahebub, V.**, Kevin, V., (2014), 'Comparative Finite Element Analysis Of Metallic And Non Metallic Spur Gear', IOSR Journal of Mechanical and Civil Engineering, Vol. 11(3), pp. 136-145.

100. **Maine, F. W.** and Newson, W. R., (2006), 'Oriented composite thermoplastic material with reactive filler', US papent, Pub. No.: US2006/0057348 A1.

101. **Makar, J. M.** and Chan, G. W., (2009), 'Growth of cement hydration products on single walled carbon nanotubes', Journal of The American Ceramic Society, Vol. 92(6), pp. 1303-1310.

102. **Manchado, M. A. L.**, Valentini, L., Biagiotti, J., Kenny, J.M., (2005), 'Thermal and mechanical properties of single-walled carbon nanotubes–polypropylene composites prepared by melt processing', Carbon, Vol. 43, pp. 1499–1505.

103. **Manjunatha, C. M.**, Taylor, A. C., Kinloch, A. J. and Sprenger, S., (2010), 'The tensile fatigue behaviour of a silica nanoparticle-modified glass fibre reinforced

epoxy composite', Composites Science and Technology, Vol. 70, pp. 193–199.

104. **Mao, K.**, (2007), 'A new approach for polymer composite gear design', Wear, Vol. 262(3-4), pp. 432-441.

105. **Marosfoi, B. B.**, Szabo, A., Marosi, G., Tabuani, D., Camin, G. and Pagliari, S., (2006), 'Thermal and spectroscopic characterization of polypropylene-carbon nanotube composites', Journal of Thermal Analysis and Calorimetry, Vol. 86(3), pp. 669–673.

106. **Marsh, G.**, (2006), '50 years of reinforced plastic boats', October 8, http://www.reinforcedplastics.com/view/1461/50-years-of-reinforced-plastic-boats

107. **Martin, C.A.**, Sandler, J.K.W., Shaffer, M.S.P., Schwarz, M.K., Bauhofer, W., Schulte, K., Windle, A.H., (2004), 'Formation of percolating networks in multi-wall carbon-nanotube–epoxy composites' Composites Science and Technology, Vol. 64, pp. 2309–2316.

108. **Medvešček, S.**, Gabrovšek, R., Kaučič, V. and Meden, A., (2006), 'Hydration products in water suspension of portland cement containing carbonates of various solubility', Acta Chimica Slovenica, Vol. 53, pp. 172–179.

109. **Melick, H. V.** and Dijk, H.V., (2010), 'High-Temperature Testing of Stanyl Plastic Gears: A Comparison with Tensile Fatigue Data', Gear Technology, March/April, pp. 59-65.

110. **Mendi, F.**, Can, H. and Kulekci, M. K. (2006), 'Fatigue properties of polypropylene involute rack gear reinforced with metallic springs', Materials and Design, Vol. 27(5), pp. 427-433.

111. **Mitra, N.**, (2010), 'A methodology for improving shear performance of marine grade sandwich composites: Sandwich composite panel with shear key', Composite Structures, Vol. 92, pp. 1065–1072.

112. **Morris, P. J. T.**, (2005), 'Polymer Pioneers: A Popular History of the Science and Technology of Large Molecules', Chemical Heritage Foundation. pp. 76. ISBN 0-941901-03-3.

113. **Mouritz, A. P.**, Gellert, E., Burchill, P. and Challis, K., (2001), 'Review of advanced composite structures for naval ships and submarines', Composite Structures, Vol. 53, pp. 21-41.

114. **Muksing, N.**, Nithitanakul, M., Grady, B. P. and Magaraphan, R., (2008), 'Melt rheology and extrudate swell of organobentonite-filled polypropylene nanocomposites', Polymer Testing, Vol. 27, pp. 470-479.

115. **Myshkin, N. K.**, Petrokovets, M. I. and Kovalev, A. V., (2005), 'Tribology of polymers: adhesion, friction, wear, and mass-transfer, Tribology International, Vol. 38, pp. 910–921.

116. **Newman, S. P.**, Clifford, S. J., Coveney, P. V., Gupta, V., Blanchard, J. D., Serafin, F., Amotz, D. B. and Diamond, S., (2005), 'Anomalous fluorescence in near-infrared Raman spectroscopy of cementitious materials', Cement and Concrete Research, Vol. 35, pp. 1620– 1628.

117. **Odegard, G. M.**, Gates, T.S., Herring, H.M., (2005), 'Characterization of Viscoelastic Properties of Polymeric Materials Through Nanoindentation', Experimental Mechanics, Vol. 45(2), pp. 130-136.

118. **Oliver W. C.** and Pharr G. M., (1992), 'An improved technique for determining hardness and elastic modulus using load and displacement sensing indentation experiments', Journal of Materials Research, Vol. 7(6), pp. 1564–83.

119. **Oprişan, G.**, Ţăranu, N., Munteanu, V. and Enţuc, I., (2010), 'Application of modern polymeric composite materials in industrial construction', buletinul institutului politehnic din iaşi, LVI (LX), Fasc. 3

120. **Ostachowicz, W. M.** and Krawczuk, M., (1991), 'Analysis of the effect of cracks on the natural frequencies of a cantilever beam', Journal of Sound and Vibration, Vol. 150(2), pp. 191-201.

121. **Parande, A. K.**, Babu, B. R., Pandi, K., Karthikeyan, M. S. and Palaniswamy, N., (2011), 'Environmental effects on concrete using Ordinary and Pozzolana Portland cement', Construction and Building Materials, Vol. 25, pp. 288–297.

122. **Park, C.**, Ounaies, Z., Watson, A. K., Crooks, R. E., Joseph S. J., Lowther, S. E., Connell, J. W., Siochi, E. J., Harrison, J. S. and Clair, T. L. S., (2002), 'Dispersion of single wall carbon nanotubes by in situ polymerization under sonication', Chemical Physics Letters, Vol. 364, pp. 303–308.

123. **Pater, J. T.**, (2001), 'Prepolymerization and morphology', PhD Thesis, University Twente, The Netherlands.

124. **Pavlidou, S.**, Papaspyrides, C.D., (2008), 'A Review on Polymer–Layered Silicate Nanocomposites', Progress in Polymer Science, Vol. 33, pp. 1119–1198.

125. **Prabhakaran, R.**, (1979), 'Tensile Fracture of Composites with Circular Holes', Materials Science and Engineering, Vol. 41, pp. 121-125.

126. **Prashantha, K.**, Soulestin, J., Lacrampe, M. F., Claes, M., Dupin, G. and Krawczak, P., (2008), 'Multi-walled carbon nanotube filled polypropylene nanocomposites based on masterbatch route: Improvement of dispersion and mechanical properties through PP-g-MA addition', eXPRESS Polymer Letters, Vol. 2(10), pp. 735-745.

127. **Price, D. M**., (2002), 'Thermomechanical, dynamic mechanical and dielectric methods', Principles of Thermal Analysis and Calorimetry Haines, P. J. (Ed.), Royal Society of Chemistry, Cambridge, pp. 94-128.

128. **Rajesh, J. J.**, Soulestin, J., Lacrampe, M. F. and Krawczak, P., (2012), 'Effect of

injection molding parameters on nanofillers dispersion in masterbatch based PP-clay nanocomposites', eXPRESS Polymer Letters, Vol. 6(3), pp. 237-248.

129. **Rajoria, H.** and Jalili, N., (2005), 'Passive vibration damping enhancement using carbon nanotube-epoxy reinforced composites', Composites Science and Technology, Vol. 65, pp. 2079–2093.
130. **Raka, L.,** Bogoeva-Gaceva, G., Lu, K. and Loos, J., (2009), 'Characterization of latex-based isotactic polypropylene/clay nanocomposites', Polymer, Vol. 50, pp. 3739–3746.

131. **Ramkumar, A.** and Gnanamoorthy, R., (2008), 'Axial fatigue behaviour of polyamide-6 and polyamide-6 nanocomposites at room temperature', Composites Science and Technology, Vol. 68, pp. 3401–3405.

132. **Ray, S. S.** and Okamoto, M., (2003), 'Polymer/layered silicate nanocomposites: a review from preparation to processing', Progress in Polymer Science, Vol. 28, pp. 1539–1641.

133. **Ristolainen, N.**, Vainio, U., Paavola, S., Torkkeli, M., Serimaa, R. and Seppala, J.,(2005), 'Polypropylene/Organoclay nanocomposites compatibilized with hydroxyl-functional polypropylenes', Journal of Polymer Science: Part B, Vol. 43, pp. 1892–1903.

134. **Saikrasuna, S.** and Saengsuwan, S., (2009), 'Thermal decomposition kinetics of in situ reinforcing composite based on polypropylene and liquid crystalline polymer', Journal of Materials Processing Technology, Vol. 209, pp. 3490–3500.

135. **Sandler, J.**, Shaffer, M. S. P., Prasse, T., Bauhofer, W., Schulte, K. and Windle, A. H., (1999), 'Development of a dispersion process for carbon nanotubes in an epoxy matrix and the resulting electrical properties', Polymer, Vol. 40, pp. 5967–5971.

136. **Sardar, J.** and Bandopadhya, D., (2010), 'Fabrication and evaluation of damping characteristics of Portland cement filled thermoplastic composites', 24th AIMTDR & 3rd International Conference Proceeding, Vol. 2, pp. 1095-1098.

137. **Sardar, J.** and Bandopadhya, D, (2014), 'Development and fabrication of cement reinforced polypropylene composite material spur gear', Journal of Polymer Engineering, Vol. 34(8), pp. 775–786.

138. **Savage, M.**, Caldwel, R.J., Wisor, G.D. and Lewicki, D.G., (1986), 'Gear mesh compliance modeling', NASA Technical Memorandum 88843.

139. **Seli, H.**, Awang, M., Ismail, A. I. M. Rachmand, E. and Ahmad, Z. A., (2013), 'Evaluation of Properties and FEM Model of the Friction Welded Mild Steel-Al6061-Alumina', Materials Research. Vol. 16(2), pp. 453-467.

140. **Sennett, M.**, Welsh, E., Wright, J. B., Li, W. Z., Wen, J. G. and Ren, Z. F., (2003), 'Dispersion and alignment of carbon nanotubes in polycarbonate', Applied Physics, Vol. 76, pp. 111–113.

141. **Senthilvelan, S.** and Gnanamoorthy, R., (2004), 'Damage Mechanisms in Injection Molded Unreinforced, Glass and Carbon Reinforced Nylon 66 Spur Gears', Applied Composite Materials, Vol. 11(1), pp. 377-397.

142. **Senthilvelan, S.** and Gnanamoorthy, R., (2004), 'Wear Characteristics of Injection Molded Unfilled and Glass Filled Nylon 6 Spur Gears', Journal of Engineering Tribology, Proceedings of the Institution of Mechanical Engineers, Part J, Vol. 218(6), pp. 495-502.

143. **Senthilvelan, S.** and Gnanamoorthy, R., (2005), 'Surface Failure Analysis of Unreinforced ,Glass and Carbon Fiber Reinforced Nylon 6/6 Spur Gears', International Journal of Plastics Technology, Vol. 9, pp. 444-452.

144. **Senthilvelan, S.** and Gnanamoorthy, R., (2005), 'Reinforced Polymer Gear Fatigue and Failure Analysis', Transactions Indian Institute of Metals, Vol. 58 (2-3), pp. 249-253.

145. **Senthilvelan, S.** and Gnanamoorthy, R., (2006), 'Selective Carbon Fiber Reinforced Nylon 66 Spur Gears Development and Performance', Applied Composite Materials, Vol. 13(1), pp. 43-56.

146. **Senthilvelan, S.** and Gnanamoorthy, R., (2006), 'Effect of Gear Tooth Fillet Radius on the Performance of Injection Molded Nylon 6/6 Gears, Materials and Design', Materials and Design, Vol. 27(8), pp. 632-639.

147. **Senthilvelan, S.** and Gnanamoorthy, R., (2007), 'Effect of rotational speed on the performance of unreinforced andglass fiber reinforced Nylon 6 spur gears', Materials and Design, Vol. 28, pp. 765–772.

148. **Seung, I. C.**, Kyung, T.K., Kyong, H.L., Chan. B.M., Yong, J.J., Soon, H.H., (2008), 'Mechanical and Electrical Properties of Cross-Linked Carbon Nanotubes', Carbon, Vol. 46, pp. 482–488.

149. **Siddique, R.**, (2003), 'Effect of fine aggregate replacement with Class F fly ash on the mechanical properties of concrete', Cement and Concrete Research, Vol. 33, pp. 539–547.

150. **Simmons, W. J.** and Simmons, W. N., (2008), 'Toughened polyethylene terephthalate', US patent No.: 7351756 B2.

151. **Sinha, J. K.**, Friswell, M. I. and Edwards, S., (2002), 'Simplified Models for the location of cracks in beam structures using measured vibration data', Journal of Sound and Vibration, Vol. 251(1), pp. 13-38.

152. **Sinha R. S.** and Biswas, M., (1999), 'Preparation and evaluation of composites from montmorillonite and some heterocyclic polymers: 3. A water dispersible nanocomposite from pyrrole-montmorillonite polymerization system', Materials Research Bulletin, Vol. 34(8), pp. 1187–1194.

153. **Sohn, M. S.**, Kim, K. S., Hong, S. H. and Kim, J. K., (2003), 'Dynamic mechanical properties of particle reinforced EPDM composites', Journal of Applied Polymer Science, Vol. 87, pp. 1595–1601.

154. **Solomon, M. J.**, Almusallam, A. S., Seefeldt, K. F., Somwangthanaroj, A. and Varadan, P., (2001), 'Rheology of Polypropylene/Clay Hybrid Materials', Macromolecules, Vol. 34, pp. 1864-1872.

155. **Sridhar, V.**, Xiu, Z. Z., Xu, D., Lee, S. H., Kim, J. K., Kang, D. J. and Bang, D. S., (2009), 'Fly ash reinforced thermoplastic vulcanizates obtained from waste tire powder', Waste Management, Vol. 29, pp. 1058–1066.

156. **Steeves, C. A.** and Fleck, N. A., (2004), 'Collapse mechanisms of sandwich beams with composite facesand a foam core, loaded in three-point bending. Part II: experimental investigation and numerical modelling', International Journal of Mechanical Sciences, Vol. 46, pp. 585–608.

157. **Subramanian, C.**, Deshpande, S. B. and Senthilvelan, S., (2011), 'Effect of Reinforced Fiber Length on the Damping Performance of Thermoplastic Composites', Advanced Composite Materials, Vol. 20, pp. 319–335.

158. **Sugimoto, T.**, Sasaki, Y., Yamasaki, M., (2007), 'Fatigue of structural plywood under cyclic shear through thickness I: fatigue process and failure criterion based on strain energy', Journal of Wood Science, Vol. 53, pp. 296–302.

159. **Sugimoto, T.**, Sasaki, Y. and Yamasaki, M., (2007), 'Fatigue of structural plywood under cyclic shear through thickness II: a new method for fatigue life prediction', Journal of Wood Science, Vol. 53, pp. 303–308.

160. **Sugimoto, T.**, Sasaki, Y. and Yamasaki, M., (2008), 'Fatigue of structural plywood under cyclic shear through thickness III: a new method for fatigue life prediction', Journal of Wood Science, Vol. 54, pp. 169–173.

161. **Sun, S.**, Li, Z. and Wang, P., (2009), 'Fabrication of Micro Gear with New Technologies', Proceedings of the 2009 IEEE International Conference on Mechatronics and Automation, August 9 - 12, Changchun, China. pp. 1427-1432.

162. **Sunil, K.**, Mishra, K. K. and Madan, J., (2010), 'Stress analysis of spur gear using FEM method', Proceding of the national conference on advancements and futuristic trends in mechanical and materials engineering, Yadavindra College of Engineering, Punjabi University, pp. 158-161.

163. **Tang, W. Z.**, Santare, M. H. and Advani, S. G., (2003), 'Melt processing and mechanical property characterization of multi-walled carbon nanotube/high density polyethylene (MWNT/HDPE) composite films', Carbon, Vol. 41(14), pp. 2779-2785.

164. **Tetsuka, H.**, Ebina, T., Nanjo, H. and Mizukami, F., (2007), 'Highly Transparent Flexible Clay Films Modified with Organic Polymer: Structural Characterization and

Intercalation Properties', Journal of Materials Chemistry, Vol. 17, pp. 3545-3550.

165. **Thome´, T.**, Fouchez, S. and Delalande, S., (2009), 'Determination of silicone coating Young's modulus using atomic force microscopy', Physica B, Vol. 404, pp. 22–25.

166. **Thuis, H. G. S. J.**, (2002), 'The development of a composite landing gear component for a fighter aircraft', SAMPE Europe International Conference, National Aerospace Laboratory NLR, Paris, France.

167. **Tong, J.**, Ma, Y. and Jiang, M., (2003), 'Effects of the wollastonite fiber modification on the sliding wear behavior of the UHMWPE composites', Wear, Vol. 255, pp. 734–741.

168. **Valentini, L.**, Biagiotti, J., Kenny, J. M. and Santucci, S., (2003), 'Morphological characterization of single-walled carbon nanotubes-PP composites', Composites Science and Technology, Vol. 63, pp. 1149–1153.

169 **Walton, D.** and Shi, Y. W., (1989), 'A comparison of ratings for plastic gears', Proceedings of the Institution of Mechanical Engineers, Vol. 203, pp. 31-38.

170. **Wang, Q.**, Liu, C. and Chen,Y., (2001), 'Studies on PA6-PP-wollastonite composite compatibilised by PP-graft-maleic anhydride prepared via pan milling', Plast. Rub. Comp. Vol. 30, pp. 363–369.

171. **Watari, T.**, T. Yamane, S. Moriyama, T. Torikai, Y. Imaoka and K. Suehiro, (1997), 'Fabrication of (expandable mica)/nylon 6 composites', Materials Research Bulletin, Vol. 32(6), pp. 719-724.

172. **Wong, S. C.**, Lee, H., Qu, S., Mall, S. and Chen, L., (2006), 'A study of global vs. local properties for maleic anhydride modified polypropylene nanocomposites', Polymer, Vol. 47, pp. 7477-7484.

173. **Wright, N. A.**, Kukureka, S. N., (2001), 'Wear testing and measurement techniques for polymer composite gears', Wear, Vol. 251, pp. 1567–1578.

174. **Xiao, K. Q.**, Zhang, L. and Zarudi, C., (2007), 'Mechanical and rheological properties of carbon nanotube-reinforced polyethylene composites', Composites Science and Technology, Vol. 67, pp. 177–182.

175. **Yakut, R.**, Düzcükoğlu, H. and Demirci, M.T., (2009), 'The load capacity of PC/ABS spur gears and investigation of gear damage', Archives of Materials Science and Engineering, Vol. 40, pp. 41-46.

176. **Yu, W. J.** and Kim, H.C., (1988), 'Double tapered FRP beam for automotive suspension leaf spring', Composite Structures, Vol. 9, pp. 279-300.

177. **Zeng, H.**, Gao, C., Wang, Y., Watts, P. C. P., Kong, H., Cui, X. and Yan, D., (2006), 'In situ polymerization approach to multiwalled carbon nanotubes-reinforced nylon 1010 composites: Mechanical properties and crystallization behavior', Polymer, Vol.

47, pp. 113–122.

178. **Zhang, Q.**, Rastogi, S., Chen, D., Lippits, D. and Lemstra, P. J., (2006), 'Low percolation threshold in single-walled carbon nanotube/high density polyethylene composites prepared by melt processing technique', Carbon, Vol. 44, pp. 778–785.

179. **Zhang, R. H.**, Shi, D., Tjong,S. C. and Li, R. K. Y., (2007), 'Study on the β to α transformation of polypropylene crystals in compatibilized blend of polypropylene/polyamide-6', Journal of Polymer Science Part B: Polymer Physics, Vol. 45(19), pp. 2674-2681.

180. **Zhou, S. E.**, Wang, K. W. and Bakis, C. E., (2004), 'Interfacial damping characteristics of carbon nanotube-based composites', Composites Science and Technology, Vol. 64, pp. 2425–2437.

181. **Zhou, X.**, Yu, Y., Lin, Q. and Chen, L., (2013), 'Effects of Maleic Anhydride-Grafted Polypropylene (MAPP) on the Physico-Mechanical Properties and Rheological Behavior of Bamboo Powder-Polypropylene Foamed Composites', BioResources, Vol. 8(4), pp. 6263-6279.

182. **Zhou, Y.**, Rangari, V., Mahfuz, H., Jeelani, S. and Mallick, P.K., (2005), 'Experimental study on thermal and mechanical behavior of polypropylene, talc/polypropylene and polypropylene/clay nanocomposites', Materials Science and Engineering A, Vol. 402, pp. 109–117.

183. **Zhuang, G.**, Yang,Y. and Li,B., (1997), 'Reinforced effect of wollastonite on phenolphthalein poly(ether ketone)', Journal of Applied Polymer Science, Vol. 65, pp. 649–653.

184. **Zou, Y.**, Feng, Y., Wang L. and Liu, X., (2004), 'Processing and properties of MWNT/HDPE composites', Carbon, Vol. 42, pp. 271–277.

185. http://en.wikipedia.org/wiki/Fibre-reinforced_plastic#cite_note-6, date: 23/0.6/2013.

186. http://www.understanding-cement.com/hydration.html, date: 12/02/2011.

187. http://www.gemmechem.com/solutions/SolutionsInfo.asp?NewsID=38, 17/02/2010

188. http://www.chemorbis.com/ChemOrbis/content/sampleReports.do, Polymer digest, 11-Dec. 2012.

189. http://www.alibaba.com/

190. http://www.chemorbis.com/ChemOrbis/content/globalpriceList.do?useFastLogin=true

191. http://www.polymerupdate.com/prices/south-asia/pp/default.aspx?product=pp&type=pp

192. Indian open market price table as of 9th September 2014, docx. file

193. http://www.polymerupdate.com/news/news-details.aspx?id=30321&vw=view_allbreakingnews&yr=2014

194. http://www.arrowgear.com/pdf_files/arrowgearpricelist.pdf

195. http://www3.nd.edu/~manufact/MPEM_pdf_files/Ch10.pdf

196. http://www.ami.ac.uk/courses/topics/0211_pmp/

197. Physical Properties of Polymers Handbook, Mark, James E. (Ed.), 2nd ed. 2007

198. http://en.wikipedia.org/wiki/PEEK

199. http://www.makeitfrom.com/material-data/?for=Polyoxymethylene-POM-Acetal

200. http://www.makeitfrom.com/material-data/?for=Polyamide-PA-Nylon

201. http://www.makeitfrom.com/material-data/?for=Polyester

202. http://www.makeitfrom.com/material-data/?for=Polymethylmethacrylate-PMMA-Acrylic-Plexiglas

203. http://tools.ticona.com/tools/mcbasei/product-tools.php?sPolymer=POM&sProduct=CELCON

204 http://asm.matweb.com/search/SpecificMaterial.asp?bassnum=MA6061t6, 12.01.2014

List of Publications

Journal Publications

1. **Jagannath Sardar** and Dibakar Bandopadhya, (**2014**) **'Development and fabrication of cement reinforced polypropylene composite material spur gear'**, Journal of Polymer Engineering, Vol. 34 (8), pp. 775–786.

2. **Jagannath Sardar** and Dibakar Bandopadhya, (**2014**), **'Effect of Notches and Evaluation of Material Performance of a Cement Filled Composite Material for Fabrication of Nonmetallic Parts'**, International Journal of Advanced Mechanical Engineering, Vol. 4 (5), pp. 481-486.

3. **Jagannath Sardar** and Dibakar Bandopadhya, (**2014**), 'Investigation and Evaluation of Wear Characteristics of a Nonmetallic Spur Gear**'**, Trends in Machine design, Vol. 1(3), pp. 1-9.

4. **Jagannath Sardar** and Dibakar Bandopadhya, (**2014**), '**A Stress Distribution Model along the Tooth Mating Surface of a Non-Metallic Spur Gear using the Hertz's Contact Theorem'**, Trends in Machine design, Vol. 1(2), pp. 23-32.

5. **Jagannath Sardar** and Dibakar Bandopadhya, (**2011**), **'Processing, Fabrication and Investigation of Thermal Characteristics of Portland Pozzolanic Cement Filled Polypropylene Composites'**, International Journal of Plastic and Polymer Technology, Vol. 1(1), pp.16-37.

Conference Publications

1. **Jagannath Sardar** and Dibakar Bandopadhya, **'Evaluation of Wear Behavior of a Nonmetallic Spur Gear'**, 3rd International and 24th All India Manufacturing Technology, Design and Research-**AIMTDR-2010**, 13-15 Dec, 2010, Visakhapatnam, India, Vol. 2, pp. 1095-1098.